OPEN ACCESS
IOP Publishing
Journal of Physics G: Nuclear and Particle Physics
J. Phys. G: Nucl. Part. Phys. **51** (2024) 090501 (163pp)
https://doi.org/10.1088/1361-6471/ad1a78

Major Report

The strong coupling constant: state of the art and the decade ahead

D d'Enterria[1,46], S Kluth[2,46], G Zanderighi[2,3,46], C Ayala[4], M A Benitez-Rathgeb[5], J Blümlein[6], D Boito[5,7], N Brambilla[3], D Britzger[2], S Camarda[1], A M Cooper-Sarkar[8], T Cridge[9], G Cvetič[10], D d'Enterria[1], M Dalla Brida[11], A Deur[12], F Giuli[1], M Golterman[13,14], A H Hoang[5,15], J Huston[16], M Jamin[5,17], S Kluth[2], A V Kotikov[18], V G Krivokhizhin[18], A S Kronfeld[19], V Leino[3], K Lipka[20], T Mäkelä[20], B Malaescu[21], K Maltman[22,23], S Marzani[24], V Mateu[25,26], S Moch[27], P F Monni[11], P Nadolsky[28], P Nason[2,29], A V Nesterenko[18], R Pérez-Ramos[30,31], S Peris[14], P Petreczky[32], A Pich[33], K Rabbertz[34], A Ramos[33], D Reichelt[35], A Rodríguez-Sánchez[36], J Rojo[37,38], M Saragnese[6], L Sawyer[39], M Schott[40], S Schumann[41], B G Shaikhatdenov[18], S Sint[42], G Soyez[43], D Teca[10], A Vairo[3], M Vos[33], C Waits[39], J H Weber[44], M Wobisch[39], K Xie[45] and G Zanderighi[2,3]

[1] CERN, EP Department, CH-1211 Geneva 23, Switzerland
[2] Max-Planck-Institut für Physik, D-80805 München, Germany
[3] Physik-Department, Technische Universität München, D-85748 Garching, Germany
[4] IAI, Univ. de Tarapacá, Arica, Chile
[5] University of Vienna, Faculty of Physics, A-1090 Wien, Austria
[6] Deutsches Elektronen–Synchrotron DESY, 15738 Zeuthen, Germany
[7] Instituto de Física de São Carlos, Universidade de São Paulo, CP 369, 13560-970, São Carlos, SP, Brazil
[8] Department of Physics, University of Oxford, United Kingdom
[9] Department of Physics and Astronomy, University College London, London, United Kingdom
[10] UTFSM, Valparaíso, Chile
[11] CERN, TH Department, CH-1211 Geneva 23, Switzerland
[12] Jefferson Lab, Newport News, VA 23606, United States of America
[13] Department of Physics and Astronomy, San Francisco State University, San Francisco, CA 94132, United States of America
[14] Department of Physics and IFAE-BIST, Universitat Autònoma de Barcelona, E-08193 Bellaterra, Barcelona, Spain
[15] Erwin Schrödinger International Institute for Mathematical Physics, University of Vienna, A-1090 Wien, Austria
[16] Department of Physics and Astronomy, Michigan State University, East Lansing, MI 48824 United States of America

[17] Central Institute of Mental Health, Medical Faculty Mannheim, Heidelberg University, Mannheim, Germany
[18] Joint Institute for Nuclear Research, Dubna, Russia
[19] Theory Division, Fermi National Accelerator Laboratory, Batavia, IL 60510, United States of America
[20] Deutsches Elektronen–Synchrotron DESY, D-22607 Hamburg, Germany
[21] LPNHE, Sorbonne Université, Université Paris Cité, CNRS/IN2P3, Paris, France
[22] Department of Mathematics and Statistics, York University, Toronto, ON M3J 1P3, Canada
[23] CSSM, University of Adelaide, Adelaide, SA 5005 Australia
[24] Dipartimento di Fisica, Università di Genova and INFN, Sezione di Genova, Via Dodecaneso 33, I-16146, Genoa, Italy
[25] Dept. de Física Fundamental e IUFFyM, Universidad de Salamanca, E-37008 Salamanca, Spain
[26] Instituto de Física Teórica UAM-CSIC, E-28049 Madrid, Spain
[27] II. Institute for Theoretical Physics, Hamburg University, D-22761 Hamburg, Germany
[28] Department of Physics, Southern Methodist University, Dallas, TX 75275-0181, United States of America
[29] Università di Milano–Bicocca and INFN, Sezione di Milano - Bicocca, I-20126 Milano, Italy
[30] DRII-IPSA, Bis, 63 Boulevard de Brandebourg, F-94200 Ivry-sur-Seine, France
[31] Sorbonne Universités, UPMC Univ Paris 06, UMR 7589, LPTHE, F-75005, Paris, France
[32] BNL, Upton, NY, United States of America
[33] IFIC, CSIC-Universitat de València, E-46980 València, Spain
[34] KIT, Karlsruhe, Germany
[35] Inst. for Particle Phys. Phenomenology, Dept. of Physics, Durham Univ., Durham DH1 3LE, United Kingdom
[36] Université Paris-Saclay, CNRS/IN2P3, IJCLab, F-91405 Orsay, France
[37] Department of Physics and Astronomy, VU Amsterdam, 1081HV Amsterdam, The Netherlands
[38] Nikhef Theory Group, Science Park 105, 1098XG Amsterdam, The Netherlands
[39] Louisiana Tech University, Ruston, LA, United States of America
[40] Johannes Gutenberg-Universitat Mainz (JGU), Saarstr. 21, D-55122 Mainz, Germany
[41] Institut für Theoretische Physik, Georg-August-Universität Göttingen, D-37077 Göttingen, Germany
[42] School of Mathematics and Hamilton Mathematics Institute, Trinity College Dublin, Dublin 2, Ireland
[43] Institut de Physique Théorique, Paris Saclay University, CEA, CNRS, F-91191 Gif-sur-Yvette, France
[44] HU & RTG2575, Berlin, Germany
[45] Department of Physics and Astronomy, University of Pittsburgh, Pittsburgh, PA 15260, United States of America

Received 6 November 2023, revised 7 December 2023
Accepted for publication 3 January 2024
Published 28 October 2024

[46] Editors.

Abstract

Theoretical predictions for particle production cross sections and decays at colliders rely heavily on perturbative Quantum Chromodynamics (QCD) calculations, expressed as an expansion in powers of the strong coupling constant α_S. The current $\mathcal{O}(1\%)$ uncertainty of the QCD coupling evaluated at the reference Z boson mass, $\alpha_S(m_Z^2) = 0.1179 \pm 0.0009$, is one of the limiting factors to more precisely describe multiple processes at current and future colliders. A reduction of this uncertainty is thus a prerequisite to perform precision tests of the Standard Model as well as searches for new physics. This report provides a comprehensive summary of the state-of-the-art, challenges, and prospects in the experimental and theoretical study of the strong coupling. The current $\alpha_S(m_Z^2)$ world average is derived from a combination of seven categories of observables: (i) lattice QCD, (ii) hadronic τ decays, (iii) deep-inelastic scattering and parton distribution functions fits, (iv) electroweak boson decays, hadronic final-states in (v) e^+e^-, (vi) e–p, and (vii) p–p collisions, and (viii) quarkonia decays and masses. We review the current status of each of these seven $\alpha_S(m_Z^2)$ extraction methods, discuss novel α_S determinations, and examine the averaging method used to obtain the world-average value. Each of the methods discussed provides a 'wish list' of experimental and theoretical developments required in order to achieve the goal of a per-mille precision on $\alpha_S(m_Z^2)$ within the next decade.

Keywords: QCD, strong coupling, colliders

1. Introduction

The strong coupling α_S sets the scale of the strength of the strong interaction, theoretically described by Quantum Chromodynamics (QCD), and is one of the fundamental parameters of the Standard Model (SM) of particle physics. In the chiral limit of zero quark masses and for fixed number of colours $N_c = 3$, the α_S coupling is the only free parameter of QCD. Starting at an energy scale of order $\Lambda_{\rm QCD} \approx 0.2$ GeV in the vicinity of the infrared Landau pole of the theory, $\alpha_S(Q)$ approximately decreases as $1/\log(Q^2/\Lambda^2_{\rm QCD})$, where Q is the energy scale of the underlying QCD process. Its value at the reference Z pole mass amounts today to $\alpha_S(m_Z^2) = 0.1179 \pm 0.0009$ [1], with a $\delta\alpha_S/\alpha_S \approx 0.8\%$ uncertainty that is orders of magnitude larger than that of the other three interaction (QED, weak, and gravitational) couplings.

Our knowledge of the QCD coupling has improved throughout the years (figure 1), from a $\mathcal{O}(100\%)$ uncertainty when it was first constrained from data-versus-theory comparisons at next-to-leading order accuracy in the mid 1980s—exploiting, already then, a variety of observables (deep-inelastic scattering cross sections, total hadronic cross section in e^+e^- annihilation, the distribution of 3-jet events in e^+e^- collisions, the energy flow of energy in e^+e^- annihilation, Υ branching fractions, the behavior of baryon form factors at large momentum transfer, measurements of the photon structure functions, and the hyperfine splittings in the J/ψ state) [2] – to the present $\mathcal{O}(1\%)$ precision [1]. Further improving our knowledge of α_S is fundamental, among other things, to reduce the theoretical 'parametric' uncertainties in the calculations of all perturbative QCD (pQCD) processes whose cross sections or decay rates depend on powers of α_S, as is the case for virtually all those measured in proton and nuclear collisions at the Large Hadron Collider (LHC), as well as in e^+e^-

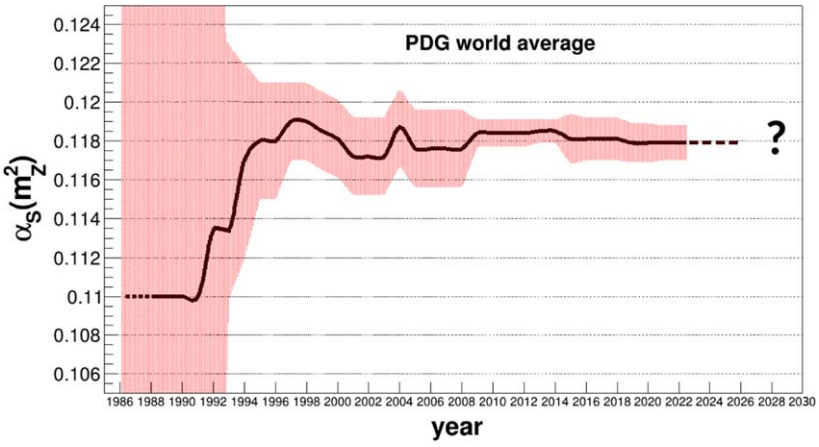

Figure 1. Evolution of the average value of the QCD coupling at the Z boson mass scale (with the red bands indicating its associated uncertainty) in the $\overline{\text{MS}}$ renormalization scheme, quoted in the Particle Data Group (PDG) review covering the last four and the current decades [1].

annihilation at future high-precision colliders. In the Higgs sector, our imperfect knowledge of α_S propagates today into total final uncertainties for key processes such as the Higgs gg-fusion and $t\bar{t}$-associated production cross sections of $\sim$2%–3% [3, 4], or of $\sim$4% for the $\mathrm{H} \to gg$ partial decay width [5, 6]. In the electroweak (EW) sector of the SM, the input $\alpha_S(m_Z^2)$ value is the leading source of uncertainty in the computation of crucial precision pseudo-observables such as the total and partial hadronic Z boson widths [6, 7]. The QCD coupling plays also a fundamental role in the calculation of key quantities in top-quark physics, such as the top mass, width, and its Yukawa coupling [8]. Last but not least, the value of $\alpha_S(m_Z^2)$ and its energy evolution have also far-reaching implications including the stability of the electroweak vacuum [9], the existence of new coloured sectors at high energies [10], and in our understanding of physics approaching the Planck scale, such as e.g. in the precise energy at which the interaction couplings may unify.

This report, co-authored by experimental and theoretical experts from all relevant subfields who participated at the α_S(2022) workshop in February 2022 (ECT*, Trento, https://indico.cern.ch/e/alphas2022), explores in depth the latest developments in the determination of α_S from the key categories where high-precision measurements and calculations are currently available. The following main questions are addressed in detail for each of the α_S extraction methods: what is the current state-of-the-art? What is the expected theoretical and experimental precision in about ten years from now (indicated by the interrogation symbol in figure 1), and what needs to be achieved in order to reach a $\mathcal{O}(0.1\%)$ precision? In particular, this report examines, for the different calculations of α_S-sensitive observables involved, what the current state-of-the-art is with regards to higher-order (pQCD, mixed QCD-EW) corrections, and what the impact of nonperturbative corrections/uncertainties is. Whenever there are new ideas or techniques to reduce them, these are illustrated. From an experimental point of view, the report discusses what the current leading systematic and statistical uncertainties of the α_S-sensitive observables are, and what future reductions of them are expected with current (p–p) and future (e^+e^-, e–p) machines. New observables are also suggested.

The review is organized as follows. Sections 2–9 discuss α_S determinations based on, consecutively, lattice-QCD methods; hadronic tau-lepton decays; deep-inelastic scattering

and parton densities fits; electroweak fits; hadronic final states in e^+e^-, and in $e^\pm-p$ and $p-p$ collisions; and quarkonium bound states. Section 10 discusses the averaging method used to currently obtain the world-average $\alpha_S(m_Z^2)$ value. The last section 10 ends with a summary of the discussions of the $\alpha_S(2022)$ workshop, and with a 'wish-list' assessment in data/theory developments needed to reach a precision of α_S at the per-mille level in the upcoming years.

2. $\alpha_S(m_Z^2)$ from lattice QCD

2.1. Prospects of lattice determinations of α_S from the FLAG perspective[47]

2.1.1. Overview of the current situation. FLAG stands for 'Flavour Lattice Averaging Group' and constitutes an effort by the lattice QCD community to supply qualified information on lattice results for selected physical quantities to the wider particle physics community. These include the QCD parameters, i.e. α_S and the quark masses. An extensive report aimed at a general particle physics audience is published every 2–3 years [11, 12] and in the meantime occasional updates are made to the online version maintained at the University of Bern[48]. We strongly encourage readers to explore this report, in particular, the α_S chapter. For a complementary pedagogical introduction see the review [13].

In the FLAG α_S working group we have recently provided the updated lattice QCD average

$$\alpha_S(m_Z^2) = 0.1184(8), \tag{2.1}$$

based on results published[49] in [14–21]. This represents a minimal change from FLAG 2019 [12], and no reduction in the error. The FLAG criteria for α_S have remained unchanged since FLAG 2019 and there are now some indications that the criteria may need to be revised in the future [11].

Lattice determinations of α_S use up, down, and strange quarks (and sometimes the charm quark) in the sea, and perturbatively evolve across the charm and bottom thresholds to obtain α_S in the 5-flavour theory. The perturbative matching across quark thresholds has been put to a nonperturbative test in [22] which demonstrates that the perturbative description of decoupling (known to 4-loop order [23–28]) provides an excellent quantitative description even for the charm quark. Hence, one may avoid the potentially large cutoff effects associated with the charm quark mass, which is usually not so small compared to the lattice cutoff scale $1/a$ (a denotes the lattice spacing).

A lattice determination of α_S starts with the choice of an observable $O(\mu)$ depending on a single scale μ with a perturbative expansion of the form

$$O(\mu) = c_0 + c_1\alpha_{\overline{\rm MS}}(\mu) + c_2\alpha^2_{\overline{\rm MS}}(\mu) + \ldots \tag{2.2}$$

It is convenient to normalize the observable as an effective coupling

$$\alpha_{\rm eff} = (O(\mu) - c_0)/c_1 = \alpha_{\overline{\rm MS}} + d_1\alpha^2_{\overline{\rm MS}} + \ldots \tag{2.3}$$

We then refer to $d_1 = c_2/c_1$ as the 1-loop matching coefficient, even though some choices of $O(\mu)$ may require a 1-loop-diagram to obtain c_0 and thus 2 more loops to obtain d_1. It should be clear that each choice of $O(\mu)$ leads to a different lattice determination of α_S, in close analogy to phenomenological determinations. The main difference therefore is whether the

[47] Authors: S Sint (Trinity College Dublin).
[48] http://flag.unibe.ch
[49] It is FLAG policy to require that the original works entering any FLAG averages to be always cited alongside the FLAG report!

original data are produced by a lattice simulation or taken from experiment. A bonus of the lattice setup is the access to observables which are not experimentally measurable, for instance, one may study QCD in a finite Euclidean space-time volume L^4 and define the observable O through a finite volume effect [29]. However, many renormalization schemes for the coupling assume large volume, i.e. in practice one needs to show that the necessarily finite L is causing negligible effects on the chosen observable. Note also that quark masses can be varied, and one may naturally define mass-independent couplings (such as the $\overline{\text{MS}}$ coupling) by imposing renormalization conditions in the chiral limit [30].

A common problem of most lattice determinations of α_S has been dubbed the 'window problem': in order to match to hadronic physics, the spatial volume L^3 must be large enough to avoid significant finite volume effects due to pion polarization 'around the world'. On the other hand, the matching to the coupling requires perturbative expansions to be reliable, so one needs to reach as high a scale μ as possible, but still significantly below the cutoff scale $1/a$ such as to avoid large lattice distortions. If taken together this means

$$\frac{1}{L} \ll m_\pi \ll \mu \ll \frac{1}{a} \quad \Rightarrow \quad \frac{L}{a} = \mathcal{O}(10^3), \tag{2.4}$$

(where the hadronic scale m_π is the pion mass) which is just a reflection of the fact that very different energy scales cannot be resolved simultaneously on a single lattice of reasonable size[50]. In addition, the continuum limit $a \to 0$ requires a range of lattice sizes satisfying the above constraint, and one would like to have a range of scales μ such as to verify that the perturbative regime has been reached. This window problem enforces various compromises; in most cases the energy scales reached for perturbative matching to the $\overline{\text{MS}}$-coupling is therefore rather low. As a consequence, even in the best cases (with 3-loop matching to the $\overline{\text{MS}}$-coupling) systematic errors due to truncation of the perturbative series and/or contributions from nonperturbative effects are dominant [11, 13].

A solution to the window problem is however known since the 1990s, in the form of the step-scaling method [31]. The method is based on a finite volume renormalization scheme with $\mu = 1/L$. It is then possible to recursively step up the energy scale by a fixed scale factor $s = 2$, and a scale difference of $\mathcal{O}(10^2)$ is thus covered in 5 to 6 steps. The window problem is by-passed, as the approach uses multiple (pairs of) lattices with size L/a and $2L/a$, covering a wide range of physical scales $\mu = 1/L$ without the need to represent simultaneously any hadronic scale, except at the lowest scale reached, $\mu_{\text{had}} = 1/L_{\text{max}}$. Once the scale μ_{had} is matched to a hadronic quantity such as the proton mass, all the higher scales are known too, as the scale ratios are powers of two. At the high energy end, now orders of magnitude above the hadronic scales, perturbation theory can be safely applied to match to the $\overline{\text{MS}}$-coupling, or, equivalently to extract the 3-flavour Λ-parameter. The method has been applied in [18], with the result $\Lambda^{(3)}_{\overline{\text{MS}}} = 341(12)$ MeV, which translates to $\alpha_S(m_Z^2) = 0.1185(8)$. It is important to realize that this is the only lattice determination of α_S where the error is still statistics dominated. For this reason, we quote this error for the FLAG average (2.1) as a conservative estimate of the uncertainty, instead of combining the (mostly systematic) errors in quadrature.

2.1.2. Future prospects and conclusions. Most lattice determinations of α_S are now limited by systematic errors, due to the relatively low energy scales where perturbation theory is applied, and the limited range of available energy scales. The one exception is the step-scaling method which enables the nonperturbative scale evolution up to very high energies. Perturbation theory can be tested and then safely applied.

[50] $L/a = 100$ would be considered a large lattice by today's standards.

Is it possible to incorporate at least some elements of the step-scaling method into some of the other lattice determinations? In its original form, the step-scaling method uses a finite volume renormalization scheme, i.e. $\mu = 1/L$, which means that finite volume effects are part of the scheme definition, rather than systematic effects to worry about. In fact, all lattice determinations of α_S could incorporate the step scaling approach by simply working at fixed μL. Unfortunately, this means that perturbation theory needs to be set up in a finite volume too, which can be rather complicated, depending on the choice of boundary conditions. In particular, the perturbative results computed for infinite volume could not be used anymore, and adapting these to finite volume is no minor change. As a side remark, it would be highly desirable that experts in perturbation theory cooperate with lattice QCD practitioners to adapt and develop perturbative techniques for some selected finite volume schemes.

In the short to medium term future some progress may still be possible by taking a few steps with the step-scaling methods in large volume, perhaps with smaller scale factors, e.g. $s = 3/2$. This would require that finite volume effects in the chosen observable are controlled and eliminated at each step. In fact, it is quite plausible that finite volume effects are smaller in the chosen observables for the coupling than in some of the other hadronic observables. An example of this strategy was presented in [32] for the force between static quarks (there for $N_\mathrm{f} = 0$ quark flavours). It is worth emphasizing that such progress requires a dedicated effort, including computational resources for the production of additional gauge configurations, which may have spatial volumes too small to serve other goals of a lattice collaboration. In the past this need for dedicated simulations has been a practical obstacle in some cases, but it seems now evident that it cannot be avoided if real progress is to be achieved.

The required computational resources for the full step-scaling method are substantial, too. In particular the bulk of the statistical error in the step-scaling result of [18] is accumulated by the scale evolution at *high* energy scales. While a further reduction of the error would be feasible by brute force, the ALPHA collaboration has instead proposed the decoupling strategy ([33], for an introduction see [34]). The scale evolution is traced in the $N_\mathrm{f} = 0$ pure gauge theory, with less resources and to better precision than in $N_\mathrm{f} = 3$ QCD [35, 36]. When combined with a nonperturbative computation for the simultaneous decoupling of $N_\mathrm{f} = 3$ dynamical quarks, the resulting error is currently comparable to the direct $N_\mathrm{f} = 3$ result of [18] and still statistics dominated [37]. I refer to section 2.2 for details. One aspect of this strategy is the importance acquired by results in the $N_\mathrm{f} = 0$ theory. Rather than being a mere test bed for the development of new methods, the pure gauge theory now indirectly contributes to α_S. The FLAG α_S working group will therefore keep monitoring $N_\mathrm{f} = 0$ results for the Λ-parameter.

In conclusion, significant progress in lattice determinations of $\alpha_S(m_Z^2)$ will require at least some elements of the step-scaling method in order to reach larger energy scales and at least partially evade the window problem. A total error clearly below half a percent for $\alpha_S(m_Z^2)$ seems achievable within the next few years by pushing the step-scaling method further, possibly in combination with the decoupling strategy. In order to corroborate such results it is very desirable to apply the step-scaling method to further observables in a finite space-time volume. Developing the necessary perturbative techniques then constitutes a challenge where cooperation with experts in perturbation theory might have a significant impact.

Acknowledgments—I thank my colleagues in the FLAG α_S-WG, Peter Petreczky and Roger Horsley for the pleasant collaboration and feedback on a draft of this contribution. Partial support by the EU unter grant agreement H2020-MSCA-ITN-2018-813942 (EuroPLEx) is gratefully acknowledged.

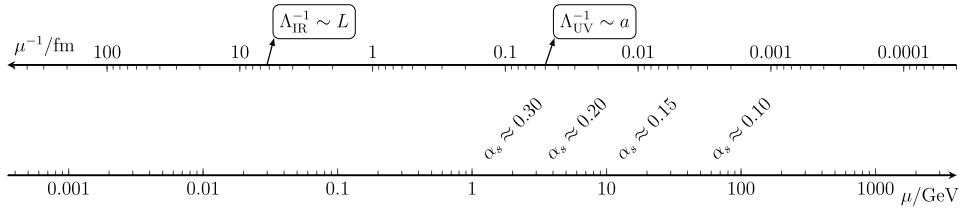

Figure 2. Lattice QCD simulations come with an IR cutoff $\Lambda_{\rm IR} = L^{-1}$ (where L is the size of the finite space-time volume of the simulation), and an ultraviolet cutoff $\Lambda_{\rm UV} = a^{-1}$ (where a is the lattice spacing). All relevant physical scales must lie far away from both these cutoffs in order to be free from finite-volume and discretization effects. As a result, given the current computational and algorithmic capabilities, if one wants to compute some hadronic quantities, the range of high-energy scales that can simultaneously be probed is limited.

2.2. A precise determination of α_S from lattice QCD using decoupling of heavy quarks[51]

The determination of the strong coupling using lattice QCD uses a nonperturbatively defined quantity $O(q)$ that depends on a single short distance scale $1/q$. Using the perturbative expression for this quantity[52]

$$O(q) \overset{q\to\infty}{\sim} \alpha_S(q) + \sum_{n=2}^{N} c_n \alpha_S^n(q) + \mathcal{O}(\alpha_S^{N+1}(q)) + \mathcal{O}\left(\frac{\Lambda}{q}\right)^p + ..., \tag{2.5}$$

where N is the number of known coefficients of the perturbative series, one can estimate the value of $\alpha_S(q)$. On the lattice, apart from the value of $O(q)$, one needs to determine the value of the scale q in units of some well-measured hadronic quantity (e.g. the ratio q/m_p with m_p being the proton mass).

There are two types of corrections in equation (2.5). First, we have the nonperturbative ('power') corrections. They are of the form $(\Lambda/q)^p$. Second, we have the perturbative corrections. Their origin is the truncation of the perturbative series to a finite order N, and parametrically these corrections are of the form $\alpha_S^{N+1}(q)$.

In principle, both kind of uncertainties decrease by taking $q \to \infty$. Unfortunately, though, a single lattice simulation can only cover a limited range of energy scales (figure 2). Thus, if one insists on determining the hadronic scale (e.g. m_p) and the value of the observable $O(q)$ using the *same* lattice simulation, the volume has to be large, $L \gtrsim 1/m_\pi$, and therefore the energy scales q that can be reached are at most a few GeV. Power corrections decrease quickly with the energy scale q, but due to the logarithmic dependence of the strong coupling with the energy scale,

$$\alpha_S(q) \overset{q\to\infty}{\sim} \frac{1}{\log(q/\Lambda_{\rm QCD})}, \tag{2.6}$$

perturbative uncertainties decrease very slowly. In fact, most lattice QCD extractions of the strong coupling are dominated by the truncation uncertainties of the perturbative series.

What can be said about such perturbative uncertainties? First, it has to be noted that due to the asymptotic nature of perturbative expansions, it is in general very difficult to estimate the difference between the truncated series for $O(q)$ and its nonperturbative value (see the original works [38, 39] and the review [13]). Second, an idea of the size of such uncertainties can be

[51] Authors: M Dalla Brida (CERN), A Ramos (IFIC, València).
[52] It is convenient to normalize the observable $O(q)$ so that the perturbative expansion starts with $\alpha_S(q)$.

obtained by using the scale-variation method. If one assumes that at scales q power corrections are negligible, one can use an arbitrary renormalization scale in the perturbative expansion equation (2.5),

$$O(q) \overset{q\to\infty}{\sim} \alpha_S(\mu) + \sum_{n=2}^{N} c_n(\mu/q)\alpha_S^n(\mu) + \mathcal{O}(\alpha_S^{N+1}(\mu)) + ... \tag{2.7}$$

The dependence on μ on the r.h.s. is spurious, and due to the truncation of the perturbative series. This dependence can be exploited to estimate the truncation effects: the value of α_S can be extracted for different choices of μ, and the differences among these extractions will give us an estimate of the effects due to missing higher-order pQCD corrections. Moreover, following [13], the estimate of the truncation uncertainties *can be obtained from the known perturbative coefficients alone*. No nonperturbative data for $O(q)$ is needed to estimate these uncertainties.

In [13] a detailed analysis of several lattice methods to extract the strong coupling is performed along these lines. What are their conclusions? Most 'large volume' approaches (those that aim at computing the scale q in physical units and the observable $O(q)$ using the same lattices) have perturbative uncertainties between about 1% and 3% in $\alpha_S(m_Z^2)$.

It is important to emphasize that this generic approach cannot say what the errors of a specific determination are. However, given the fact that *scale uncertainties can underestimate the true truncation errors* (see [38] for a concrete example), this exercise draws a clear picture: a *substantial reduction in the uncertainty of the strong coupling will only come from dedicated approaches*, where the multiscale problem discussed above is solved. In this contribution, we will summarize the efforts of the ALPHA collaboration in solving this challenging problem (see [34, 40] for a review).

2.2.1. Finite-volume schemes. A first step towards solving the difficult multiscale problem of extracting α_S using lattice QCD comes from the following simple realization. The computation of the hadronic quantities $m_{\rm had}$, needed for fixing the bare parameters of the lattice QCD action, and the determination of the nonperturbative coupling $\alpha_O(q) \equiv O(q)$ at large q, from which we extract α_S, are two distinct problems.[53] Hence, in order to best keep all relevant uncertainties under control, we need dedicated lattice simulations for the calculation of $\alpha_O(q)$. In fact, as mentioned above, despite being convenient in practice, determinations of $\alpha_O(q)$ based on simulations originally intended for the computation of low-energy quantities come with severe limitations on the energy scales q at which α_S can be extracted. As a concrete example, consider a typical state-of-the-art hadronic lattice simulation, with e.g. $L/a = 128$ points in each of the four space-time dimensions, and a spatial size L large enough to comfortably fit all the relevant low-energy physics, say, $m_\pi L \approx 4$ with $m_\pi \approx 135\,\text{MeV}$. This results in a lattice spacing $a \approx 0.045\,\text{fm}$, which sets the constraint, $q \ll a^{-1} \approx 4\,\text{GeV}$. With such a low upper-limit on q, reaching high precision on α_S is very likely impeded by the systematic uncertainties related to perturbative truncation errors and nonperturbative corrections.

The most effective way to determine nonperturbatively the coupling $\alpha_O(q)$ at high-energy is to consider a *finite-volume* renormalization scheme [31]. These schemes are built in terms of observables O defined in a finite space-time volume. The renormalization scale of the coupling q is then identified with the inverse spatial size of the finite volume, i.e. $q = L^{-1}$. In order words, a running coupling is defined through the response of some correlation function

[53] In this and the following sections, we find convenient to use the notation $\alpha_O(q) \equiv O(q)$, and interpret the extraction of α_S as the matching between the nonperturbative scheme for the QCD coupling α_O and the $\overline{\rm MS}$-scheme.

(s) as the volume of the system is varied. As a result, finite volume effects are part of the definition of the coupling, rather than a systematic uncertainty in its determination. This is clearly an advantage, since for these schemes lattice systematics are under control once a single condition, $L^{-1} = q \ll a^{-1} \Rightarrow L/a \gg 1$, is met. This is a much simpler situation than having to simultaneously satisfy: $L^{-1} \ll q \ll a^{-1}$. In principle, there is lots of freedom in choosing a finite-volume scheme. However, in practical applications several technical aspects need to be taken intro consideration. We refer the reader to [40] for a detailed discussion about these points and for concrete examples of schemes.

2.2.2. Step-scaling strategy. The way we exploit finite-volume schemes for the determination of α_S can be summarized in a few key steps,which we typically refer to as *step-scaling* strategy [31, 40, 41]. (1) We begin at low-energy by implicitly defining a hadronic scale $\mu_{\rm had}$ through a specific value of a chosen finite-volume coupling. Taking $\alpha_O(\mu_{\rm had} = L_{\rm had}^{-1}) \sim 1$, we expect $\mu_{\rm had} \approx \Lambda_{\rm QCD}$. (2) Using results from hadronic, large volume simulations, we can accurately establish the value of $\mu_{\rm had}$ in physical units. This is done by computing the ratio $\mu_{\rm had}/m_{\rm had} \sim \mathcal{O}(1)$,where $m_{\rm had}$ is an experimentally measurable low-energy quantity, e.g. a hadronic mass or decay constant. (3) We simulate pairs of lattices with physical sizes L and $L/2$,and determine the nonperturbative running of the finite-volume coupling $\alpha_O(1/L)$ with the energy scale.[54] This is encoded in the (inverse) step-scaling function: $\sigma_O^{-1}(u) = \alpha_O(2/L)|_{u=\alpha_O(1/L)}$, which measures the variation of the coupling as the energy scale is increased by a factor of two. (4) Starting from $\mu_{\rm had} = L_{\rm had}^{-1} \sim \mathcal{O}(100)\,\text{MeV}$, after $n \sim \mathcal{O}(10)$ steps as in 3), we reach nonperturbatively high-energy scales, $\mu_{\rm PT} = 2^n/L_{\rm had} \sim \mathcal{O}(100)\,\text{GeV}$. (5) Using the perturbative expansion of $\alpha_O(\mu_{\rm PT})$ in terms of $\alpha_{\overline{\rm MS}}(\mu_{\rm PT})$ we extract the latter (see equation (2.5)). (6) Given $\alpha_{\overline{\rm MS}}(\mu_{\rm PT})$, through the perturbative running in the $\overline{\rm MS}$-scheme, we obtain a value for $\Lambda_{\overline{\rm MS}}/\mu_{\rm PT}$, from which $\Lambda_{\overline{\rm MS}}/m_{\rm had}$ can be readily inferred.

2.2.3. α_S from a nonperturbative determination of $\Lambda_{\overline{\rm MS}}^{(N_{\rm f}=3)}$. Following a step-scaling strategy, the ALPHA collaboration has obtained a subpercent precision determination of $\alpha_S(m_Z^2)$ from a nonperturbative determination of $\Lambda_{\overline{\rm MS}}^{(3)}$ [18, 38, 39, 42]. We refer the reader to these references for the details on our previous calculation. Here we simply want to recall a few points which are relevant for the following discussion. In [38, 42] the nonperturbative running of some convenient finite-volume couplings in $N_{\rm f} = 3$ QCD was obtained, from $\mu_{\rm had} = 197(3)\,\text{MeV}$, up to $\sim$140 GeV.[55] Using NNLO perturbation theory, $\alpha_{\overline{\rm MS}}^{(3)}(\mu_{\rm PT})$ was then extracted at $\mu_{\rm PT} \approx 70\,\text{GeV}$, and from it the result: $\Lambda_{\overline{\rm MS}}^{(3)} = 341(12)\,\text{MeV}$. Thanks to the fact that we covered nonperturbatively a wide range of high-energy scales, a careful assessment of the accuracy of perturbation theory in matching the finite-volume and $\overline{\rm MS}$ schemes was possible. The result is that the error on $\Lambda_{\overline{\rm MS}}^{(3)}$ is entirely dominated by the statistical uncertainties associated with the determination of the nonperturbative running from low to high energy [18]. In particular, perturbative truncation errors and nonperturbative corrections are completely negligible within the statistical uncertainties [38]. Finally, from the result for $\Lambda_{\overline{\rm MS}}^{(3)}$, using perturbative decoupling relations, we included the effect of the charm and bottom quarks in the running to arrive at: $\alpha_{\overline{\rm MS}}^{(5)}(m_Z) = 0.1185(8)$ [18]. From these observations, it is clear that an improved determination of α_S may be obtained by reducing the

[54] In practice, several pairs of lattices with fixed spatial sizes L and $L/2$ but different lattice spacing a are simulated in order to extrapolate the lattice results to the continuum limit, $a \to 0$. Within this approach the simulated lattices cover at most a factor of two in energy. This allows for having control on discretization errors at any energy scale.
[55] The physical units of $\mu_{\rm had}$ were accurately established from a combination of pion and kaon decay constants [18].

statistical uncertainties on $\Lambda^{(3)}_{\overline{\rm MS}}$ due to the nonperturbative running of the finite-volume couplings. On the other hand, to which extent this is possible very much depends on how accurate it is to rely on perturbative decoupling for including charm effects.

2.2.4. How accurate is $N_f = 3$ QCD? Including the charm is particularly challenging in hadronic, large volume simulations. The charm has a mass $m_c \approx 1.3\,\text{GeV}$. In units of the typical cutoffs set in hadronic simulations this means $am_c \gtrsim 0.3$. It is thus difficult to comfortably resolve the characteristic energy scales associated with the charm in current large volume simulations: it requires very fine lattice spacings, which are computationally very demanding.[56] In addition, simulations become more expensive as the number of quarks increases, and the tuning of the parameters in the lattice QCD action is more involved. It is therefore important to assess whether the computational effort required to include the charm is actually needed to significantly improve our current precision on α_S. If that is not the case, the resources are better invested in improving the results from $N_{\rm f} = 3$ QCD.

In order to answer this question, we must study the systematics that enter in the $\Lambda^{(3)}_{\overline{\rm MS}} \to \Lambda^{(4)}_{\overline{\rm MS}}$ step. The first class is related to the use of perturbative decoupling relations for estimating the ratio $\Lambda^{(3)}_{\overline{\rm MS}}/\Lambda^{(4)}_{\overline{\rm MS}}$. As we shall recall below, the ratio of Λ-parameters with different flavour content is given by a function $P_{\ell,{\rm f}}\big(M/\Lambda^{(N_{\rm f})}_{\overline{\rm MS}}\big) = \Lambda^{(N_\ell)}_{\overline{\rm MS}}\big/\Lambda^{(N_{\rm f})}_{\overline{\rm MS}}$, which depends on the renormalization group invariant (RGI) mass M of the decoupling quark(s) and the theories considered. The function $P_{\ell,{\rm f}}$ can in principle be nonperturbatively defined (section 2.2.6). In phenomenological applications, however, we approximate it with its asymptotic, perturbative expansion at some finite loop-order, i.e. $P_{\ell,{\rm f}}\big(M/\Lambda^{(N_{\rm f})}_{\overline{\rm MS}}\big) \sim P^{(n-\text{loop})}_{\ell,{\rm f}}\big(M/\Lambda^{(N_{\rm f})}_{\overline{\rm MS}}\big) + \mathcal{O}(\alpha^{n-1}(M)) + \mathcal{O}(M^{-2})$. Whether this is appropriate, it all depends on the size of the perturbative and nonperturbative corrections to this approximation for values of the quark masses $M \sim M_c$, with M_c the RGI charm mass.

The second class of charm effects concerns the hadronic renormalization of the lattice theory. Normally, the bare parameters entering the lattice QCD action are tuned by requiring that a number of ratios of hadronic quantities R_H (as many as parameters to tune), reproduce their experimental counter-parts. Typical examples are, for instance, $R_H = m_\pi/f_\pi, m_K/f_\pi, \ldots$[57] On the other hand, $N_{\rm f} = 3$ QCD simulations do not include charm effects, while these are obviously present in the experimental determinations. Whether this mismatch is relevant in practice, it all depends on the actual size of charm effects in the ratios R_H.

2.2.5. Effective theory of decoupling and perturbative matching. For the ease of presentation, we define our *fundamental theory* as $N_{\rm f}$-flavour QCD (QCD$_{N_{\rm f}}$) with N_ℓ massless quarks, and $N_{\rm h} = N_{\rm f} - N_\ell$ mass-degenerate heavy quarks of mass M. In the limit where M is larger than any other scale in the problem, this theory can be approximated by an *effective theory* (EFT) with Lagrangian [43]

$$\mathcal{L}_{\rm dec} = \mathcal{L}_{{\rm QCD}_{N_\ell}} + \frac{1}{M^2}\sum_i \omega_i \Phi_i + \mathcal{O}(M^{-4}). \tag{2.8}$$

The leading order term in the $1/M$ expansion is the Lagrangian $\mathcal{L}_{{\rm QCD}_{N_\ell}}$ of massless QCD$_{N_\ell}$, while the effect of the heavy quarks is represented by nonrenormalizable interactions Φ_i suppressed by higher powers of $1/M$. Massless QCD$_{N_\ell}$ has a single parameter, the gauge coupling $\bar{g}^{(N_\ell)}$. The EFT is hence predictive once its coupling is given as a proper function of the coupling of the fundamental theory, $\bar{g}^{(N_{\rm f})}$, and the quark masses M. In this situation, we

[56] We recall that the computational cost of lattice simulations grows roughly $\propto a^{-7}$ as $a \to 0$.

[57] The experimental numbers for the hadronic quantities of interest are usually 'corrected' for QED and strong isospin breaking effects, if these are not included in the lattice simulations (see [11]).

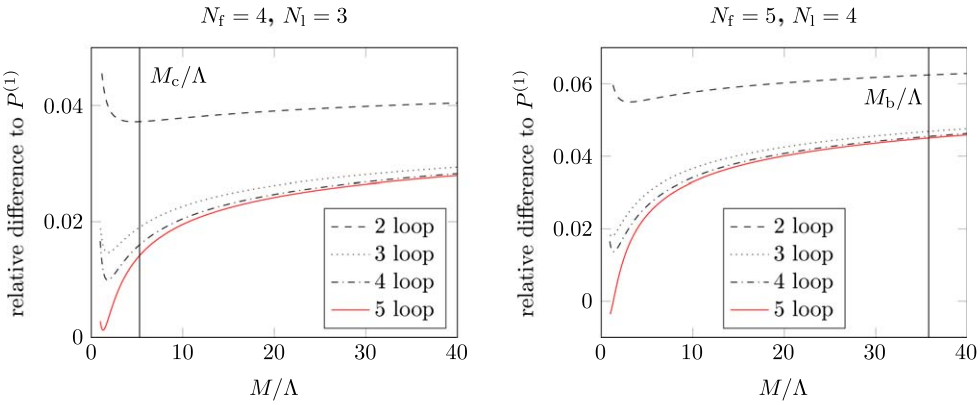

Figure 3. Relative differences from the (unsystematic) 1-loop approximation $P^1_{\ell,\mathrm{f}}(M/\Lambda) = M/\Lambda^{\eta_0}$, $\eta_0 = 2N_\mathrm{h}/(33 - 2N_\ell)$, for different orders of the perturbative expansion of $P_{\ell,\mathrm{f}}(M/\Lambda)$ as a function of M/Λ [22]. The results for $N_\ell = 3$, $N_\mathrm{f} = 4$ ($N_\ell = 4$, $N_\mathrm{f} = 5$) are given in the left (right) panel. The values for the RGI charm (M_c) and bottom (M_b) quark masses in units of the proper Λ-parameters are marked by vertical lines.

say that the couplings are matched,

$$\bar{g}^{(N_\ell)}(\mu) = F_O(\bar{g}^{(N_\mathrm{f})}(\mu), M/\mu). \tag{2.9}$$

The function F_O depends in principle on the observable O that is used to establish the matching. At leading order in the EFT, however, it is consistent to drop any correction of $\mathcal{O}(M^{-2})$ in the relation (2.9), which thus becomes universal, i.e. it only depends on the renormalization scheme chosen for the couplings. In the $\overline{\mathrm{MS}}$-scheme, the so-called decoupling relation (2.9) is known at 4-loop order [23–28], and it is usually evaluated at the scale $\mu = m_\star$, where $m_\star = \overline{m}_{\overline{\mathrm{MS}}}(m_\star)$ with $\overline{m}_{\overline{\mathrm{MS}}}(\mu)$ the mass of the heavy quarks in the $\overline{\mathrm{MS}}$-scheme. In formulas,

$$\bar{g}^{(N_\ell)}_{\overline{\mathrm{MS}}}(m_\star) = g_\star\, \xi(g_\star), \quad g_\star \equiv \bar{g}^{(N_\mathrm{f})}_{\overline{\mathrm{MS}}}(m_\star), \quad \xi(g) = 1 + c_2 g^4 + c_3 g^6 + c_4 g^8 + \mathcal{O}(g^{10}). \tag{2.10}$$

The relation between the couplings can be reexpressed in terms of the corresponding Λ-parameters of the two theories,

$$P_{\ell,\mathrm{f}}(M/\Lambda^{(N_\mathrm{f})}_{\overline{\mathrm{MS}}}) = \Lambda^{(N_\ell)}_{\overline{\mathrm{MS}}}/\Lambda^{(N_\mathrm{f})}_{\overline{\mathrm{MS}}} = \varphi^{(N_\ell)}_{\overline{\mathrm{MS}}}(g_\star\, \xi(g_\star))/\varphi^{(N_\mathrm{f})}_{\overline{\mathrm{MS}}}(g_\star), \tag{2.11}$$

where the RGI-parameters are given by $\Lambda^{(N_\mathrm{f})}_\mathrm{X} = \mu\, \varphi^{(N_\mathrm{f})}_\mathrm{X}(\bar{g}^{(N_\mathrm{f})}_\mathrm{X}(\mu))$ and $M = \overline{m}_\mathrm{X}(\mu)\varepsilon^{(N_\mathrm{f})}_\mathrm{X}(\bar{g}^{(N_\mathrm{f})}_\mathrm{X}(\mu))$. Explicit expressions for the functions $\varphi^{(N_\mathrm{f})}_\mathrm{X}$ and $\varepsilon^{(N_\mathrm{f})}_\mathrm{X}$ in terms of the β- and τ-functions in a generic scheme X can be found in e.g. [40].

In figure 3 we present the perturbative results from [22] for $P_{\ell,\mathrm{f}}\big(M/\Lambda^{(N_\mathrm{f})}_{\overline{\mathrm{MS}}}\big)$, for the phenomenological relevant cases of $N_\ell = 3$, $N_\mathrm{f} = 4$ and $N_\ell = 4$, $N_\mathrm{f} = 5$. More precisely, we show the relative deviation with respect to the 1-loop approximation, $P^{(1)}_{\ell,\mathrm{f}}$, for different orders of the perturbative expansion of $P_{\ell,\mathrm{f}}$. Focusing on the case of $P_{3,4}$, we see how the perturbative corrections at 4- and 5-loop order are very small already for values of M comparable to that of the charm. Judging from the perturbative behavior alone, the series thus appears to be well within its regime of applicability. As a result, any estimate for the perturbative truncation errors on $P_{\ell,\mathrm{f}}$ based on the last-known contributions to the series leads

to very small uncertainties. When translated to the coupling we find, for instance, $\alpha^{(5)}_{\overline{\rm MS}}(m_{\rm Z}) = 0.1185(8)(3)_{\rm PTdec}$, where the second error is estimated as the sum of the full 4- and 5-loop contributions due to the decoupling of both charm and bottom quarks [18]. As anticipated, the perturbative error estimate is well-below the uncertainties from other sources.

2.2.6. How perturbative are heavy quarks? Above we have shown how, within perturbation theory, the perturbative decoupling of the charm appears to be very accurate. A natural question to ask at this point is how reliable this picture is at the nonperturbative level. In other words, can we quantify the accuracy of perturbative decoupling for the charm by comparing it directly to nonperturbative results, thus getting an estimate for the size of nonperturbative corrections? In order to answer this question, we start by formulating the matching of Λ-parameters (2.11) in nonperturbative terms [22, 44],

$$\frac{\Lambda^{(N_\ell)}_{\overline{\rm MS}}}{m^{(N_\ell)}_{\rm had,1}} = P^{\rm had,1}_{\ell,\rm f}(M/\Lambda^{(N_{\rm f})}_{\overline{\rm MS}})\frac{\Lambda^{(N_{\rm f})}_{\overline{\rm MS}}}{m^{(N_{\rm f})}_{\rm had,1}(M)}. \tag{2.12}$$

We thus say that the EFT is matched to the fundamental theory if its Λ-parameter $\Lambda^{(N_\ell)}_{\overline{\rm MS}} \equiv \Lambda^{(N_\ell)}_{\overline{\rm MS}}\big(M,\, \Lambda^{(N_{\rm f})}_{\overline{\rm MS}}\big)$ in units of a hadronic quantity $m^{(N_\ell)}_{\rm had,1}$, is a proper function of the heavy quark masses M, and the Λ-parameter of the fundamental theory $\Lambda^{(N_{\rm f})}_{\overline{\rm MS}}$ in units of the same hadronic quantity $m^{(N_{\rm f})}_{\rm had,1}(M)$, computed in QCD$_{N_{\rm f}}$ where $N_{\rm h}$ quarks are heavy with mass $M \gg \Lambda_{\rm QCD}$.[58] Once the theories are matched, decoupling predicts that for any other hadronic quantity $m^{(N_\ell)}_{\rm had,2}$ computed in the EFT, we should expect: $m^{(N_\ell)}_{\rm had,2} = m^{(N_{\rm f})}_{\rm had,2}(M) + \mathcal{O}(M^{-2})$ (see section 2.2.5). As anticipated by our notation, the function $P^{\rm had}_{\ell,\rm f}$ depends on the hadronic quantity considered for the matching. If we were to choose a different quantity, we expect: $P^{\rm had,1}_{\ell,\rm f}\big(M/\Lambda^{(N_{\rm f})}_{\overline{\rm MS}}\big) \sim P^{\rm had,2}_{\ell,\rm f}\big(M/\Lambda^{(N_{\rm f})}_{\overline{\rm MS}}\big) + \mathcal{O}(M^{-2})$.

The relation (2.12) leads to the interesting *factorization formula* [22, 44],

$$\frac{m^{(N_{\rm f})}_{\rm had}(M)}{m^{(N_{\rm f})}_{\rm had}(0)} = Q^{\rm had}_{\ell,\rm f} \times P^{\rm had}_{\ell,\rm f}(M/\Lambda^{(N_{\rm f})}_{\overline{\rm MS}}), \qquad Q^{\rm had}_{\ell,\rm f} = \frac{m^{(N_\ell)}_{\rm had}/\Lambda^{(N_\ell)}_{\overline{\rm MS}}}{m^{(N_{\rm f})}_{\rm had}(0)/\Lambda^{(N_{\rm f})}_{\overline{\rm MS}}}. \tag{2.13}$$

On the l.h.s. of this equation we have the hadronic quantity $m^{(N_{\rm f})}_{\rm had}(M)$ computed in QCD$_{N_{\rm f}}$ where $N_{\rm h}$ quarks have mass M, over the same hadronic quantity $m^{(N_{\rm f})}_{\rm had}(0)$ computed in the chiral limit, i.e. where all $N_{\rm f}$ quarks are massless. This ratio can be expressed as the product of a nonperturbative, M-independent factor $Q^{\rm had}_{\ell,\rm f}$, and the function $P^{\rm had}_{\ell,\rm f}\big(M/\Lambda^{(N_{\rm f})}_{\overline{\rm MS}}\big)$, which encodes all the M-dependence. As we recalled in section 2.2.5, for $M \to \infty$ the function $P^{\rm had}_{\ell,\rm f}$ admits an asymptotic perturbative expansion. Hence, by measuring nonperturbatively on the lattice the l.h.s. of equation (2.13), we can compare the M-dependence of several such ratios with what is predicted by a perturbative approximation for $P^{\rm had}_{\ell,\rm f}$. In this way, we can assess the typical size of nonperturbative effects in $P^{\rm had}_{\ell,\rm f}$ as a function of M. In [22] a careful study was carried out considering the case of the decoupling of two heavy quarks with mass $M \sim M_c$, for the case of $N_\ell = 0$, $N_{\rm f} = 2$.[59] Under very reasonable assumptions, it is possible to extract from these results quantitative information on the nonperturbative corrections in the phenomenological interesting case of $P_{3,4}\big(M_c/\Lambda^{(4)}_{\overline{\rm MS}}\big)$. The conclusions of [22] are that these effects are

[58] Here we use the $\overline{\rm MS}$-scheme as reference scheme for the Λ-parameters. As we have seen in section 2.2.2, $\Lambda_{\overline{\rm MS}}$ can be indirectly expressed in terms of any nonperturbative scheme of choice.

[59] The reason why the authors of [22] considered $N_\ell = 0$, $N_{\rm f} = 2$ instead of $N_\ell = 3$, $N_{\rm f} = 4$, has to do with the technical difficulties of simultaneously simulating heavy and light quarks on the lattice (see section 2.2.4). The effect of decoupling two heavy quarks rather than just one is however expected to more than compensate the effects on decoupling induced by the presence of the light quarks (see [22] for a detailed discussion about this point).

very much likely below the per-cent level. This means that it is safe to use a perturbative estimate for $P_{3,4}\left(M_c/\Lambda^{(4)}_{\overline{\rm MS}}\right)$ in transitioning from $\Lambda^{(3)}_{\overline{\rm MS}} \to \Lambda^{(4)}_{\overline{\rm MS}}$, as long as, say, $\delta\Lambda^{(3)}_{\overline{\rm MS}} \gtrsim 1.5\%$ or so.

If we now consider ratios of hadronic quantities, where the dependence on the Λ-parameters drops out, we immediately conclude that

$$m^{(N_\ell)}_{\rm had,1}/m^{(N_\ell)}_{\rm had,2} = m^{(N_{\rm f})}_{\rm had,1}(M)/m^{(N_{\rm f})}_{\rm had,2}(M) + \mathcal{O}(M^{-2}). \tag{2.14}$$

In this case, one can obtain estimates for the typically size of $\mathcal{O}(M^{-2})$ effects in these ratios by comparing both sides of the above equation computed through lattice simulations. In [45, 46] careful studies have been conducted considering both the case of the decoupling of two heavy quarks of mass $M \sim M_c$ with $N_\ell = 0$, $N_{\rm f} = 2$, and more recently for the decoupling of a single charm quark with $N_\ell = 3$, $N_{\rm f} = 3 + 1$, i.e. in the presence of three mass-degenerate lighter quarks. From these calculations, the authors conclude that the typical effects due to the charm on dimensionless ratios of low-energy quantities are well-below the per-cent level. This means that these effects are not relevant for a per-cent precision determinations of $\Lambda^{(3)}_{\overline{\rm MS}}$.

In summary, thanks to recent dedicated studies, we are able to conclude that it is safe to rely on perturbative decoupling for the charm quark in connecting $\Lambda^{(3)}_{\overline{\rm MS}}$ and $\Lambda^{(4)}_{\overline{\rm MS}}$, as long as $\delta\Lambda^{(3)}_{\overline{\rm MS}} \gtrsim 1.5\%$. The 0.7% precision extraction of α_S from [18] is based on a determination of $\Lambda^{(3)}_{\overline{\rm MS}}$ with an uncertainty of $\delta\Lambda^{(3)}_{\overline{\rm MS}} \approx 3.5\%$ (see section 2.2.3). Hence, there is still about a factor of two of possible improvement within the $N_{\rm f} = 3$ flavour theory.

2.2.7. The strong coupling from the decoupling of heavy quarks. The previous section suggests a method to relate the Λ-parameters in theories with a different number of quark flavours (see equation (2.12)). Taking this relation to the extreme, one should be able to determine $\Lambda^{(N_{\rm f})}_{\overline{\rm MS}}$ from the pure-gauge one, $\Lambda^{(0)}_{\overline{\rm MS}}$. Of course this requires to decouple $N_{\rm f}$ heavy quarks with $M \gg \Lambda^{(N_{\rm f})}_{\overline{\rm MS}}$. The physical world is very different from this limit, but lattice QCD can simulate such *unphysical* situation.

A possible strategy for the determination of the strong coupling based on this idea is the following:

1. Starting from a scale $\mu_{\rm dec}$ in QCD$_{N_{\rm f}}$, one determines the value of a nonperturbatively defined coupling at such scale in a massless renormalization scheme, $\bar{g}^{(N_{\rm f})}_O(\mu_{\rm dec})$.
2. By performing lattice simulations at increasing values of the quark masses, one is able to determine the value of the coupling in a massive scheme, $\bar{g}^{(N_{\rm f})}_O(\mu_{\rm dec}, M)$.
3. For M larger than any other scale in the problem (i.e. $M \gg \Lambda_{\rm QCD}$, $\mu_{\rm dec}$), the massive coupling is, up to heavy-mass corrections, the same as the corresponding coupling in the pure-gauge theory, i.e.

$$\bar{g}^{(N_{\rm f})}_O(\mu_{\rm dec}, M) = \bar{g}^{(0)}_O(\mu_{\rm dec}), \tag{2.15}$$

   where corrections of $\mathcal{O}(1/M^2)$ have been dropped.
4. From the running of the coupling $\bar{g}^{(0)}_O(\mu_{\rm dec})$ in the pure-gauge theory we can determine the pure-gauge Λ-parameter in units of $\mu_{\rm dec}$,

$$\frac{\Lambda^{(0)}_{\overline{\rm MS}}}{\mu_{\rm dec}} = \frac{\Lambda^{(0)}_{\overline{\rm MS}}}{\Lambda^{(0)}_O} \times \varphi^{(0)}_O(\bar{g}^{(0)}_O(\mu_{\rm dec})). \tag{2.16}$$

   (Note that the ratio of Λ-parameters in different schemes can be exactly determined via a perturbative, 1-loop computation (see e.g. [40]).)

5. Since all $N_{\rm f}$ quarks are heavy, one can employ the decoupling relations to estimate the $N_{\rm f} \geqslant 3$ flavour Λ-parameter as (see equation (2.12)),

$$\Lambda_{\overline{\rm MS}}^{(N_{\rm f})} = \mu_{\rm dec} \times \frac{\Lambda_{\overline{\rm MS}}^{(0)}}{\Lambda_{O}^{(0)}} \times \varphi_{O}^{(0)}(\bar{g}_{O}^{(0)}(\mu_{\rm dec})) \times \frac{1}{P_{0,N_{\rm f}}^{(5-\text{loop})}(M/\Lambda_{\overline{\rm MS}}^{(N_{\rm f})})} + \mathcal{O}(\alpha_{S}^{4}(m_{\star})) + \mathcal{O}(M^{-2}). \tag{2.17}$$

Equation (2.17) is our master formula to determine $\Lambda_{\overline{\rm MS}}^{(N_{\rm f}=3)}$ from precise results for the nonperturbative running of the gauge coupling in the pure-gauge theory (i.e. for the function $\varphi_{O}^{(0)}$). Several comments are in order at this point:

- There are two types of corrections in equation (2.17). First, 'perturbative' ones of $\mathcal{O}(\alpha_{S}^{4}(m_{\star}))$. They come from using perturbation theory for the function $P_{0,N_{\rm f}}$. Second, we have nonperturbative 'power' corrections. Their origin is the decoupling condition, equation (2.15), as well as the use of a perturbative approximation for the function $P_{0,N_{\rm f}}$.
- Both perturbative and power corrections vanish for $M \to \infty$. In fact, the following relation is exact

$$\Lambda_{\overline{\rm MS}}^{(N_{\rm f})} = \lim_{M\to\infty} \mu_{\rm dec} \times \frac{\Lambda_{\overline{\rm MS}}^{(0)}}{\Lambda_{O}^{(0)}} \times \varphi_{O}^{(0)}(\bar{g}_{O}^{(0)}(\mu_{\rm dec})) \times \frac{1}{P_{0,N_{\rm f}}^{(n-\text{loop})}(M/\Lambda_{\overline{\rm MS}}^{(N_{\rm f})})}, \tag{2.18}$$

  with $\bar{g}_{O}^{(0)}(\mu_{\rm dec}) = \bar{g}_{O}^{(N_{\rm f})}(\mu_{\rm dec}, M)$.
- The situation and challenges in this approach might look similar to those present in more 'conventional' extractions of the strong coupling (see equation (2.5)). The subtle difference however is that, in the present case, perturbative corrections are very small even for scales $\sim M_{c}$ (see section 2.2.5). In particular, if one is considering quarks with masses of a few GeV, they are completely negligible in practice, and one has only to deal with the power corrections, which decrease much faster with the relevant energy scale.

This method to extract the strong coupling was proposed in [33] (for a recent review see [34]). Here we present first results using this strategy [37].[60] We follow closely the strategy described above, skipping the technical details. The reader interested in the details is encouraged to look at the original references [33, 34, 37].

1. A scale $\mu_{\rm dec} = 789(15)$ MeV is determined in a finite-volume renormalization scheme in three-flavour QCD using results from [42]. This corresponds to a value of the renormalized nonperturbative coupling $\bar{g}^{(3)}(\mu_{\rm dec}) \approx 1.9872$.
2. For technical reasons the massive coupling is determined in a slightly different renormalization scheme than the massless one. The value of the massive coupling is then determined by keeping the value of the bare coupling (and therefore the lattice spacing) fixed and increasing the value of the quark masses. This determination is performed for several values of the quark masses, $z = M/\mu_{\rm dec} = 1.972,\ 4,\ 6,\ 8,\ 10,\ 12$, and several values of the lattice spacing with $1/(a\mu_{\rm dec}) = 12, \ldots, 48$. The results are extrapolated to the continuum limit for each value of the quark masses labeled by z (see figure 4). We refer the reader to [37] for a detailed discussion.
3. The values of the massive coupling are used as matching condition between QCD$_{N_{\rm f}}$ and the pure-gauge theory (see equation (2.15)). The running in the pure-gauge theory is

[60] At the time of the workshop only a preliminary analysis of these results was available [47].

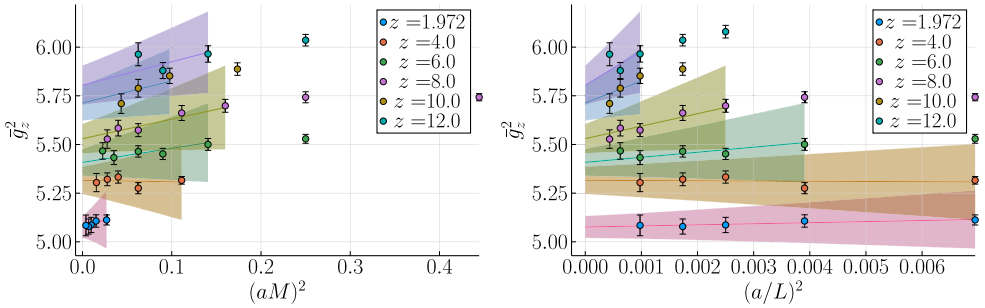

Figure 4. Continuum extrapolations of the massive coupling $\bar{g}_z^2 = [\bar{g}^{(3)}(\mu_{\rm dec}, M)]^2$ for different values of the quark masses labeled by $z = M/\mu_{\rm dec}$. Only data at fine enough lattice spacings (i.e. for which $(aM)^2 < 0.16$) are included in the fit. Note that the fit error bands include an estimate for the remaining $\mathcal{O}(a)$ effects (see [37] for a full discussion).

Table 1. Values of the massive three-flavour coupling $\bar{g}^{(3)}(\mu_{\rm dec}, M)$ and the corresponding values of $\Lambda^{(3)}_{\overline{\rm MS},\rm eff}$ obtained by applying our master formula equation (2.17) and ignoring perturbative and power corrections.

z	$[\bar{g}^{(3)}(\mu_{\rm dec}, M)]^2$	$\Lambda^{(3)}_{\overline{\rm MS},\rm eff}$ [MeV]
1.972	5.076(56)	426(14)
4	5.316(70)	388(13)
6	5.408(69)	363(12)
8	5.530(76)	351(12)
10	5.713(90)	349(12)
12	5.80(10)	343(12)

known very precisely from the literature [35]. The ratio $\Lambda^{(0)}_{\overline{\rm MS}}/\mu_{\rm dec}$ can thus be accurately determined.

4. Given this result, by applying the master formula equation (2.17), one obtains the estimates, $\Lambda^{(3)}_{\overline{\rm MS},\rm eff}$, for $\Lambda^{(3)}_{\overline{\rm MS}}$ given in table 1. These estimates should approach the correct three-flavour Λ-parameter in the limit $M \to \infty$. Figure 5 shows that this is indeed the case. Our data are consistent with a linear extrapolation in $\mu_{\rm dec}^2/M^2$, which results in

$$\Lambda^{(3)}_{\overline{\rm MS}} = 336(10)(6)(3)\text{MeV}, \tag{2.19}$$

where the first uncertainty is statistical, the second is due to an estimate of the $\mathcal{O}(a)$ effects present in our setup, and the last is due to different parameterizations of the $M \to \infty$ limit.

This result for the three-flavour Λ-parameter translates, after crossing the charm and bottom thresholds, into

$$\alpha_S(m_Z^2) = 0.11823(84). \tag{2.20}$$

The result has a 0.7% uncertainty, which is in fact dominated by the statistical uncertainties in the scale $\mu_{\rm dec} = 789(15)$ MeV and in the running of the pure-gauge theory. These statistical uncertainties can be reduced with a modest computational effort. The effects of the truncation of the perturbative series are subdominant in our approach. A nonperturbative determination

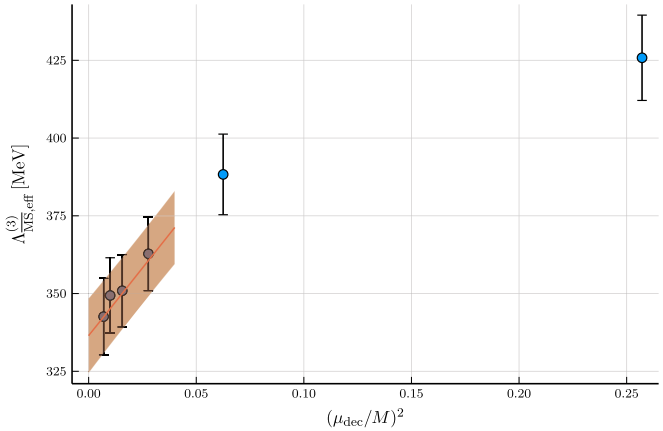

Figure 5. Estimates of the three-flavour Λ-parameter (table 1) and its $M \to \infty$ extrapolation yielding our final result for $\Lambda^{(3)}_{\overline{\rm MS}}$.

of the relevant improvement parameter would eliminate entirely the systematics related to $\mathcal{O}(a)$ effects, and make possible a further reduction of the uncertainty by a factor of two with this approach (see [37] for a full discussion). Going beyond this precision would require including charm effects nonperturbatively and also some serious thinking on how to include electromagnetic effects in the determination of both the scale and the running.

2.3. Strong coupling constant α_S from moments of quarkonium correlators[61]

A lattice method conceptually similar to the determination of $\alpha_S(m_Z^2)$ or heavy-quark masses from the R-ratio via quarkonium sum rules [48, 49] uses heavy-quark two-point correlators; for a recent review see [50]. Renormalization group invariant pseudoscalar correlators $G(t)$ and their nth time moments G_n are defined as

$$G_n = \sum_t t^n (G(t) + G(N_t - t)), \quad G(t) = a^6 \sum_{\boldsymbol{x}} am_{h0}{}^2 \langle j_5(\boldsymbol{x}, t) j_5(0, 0) \rangle,$$
$$j_5(\boldsymbol{x}, t) = \bar{\psi}(\boldsymbol{x}, t) \gamma_5 \psi(\boldsymbol{x}, t). \tag{2.21}$$

The symmetrization accounts for (anti)periodic boundary conditions in time. Here, am_{h0} is the corresponding bare heavy-quark mass in the lattice scheme; am_{h0}, resp. m_h, can be varied quite liberally for valence quarks in the charm- and bottom-quark regions and in between. Since sea quark mass variation is expensive, most results have partially quenched heavy quarks, i.e. heavy-quark masses in sea and valence sectors can be different in (2+1+1)-flavour QCD, or heavy quarks are left out from the sea in (2+1)-flavour QCD.

The weak-coupling series of G_n, which are finite for $n \geqslant 4$, is known up to N^{3}LO, resp. $\mathcal{O}(\alpha_S^3(\nu_h))$, for $N_{\rm f}$ massless and one massive quark flavour [51–53],

$$G_n = \frac{g_n(\alpha_S(\nu), \nu/m_h)}{am_h^{n-4}(\nu_m)}, \tag{2.22}$$

where $\nu = xm_h$, proportional to the heavy-quark mass m_h, is the $\overline{\rm MS}$ renormalization scale of the coupling; and $\nu_m = x_m m_h$, the scale at which the $\overline{\rm MS}$ heavy-quark mass $m_h(\nu_m)$ is defined, could be different from ν [48]. In published weak-coupling results, heavy-quark masses on

[61] Authors: P Petreczky (BNL), J H Weber (HU, Berlin).

internal (sea) and external (valence) quark lines must agree [51–53]. This restriction has profound implications for α_S extractions in (2+1+1)-flavour QCD.

As the bare heavy-quark mass in lattice units, am_{h0}, is a large parameter, improved quark actions are needed; so far most calculations have employed the highly improved staggered quarks (HISQ) [16, 17, 54–57], while domain-wall fermions have been used as well [58]. Some data sets involved values of am_{h0} corresponding to different heavy-quark masses m_h [16, 17, 56, 57]; for this reason even (2+1+1)-flavour QCD lattice results still involve partially quenched heavy quarks [17]. Enforcing an upper bound $am_{h0} \lesssim 1$ to limit the size of lattice artifacts implies that fewer independent ensembles can constrain the data at larger m_h and entail larger errors of the respective continuum limit.

The so-called (tree-level) reduced moments, known perturbatively at $\mathcal{O}(\alpha_S^3(\nu_h))$,

$$R_4 = \left(\frac{G_4^{\rm QCD}}{G_4^0}\right), \qquad R_4\left(\alpha_S(\nu), \frac{\nu}{m_h}\right) = 1 + \sum_{j=1}^{3} r_{nj}\left(\frac{\nu}{m_h}\right)\left(\frac{\alpha_S(\nu)}{\pi}\right)^j \tag{2.23}$$

$$R_n = \left(\frac{G_n^{\rm QCD}}{G_n^0}\right)^{\frac{1}{(n-4)}}, \qquad R_n\left(\alpha_S(\nu), \frac{\nu}{m_h}\right) = \left(\frac{m_{h0}}{m_h(\nu_m)}\right)\left(1 + \sum_{j=1}^{3} r_{nj}\left(\frac{\nu}{m_h}\right)\left(\frac{\alpha_S(\nu)}{\pi}\right)^j\right), \ n > 4, \tag{2.24}$$

eliminate the tree-level contribution, thus cancelling the leading lattice artifacts [54]. The coefficients r_{nj} are numbers of order 1 without any obvious pattern, see, e.g. table 1 of [50]. On the one hand, the lowest reduced moment R_4 and ratios of higher reduced moments, i.e. R_6/R_8 or R_8/R_{10}, are dimensionless; their respective continuum extrapolations turned out to be challenging, in particular due to $\log(a\Lambda_{\rm QCD})$ and $\log(am_{h0})$ dependence [57]. Such $\log(a)$ dependence is manifest in slopes that decrease for larger am_{h0}. On the other hand, higher moments R_n/m_{h0}, $n \geqslant 6$, are dimensionful and scale with $1/m_{h0} = a/(am_{h0})$; thus, because the scale uncertainty and the uncertainty of the tuned bare heavy-quark mass (am_{h0}) strongly impact the results, these are insensitive to any $\log(a)$ effects, and continuum extrapolations are straightforward. For the improved actions used in published results, lattice spacing dependence could be parameterized for functions of the reduced moments, i.e. $R(m_h) = \{R_4(m_h), R_n(m_h)/m_{h0}, R_n(m_h)/R_{n+2}(m_h), \}$, $n \geqslant 6$, as

$$R(m_h) = R^{\rm cont}(m_h) + \sum_{i=1}^{N}\sum_{j=1}^{M_i} b_{ij}^{(R)}(\alpha_S^b)^i\left[1 + \sum_{k=1}^{i} d_{ijk}^{(R)}\ln^k(am_{h0})\right](am_{h0})^{2j}, \tag{2.25}$$

where $\alpha_S^b = g_0^2/(4\pi u_0^4)$ is the boosted lattice coupling [59]; the tadpole factor u_0 is defined in terms of the plaquette, $u_0^4 = \langle \mathrm{Tr}\, U_{\mu\nu} N_c\rangle$, and partially accounts for the expected $\log(a\Lambda_{\rm QCD})$ dependence.

For R_4 and R_6/R_8, separate continuum extrapolations for each heavy-quark mass proved feasible only for $m_h \leqslant 1.5m_c$ [56]. Continuum extrapolation for $m_h \geqslant 2m_c$ required joint fits including $m_h < 2m_c$ [57]; similar joint fits with Bayesian priors were used in [16, 17]. The published continuum results for R_4 and R_6/R_8 at $m_h = m_c$ or $1.5m_c$ are consistent among each other [50, 57]; any significant deviations can be traced back to known deficiencies in the respective analyses [55, 58], see e.g. table 65 of [11]. For R_n/m_{h0}, $n \geqslant 6$ fits with $N = 1$, $M_1 = 2$ are sufficient for any m_h, and published results for $R_n(m_c)/m_{c0}$, $n \geqslant 6$ are consistent. Severe finite volume effects affect R_8/R_{10}; R_8/R_{10} at m_c is systematically low (and inconsistent with R_4), while continuum extrapolation with joint fits proved reliable for $m_h \geqslant 1.5m_c$ [57]. With the aforementioned exceptions the continuum results in (2+1)-flavour QCD span the region $m_h = m_c, \ldots, 4m_c$ for valence quarks, see tables 1 and 4 of [57]; with increasing

Table 2. $\Lambda_{\overline{\rm MS}}^{(N_{\rm f}=3)}$ obtained for different values of m_h and different choices of the renormalization scale ν (using $\nu = \nu_m$). The first error comes from the lattice calculations, the second error is the perturbative error, and the last error is due to the gluon condensate. From [57].

m_h/m_c	$\nu/m_h = 2/3$	$\nu/m_h = 1$	$\nu/m_h = 3/2$	$\nu/m_h = 2$	$\nu/m_h = 3$
1.0	—	323(4)(6)(3)	323(4)(7)(3)	327(4)(13)(3)	340(4)(21)(3)
1.5	314(8)(23)(1)	326(9)(4)(1)	326(8)(5)(1)	329(8)(10)(1)	341(9)(18)(1)
2.0	—	327(13)(3)(0)	327(13)(4)(0)	330(13)(9)(0)	341(14)(16)(0)
3.0	325(20)(20)(0)	332(21)(2)(0)	332(21)(4)(0)	335(22)(22)(0)	344(22)(14)(0)
4.0	—	336(26)(2)(0)	336(26)(3)(0)	339(27)(7)(0)	347(28)(17)(0)

heavy-quark mass m_h, R_4 and the ratios decrease towards 1, while the errors of the lattice calculations increase. Continuum results in (2+1+1)-flavour QCD have not been published.

Comparing $R_4(m_h)$ to $R_4(\alpha_S(\nu), \nu/m_h)$ permits extraction of $\alpha_S(\nu)$; truncation errors, estimated via inclusion of terms $\pm 5 r_{n3}\, \alpha_S^4(\nu)$, turn out to be too large for the ratios to provide more than a cross-check [57]. Once $\alpha_S(\nu)$ is given, R_n/m_{h0} permits obtaining the $\overline{\rm MS}$ heavy-quark mass $m_h(\nu_m)$; combining both yields $\Lambda_{\overline{\rm MS}}^{(N_{\rm f})}$. Whether or not the two scales $\nu_h = x m_h$ and $\nu_m = x_m m_h$, should be varied jointly ($x = x_m$) or independently ($x \neq x_m$) is under investigation; the latter has yielded in a reanalysis of published lattice results at $m_h = m_c$ about 50% larger estimates of truncation errors [49]. $\alpha_S(\nu)$ or $m_h(\nu_m)$ for different $a m_{h0} = x_{\rm lat} a m_{c0}$ are consistent with perturbative running [57]. Nonperturbative contributions—parametrized in terms of QCD condensates—are negligible for $m_h \geqslant 1.5 m_c$ due to suppression by powers of at least $1/m_h^4$; similarly, truncation errors diminish dramatically for $m_h \geqslant 1.5 m_c$ [57].

A recent analysis has exposed that the choice of the lattice scale ratio, i.e. $x_{\rm lat} = m_h/m_c = (a m_{h0})/(a m_{c0})$, and the perturbative scale ratio, $x_{\rm pert} = \nu/m_h$, both have a significant and systematic impact on the extracted $\Lambda_{\overline{\rm MS}}^{(N_{\rm f})}$, and consequently on $\alpha_S(m_{\rm Z}^2)$ [57], while the composition of the error budget is very different (table 2). Neglecting the spread due to varying either of these two scale ratios led in most past determinations to significantly underestimated errors [16, 17, 54–56]. Nonetheless, the central value of [16] is in good agreement with the corresponding entry of table 2.

The current FLAG sub-average—taking the latest results [57] partially into account, and using error estimates from independent scale variation [49]—reports

$$\alpha_S(m_{\rm Z}^2) = 0.11826(200) \quad (\text{FLAG sub}-\text{average for heavy}-\text{quark two}-\text{point correlators}) \text{ [11]}. \tag{2.26}$$

Table 2 suggests that a viable approach on the lattice side to reducing the errors in the next decade may be by performing more accurate lattice calculations using masses $m_h \geqslant 2 m_c$, where the truncation errors are subleading in current results. The corresponding continuum extrapolations could be made more robust in two ways. First, by including more intermediate heavy-quark mass values (e.g. $m_h/m_c = 1.75,\ 2.25,\ 2.5,\ 2.75,\ 3.25$, etc) in the joint fits, equation (2.25), one may hope to significantly reduce the lattice errors of the continuum results for $m_h \geqslant 2 m_c$. Second, by relying on one-loop instead of tree-level reduced moments at finite lattice spacing as suggested in [60], one may simplify the approach to the continuum limit; while cumbersome, these calculations in lattice perturbation theory are in principle straightforward and are expected to eliminate all $i = 1$ terms from the series corresponding to equation (2.25). The availability of lattice results in (2+1+1)-flavour QCD with partially quenched heavy quarks suggests that a viable approach on the perturbative side to reducing the errors may be to permit partially quenched heavy quarks, i.e. different heavy-quark

masses on internal (sea) and external (valence) lines. In particular, application of this method in (2+1+1)-flavour QCD permits no α_S extraction for valence quarks at $m_h > m_c$, the only readily available strategy to alleviate the truncation error, on the basis of the currently available weak-coupling calculations that require $m_{\mathrm{h,sea}} = m_{\mathrm{h,val}}$. If this deficiency were remedied, the constraining power could be improved in a joint analysis of partially quenched lattice calculations with different m_h in (2+1+1)-flavour QCD similar to the recent analysis in (2+1)-flavour QCD [57], or by even combining (2+1)- and (2+1+1)-flavour QCD continuum results in a joint analysis that assumes perturbative decoupling of the heavy quark. Last but not least, the expected accuracy would obviously benefit from N^{4}LO, resp. $\mathcal{O}(\alpha_S^4(\nu_h))$, calculations.

Acknowledgments—PP was supported by US Department of Energy under Contract No. DE-SC0012704. JHW's research was funded by the Deutsche Forschungsgemeinschaft (DFG, German Research Foundation)–Projektnummer 417 533 893/GRK2575 'Rethinking Quantum Field Theory'.

2.4. Strong coupling constant α_S from the static energy, the free energy and the force[62]

QCD observables that have been computed with high precision in perturbative- and lattice-QCD with $2+1$ or $2+1+1$ flavours are well suited to provide determinations of α_S in the kinematic regions where pQCD applies. The advantage of looking at observables is that continuum analytical and lattice results may be compared without having to deal with renormalization issues and change of scheme. Moreover, if in the kinematic regions where pQCD is used the perturbative series converges well, and nonperturbative corrections turn out to be small, and if lattice data can be extrapolated to continuum, then a very precise extraction of α_S is possible even by comparing few lattice data with the perturbative expression. The comparison provides $\Lambda_{\overline{\mathrm{MS}}}$ times the lattice scale. By supplying a precise determination of the lattice scale, one obtains $\Lambda_{\overline{\mathrm{MS}}}$. Finally, $\Lambda_{\overline{\mathrm{MS}}}$ may be traded with α_S conventionally expressed at the mass of the Z, $\alpha_S(m_Z^2)$.

2.4.1. The QCD static energy. The QCD static energy $E_0(r)$, i.e. the energy between a static quark and a static antiquark separated by a distance r, is one of these golden observables for the extraction of α_S and it is also a basic object to study the strong interactions [61]. The QCD static energy, $E_0(r)$, is defined (in Minkowski spacetime) as

$$E_0(r) = \lim_{T\to\infty} \frac{i}{T} \ln \left\langle \mathrm{Tr\,P} \exp\left\{ ig \oint_{r\times T} dz^\mu A_\mu \right\} \right\rangle \equiv \lim_{T\to\infty} \frac{i}{T} \ln \langle W_{r\times T} \rangle, \tag{2.27}$$

where the integral is over a rectangle of spatial length r, the distance between the static quark and the static antiquark, and time length T; $\langle ... \rangle$ stands for the path integral over the gauge fields A_μ and the light quark fields, P is the path-ordering operator of the colour matrices and g is the SU(3) gauge coupling ($\alpha_S = g^2/(4\pi)$); $W_{r\times T}$ is the static Wilson loop. The above definition of $E_0(r)$ is valid at any distance r.

On the lattice side, the Wilson loop is one of the most accurately known quantities that has been computed since the establishment of lattice QCD. In the short distance range, $r\Lambda_{\mathrm{QCD}} \ll 1$ for which $\alpha_S(1/r) \ll 1$, $E_0(r)$ may be computed in pQCD and expressed as a series in α_S (computed at a typical scale of order $1/r$):

[62] Authors: N Brambilla (TUM), V Leino (TUM), P Petreczky (BNL), A Vairo (TUM) J H Weber (HU, Berlin).

$$E_0(r) = \Lambda_s - \frac{4\alpha_S}{3r}(1 + ...), \tag{2.28}$$

where Λ_s is a constant that accounts for the normalization of the static energy and the dots stand for higher-order terms. The expansion of $E_0(r)$ in powers of α_S has been computed, in the continuum in the $\overline{\text{MS}}$ scheme, using perturbative and effective field theory techniques, in particular potential Nonrelativistic QCD [62]. It is currently known at next-to-next-to-next-to-leading-logarithmic (N^3LL) accuracy, i.e. including terms up to order $\alpha_S^{4+n}\ln^n\alpha_S$ with $n \geqslant 0$. At three loops, a contribution proportional to $\ln\alpha_S$ appears for the first time. This three-loop logarithm has been computed in [63]. The complete three-loop contribution has been computed in [64, 65]. The leading logarithms have been resummed to all orders in [66], providing, among others, also the four-loop contribution proportional to $\alpha_S^5\ln^2\alpha_S$. The four-loop contribution proportional to $\alpha_S^5\ln\alpha_S$ has been computed in [67]. Next-to-leading logarithms have been resummed to all orders in [68]. However the constant coefficient of the α_S^5 term is not yet known. $E_0(r)$ is, therefore, one of the best known quantities in pQCD lending to a perfect playground for the extraction of α_S.

The $\ln\alpha_S$ terms in $E_0(r)$ signal the cancellation of contributions coming from the soft energy scale $1/r$ and the ultrasoft (US) energy scale α_S/r. The ultrasoft scale is generated in loop diagrams by the emission of virtual ultrasoft gluons changing the colour state of the quark-antiquark pair [63, 69]. The resummation of these logarithms accounts for the running from the soft to the ultrasoft scale.

The soft and ultrasoft energy scales may be effectively factorized in potential Nonrelativistic QCD [62, 70]. The factorization of scales leads to the formula [62, 63]:

$$E_0(r) = \Lambda_s + V_s(r,\mu) - i\frac{V_A^2}{3}\int_0^\infty dt\, e^{-it(V_o-V_s)}\langle \text{Tr}\,\{\mathbf{r}\cdot g\mathbf{E}(t,0)\,\mathbf{r}\cdot g\mathbf{E}(0,0)\}\rangle(\mu) + ..., \tag{2.29}$$

where μ is the US renormalization scale, $V_s(r,\mu) = -4\alpha_S/(3r) + ...$ is the colour-singlet static potential, $V_o(r,\mu) = \alpha_S/(6r) + ...$ is the colour-octet static potential, $V_A = 1 + \mathcal{O}(\alpha_S^2)$ is a Wilson coefficient giving the chromoelectric dipole coupling, and $\mathbf{E}$ is the chromoelectric field. The colour-singlet and colour-octet static potentials encode the contributions from the soft scale $1/r$, whereas the low-energy contributions are in the term proportional to the two chromoelectric dipoles. While at short distances, $r\Lambda_{\text{QCD}} \ll 1$, the potentials V_s and V_o may be computed in perturbation theory, low-energy contributions include nonperturbative contributions.

The perturbative expansion of V_s is affected by a renormalon ambiguity of order Λ_{QCD}. The ambiguity reflects in the poor convergence of the perturbative series. A first method to cure the poor convergence of the perturbative series of V_s consists in subtracting a (constant) series in α_S from V_s and reabsorb it into a redefinition of the normalization constant Λ_s. This is the strategy we followed, for instance, in [71]. A second possibility consists in considering the force

$$F(r,\nu) = \frac{d}{dr}E_0(r). \tag{2.30}$$

It does not depend on Λ_s and is free from the renormalon of order Λ_{QCD} [72, 73]. Once integrated upon the distance, the force gives back the static energy

$$E_0(r) = \int_{r_*}^{r} dr'\, F(r', 1/r'), \tag{2.31}$$

up to an irrelevant constant determined by the arbitrary distance r^*, which can be reabsorbed in the overall normalization when comparing with lattice data. This is the strategy followed,

for instance, in [19]. We note that equation (2.29) provides also the explicit form of the nonperturbative contributions encoded in the chromoelectric correlator. They are proportional to r^3 at very short distances and to r^2 at somewhat larger distances.

In summary, $E_0(r)$ is one of the best known quantities in pQCD lending an ideal observable for the extraction of α_S by comparing lattice data and perturbative calculation in the appropriate short distance window. This way of extracting of α_S has been developed in a series of papers [71, 74, 75]. Here we report about our best determination from [19]. The method provides one of the most precise low energy determinations of α_S. The strong coupling constant extracted in this way relies typically on low energy data because the lattice cannot explore too small distances. It therefore provides a precise check of the running of the coupling constant and a determination of it that is complementary to high-energy determinations.

Concerning the power counting of the perturbative series a remark is in order. Upon inspection of the numerical size of the contributions coming from the soft and the US scale at each order, in the analysis of [19] it was decided to count the leading US resummed terms along with the three loop terms, since the $\alpha_S^4 \log \alpha_S$ terms appear to be of the same size as the α_S^4 terms, and, moreover, to partially cancel each other. It was also decided not to include subleading US logarithms in the analysis, as the finite four loop contribution is unknown and a cancellation similar to the one happening at three loops may also happen at four loops. Nevertheless, it may be also legitimate to count leading US resummed terms as if they were parametrically of order α_S^3 and count subleading US logarithms of order $\alpha_S^5 \log \alpha_S$ as if they were parametrically of order α_S^4, including them in the analysis. This is the procedure adopted in [20]. Most of the difference between the central value of α_S obtained in the analysis of [19] and in the one of [20] is due to this different counting of the perturbative series. The two analyses are consistent once errors, in particular those due to the truncation of the perturbative series, are accounted for.

The static energy can be computed on the lattice as the ground state of Wilson loops or temporal Wilson line correlators in a suitable gauge, typically in Coulomb gauge. Polyakov loops at sufficiently low temperatures could be employed as well. All energy levels from any of these correlators are affected by a constant, lattice spacing dependent self-energy contribution that diverges in the continuum limit. It can be removed by matching the static energy at each finite lattice spacing to a finite value at some distance. In calculations with an improved action, all these correlators, which are obtained from spatially extended operators, are affected by nonpositive contributions at very small distance and time, which cannot be resolved on coarse lattices or with insufficient suppression of the lowest excited states. Although Wilson line correlators retain an advantage in terms of the excited state suppression, the relative disadvantage of Wilson loops could be alleviated to some extent with smeared spatial links.

The ground state energy $E_0(\boldsymbol{r}, a)$ can be extracted from such correlators, e.g. via multi-exponential fits, in the large Euclidean time region for each lattice three-vector $\boldsymbol{r}/a = (n_1, n_2, n_3)$, where $0 \leqslant n_i \leqslant L_i/2a$. Obviously, small lattice spacing a is indispensable in order to access small distances $|\boldsymbol{r}| \lesssim 0.15$ fm [75]. Yet simulations with periodic boundary conditions fail to sample the different topological sectors of the QCD vacuum properly at small a. This topological freezing, which is known to be a quantitatively small but significant problem in low-energy hadron physics, does not lead in high-energy quantities (such as $E_0(\boldsymbol{r}, a)$ at small distances) to statistically significant effects due to small changes of the topological charge [76]. Although significant effects in $E_0(\boldsymbol{r}, a)$ due to large changes of the topological charge cannot be completely ruled out, they seem very unlikely, given that the topology does not

contribute at all in the weak-coupling calculations used in the comparison. Furthermore, sea quark mass effects due to light or strange quarks do not play a role in this range [76, 77], while dynamical charm effects are significant [78, 79]. At distance larger than $|\boldsymbol{r}| \gtrsim 0.15$ fm light sea quark mass effects become nonnegligible [76, 77].

Continuum extrapolation is only possible for somewhat larger distances probed by multiple lattice spacings, or if the functional form of $E_0(\boldsymbol{r}, a)$ were known to sufficient accuracy to predict the shape at small $\boldsymbol{r}/a$ on the fine lattices. Due to the breaking of the continuous $O(3)$-symmetry group to the discrete W_3-symmetry group the lattice gluon propagator, and hence $E_0(\boldsymbol{r}, a)$, is a non-smooth function of $|\boldsymbol{r}|/a$; geometrically inequivalent combinations of the n_i, i.e. belonging to different representations of W_3 but corresponding to the same geometric distance $|\boldsymbol{r}|/a = \sqrt{n_1^2 + n_2^2 + n_3^2}$, e.g. (3, 0, 0) or (2, 2, 1), yield inconsistent $E_0(|\boldsymbol{r}|, a)$ due to lattice artifacts. Moreover, the same $|\boldsymbol{r}|$ accessed through different lattice spacings a is generally affected by different types of non-smooth lattice artifacts corresponding to the different underlying $\boldsymbol{r}/a$. For this reason, a continuum extrapolation of $E_0(|\boldsymbol{r}|, a)$ at fixed $|\boldsymbol{r}|$ utilizing a parametrization of lattice artifacts in terms of a smooth function in $|\boldsymbol{r}|$ is incapable of describing the small $|\boldsymbol{r}|/a$ region, see e.g. [50]. These inconsistencies are much larger than the statistical errors at small $|\boldsymbol{r}|/a$, but covered by the statistical errors at large $|\boldsymbol{r}|/a$. A tree-level correction (TLC) procedure defines the (tree-level) improved distance $r_I/a = f(n_1, n_2, n_3)$ and alleviates these inconsistencies somewhat: at $|\boldsymbol{r}|/a \gtrsim 3$ this is sufficient, while further effort is needed at smaller $|\boldsymbol{r}|/a$. A nonperturbative correction (NPC) procedure heuristically estimates the lattice artifacts remaining in $E_0(r_I, a)$ by comparing to a suitable smooth function, either obtained at a finer lattice spacing, or in a continuum calculation, which, however, potentially introduces systematic errors. Both approaches have been used yielding consistent results; for details see [19].

For Wilson line correlators, all combinations of $0 \leqslant n_1, n_2, n_3 \leqslant L/2a$ are accessible, thus permitting access to noninteger distances in units of the lattice spacing; this entails all of the aforementioned complications. After the nonperturbative correction, $E_0^{\mathrm{NPC}}(r_I, a)$ from Wilson line correlators computed in (2+1)-flavour QCD on lattices with highly improved staggered quarks (HISQ) was shown to exhibit no statistically significant lattice artifacts anymore [19] (figure 6). With this data set the range of interest can be probed using a rather large number of r_I/a values and many lattice spacings (up to six spacings in the range $a \in (0.024, \ldots, 0.06)$ fm), where the underlying high statistics ensembles had been generated for studies of the QCD equation of state [77, 82]. The uncertainty due to the lattice scale, lattice spacing dependence, estimates of the uncertainty due to treating residual lattice artifacts with the nonperturbative correction, or due to changes of the fit range are within the the statistical error and subleading in the error budget. Instead it was found that estimates of the continuum perturbative truncation error dominate the error budget. In [19] these have been estimated by a scale variation between $2/r$ and $1/2r$, inclusion of a parametric estimate of a higher order term $\pm 4/3\alpha_S^5/r$, and variation between resummation or no resummation of the leading ultrasoft logarithms $\alpha_S^{3+n} \ln^n \alpha_S/r$. The scale dependence becomes nonmonotonic below $1/\sqrt{2}\,r$ at large r, which makes robust error estimates challenging unless the range is restricted to $\max(|\boldsymbol{r}|) \leqslant 0.1$ fm. As lattice data at larger $|\boldsymbol{r}|$ are discarded, the statistical error increases while the truncation error decreases. Eventually, for $\max(|\boldsymbol{r}|) \ll 0.1$ fm, the nonperturbative correction to the lattice data becomes essential to having enough data, while the central value hardly changes. For our joint fit using nonperturbatively corrected HISQ data at five lattice spacings we report the best compromise between the different contributions to the error budget as

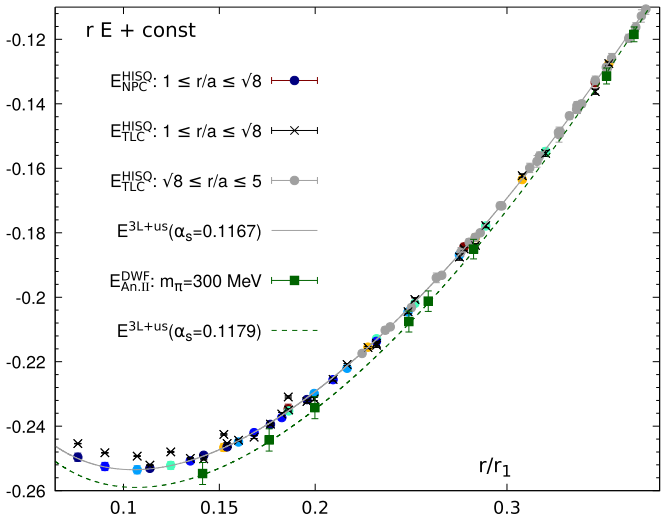

Figure 6. The nonperturbative lattice and the perturbative continuum results for the static energy multiplied by the distance, $rE(r)$ ($E \equiv E_0$). The HISQ data [19] are nonperturbatively corrected (NPC, coloured bullets) or tree-level corrected (TLC, black crosses and gray bullets). The colour indicates the lattice spacing in units of the scale r_1, a/r_1. The DWF data [80, 81] are from a one-step analysis II that mixes the continuum extrapolation with the fit to the OPE result at N^{3}LO, using a parametrization of discretization artifacts (green squares). The lines represent the three-loop result with resummed leading ultrasoft logarithms, corresponding to $\alpha_S(m_Z^2) = 0.1167$ (gray, solid) or $\alpha_S(m_Z^2) = 0.1179$ (green, dashed). The former uses the central value $\alpha_S(m_Z^2) = 0.1167$ of the analysis of the (TLC or NPC) HISQ data with $|\boldsymbol{r}|/a \geqslant \sqrt{8}$ (gray bullets), the latter uses the central value $\alpha_S(m_Z^2) = 0.1179$ of the OPE-based one-step analysis II of the DWF data [80, 81]. The NPC HISQ data with $|\boldsymbol{r}|/a < \sqrt{8}$ are well-aligned with the fit excluding these data, while the TLC HISQ data with $|\boldsymbol{r}|/a < \sqrt{8}$ cannot be consistently described by a continuum result for any value of $\alpha_S(m_Z^2)$. The figure is taken from [50].

$$\alpha_S(m_Z^2) = 0.11660^{+0.00110}_{-0.00056}, \tag{2.32}$$

where the total, symmetric lattice error amounts to 0.00047 for $|\boldsymbol{r}| \leqslant 0.073$ fm.

In [20], a reanalysis of a subset of these data ($a = 0.024$ fm, $\sqrt{8} \leqslant |\boldsymbol{r}|/a \leqslant 4$) was carried out that included resummation of next-to-leading ultrasoft logarithms $\alpha_S^{4+n} \ln^n \alpha_S/r$, i.e. the full N^{3}LL accuracy, and hyperasymptotic expansion, resulting in $\alpha_S(m_Z^2) = 0.1181(9)$. Concerning the central value, we have already commented that it differs from (2.32) mostly because of the inclusion of the subleading ultrasoft logarithms. Concerning the error budget, it may possibly increase by including an estimate of the lattice spacing dependence and a variation of $\min(|\boldsymbol{r}|)$ or $\max(|\boldsymbol{r}|)$ to smaller values. Nevertheless, even inside the quoted errors the result is consistent with (2.32).

For Wilson loops, spatial Wilson lines connecting the temporal ones entail additional, $\boldsymbol{r}/a$-dependent self-energy divergences. The static energy from Wilson loops is usually computed only for few specific geometries, and spatial link smearing is applied to suppress these divergences. The static energy has been obtained from Wilson loops for two different geometries $\boldsymbol{r}/a \propto (1, 0, 0)$ or $(1, 1, 0)$ [80, 81] in (2+1)-flavour QCD on lattices with Möbius domain-wall fermions with a pion mass of $m_\pi \approx 300$ MeV and three lattice spacings

$a \in (0.04, \ldots, 0.08)$fm that had been generated by the JLQCD collaboration [83]. Two separate analyses were performed: a two-step analysis (I) with a continuum extrapolation at large distances sequentially followed by the α_S extraction, and another one-step analysis (II) using a single joint fit to achieve both at once. Both analyses relied on a particular form of operator product expansion, and used data in the range $0.24\,\text{fm} \leqslant |\boldsymbol{r}| \leqslant 0.6\,\text{fm}$ or $0.044\,\text{fm} \leqslant |\boldsymbol{r}| \leqslant 0.36\,\text{fm}$, respectively. The reported values from the two analyses are $\alpha_S(m_Z^2) = 0.1166^{+0.0021}_{-0.0020}$ and $\alpha_S(m_Z^2) = 0.1179^{+0.0015}_{-0.0014}$. They are both dominated by the estimate of the truncation errors. As both analyses extend far into ranges where $E_0(|\boldsymbol{r}|, a)$ is known to be sensitive to the pion mass [76], the authors had to include condensate terms, while reporting no significant mass dependence when assuming only a perturbative contribution from massive light quarks. The first analysis has no data for $|\boldsymbol{r}| \lesssim 0.10\,\text{fm}$. The second analysis does have data in that region, but has to fit $\Lambda_{\overline{\text{MS}}}$ simultaneously with the lattice artifacts at small $\boldsymbol{r}/a$. As a result the continuum extrapolated static energy from this analysis has large errors for $|\boldsymbol{r}| \lesssim 0.10\,\text{fm}$ and lies systematically below the HISQ result from [19] (figure 6).

2.4.2. Static force. Another possibility consists of computing the force directly from the lattice, i.e. not as the slope of the static energy. The force, F, between a static quark located in $\mathbf{r}$ and a static antiquark located in 0 can be defined as [84]

$$F(r) = \partial_r E_0(r) = \lim_{T\to\infty} -i\frac{\left\langle \text{Tr}\left\{W_{r\times T}\ \hat{\mathbf{r}}\cdot g\mathbf{E}(\mathbf{r}, t^*)\right\}\right\rangle}{\langle \text{Tr}\{W_{r\times T}\}\rangle}. \tag{2.33}$$

The chromoelectric field $\mathbf{E}(\mathbf{r}, t^*)$ is located at the quark line of the Wilson loop.

This definition permits to obtain the force directly from the lattice instead of reconstructing it, after interpolation, from the lattice data of the static energy. The perturbative calculation of the force in continuum QCD is free of the leading renormalon and it is known at N^3LL. Therefore the force provides a clean way to extract α_S. In [85], we have used the multilevel algorithm to perform a preliminary quenched lattice study of the chromoelectric insertion in a static Wilson loop given by equation (2.33) both with smeared Wilson loops and with Polyakov loops. The result is consistent with the force obtained via derivative of the static energy upon multiplication with a constant renormalization factor Z_E that encodes the very slow convergence of lattice operators containing gluonic operators. Recently in [86] we have performed the same calculation with gradient flow, which eliminates the necessity of Z_E and makes the lattice calculation more efficient. We plan to go to very fine lattice spacings and perform an extraction of $\Lambda_{\overline{\text{MS}}} r_0$.

2.4.3. Static singlet free energy. One reason for which it is challenging to reach the fine lattice spacings needed for the best extraction of α_S is that one has to simultaneously maintain the control over finite volume effects from the propagation of the lightest hadronic modes, namely, the pions. A lattice simulation at high enough temperature avoids this infrared problem, and thus enables reaching much finer lattice spacings using smaller volumes. In [19], we considered the extraction of the strong coupling from the singlet free energy at nonzero temperature, as it is expected that at small distances medium effects are small. The singlet free energy in terms of the correlation function of two thermal Wilson lines in Coulomb gauge is given by (T is now the temperature)

$$F_S(r,\,T) = -T\ln\left(\frac{1}{N_c}\langle \mathrm{Tr}\,[W(r)W^\dagger(0)]\rangle\right). \tag{2.34}$$

At distances much smaller than the inverse temperature, $rT \ll 1$, we can write using potential nonrelativistic QCD [87]

$$F_S(r,\,T) = V_s(r,\,\mu) + \delta F_S(r,\,T,\,\mu). \tag{2.35}$$

The form of the US correction depends on the scale hierarchy that is now featuring also the temperature and the Debye mass $m_D \sim gT$: if $1/r \gg \alpha_S/r \gg T \gg m_D$ then $\mu \sim \alpha_S/r$ and $\delta F_S(r,\,T,\,\mu) = \delta E_{US}(\mu) + \Delta F_S(r,\,T)$, with $\delta E_{US}(\mu)$ being the US contribution to E_0 in vacuum that we already discussed. The singlet free energy has been studied on the lattice in [88] using a wide temperature range and several lattice spacings, i.e. several temporal extents N_τ. The shortest distance that we can access, due to a single lattice spacing on our finest lattice at $T > 0$, is 0.00814 fm. For our analysis the relevant data correspond to $N_\tau = 10,\ 12$ and 16, since rT has to be small. From the analysis of Ref. [88], we see that thermal effects are small for $rT \lesssim 0.3$. In particular we see that for $|\boldsymbol{r}|/a \leqslant \sqrt{6}$ the difference between the singlet free energy at $(T > 0)$ and the static energy at $(T = 0)$ approaches a constant proportional to the temperature. No temperature effects beyond a constant can be seen in this range within the errors of the lattice results. Therefore we treat the finite temperature data in this range as if they were at zero temperature and fit them with the three-loop plus leading ultrasoft resummed result of the static energy at $T = 0$.

A drawback of this analysis is the restriction to very small $|\boldsymbol{r}|/a$, which implies that the nonperturbative correction (NPC) is indispensable. Yet the main advantage of the analysis is that at very small distances, $\max(|\boldsymbol{r}|) \leqslant 0.03$ fm, the truncation error becomes very small. Beyond what has been necessary at zero temperature, one must verify that $T > 0$ effects do not become significant when including larger $|\boldsymbol{r}|/a$ or when varying the temperature $T = 1/aN_\tau$ at fixed lattice spacing. We confirmed the statistical irrelevance in these two measures of $T > 0$ effects by comparing $|\boldsymbol{r}|/a \leqslant 2$ with $|\boldsymbol{r}|/a \leqslant 3$ and $N_\tau = 12,\ 16$, and, where possible, 64, and included these error estimates with the other lattice errors in the error budget. The key ingredient to making this extraction work with substantial constraining power is that a wide range in $|\boldsymbol{r}|$ can be covered using only narrow windows in $|\boldsymbol{r}|/a$ by performing a joint analysis using multiple lattice spacings a that cover $|\boldsymbol{r}|$ in multiple, overlapping segments. For our joint fit using nonperturbatively corrected $T > 0$ HISQ data at eight lattice spacings and an $|\boldsymbol{r}|$ region and set of lattice spacings nonoverlapping with the zero temperature analysis we report

$$\alpha_S(m_Z^2) = 0.11638^{+0.00095}_{-0.00087} \tag{2.36}$$

(the total, symmetric lattice error amounts to 0.000 85) for $|\boldsymbol{r}| \leqslant 0.03$ fm [19]. This result is marginally lower than the result from our zero temperature analysis. Remarkably, however, the zero temperature result is still compatible with the $T > 0$ data over a much wider range in $|\boldsymbol{r}|/a$, a factor of sixteen in $|\boldsymbol{r}|$, and over almost a factor of ten in lattice spacings (figure 7).

2.4.4. Outlook. In summary, in order to reach a few permil accuracy in the extraction of α_S with the outlined methods we need:

- Lattice calculations of the static energy at smaller distances, ideally extrapolated to the continuum. The one-loop correction should be computed in lattice perturbation theory. Based on the experience with the nonperturbative correction, the one-loop correction is expected to substantially alleviate the restriction of $|\boldsymbol{r}|/a$ (from $|\boldsymbol{r}|/a \gtrsim 3$ to $|\boldsymbol{r}|/a \gtrsim 2$) in a field-theoretically rigorous manner.

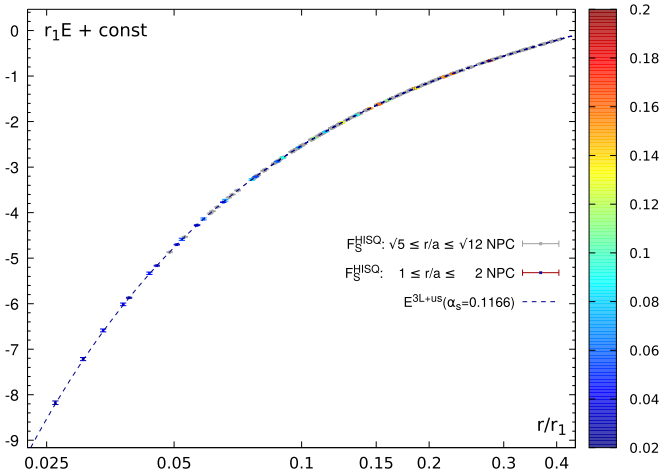

Figure 7. The nonperturbative lattice result $r_1E(r)$ ($E \equiv E_0$) using the singlet free energy at $T > 0$ and the perturbative continuum results for the static energy. The HISQ data [19] are nonperturbatively corrected (NPC, coloured bullets and gray bullets). The colour indicates the lattice spacing in units of the r_1 scale, a/r_1. The dashed line represents the three-loop result with resummed leading ultrasoft logarithms, corresponding to the result of the optimal $T = 0$ analysis $\alpha_S(m_Z^2) = 0.1166$. Only the NPC HISQ data at $T > 0$ with $|\boldsymbol{r}|/a \leqslant 2$ (coloured) are used in the fit, but all data in the range $2 < |\boldsymbol{r}|/a \leqslant \sqrt{12}$ (gray) are still consistent with it. The figure is taken from [19].

- To exploit more systematically finite temperature simulations in order to go to shorter distances. On the lattice side there is no major impediment to further increasing the temperature and decreasing the lattice spacing.
- To have the nonlogarithmic four-loop contribution to the static potential. This would be important to verify if large numerical cancellations between soft and US contributions also happen beyond three loops.
- To further exploit the definition of the force in terms of a chromoelectric field insertion in the static Wilson loop in order to generate high precision quenched and unquenched lattice data at short distances and to compare with the perturbative expression at N^3LO or N^3LL.
- To use recent high quality lattice data at $2 + 1 + 1$ flavours to extract α_S from the static energy with an active charm quark [78, 79]. To achieve precision competitive with $2 + 1$ flavour QCD, a full three-loop calculation of the contribution to the static potential due to the finite charm quark mass may be necessary.

Acknowledgments— PP was supported by U.S. Department of Energy under Contract No. DE-SC0012704. JHW's research was funded by the Deutsche Forschungsgemeinschaft (DFG, German Research Foundation) - Projektnummer 417 533 893/GRK2575 'Rethinking Quantum Field Theory'.

2.5. Remarks on determining α_S[63]

Every method to determine the strong coupling α_S starts with an observable that depends on a short distance, $1/Q$ (or high energy Q). The notion of 'short' or 'high' relates to other scales

[63] Authors: A S Kronfeld (Fermilab).

in the problem. The observable can be multiplied by the appropriate power of Q to obtain a dimensionless quantity, $\mathcal{R}(Q)$, which can be written

$$\mathcal{R}(Q) = R(Q) + Q^{-p}S(M, Q), \tag{2.37}$$

where M is another (energy) scale, $M \ll Q$, the first term R does not depend on M, and the power $p > 0$ is something like 2, 4, or 1. The separation can be justified with tools such as the operator product expansion (OPE) [89] or an effective field theory (EFT) [90, 91]. (Sometimes equation (2.37) is posited on the basis of arguments or assumptions.) With the OPE or an EFT, the power p corresponds to the dimension of an operator. For example, R might be the short-distance (or 'Wilson') coefficient of the unit operator, and S the product of another coefficient and the matrix element of a dimension-4 operator, in which case $p = 4$.

In an asymptotically free quantum field theory, such as QCD, the short-distance part can be well approximated with perturbation theory:

$$R(Q) = \sum_{l=0}^{\infty} R_l(Q/\mu)\alpha_S^l(\mu) = \sum_{l=0}^{\infty} R_l\alpha_S^l(Q), \tag{2.38}$$

where μ is a separation scale introduced by the OPE, EFT, or other consideration; in the last expression, $R_l = R_l(1)$. Because μ is unphysical, it can be chosen, at least after thorough analysis of the scale-separation details, equal or proportional to Q. At this stage, it is useful to introduce (with $\mu = Q$)

$$\alpha_{\mathcal{R}}(Q) = \frac{\mathcal{R}(Q) - R_0}{R_1}, \tag{2.39}$$

which is known as the effective charge (or effective coupling) for the observable $\mathcal{R}$. It may be more apt to note that $\alpha_{\mathcal{R}}$ is simply a physical, regularization-independent choice of renormalization scheme.

It is tempting to identify 'short distance' with 'perturbative' and 'long distance' with 'nonperturbative'. In the OPE or an EFT, however, the home for small instantons (for example) of diameter $1/Q$ is in short-distance coefficients. Fortunately, small-instanton contributions scale with a large power, $11 - 2N_f/3 \geqslant 7$ (where N_f is the number of active quark flavours), so they are small enough that neglecting them is safer than other compromises that must be made. Further complications in separating scales arise, such as renormalons. In the end, the point of equation (2.37) is that short-distance quantities depend on Q logarithmically with power-law corrections.

A practical version, then, of equation (2.37) is

$$\alpha_{\mathcal{R}}(Q) = \sum_{l=1}^{n_{\text{loop}}} r_l\alpha_S^l(Q) + \sum_{l=1+n_{\text{loop}}} r_l\alpha_S^l(Q) + \sum_p d_p(M/Q)^p, \quad r_1 = 1, \tag{2.40}$$

presupposing a preferred renormalization scheme (such as $\overline{\text{MS}}$), truncating the perturbative series at n_{loop} terms (those available from explicit perturbative calculation), acknowledging that the remaining terms do not vanish, and allowing for several power corrections. The renormalization group provides more information, in particular showing how to relate $\alpha_{\mathcal{R}}(Q)$ at one scale to $\alpha_{\mathcal{R}}(Q_0)$ at a fiducial scale Q_0. Instead of using the r_l to relate $\alpha_{\mathcal{R}}$ to $\alpha_{\overline{\text{MS}}}$, they can be used to convert the coefficients of the β function in the $\overline{\text{MS}}$ scheme to the $\mathcal{R}$ scheme. Thus, perturbation theory predicts the logarithmic Q dependence of $\alpha_{\mathcal{R}}(Q)$ without explicit reference to the ultraviolet regularization.

Equation (2.40) provides a guide to controlling a determination of α_S. The quantity $\mathcal{R}$ should be something that can be measured (in a laboratory experiment) or computed (with numerical lattice QCD) precisely. The higher the order in α_S, n_{loop}, the better. One wants Q to

Table 3. Ingredients of α_S determinations, with nonperturbative 'measurements' directly from lattice gauge theory (LGT), from the continuum limit of lattice QCD, or (to choose one example) scaling violations of the moments of structure functions in deep inelastic scattering (DIS). Effects beyond the Standard Model (BSM) may be present in experimental data (no one knows) and are omitted (as a rule) from the theory.

Ingredient	Small Wilson loops	LGT with $a \to 0$	DIS scaling violation
Obtain $\mathcal{R}(Q)$	Compute from QCD Lagrangian		Measure e−p scattering
Large energy scale	a^{-1}	L^{-1}, $2m_Q$, ...	Momentum transfer Q
Scale separation	OPE	Various	OPE
Perturbation theory	Lattice (NLO, maybe NNLO)	Dimensional regularization (NNLO, N^3LO)	
Number of quantities	Several	one or few	Several
Electroweak	Omitted by construction		Included in data and theory
BSM	Omitted by construction		Unknown/omitted
Units in GeV	Hadronic quantity, viz., $Q = M_{\rm PDG}[(Qa)/(Ma)]_{\rm lat}$		Detector calibration

be as large as possible, both to reduce the power corrections and to reduce the truncation error. Even better is a wide range of Q, both to verify the running of $\alpha_{\mathcal{R}}$ and to separate the logarithmic dependence on Q from the power-law behavior of the remainder. An observable is better suited when p can be proven, argued, or demonstrated to be large. Another desirable feature is to have several similar quantities, especially if the power corrections are related.

The quantity $\mathcal{R}$ can be computed in lattice QCD or measured in high-energy scattering or heavy-particle decays. Many reviews separate the two as if they are completely different objects. Table 3 compares the ingredients in the two approaches.

The scaling violations of moments of deep-inelastic structure functions are taken as a textbook example of high-energy scattering (further columns could be added without much work). Table 3 shows two classes of methods based on lattice gauge theory: small Wilson loops and every observable for which the continuum limit is taken (including everything else discussed in the subsections below). Even if one starts with a spacetime lattice as an ultraviolet regularization, the continuum limit is the same QCD as probed by high-energy experiments. In particular, the same methods for perturbation theory—based on dimensional regularization—apply and, thus, the issues related to truncating the series, the size of and range in Q, etc, are *the same*. Indeed, moments of quarkonium correlation functions can be calculated with lattice QCD or measured in $e^+e^- \to$ hadrons: the perturbative series are exactly the same. We have here an example of a lattice-QCD method that has more in common with a high-energy-scattering method than it has with other lattice-QCD methods (see sections 2.3 and 9.1 for details).

Because of the similarities, criteria for assessing issues such as truncation of perturbation theory and the range in Q should be the same for both. Ideally, the $\alpha_S(m_Z^2)$ averaging approaches used by the PDG from the world data [92] and by the FLAG collaboration from lattice results [12] should be more closely aligned. Some remarks on the criteria are provided below.

In table 3, small Wilson loops are listed separately because they are defined at the scale of the lattice spacing, i.e. at the ultraviolet cutoff. There are further such quantities, including the bare coupling. They are a different object because the lattice—including details of the chosen lattice action—is present. The lattice is like 'new physics' at the highest energies, except that

the action of the new physics is exactly known. Determinations of α_S from small Wilson loops warrant discussion here in order to clarify discussions in [11, 13, 50].

In continuum language, a Wilson loop is a path-ordered exponential integrating $dz \cdot A$ around a closed loop [61]:

$$W_P = \mathbb{P} \exp ig \oint_P dz \cdot A(z), \tag{2.41}$$

where $A = t^a A^a$ is the gauge potential, and $\mathbb{P}$ denotes path ordering. For small loops of linear size a, this operator admits an OPE:

$$W_P \doteq Z_P[\mathbb{1} + C_P^{(FF)} a^4 \alpha_S F^2 + C_P^{(\bar{q}q)} a^4 m \bar{q} q + \mathcal{O}(a^6)], \tag{2.42}$$

where the equivalence $\doteq$ is in the weak sense of matrix elements between low-energy states. Here, Z_P, $Z_P C_P^{(FF)}$, and $Z_P C_P^{(\bar{q}q)}$, are short distance coefficients, so they can be calculated in perturbation theory. Note that the operators that appear do not depend on the path: when taking matrix elements, the same quantities enter over and over again. Note also the high power 4 in the power corrections.

Equation (2.42) applies equally well in a lattice gauge theory. Indeed, in pure gauge theory, the OPE is on a very solid footing [93, 94]. The short-distance coefficients must be calculated in lattice perturbation theory, which is less developed than perturbation theory with dimensional regularization. It is instructive to show the tree-level expression for the coefficient $Z_P C_P^{(FF)}$ of a planar Wilson loop of size $ma \times na$,

$$Z_{m\times n} C_{m\times n}^{(FF)} = -\frac{\pi (mn)^2}{36}, \tag{2.43}$$

where a is now the lattice spacing. The condensate contribution to the 1×1 loop is 16 times smaller than that of the 2×2 loop.

Vacuum expectation values $\mathcal{R}_P \equiv \frac{1}{3}\langle \mathrm{Re\,tr} W_P \rangle$ or $\mathcal{R}'_P \equiv -\ln \frac{1}{3}\langle \mathrm{Re\,tr} W_P \rangle$, and combinations thereof, satisfy equation (2.40). They can be computed very precisely. (The bare coupling, mentioned above, is known exactly.) Fits of the precise data can include several orders beyond the $n_{\mathrm{loop}}^{\mathrm{th}}$ term [14, 95, 96], which is not a shortcoming but a strength of the method. Such fitting could be applied to any quantity $\mathcal{R}$ with per mil uncertainties, because assuming that the higher-order terms vanish is obviously wrong. In practice, the fits include terms that cannot be determined by the data, but the correct interpretation of these parameters is a marginalization over terms whose Q dependence is known, even if their strength is not. For determining α_S, one is not interested in the values (and errors) of higher-order or power-law coefficients. One is interested is how imperfect knowledge of these terms propagates to uncertainty in $\alpha_S(m_Z^2)$.

Incorporating the next few terms via fit parameters, with suitable priors, can be seen as more conservative and more robust than the popular method of varying the scale by a factor of two up and down. The popular method sets $\mu = sQ$ and moves $\ln s \in [-\ln 2, +\ln 2]$. It picks out a one-dimensional curve in a multidimensional space, rather than allowing a data-guided exploration of the space. Reference [13] uses the scale variation method to estimate the truncation uncertainty in analyses such as those in [14, 95, 96], not discussing that the additional fitted terms could absorb such a variation.

The FLAG collaboration [11] is considering making its quality criteria stricter. It is worth scrutinizing the criteria and asking whether they are the most apt. One of the criteria requires $\alpha_{\mathcal{R}}$ to be sufficiently small. The bare coupling of lattice QCD satisfies the 2021 criterion and probably any future one, but it has been deprecated (for well-known reasons) as a route to α_S. Another criterion demands that the truncation error, $\alpha_{\mathcal{R}}^{m_{\mathrm{loop}}+1}$, be smaller than the statistical

(and systematic) error. This criterion, as it stands, can exclude quantities that are precise enough to verify higher-order perturbative behavior by fitting.

Because small Wilson loops are defined at the scale of the lattice spacing, effects of QED and strong isospin breaking ($m_u \neq m_d$) are often very small. The leading effect arises not in the effective α_S but in the conversion from lattice units to GeV. The ensembles of lattice gauge fields best suited to a future study of small Wilson loops are those being used for the hadronic-vacuum-polarization contribution to the muon's anomalous magnetic moment, because they have the widest range in a, highest statistics, and include QED and strong isospin contributions in the determination of the lattice spacing. A typical target is $\delta a/a \lesssim 0.5\%$, leading to a $\delta\alpha_S/\alpha_S$ that is $\beta_0\alpha_S$ times smaller, or $\lesssim 0.1\%$.

3. $\alpha_S(m_Z^2)$ from hadronic tau decays

3.1. Determination of $\alpha_S(m_\tau^2)$ from ALEPH τ decay data[64]

The inclusive distribution of the final hadrons in τ decay provides the needed information to perform a clean low-energy determination of the strong coupling [97]. The relevant dynamical quantities are the two-point correlation functions for the vector $V^\mu = \bar{u}\gamma^\mu d$ and axial-vector $A^\mu = \bar{u}\gamma^\mu\gamma_5 d$ colour-singlet charged currents:

$$i\int d^4x\; e^{iqx}\;\langle 0|T[\mathcal{J}^\mu(x)\mathcal{J}^{\nu\dagger}(0)]|0\rangle = (-g^{\mu\nu}q^2 + q^\mu q^\nu)\;\Pi_{\mathcal{J}}(q^2) + g^{\mu\nu}q^2\;\Pi_{\mathcal{J}}^{(0)}(q^2), \qquad (3.1)$$

with $\mathcal{J} = V, A$. If the tiny up and down quark masses are neglected, $q^2\;\Pi_{\mathcal{J}}^{(0)}(q^2) = 0$ and only the first term needs to be considered. The correlators $\Pi_{\mathcal{J}}(s)$ are analytic functions in the entire complex s plane, except for a cut along the positive real axis where their imaginary parts (spectral functions) have discontinuities. This implies the exact mathematical identity [98]

$$A_{\mathcal{J}}^{\omega}(s_0) \;\equiv\; \int_{s_{\rm th}}^{s_0}\frac{ds}{s_0}\;\omega(s)\,{\rm Im}\,\Pi_{\mathcal{J}}(s) \;=\; \frac{i}{2}\oint_{|s|=s_0}\frac{ds}{s_0}\;\omega(s)\Pi_{\mathcal{J}}(s), \qquad (3.2)$$

where $\omega(s)$ is any weight function analytic in $|s| \leqslant s_0$, $s_{\rm th}$ is the hadronic mass-squared threshold, and the complex integral in the right-hand side runs counter-clockwise around the circle $|s| = s_0$. The inclusive Cabibbo-allowed hadronic decay width of the τ just corresponds to the weight $\omega_\tau(x) = (1-x)^2(1+2x)$ with $x = s/s_0$ and $s_0 = m_\tau^2$. The measured invariant-mass distribution determines then the left-hand-side integral for $s_0 \leqslant m_\tau^2$.

For large-enough values of s_0, the operator product expansion (OPE) [99],

$$\Pi_{\mathcal{J}}^{\rm OPE}(s) \;=\; \sum_D \frac{1}{(-s)^{D/2}}\sum_{\dim\mathcal{O}=D} C_{D,\mathcal{J}}(-s,\,\mu)\;\langle 0|\mathcal{O}(\mu)|0\rangle \;\equiv\; \sum_D \frac{\mathcal{O}_{D,\mathcal{J}}}{(-s)^{D/2}}, \qquad (3.3)$$

can be used to expand the contour integral in inverse powers of s_0. The first term ($D = 0$) contains the perturbative QCD contribution, which is known to $\mathcal{O}(\alpha_S^4)$ [100], while nonperturbative power corrections have $D \geqslant 4$. The small differences between the physical values of the integrated moments $A_{\mathcal{J}}^{\omega}(s_0)$ and their OPE approximations are known as quark-hadron duality violations. They are very efficiently minimized by taking 'pinched' weight functions which vanish at $s = s_0$, suppressing in this way the contributions from the region near the real axis where the OPE is not valid [98, 101, 102].

The high sensitivity of the τ hadronic width to the strong coupling follows from four important facts:

[64] Authors: A Pich (IFIC València), A Rodríguez-Sánchez (IJCLab Orsay).

1. The perturbative contribution amounts to a sizeable 20% effect because $\alpha_S(m_\tau^2) \sim 0.3$ is large.
2. The OPE can be safely used at $s_0 \sim m_\tau^2$. The weight $\omega_\tau(x)$ contains a double zero at $s = s_0$, heavily suppressing the numerical impact of duality violations.
3. Since $\omega_\tau(x) = 1 - 3x^2 + 2x^3$, the contour integral is only sensitive to OPE corrections with $D = 6$ and 8, which are strongly suppressed by the corresponding powers of m_τ. Moreover, these power corrections appear with opposite signs in the vector and axial-vector correlators [98, 103, 104], which implies an additional numerical cancellation in the total vector + axial ($V + A$) decay width.
4. The opening of high-multiplicity hadronic thresholds dilutes very soon the prominent $\rho(2\pi)$ and $a_1(3\pi)$ resonances, leading to a quite flat $V + A$ spectral distribution that approaches very fast the perturbative QCD predictions.

The small nonperturbative contributions can be extracted from data, analysing moments more sensitive to power corrections [101]. The detailed analyses performed by ALEPH [105], CLEO [106] and OPAL [107] confirmed a long time ago that these corrections are smaller than the perturbative uncertainties. The latest and more precise experimental determination of the strong coupling obtains $\alpha_S^{(N_f=3)}(m_\tau^2) = 0.332 \pm 0.005_{\rm exp} \pm 0.011_{\rm th}$ [103]. Taking as input their measured nonperturbative correction, the strong coupling can be directly extracted from the total τ hadronic width (and/or lifetime), which results in $\alpha_S^{(N_f=3)}(m_\tau^2) = 0.331 \pm 0.013$ [108].

An exhaustive reanalysis with the updated ALEPH τ data [103] has been performed in [104], in order to carefully assess any possible source of systematic uncertainties. A large variety of methodologies, including all previously considered strategies, have been explored, looking for potential hidden weaknesses and testing the stability of the fitted results under slight variations of the assumed inputs. The most reliable determinations of $\alpha_S(m_\tau^2)$, obtained with the total $V + A$ distribution, are summarized in table 4. The dominant uncertainties are the perturbative errors associated with the unknown higher-order corrections. This is clearly illustrated in the table, which shows the results obtained under two different procedures, either performing the contour integrals with a running $\alpha_S(-s)$, by solving numerically the five-loop β-function equation (contour-improved perturbation theory, CIPT) [109, 110], or naively expanding them in powers of $\alpha_S(m_\tau^2)$ (fixed-order perturbation theory, FOPT). FOPT generates a somewhat larger perturbative contribution and, therefore, leads to a slightly smaller fitted value of α_S. Within each procedure, the perturbative error has been estimated taking a very conservative range for the fifth-order coefficient of the Adler series, $K_5 = 275 \pm 400$, and varying the renormalization scale in the interval $\mu^2/(-s) \in (0.5, 2)$. The values obtained with the two procedures are finally combined, adding quadratically half their difference as an additional systematic error.

The different rows in the table correspond to different choices of pinched weights:

$$\begin{aligned}
&\omega_{kl}(x) = (1 - x)^{(2+k)}\, x^l\, (1 + 2x), && (k, l) = \{(0, 0), (1, 0), (1, 1), (1, 2), (1, 3)\},\\
&\hat{\omega}_{kl}(x) = (1 - x)^{(2+k)}\, x^l, && (k, l) = \{(0, 0), (1, 0), (1, 1), (1, 2), (1, 3)\},\\
&\omega^{(2,m)}(x) = 1 - (m + 2)x^{m+1} + (m + 1)x^{m+2}, && 1 \leqslant m \leqslant 5,\\
&\omega_a^{(1,m)}(x) = (1 - x^{m+1})\mathrm{e}^{-ax}, && 0 \leqslant m \leqslant 6.
\end{aligned} \tag{3.4}$$

In all cases, we find a high sensitivity to the strong coupling and a very small sensitivity to power corrections, which gets reflected in large uncertainties for the fitted condensates. The first set of weights was adopted by ALEPH and allows for a direct use of the measured distribution. With the five indicated moments, we have fitted $\alpha_S(m_\tau^2)$ and the nonperturbative

Table 4. Determinations of $\alpha_S^{(N_f=3)}(m_\tau^2)$ from τ decay data, in the $V+A$ channel [104].

Method	$\alpha_S^{(N_f=3)}(m_\tau^2)$		
	CIPT	FOPT	Average
$\omega_{kl}(x)$ weights	$0.339^{+0.019}_{-0.017}$	$0.319^{+0.017}_{-0.015}$	$0.329^{+0.020}_{-0.018}$
$\hat{\omega}_{kl}(x)$ weights	$0.338^{+0.014}_{-0.012}$	$0.319^{+0.013}_{-0.010}$	$0.329^{+0.016}_{-0.014}$
$\omega^{(2,m)}(x)$ weights	$0.336^{+0.018}_{-0.016}$	$0.317^{+0.015}_{-0.013}$	$0.326^{+0.018}_{-0.016}$
s_0 dependence	0.335 ± 0.014	0.323 ± 0.012	0.329 ± 0.013
$\omega_a^{(1,m)}(x)$ weights	$0.328^{+0.014}_{-0.013}$	$0.318^{+0.015}_{-0.012}$	$0.323^{+0.015}_{-0.013}$
Average	0.335 ± 0.013	0.320 ± 0.012	0.328 ± 0.013

corrections $\mathcal{O}_{4,6,8}$. The impact on α_S from neglected condensates of higher dimensions (the highest moment involves corrections with $D \leqslant 16$) has been estimated including $\mathcal{O}_{10}$ in the fit and taking the difference as an additional uncertainty. Additional power corrections with $D > 10$ would certainly modify the poorly determined values of the fitted condensates, specially those with higher dimensions, but they have a negligible impact on α_S, compared with the errors already included. Our results (first line in the table) are in good agreement with [103]. Very similar values are obtained with the modified weights $\hat{\omega}_{kl}(x)$ (second line), which eliminate the highest-D power correction from every moment, showing that these contributions do indeed play a minor numerical role.

Moments constructed with the optimized (double-pinched) weights $\omega^{(2,m)}(x)$ only receive power corrections with $D = 2(m+2)$ and $2(m+3)$. The third line in the table shows that they give values of $\alpha_S(m_\tau^2)$ in very good agreement with those in the first two lines. Similar results (not shown in the table) are obtained from a fit to four moments, based on the weights $\omega^{(n,0)}(x) = (1-x)^n$, with $0 \leqslant n \leqslant 3$, which have a different sensitivity to power corrections and (for n=0,1) are less protected against duality violations and experimental uncertainties. The values of $\alpha_S(m_\tau^2)$, $\mathcal{O}_{2(m+2)}$ and $\mathcal{O}_{2(m+3)}$ can also be extracted from a fit to the s_0 dependence of a single $A^{(2,m)}(s_0)$ moment, above some $\hat{s}_0 \geqslant 2.0$ GeV^2. One finds a quite poor sensitivity to power corrections, as expected, but a surprising stability in the extracted values of $\alpha_S(m_\tau^2)$ at different $\hat{s}_0$. Combining the information from three different moments ($m = 0$, 1, 2), and adding as an additional theoretical error the fluctuations with the number of fitted bins, one gets the $\alpha_S(m_\tau^2)$ values given in the fourth line of table 4. This determination is much more sensitive to violations of quark-hadron duality because the s_0 dependence of consecutive bins feels the local structure of the spectral function.[65] The agreement with the determinations in the other lines of the table confirms the small size of duality violations in the $V+A$ distribution above $\hat{s}_0$.

A completely different sensitivity to nonperturbative corrections is achieved with the weights $\omega_a^{(1,m)}$. Their exponential suppression nullifies the high-s region, strongly reducing the violations of quark-hadron duality, at the price of enhancing the exposition to power

[65] [104, 111–113] have also analysed a different strategy, advocated in some recent works (see section 3.2), that maximises duality violations: the experimental spectral function is fitted in the interval $\hat{s}_0 < s < m_\tau^2$ with an ad-hoc 4-parameter ansatz, and the resulting model is used to correct the perturbative prediction of $A_J^\omega(\hat{s}_0)$ with $\omega(x) = 1$ (no weight). This is a dangerous procedure because (1) the OPE is not valid in the real axis, (2) α_S is fixed at a very low scale $\hat{s}_0 = (1.2\ \text{GeV})^2$ where theoretical errors are large, and (3) the subtracted duality-violation contribution is large and model dependent. Slight changes on the functional form of the assumed ansatz result in large variations of the fitted value of $\alpha_S(\hat{s}_0)$ [104, 113] that have not been taken into account in the quoted uncertainties. [113] provides a very detailed anatomy of this duality-violation approach to the strong coupling, exhibiting unaccounted systematic errors, some formal inconsistencies of the adopted assumptions and the tautological nature of some of the tests.

corrections of any dimensionality. In a pure perturbative analysis the neglected power corrections should manifest as large instabilities of α_S under variations of s_0 and $a \neq 0$; however, stable results are found for a broad range of both s_0 and a, which indicates that power corrections are small. The last line in the table has been obtained combining the information from seven different moments with $\omega_a^{(1,m)}$ $(0 \leqslant m \leqslant 6)$ weights.

Fully compatible results with slightly larger uncertainties are also obtained from the separate V and A distributions [104]. The excellent overall agreement among determinations obtained with a broad variety of numerical approaches that have very different sensitivities to nonperturbative corrections, and the many complementary tests successfully performed in [104], demonstrate the robustness and reliability of the results shown in table 4. The final average value

$$\alpha_S^{(N_f=3)}(m_\tau^2) = 0.328 \pm 0.013 \tag{3.5}$$

is in good agreement with the results of [103] and with a recent determination (see section 3.3) based on Borel–Laplace sum rules and a renormalon-motivated model [114]. After evolution up to the scale m_Z, the strong coupling decreases to

$$\alpha_S^{(N_f=5)}(m_Z^2) = 0.1197 \pm 0.0015, \tag{3.6}$$

in excellent agreement with the direct N^3LO determination at the Z peak.

A much better control of the small nonperturbative contributions could be achieved with more precise data, specially at the highest energy bins. The high-statistics expected from Belle-II or a future TeraZ facility should make that possible. A reduction of the dominant perturbative error requires a better theoretical understanding of higher-order corrections (CIPT versus FOPT, renormalons, etc). In the long term, an explicit calculation of the K_5 term in the Adler series would have a major impact.

Acknowledgments—This work has been supported by MCIN/AEI/10.13039/501100011033, Grant No. PID2020-114473GB-I00, by the Generalitat Valenciana, Grant No. Prometeo/2021/071, and by the Agence Nationale de la Recherche (ANR), Grant ANR-19-CE31-0012 (project MORA).

3.2. The strong coupling from hadronic τ decays: present and future[66]

We review the sum-rule framework for determining the strong coupling, α_S, from inclusive spectral functions measured in hadronic τ decays. We then discuss a new inclusive vector isovector spectral function, obtained from combining the dominant exclusive-mode spectral-function data from ALEPH and OPAL with BaBar data for $\tau \to K^- K^0 \nu_\tau$ and several CVC-converted R-ratio data sets for small exclusive-mode contributions that had previously been estimated using Monte Carlo methods. We summarize our most recent results for α_S, and discuss prospects for future improvements.

3.2.1. Review. Finite-energy sum rules (FESRs) allow for the extraction of the strong coupling at the τ mass, $\alpha_S(m_\tau^2)$, from inclusive vector (V) and/or axial (A) non-strange spectral functions, which can and have been measured through hadronic τ decays [105, 107, 115]. Such sum rules have the form

[66] Authors: D Boito (U Vienna and U Sao Paulo), M Golterman (SF State Univ. and IFAE Barcelona), K Maltman (YU Toronto and CSSM Adelaide), S Peris (IFAE Barcelona).

$$I^{(w)}(s_0) \equiv \frac{1}{s_0}\int_0^{s_0} ds\; w(s)\rho(s) = -\frac{1}{2\pi i s_0}\oint_{|z|=s_0} dz\; w(z)\Pi(z), \tag{3.7}$$

where $\Pi(z)$ is a vacuum polarization, $\rho(s) = \frac{1}{\pi}\,\mathrm{Im}\,\Pi(s)$, with $s = q^2$, is the corresponding spectral function, $s_0 > 0$, and $w(s)$ is typically a polynomial in s/s_0. The left-hand side of equation (3.7) can be determined from data for $s_0 \leqslant m_\tau^2$, while, for s_0 large enough, the right-hand side can be represented in QCD perturbation theory, with nonperturbative (NP) corrections. The latter are needed because of the relatively low value of m_τ.

The perturbative expansion for $\Pi(z)$ in powers of $\alpha_S(\mu^2)$ and $\log(-z/\mu^2)$ is known to order α_S^4 [100], where μ is the renormalization-group scale. In most of the literature, two scale-choice prescriptions have been considered, either FOPT, in which $\mu^2 = s_0$, or CIPT [109, 110], in which μ^2 is set equal to z when evaluating the perturbative contribution to the contour integral on the right-hand side of equation (3.7).

NP corrections (away from the positive real axis, see below) are incorporated through the operator product expansion (OPE), which schematically takes the form

$$\Pi_{\rm OPE}(z) = \sum_{k=0}^{\infty}(-1)^k\frac{C_{2k}(z)}{z^k}. \tag{3.8}$$

The $k = 0$ term represents purely perturbative contributions, the $k = 1$ term perturbative mass corrections (in the non-strange channels, C_2 can be set to zero because of the smallness of the up and down quark masses); NP condensate contributions start at $k = 2$. The presence of a cut in the complex $z = q^2$ plane extending to infinity along the positive real axis, means the OPE is not convergent; it is, at best, an asymptotic series. It is also generally believed that the $D = 2k$ terms (for $k > 1$) are related to renormalon ambiguities in the perturbative expansion [116–118]. While the higher-dimension coefficients C_{2k} in principle depend logarithmically on z, they are generally taken as constants, as their z dependence is suppressed by two powers of α_S, in addition to the $1/z^k$ suppression.

Recently, it was shown that the Borel sums of the FOPT and CIPT versions of the perturbative expansion of the right-hand side of equation (3.7) are not the same and, related, that the OPE (3.8) does not reflect the renormalon ambiguities for CIPT [119, 120], creating a mismatch between the use of CIPT and the OPE in the form (3.8). Because of this, we will always employ FOPT [121]. The recent work of [122] (see section 3.4) paves the way for a reconciliation between the FOPT and CIPT series but, until this is realized in practice, averaging the results obtained using FOPT and CIPT should be avoided.

The nonconvergent, at-best-asymptotic, nature of the OPE noted above has two implications. First, it is advisable to restrict the use of the OPE to low orders in the expansion (3.8), as little is known about where it starts to diverge (at the energies relevant in τ decays). Second, one expects NP corrections *beyond* the OPE, just as the OPE represents NP corrections beyond perturbation theory. This phenomenon, known as the violation of quark-hadron duality [123–125], manifests itself physically in the presence of overlapping resonance contributions in $\rho(s)$. These duality violations (DVs) need to be modeled (as long as a NP solution to QCD is not known). We have developed a theoretical framework, based on generally accepted assumptions about QCD in the framework of hyperasymptotics [126], which leads to the following large-s asympotic form for the duality-violating part of the spectral function:

$$\rho_{\rm DV}(s) = e^{-\delta-\gamma s}\sin(\alpha + \beta s)\left[1 + \mathcal{O}\left(\frac{1}{\log s};\,\frac{1}{s};\,\frac{1}{N_c}\right)\right]. \tag{3.9}$$

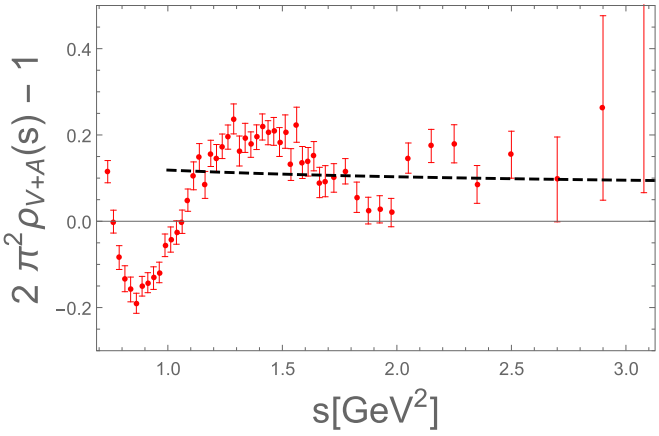

Figure 8. Blow-up of the large-s region of the parton-model-subtracted ALEPH $V+A$ non-strange spectral function [103]. The dashed curve represents QCD perturbation theory.

With this *ansatz*, the sum rule (3.7) can be reformulated as [127]

$$\frac{1}{s_0}\int_0^{s_0} ds\; w(s)\rho(s) = -\frac{1}{2\pi i s_0}\oint_{|z|=s_0} dz\; w(z)\Pi_{\rm OPE}(z) - \frac{1}{s_0}\int_{s_0}^{\infty} ds\; w(s)\rho_{\rm DV}(s). \qquad (3.10)$$

This introduces a new set of parameters into the theory representation of the right-hand side of equation (3.7). A separate set of DV parameters is needed for each of the V and A channels. The main assumption is that the form (3.9) can be used at values of s below m_τ^2—whether this is the case can be tested by a variety of fits to data. For a more detailed version of this very brief review, and many more references, we refer to [121].

At this point, a quick look at data is instructive. Figure 8 shows a rescaled version of the sum of the non-strange V and A spectral functions from [103], with the α_S-independent parton-model contribution subtracted. Resonance oscillations are immediately evident, with an amplitude comparable in size to the α_S-dependent pQCD contribution, represented by the dashed curve. The figure makes clear that DVs are important, though, because of the large errors, it is difficult to tell whether oscillations above $s = m_\tau^2$ (relevant to determining DV contributions to the sum rules (3.10) with $s_0 = m_\tau^2$) will be numerically relevant or not. Clearly, DVs need to be accounted for, and their contributions quantitatively assessed, even in the $V+A$ channel.

Two different strategies, which we refer to as the 'truncated OPE' (tOPE) [101] and the 'DV-model' strategies [128, 129], have been developed to deal with the NP contributions discussed above.

In the tOPE approach, s_0 is taken equal to m_τ^2, and, to suppress contributions to the contour integral from the region near the positive real axis, and thus from DVs, weights with a double or triple zero at $s = s_0 = m_\tau^2$ are employed. The set of such multiple-zero ('pinched') polynomial weights typically extends up to degree $k = 7$, and thus probes the OPE up to dimension $D = 2k+2 = 16$. The number of OPE parameters to be fitted (α_S and the condensates C_D, $D = 4,\ 6,\ \cdots,16$) necessarily exceeds the number of such independent weights, and hence the number of independent $s_0 = m_\tau^2$ spectral integrals available to fix these parameters. Some subset of the C_D in principle present must thus be set to zero by hand

to leave a fit with fewer parameters than data points. DVs are also neglected (in terms of equation (3.9), δ is set to ∞) under the assumption that the use of pinched moments sufficiently suppressess these contributions.

The main problem with this strategy, employed most recently in [103, 104], is the neglect of these higher-D OPE contributions. Several tests of the tOPE strategy were carried out in [130, 131], exposing clear inconsistencies. Such inconsistencies can arise because integrated dimension-D OPE contributions scale as $1/s_0^{D/2}$. If contributions from omitted higher-D condensates are, in fact, not numerically negligible, then when these are absorbed into the values of the lower-D OPE parameters obtained in a fixed-s_0 tOPE fit, the resulting theory representation will, in general, have an s_0 dependence which is incorrect. The tOPE truncation can thus be tested for selfconsistency by comparing spectral-integral predictions obtained using the theory parameters obtained from the single-s_0 tOPE fit to the experimental values of these same spectral integrals over a range of s_0 values. Such tests, designed to take into account the impact of the very strong correlations between (i) spectral integrals at different s_0, (ii) theory integrals at different s_0, and (iii) fitted theory parameters and spectral integrals, were carried out in [131], with related tests also carried out in [130]. The s_0 dependence of the theory predictions was found to be in clear disagreement with that of the corresponding experimental spectral integral combinations.[67]

In a recent publication [113], Pich and Rodriguez-Sanchez have addressed the relative merits of the tOPE and DV-model based approaches, commenting on [130, 131]. In this brief overview, there is not enough space to discuss, in sufficient detail, a number of the ongoing misconceptions and/or mis-statements concerning the tOPE and DV model approaches contained in both this new work and in section 3.1 of this review. Neither, in fact, addresses the points raised in [131] beyond a few vague comments, while the discussion of [130] in [113] is based on a number of assumptions/prejudices about the OPE and misinterpretations of the results presented in [130]. Some further discussion of these shortcomings can be found in the Mattermost forum provided for the recent ECT* Trento α_S(2022) Workshop on Precision Measurements of the QCD Coupling Constant.[68] We leave further discussion, including of [113], to a future publication.

In the alternate DV-model strategy, recent implementations employ weights sensitive to terms in the OPE only up to $D = 8$, avoiding potential problems with higher-D OPE contributions.[69] DVs cannot, in general, be ignored, and are instead modeled by equation (3.9), with fits performed to spectral integrals for a range of s_0 between a minimum value $s_0^{\min}$ and m_τ^2, where $s_0^{\min}$ is determined by the quality of the fits and turns out to be $\sim 1.5\,\text{GeV}^2$. Results are found to be very stable against variations of $s_0^{\min}$.

To determine both DV parameters and α_S, the analysis should include at least one weight with good sensitivity to DVs. The choice $w = 1$, which produces no DV suppression, is ideal for this purpose. Stability of the DV-model approach has been tested using various combinations of weight functions in analyses of purely V-channel τ data, both V- and A-channel τ data [132], and the KNT [133, 134] compilation of R-ratio (inclusive $e^+e^- \to$ hadrons) data [135]. [121] contains our most recent application of this strategy. Earlier applications, laying out the framework in more detail, can be found in [128]. The DV-model strategy uses a range of s_0 as it is important to check the s_0 dependence of the match between experiment and theory (left-hand and right-hand sides of equation (3.10),

[67] See, for example, figure 8 of [131].
[68] See https://mattermost.web.cern.ch/alphas-2022/channels/town-square.
[69] Some tests were also performed with a degree-4 weight, sensitive to C_{10}. We avoid weights that project onto C_4 [118, 128, 129].

respectively), to test the validity of the theory representation employed for $\Pi(z)$. One also needs to check that oscillations in the V and A (hence also $V+A$) spectral functions are well represented by the *ansatz* (3.9), for at least some range of s below m_τ^2.

3.2.2. Data. Traditionally, in most papers since the appearance of the perturbative result to order α_S^4 in [100], the τ-based α_S has been obtained from the ALEPH data [103, 104, 114, 132, 136]. However, the value obtained from OPAL data [128, 129] is consistent with the ALEPH-based result [132], and it thus makes sense to combine the ALEPH and OPAL data sets prior to integration, following the approach now routinely employed for electroproduction data when obtaining dispersive estimates for the leading hadronic contribution to the muon anomalous magnetic moment. Moreover, while the bulk of the inclusive spectral functions comes from the 2-pion and the 4-pion modes (in the V channel), and the 3-pion and 5-pion modes (in the A channel), most of the residual exclusive channels (including some of the 5-pion channels) were obtained from Monte Carlo simulations rather than from experimental data in [105, 107, 115]. In the V channel, this can now be remedied by using, in addition to BaBar results for $\tau \to K^- K^0 \nu_\tau$ [137], recent high-precision results for higher-multiplicity, G-parity positive (hence $I=1$) exclusive-mode electroproduction cross sections. CVC allows these to be converted to the equivalent higher-multiplicity contributions to the $I=1$, V τ-based spectral function.[70] The detailed construction of the combined inclusive $I=1$, V spectral function along these lines is described in [121]. With 98% of the inclusive total by branching fraction (BF) coming from the combined ALEPH and OPAL 2-pion and 4-pion modes, and the support for the residual modes lying well above the ρ/ω meson interference region, isospin-breaking corrections, which should in principle be applied to the CVC relations, will be safely negligible.

The new V spectral function is shown in figure 9. The increased precision in the large-s region, coming from the replacement of Monte Carlo data with electroproduction data (which are not kinematically limited by the τ mass) is immediately evident. A more quantitative measure of the improved precision is provided in table 5, which shows a dramatically reduced statistical error on the $w=1$ spectral moment $I^{(w=1)}(s_0)$ resulting from the improved precision of the combined spectral function, compared to the ALEPH or OPAL spectral functions, in the larger s region.

3.2.3. Results. The increased precision of the new non-strange $I=1$ V spectral function constructed in [121] produces an improved determination of $\alpha_S(m_\tau^2)$, with the CVC-based improvement of residual-mode contributions playing a particularly important role. Since electroproduction data are purely vector, a similar improvement is not possible for the axial channel. Higher precision is thus now obtainable from V-channel than from $V+A$-channel analyses.[71]

Our result for α_S at the τ-mass is [121]

$$\alpha_S(m_\tau^2) = 0.3077 \pm 0.0065_{\rm exp} \pm 0.0038_{\rm theory} = 0.3077 \pm 0.0075 \qquad (N_{\rm f}=3,\ {\rm FOPT}), \tag{3.11}$$

where the first error is the fit error, and the second an estimate of the systematic uncertainty associated with the truncation of perturbation theory and the use of equation (3.9) to model DVs. For comparison, analyses of ALEPH or OPAL data alone produce combined errors of ± 0.010 and ± 0.018, respectively.

[70] The existence of a Dalitz-plot-based $I=0/1$ separation of the $e^+e^- \to K\bar{K}\pi$ cross sections means CVC can also be used to determine the $K\bar{K}\pi$ contribution to the τ V spectral function [138].

[71] Note, however, that combined V- and A-channel analyses of both OPAL data [128, 129] and ALEPH data [132] produced results in very good agreement with those of the corresponding V-channel analyses.

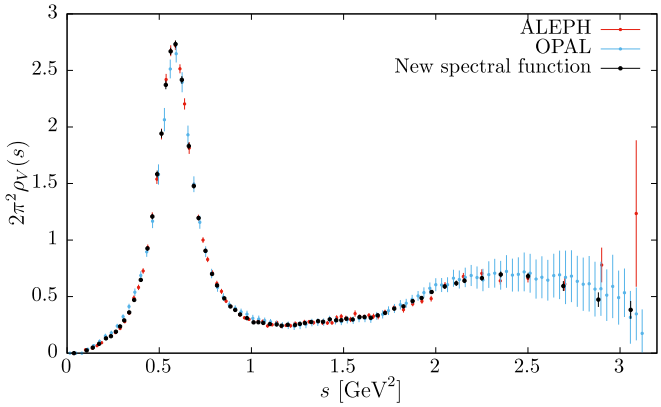

Figure 9. New non-strange V spectral function [121], compared with the ALEPH and OPAL spectral functions.

Table 5. Comparison of the left-hand side of equation (3.7) for $w = 1$, at two values of s_0, for the combined, ALEPH, and OPAL versions of the V spectral function. $s_0{}^*$ is a value close to 1.5 GeV^2 for each case, and $s_0{}^{**}$ is close to 2.9 GeV^2 for each case. Note that, because the values of $s_0{}^*$ and $s_0{}^{**}$ are slightly different for the three cases, the central values cannot be directly compared. The errors can, however, be compared, as they vary slowly with s_0. For details, see [121].

	Combined	ALEPH	OPAL
$s_0{}^* \approx 1.5$ GeV^2	0.03137(14)	0.03145(17)	0.03140(46)
$s_0{}^{**} \approx 2.9$ GeV^2	0.02952(29)	0.03133(65)	0.03030(170)

Converting equation (3.11) to the $N_f = 5$, Z-mass scale using five-loop running and four-loop matching at the charm and bottom thresholds, one finds

$$\alpha_S(m_Z^2) = 0.1171 \pm 0.0010 \qquad (\tau,\ N_f = 5,\ \text{FOPT}). \tag{3.12}$$

This is in good agreement with an independent determination from electroproduction data using the same theoretical framework [135]:

$$\alpha_S(m_Z^2) = 0.1158 \pm 0.0022 \qquad (\text{EM},\ N_f = 5,\ \text{FOPT}). \tag{3.13}$$

The latter determination was obtained from FESRs with $3.25\,\text{GeV}^2 \leqslant s_0^{min} \leqslant 4\ \text{GeV}^2$, significantly higher than the interval $\sim 1.5\,\text{GeV}^2 \leqslant s_0^{min} \leqslant m_\tau^2$ available from τ decays. The wider range of accessible s_0 allowed tests of our model for DVs, equation (3.9), to be performed by comparing values of $\alpha_S(m_\tau^2)$ obtained from the $w = 1$ FESR (which is maximally sensitive to DV effects, and hence provides a good probe of their effect) with and without DV contributions included. The effect found was small (of order 0.005)[72] for $3.25\,\text{GeV}^2 \leqslant s_0^{min} \leqslant 4\ \text{GeV}^2$ but increased rapidly as $s_0^{\min}$ was lowered below m_τ^2.[73]

3.2.4. Future improvements. The value of α_S obtained from hadronic τ decays, in addition to being competitive, provides a particularly strong test of the running predicted by QCD

[72] This systematic effect is included in the error shown in equation (3.13).
[73] Recall that the dependence of equation (3.9) on s is exponential.

since the τ mass is much lower than the energies at which other determinations have been carried out. Important questions are, of course, what future data or theory improvements might produce a reduction in the error on the current best result, equation (3.11), and how to test the assumed NP behavior of the spectral function around and below the τ mass. As we will now discuss, the best prospect for improvement appears to be from future, more precise data for hadronic τ decays.

Improved τ data will allow for a reduction in the experimental part of the error on $\alpha_S(m_\tau^2)$, currently± 0.0065. The theory error in equation (3.11) has two (to some extent related) sources: the truncation of perturbation theory, and the unavoidable need to estimate NP effects. A calculation of the order-α_S^5 term in QCD perturbation theory would be interesting, given the sometimes slow convergence of $I^{(w)}(s_0)$ for typical weights w. On the nonperturbative side, increased data precision would allow more stringent tests, in particular of the DV contribution from equation (3.9). Subleading effects predicted by [126] might become accessible, and either further confirmation, or a breakdown of this representation of DVs would increase our ability to probe the limits on the potential precision of the strong-coupling determination from hadronic τ decays.

A further point, of relevance to improving tests of the reliability of the theoretical assumptions underlying the two FESR approaches, concerns how such tests should be carried out. In the past, overlapping experimental spectral integral and theory integral error bands were often taken as evidence of the compatibility of the underlying theory representation with data. Such a conclusion is, however, statistically unjustified since the theory errors, which result from a fit to the experimental spectral integrals, are necessarily very strongly correlated with their experimental counterparts. Plotting both, and interpreting their overlap as if the two were independent runs the risk of serious double counting. To properly test underlying theory assumptions, it is crucial to make comparisons that account for not just correlations between the spectral integrals at different s_0 and theory integrals at different s_0, but also those between fitted theory and experimental integrals.

While FCC-ee would produce τ-leptons copiously [139, 140], the best near-future prospect is Belle-II [141], which has access to many more τ-leptons than were produced at LEP. Our construction of the new inclusive V spectral function, moreover, suggests a clear path forward: *no fully-inclusive spectral function* needs to be obtained from Belle-II data. Residual-mode contributions (which, though representing only 2% of the inclusive total by BF, are important in the upper part of the τ kinematic range) have already been brought under good control using CVC and electroproduction data [121]. More precise 2-pion and 4-pion exclusive-mode τ data would thus suffice to produce a new $I=1$ V spectral function with even smaller errors than those of [121], and hence to reduce the experimental error in equation (3.11). Details will need to be carefully considered. For instance, while the existing Belle unit-normalized 2-pion distribution is more precise than that of ALEPH or OPAL, the $\tau\to\pi^-\pi^0\nu_\tau$ BF has been measured less well by Belle, with the HFLAV [142] value still dominated by ALEPH. An improved, BF-normalized 2-pion distribution will thus require combining input from different experiments. The situation is, presumably, similar for the two 4-pion modes.

Acknowledgments—DB is supported by the São Paulo Research Foundation (FAPESP) Grant No. 2021/06756-6, by CNPq Grant No. 309847/2018-4, and by the Coordenação de Aperfeiçoamento de Pessoal de Nível Superior—Brazil (CAPES)—Finance Code 001. MG is supported by the U.S. Department of Energy, Office of Science, Office of High Energy Physics, under Award No. DE-SC0013682. KM is supported by a grant from the Natural Sciences and Engineering Research Council of Canada. SP is supported by the Spanish Ministry of Science, Innovation and Universities (project PID2020-112965GB-I00/AEI/

10.13039/501100011033). IFAE is partially funded by the CERCA program of the Generalitat de Catalunya.

3.3. Extraction of α_S using Borel–Laplace sum rules for tau decay data[74]

The application of double-pinched Borel–Laplace sum rules to ALEPH τ-decay data is discussed. For the leading-twist ($D = 0$) Adler function a renormalon-motivated extension is used, and the 5-loop coefficient is taken to be $d_4 = 275 \pm 63$. Two $D = 6$ terms appear in the truncated OPE ($D \leqslant 6$) to enable cancellation of the corresponding renormalon ambiguities. Two variants of the fixed order perturbation theory, and the inverse Borel transform, are applied to the evaluation of the $D = 0$ contribution. The truncation index N_t is fixed by the requirement of local insensitivity of the momenta $a^{(2,0)}$ and $a^{(2,1)}$ under variation of N_t. The averaged value of the coupling obtained is $\alpha_S(m_\tau^2) = 0.3235^{+0.0138}_{-0.0126}$ (corresponding to $\alpha_S(m_Z^2) = 0.1191 \pm 0.0016$). The theoretical uncertainties are significantly larger than the experimental ones.

The sum rule corresponding to the application of the Cauchy theorem to a contour integral containing the (u-d) quark $V + A$ correlator $\Pi(Q^2)$ ($Q^2 \equiv -q^2$) and a weight function $g(Q^2)$, $\oint_{C_1+C_2} dQ^2 g(Q^2)\Pi(Q^2) = 0$, gives the sum rule

$$\int_0^{\sigma_m} d\sigma g(-\sigma)\omega_{\rm exp}(\sigma) = \frac{1}{2\pi}\int_{-\pi}^{\pi} d\phi\ \mathcal{D}_{\rm th}(\sigma_m e^{i\phi})G(\sigma_m e^{i\phi}), \tag{3.14}$$

where $\sigma_m \equiv \sigma_{\rm max}$ is the maximal used energy in the data, and $\omega(\sigma)_{\rm exp}$ is the ALEPH-measured discontinuity (spectral) function of the $(V + A)$-channel polarization function

$$\omega(\sigma) \equiv 2\pi\ {\rm Im}\ \Pi(Q^2 = -\sigma - i\epsilon). \tag{3.15}$$

The function $g(Q^2)$ is the double-pinched Borel–Laplace weight function

$$g_{M^2}(Q^2) = \left(1 + \frac{Q^2}{\sigma_m}\right)^2 \frac{1}{M^2}\exp\left(\frac{Q^2}{M^2}\right), \tag{3.16}$$

$G(Q^2)$ is the integral of g

$$G(Q^2) = \int_{-\sigma_m}^{Q^2} dQ'^2 g(Q'^2), \tag{3.17}$$

and $\mathcal{D}_{\rm th}(Q^2)$ is the full Adler function $\mathcal{D}(Q^2) \equiv -2\pi^2 d\Pi(Q^2)/d\ln Q^2$, whose OPE truncated at dimension $D = 6$ terms has the form

$$\mathcal{D}_{\rm th}(Q^2) = d(Q^2)_{D=0} + 1 + 4\pi^2\frac{\langle O_4\rangle}{(Q^2)^2} + \frac{6\pi^2}{(Q^2)^3}\left[\frac{\langle O_6^{(2)}\rangle}{a(Q^2)} + \langle O_6^{(1)}\rangle\right]. \tag{3.18}$$

Here, $a(Q^2) \equiv \alpha_S(Q^2)/\pi$. The two terms of $D = 6$ in the above OPE are needed to enable the cancellation of the corresponding $u = 3$ IR renormalon ambiguities originating from the $D = 0$ contribution $d(Q^2)_{D\ =\ 0}$. The latter contribution has the perturbation expansion

$$d(Q^2)_{D=0,{\rm pt}} = d_0 a(\kappa Q^2) + d_1(\kappa)\ a(\kappa Q^2)^2 + \ldots + d_n(\kappa)\ a(\kappa Q^2)^{n+1} + \ldots, \tag{3.19}$$

where $\kappa \equiv \mu^2/Q^2$ is the renormalization scale parameter ($0 < \kappa \lesssim 1$; usually $\kappa = 1$), the first four terms ($d_0 = 1$; d_1, d_2, d_3) are exactly known [100], and for the coefficient d_4 [$\equiv d_4(\kappa)$ with $\kappa = 1$ and $N_f = 3$] we take the following values based on various specific estimates in the

[74] Authors: C Ayala (U Tarapacá), G Cvetič (UTFSM, Valparaiso), D Teca (UTFSM, Valparaiso).

literature [100, 117, 143–145]:

$$d_4 = 275 \pm 63. \tag{3.20}$$

The expansion of the Borel transform of $d(Q^2)_{D\,=\,0}$ is $\mathcal{B}[d](u;\,\kappa)_{\rm ser.} = \sum_{n\geqslant 0} d_n(\kappa) u^n/n!/\beta_0^n$. The extension of $d(Q^2)_{D\,=\,0}$ beyond $\sim a^5$ is performed with a renormalon-motivated model [145] in which the Borel transform is constructed first for an auxiliary quantity $\widetilde{d}(Q^2)$ of the Adler function [145], resulting in the Borel transform $\mathcal{B}[d](u)$ having terms $\sim 1/(2-u)^{\widetilde{\gamma}_2}$, $1/(3-u)^{\widetilde{\gamma}_3\,+\,1}$, $1/(3-u)^{\widetilde{\gamma}_3}$ and $1/(1+u)^{1+\overline{\gamma}_1}$, and similar terms with lesser powers, where $\widetilde{\gamma}_p = 1 + p\beta_1/\beta_0^2$ ($\overline{\gamma}_p = 1 - p\beta_1/\beta_0^2$), and $\beta_0 = (11 - 2N_f/3)/4$ and $\beta_1 = (1/16)(102 - 38N_f/3)$ are the first two β-function coefficients ($N_f = 3$).[75] This extension gives, for the choice $d_4 = 275.$, the coefficients of the expansion (3.19): $d_5 = 3159.5$; $d_6 = 16136.$; $d_7 = 3.4079 \times 10^5$; $d_8 = 3.7816 \times 10^5$; $d_9 = 6.9944 \times 10^7$; $d_{10} = -5.8309 \times 10^8$; etc.

The cancellation of the IR renormalon ambiguity requires: (i) for $u = 2$ IR renormalon term $\mathcal{B}[d](u) \sim 1/(2-u)^{\widetilde{\gamma}_2}$, the $D = 4$ OPE term of the Adler function to be of the form $1/(Q^2)^2$; (ii) for the $u = 3$ IR renormalon term $\mathcal{B}[d](u) \sim 1/(3-u)^{\widetilde{\gamma}_3}$ to be of the form $1/(Q^2)^3$; (iii) and for the $u = 3$ IR renormalon term $\mathcal{B}[d](u) \sim 1/(3-u)^{\widetilde{\gamma}_3\,+\,1}$ to be of the form $1/(Q^2)^3/a(Q^2)$. These three terms ($D = 4$, 6) are taken into account in the OPE (3.18).

The $D = 0$ contribution $d(Q^2)_{D\,=\,0}$ to the Adler function in the sum rule contour integral (3.14) is evaluated in three different ways. We apply two variants of fixed order perturbation theory (FOPT). In the first variant, the powers of $a(\kappa\sigma_{\rm m}e^{i\phi})^n$ are expressed as truncated Taylor series in powers of $a(\kappa\sigma_{\rm m})$ (FO). In the second variant, $d(Q^2)_{D\,=\,0}$ is expressed as the sum of the logarithmic derivatives $\widetilde{a}_n(Q^2)$ [$\propto (d/d\ln Q^2)^{n-1} a(Q^2)$], and then $\widetilde{a}_n(\kappa\sigma_{\rm m}e^{i\phi})$ are expressed as truncated Taylor series of $\widetilde{a}_k(\kappa\sigma_{\rm m})$ ($\widetilde{\rm FO}$). The third way of evaluation is the use of the inverse Borel transformation of $d(Q^2)_{D\,=\,0}$, where the Borel integral is evaluated with the Principal Value (PV) prescription; in the integrand, the Borel transform $\mathcal{B}[d](u)$ is taken as as a series consisting of the mentioned (renormalon-related) inverse powers $\sim (p-u)^k/(p-u)^\gamma$ ($k = 0,\,1,\,\ldots$), where the series is truncated; this truncation requires for $d(\sigma_{\rm m}e^{i\phi})_{D\,=\,0}$ introduction of an additional correction polynomial $\delta d(\sigma_{\rm m}e^{i\phi})^{[N_t]}_{D\,=\,0}$ in powers of $a(Q^2)$. In all the three methods, a truncation index N_t is involved, i.e. only the terms up to the power a_t^N (or $\widetilde{a}_{N_t}$ in $\widetilde{\rm FO}$) are taken into account.

We apply the Laplace–Borel sum rules, with the weight function (3.16), to the ALEPH $V+A$ data with $\sigma_{\rm max}(\equiv\sigma_{\rm m}) = 2.8\,{\rm GeV}^2$ (i.e. the last two bins are excluded due to large uncertainties). In the sum rule (3.14), this gives on both sides the Borel–Laplace sum rule quantity $B(M^2;\sigma_{\rm m})$. In practice, the rule is applied to the real parts only, ${\rm Re}\,B_{\rm exp}(M^2;\,\sigma_{\rm m}) = {\rm Re}\,B_{\rm th}(M^2;\,\sigma_{\rm m})$, and for the scale parameters M^2 along rays in the first quadrant: $M^2 = |M^2|\exp(i\Psi)$ with $0 \leqslant \Psi < \pi/2$. We minimise (with respect to α_S, $\langle O_4\rangle$, $\langle O_6^{(1)}\rangle$ and $\langle O_6^{(2)}\rangle$) the following sum of squares:

$$\chi^2 = \sum_{\alpha=0}^{n} \left(\frac{{\rm Re}\,B_{\rm th}(M_\alpha^2;\,\sigma_{\rm m}) - {\rm Re}\,B_{\rm exp}(M_\alpha^2;\,\sigma_{\rm m})}{\delta_B(M_\alpha^2)} \right)^2, \tag{3.21}$$

where $\{M_\alpha^2\}$ was taken as a dense set of points along the chosen rays with $\Psi = 0$, $\pi/6$, $\pi/4$ and $0.9\,{\rm GeV}^2 \leqslant |M_\alpha|^2 \leqslant 1.5\,{\rm GeV}^2$. We chose 11 equidistant points along each of the three rays, and the series (3.21) thus contains 33 terms (the fit results remain practically unchanged

[75] In our ansatz [145] and notation, the effective one-loop $D = 6$ anomalous dimensions $-\gamma^{(1)}_{O_6}/\beta_0$ (appearing beside $\widetilde{\gamma}_3$ in the mentioned powers $\widetilde{\gamma}_3 - \gamma^{(1)}_{O_6}/\beta_0$) were taken to be large-β_0, i.e. $-\gamma^{(1)}_{O_6}/\beta_0 = 1,\,0$. The work [146] implies that these quantities can be evaluated beyond large-β_0, resulting in a decreasing sequence of nine numbers $-\gamma^{(1)}_{O_6}/\beta_0 \approx -0.197;\,-0.247;\ldots$. It remains an open question how to extend the renormalon-motivated [145] model to include these results.

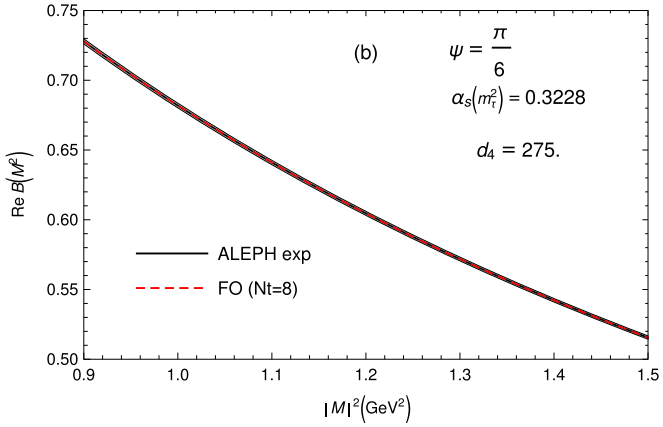

Figure 10. The values of $\mathrm{Re}\,B(M^2;\sigma_\mathrm{m})$ along the ray $M^2 = |M^2|\exp(i\Psi)$ with $\Psi = \pi/6$. The narrow grey band are the experimental predictions. The red dashed line inside the band is the result of the FOPT global fit with truncation index $N_t = 8$. Similar fitting curves are obtained for the rays with $\Psi = 0$ and $\Psi = \pi/4$.

when the number of points is increased). In the sum (3.21), the quantities $\delta_B(M_\alpha^2)$ are the experimental standard deviations of $\mathrm{Re}\,B_\mathrm{exp}(M_\alpha^2;\sigma_\mathrm{m})$, with the ALEPH covariance matrix for the $(V+A)$-channel taken into account (see appendix C of [147] for more explanation). For each evaluation method (FO, $\widetilde{\mathrm{FO}}$, PV) and for each chosen truncation index N_t, the fit procedure gives us results, and the fit is usually of good quality, $\chi^2 \lesssim 10^{-3}$ (figure 10).

The truncation index N_t is then fixed by considering the first two double-pinched momenta $a^{(2,0)}(\sigma_\mathrm{m})$ and $a^{(2.1)}(\sigma_\mathrm{m})$[76] and requiring local stability of their values under the variation of N_t. The resulting extracted values of the coupling are

$$\begin{aligned}\alpha_S(m_\tau^2)^{(\mathrm{FO})} &= 0.3228 \pm 0.0003\,(\mathrm{exp})^{-0.0026}_{+0.0070}\,(\kappa)^{-0.0103}_{+0.0079}(d_4)^{+0.0081}_{-0.0057}(N_t)\\ &= 0.3228^{+0.0134}_{-0.0121} \approx 0.323^{+0.013}_{-0.012} \qquad (N_t = 8^{+2}_{-3}).\end{aligned} \tag{3.22}$$

$$\begin{aligned}\alpha_S(m_\tau^2)^{(\widetilde{\mathrm{FO}})} &= 0.3209 \pm 0.0003\,(\mathrm{exp})^{-0.0038}_{+0.0201}\,(\kappa)^{-0.0039}_{+0.0047}(d_4)^{+0.0293}_{-0.0084}(N_t)\\ &= 0.3209^{+0.0359}_{-0.0100} \approx 0.321^{+0.036}_{-0.010} \qquad (N_t = 5 \pm 2).\end{aligned} \tag{3.23}$$

$$\begin{aligned}\alpha_S(m_\tau^2)^{(\mathrm{PV})} &= 0.3269 \pm 0.0003\,(\mathrm{exp})^{+0.0007}_{+0.0102}(\kappa)^{-0.0064}_{+0.0155}(d_4)^{+0.0092}_{-0.0006}(N_t)^{+0.0167}_{-0.0067}(\mathrm{amb})\\ &= 0.3269^{+0.0266}_{-0.0093} \approx 0.327^{+0.027}_{-0.009} \qquad (N_t = 8^{+2}_{-3}).\end{aligned} \tag{3.24}$$

$$\begin{aligned}\alpha_S(m_\tau^2)^{(\mathrm{CI})} &= 0.3488 \pm 0.0005\,(\mathrm{exp})^{+0.0078}_{+0.0004}(\kappa) \pm 0.0000(d_4)^{-0.0027}_{+0.0119}(N_t)\\ &= 0.3488^{+0.0142}_{-0.0028} \approx 0.349^{+0.014}_{-0.003} \qquad (N_t = 4^{+2}_{-1}).\end{aligned} \tag{3.25}$$

The uncertainties are presented as separate terms. The variation of the renormalization scale parameter $\kappa \equiv \mu^2/Q^2$ was taken in the range $2/3 \leqslant \kappa \leqslant 2$ ($\kappa = 1$ for the central values). The truncation index is $N_t = 8$, 5, 8 for the central cases of FO, $\widetilde{\mathrm{FO}}$ and PV.

[76] The weight functions for double-pinched momenta $a^{(2,n)}$ are: $g^{(2,n)}(Q^2) = ((n+3)/(n+1))(1/\sigma_\mathrm{m})(1 + Q^2/\sigma_\mathrm{m})^2\sum_{k=0}^{n}(k+1)(-1)^k(Q^2/\sigma_\mathrm{m})^k$. The obtained values of $a^{(2,0)}(\sigma_\mathrm{m})$ and $a^{(2.1)}(\sigma_\mathrm{m})$ are well within the experimental band.

The (truncated) Contour Improved perturbation theory (CIPT) results are also included in the above results, for comparison. However, the truncated CIPT approach for $d(Q^2)_{D\,=\,0}$ evaluation appears to require a different type of OPE in the $D > 0$ part of the contributions, because the renormalon structure and the related renormalon ambiguities are not reflected in the truncated CIPT series [120]. We thus include only FO, $\widetilde{\text{FO}}$ and PV results in the average

$$\begin{aligned} \alpha_S(m_\tau^2) &= 0.3235^{+0.0138}_{-0.0126} \qquad (\text{FO} + \widetilde{\text{FO}} + \text{PV}) \\ \Rightarrow\ \alpha_S(m_Z^2) &= 0.1191 \pm 0.0016. \end{aligned} \tag{3.26}$$

In table 6 we compare these results with some other in the literature.

The results (3.26) can be significantly affected when the assumptions or methods are changed. For example, if we chose, instead of the central value $d_4 = 275.$, the upper upper bound $d_4 = 338.$ of equation (3.20) as the central value, the results would decrease somewhat, to $\alpha_S(m_\tau^2) \approx 0.320 \pm 0.015$ (corresponding to $\alpha_S(m_Z^2) \approx 0.1187^{+0.0016}_{-0.0019}$), i.e. $\delta\alpha_S(m_\tau^2) \approx -0.0004$. If we took, instead of the two mentioned $D = 6$ terms in the OPE, the simple $D = 6$ and $D = 8$ OPE terms [$\sim 1/(Q^2)^3$ and $\sim 1/(Q^2)^4$], the central value would decrease by about $\delta\alpha_S(m_\tau^2) \approx -0.008$. In our previous work [136] we used the OPE with simple $D = 6{,}8$ terms, and took for d_4 higher values $d_4 = 338 \pm 63$ than here equation (3.20). If we took $N_t = 5$ in all three methods (i.e. no extension of Adler function beyond $d_4 a^5$), then the central value of $\alpha_S(m_\tau^2)$ in FO changes from 0.3288 to 0.3171, and in PV from 0.3269 to 0.3277 $\Rightarrow$ for the average of the three methods the central value changes from 0.3235 to 0.3219 (correspondingly, $\alpha_S(m_Z^2)$ goes from 0.1191 to 0.1189), i.e. $\delta\alpha_S(m_\tau^2) = -0.0016 \approx -0.002$, smaller.

According to the results (3.22)–(3.24), Borel–Laplace sum rules indicate that the theoretical uncertainties dominate over the experimental ones. Even if maximally strong correlations were assumed among the experimental Borel–Laplace sum rule values at different M_α^2, the presented experimental uncertainty of α_S would increase by a factor of less than five. Part of these theoretical uncertainties would be reduced by: (1) the calculation of the five-loop Adler function coefficient d_4; (2) the use of the more complicated structure of the $D = 6$ OPE terms [146] and the corresponding terms in the $D = 0$ $u = 3$ IR renormalon structure; (3) the use of a variant of the QCD coupling $a(Q^2)$ without the Landau singularities in the $D = 0$ contribution, because this would allow for the resummation to all orders (no truncation) of the renormalon-motivated contribution $D = 0$ and would eliminate the renormalization scale ambiguity (κ). The high precision ALEPH determination of the τ spectral function represents an important source of data for better understanding the behaviour of QCD at the limit between the perturbative and nonperturbative regimes.

3.4. Reconciling the fixed order and contour improved perturbative series in hadronic τ decays[77]

In [122, 149] an approach was proposed to reconcile the long-standing discrepancy between the fixed order (FOPT) and contour improved (CIPT) pQCD expansions of hadronic spectral function moments relevant for the precise determination of α_S from τ decays. This is achieved by a simple change of scheme of the gluon condensate matrix element so that it becomes renormalon-free. The technical aspects of the scheme change are similar to the well-known implementation of short-distance mass schemes for massive-quark-sensitive observables. The scheme relies on external knowledge about the gluon condensate renormalon norm and is

[77] Authors: M A Benitez-Rathgeb (U Vienna), D Boito (U Vienna and U Sao Paulo), A H Hoang (U Vienna and E Schrödinger Inst. for Math Phys.), M Jamin (U Vienna and Heidelberg Univ.).

Table 6. $\alpha_S(m_\tau^2)$ values extracted by various groups from ALEPH τ-decay data applying sum rules and other methods.

Group	Sum rule	FO	CI	PV	Average
Baikov *et al*. 2008 [100]	$a^{(2,1)} = r_\tau$	0.322 ± 0.020	0.342 ± 0.011	—	0.332 ± 0.016
Beneke and Jamin, 2008 [117]	$a^{(2,1)} = r_\tau$	$0.320^{+0.012}_{-0.007}$	—	0.316 ± 0.006	0.318 ± 0.006
Caprini, 2020 [148]	$a^{(2,1)} = r_\tau$	—	—	0.314 ± 0.006	0.314 ± 0.006
Davier *et al*. 2013 [103]	$a^{(i,j)}$	0.324	0.341 ± 0.008	—	0.332 ± 0.012
Pich and Sánchez, 2016 [104]	$a^{(i,j)}$	0.320 ± 0.012	0.335 ± 0.013	—	0.328 ± 0.013
Boito *et al*. 2014 [132]	DV in $a^{(i,j)}$	0.296 ± 0.010	0.310 ± 0.014	—	0.303 ± 0.012
Our prev. work, 2021 [136]	BL (O_6, O_8)	0.308 ± 0.007	—	$0.316^{+0.008}_{-0.006}$	0.312 ± 0.007
This work, 2022 (also [114])	BL ($O_6^{(1)}$, $O_6^{(2)}$)	$0.323^{+0.013}_{-0.012}$(FO) $0.321^{+0.021}_{-0.030}(\widetilde{\text{FO}})$	—	$0.327^{+0.027}_{-0.009}$	0.324 ± 0.013

capable of resolving the long-standing discrepancy between FOPT and CIPT predictions, under the assumption that the gluon condensate renormalon gives a sizeable contribution to QCD perturbative coefficients at the accessible intermediate orders. The approach is briefly outlined in the following. For details we refer to [122, 149].

As outlined in section 3.2, strong coupling determinations from hadronic τ decay data are based on weighted integrals of the experimental spectral functions with an upper bound $s_0 \leqslant m_\tau^2$ and to integrals of the QCD Adler function over a closed contour in the complex momentum plane. For the latter one must set the renormalization scale in α_S when performing the contour integrals. The two widely used prescriptions are based on FOPT and CIPT. In FOPT, the renormalization scale is fixed at $\mu^2 = s_0$, which leads to a power series in $\alpha_S(s_0)$. In CIPT, the scale is tied to the contour's momentum variable such that logarithms related to the QCD β-function are summed, so that the resulting series is not any more a power series in α_S. These two expansion methods exhibit a sizeable discrepancy at orders $\mathcal{O}(\alpha_S^4)$ and $\mathcal{O}(\alpha_S^5)$ that is larger than the individual renormalization scale variations. As a consequence, α_S determinations based on CIPT tend to yield higher values than those based on FOPT. This discrepancy has been one of the main sources of theory uncertainty in α_S from τ decays.

In [119, 120], Hoang and Regner suggested that the discrepancy is of infrared (IR) origin and largely dominated by the leading IR renormalon of the massless-quark QCD Adler function, which is associated with the gluon condensate (GC). This entails that, once this renormalon is subtracted from the Adler function's perturbation series, the truncated series of the two expansion methods should yield more consistent values already at intermediate orders, reducing the theoretical uncertainty in the extractions of α_S. In [122, 149] a concrete subtraction method of the gluon condensate renormalon was devised and its practical value was demonstrated.

The subtraction method is based on two premises. First, it is assumed that the GC renormalon gives a sizeable contribution to the Adler function's perturbative coefficients at intermediate orders ($\mathcal{O}(\alpha_S^3)$ to $\mathcal{O}(\alpha_S^5)$). This assumption can be considered as natural, since the GC represents the leading IR sensitivity. It is also supported by all-order results in the large-β_0 limit and by renormalon models [117, 118] built for the Adler function in QCD. Second, our framework relies on the fact that the OPE condensate corrections not only provide nonperturbative corrections but also compensate for the associated factorial renormalon growth of the perturbative series coefficients, thus leading to an unambiguous theoretical description. The first premise is important. If it were not true, the CIPT-FOPT discrepancy problem would be unrelated to IR renormalons and no information on the norm of the GC renormalon could be gained from the known QCD corrections for the Adler function. The second premise is an established characteristics of multiloop QCD calculations in the limit of vanishing IR cutoff, where sensitivities to IR momenta are a cause of QCD perturbation series to be asymptotic. Since this is the common approach for the loop corrections for inclusive quantities based on dimensional regularization and the $\overline{\rm MS}$ scheme for the strong coupling, we call this approach to regularize IR momenta '$\overline{\rm MS}$ scheme' as well. This should not be confused with the $\overline{\rm MS}$ scheme for α_S, which refers to the regularization of UV momenta. The concrete analytic expressions shown in this subsection below actually use the strong coupling in the C scheme (for the concrete value $C = 0$) [150], referred to as $\bar{\alpha}_S$ below. (See the appendix of [122] for concrete formulae to obtain the results for the strong coupling in the $\overline{\rm MS}$ scheme.)

In heavy-quark physics, it is well established that the leading (linear) IR sensitivity that arises in the pole mass renormalization scheme can be eliminated by switching to short-distance mass schemes [8, 151]. In [122, 149] a similar approach is proposed for the GC matrix element. One starts from the operator product expansion (OPE) for the massless quark

Adler function. Using the $\overline{\text{MS}}$ scheme (to regularize IR momenta), it can be cast in the form (using $\mu^2 = -s$ as renormalization scale for the strong coupling)

$$D(s) = \sum_{n=1}^{\infty} \bar{c}_{n,1} \left(\frac{\bar{\alpha}_S(-s)}{\pi} \right)^n + \frac{C_{4,0}(\bar{\alpha}_S(-s))}{s^2} \langle \bar{\mathcal{O}}_{4,0} \rangle + \sum_{d=6}^{\infty} \frac{1}{(-s)^{d/2}} \sum_i C_{d,i}(\bar{\alpha}_S(-s)) \langle \bar{\mathcal{O}}_{d,\gamma_i} \rangle, \tag{3.27}$$

where the first term is the perturbative contribution, and the $1/s$ OPE power corrections, starting from the term with $d = 4$, are the nonperturbative corrections. The perturbative coefficients $\bar{c}_{n,1}$ are exactly known up $\mathcal{O}(\alpha_S^4)$ [100, 152]. It is customary to also include an estimate for the $\mathcal{O}(\alpha_S^5)$ coefficient $\bar{c}_{5,1}$ in phenomenological analyses [104, 121, 132, 136]. The terms $\langle \bar{\mathcal{O}}_{d,\gamma_i} \rangle$ are nonperturbative vacuum matrix elements (condensates) and the $C_{d,i}$ are the respective Wilson coefficients which are a power series in $\alpha_S(-s)$. The bar over the operator indicates that the condensates are defined in the $\overline{\text{MS}}$ scheme (to regularize IR momenta).

The leading $d = 4$ OPE power correction arises from the GC and is central to this work. It can be cast in terms of the renormalization scale invariant GC matrix element $\langle \bar{G}^2 \rangle$ as ($\bar{a}(-s) \equiv \beta_0 \, \bar{\alpha}_S(-s)/(4\pi)$, $\beta_0 = 11 - 2N_f/3$)

$$\delta D_{4,0}^{\text{OPE}}(s) = \tfrac{1}{s^2} \frac{2\pi^2}{3} \left[1 - \frac{22}{81} \, \bar{a}(-s) \right] \langle \bar{G}^2 \rangle. \tag{3.28}$$

Associated with the GC OPE correction is a renormalon singularity in the Borel function of the Adler function that has the form

$$B_{4,0}(u) = \left[1 - \frac{22}{81} \, \bar{a}(-s) \right] \frac{N_{4,0}}{(2-u)^{1+4\hat{b}_1}}, \tag{3.29}$$

where $N_{4,0}$ is the Adler function's GC renormalon norm and $\hat{b}_1 = \beta_1/2\beta_0^2$, with β_1 being the two-loop QCD β-function coefficient. This GC renormalon singularity contributes to the Adler function's perturbative series coefficients $\bar{c}_{n,1}$ in the form

$$\delta \hat{D}_{4,0}(s) = N_{4,0} \left[1 - \frac{22}{81} \, \bar{a}(-s) + \ldots \right] \sum_{n=1}^{\infty} r_n^{(4,0)} \, \bar{a}(-s)^n, \tag{3.30}$$

where the terms $r_n^{(4,0)} = 2^{-(n+4\hat{b}_1)} \Gamma(n + 4\hat{b}_1)/\Gamma(1 + 4\hat{b}_1)$ diverge factorially. The use of the C-scheme [150] is convenient because the term $1/(2-u)^{1 \, + \, 4\hat{b}_1}$ in $B_{4,0}(u)$ and the coefficients $r_n^{(4,0)}$ in $\delta \hat{D}_{4,0}(s)$ are exact, i.e. they do not receive any further higher-order corrections. The first premise entails that $N_{4,0}$ is sufficiently sizeable, such that the series in $\delta \hat{D}_{4,0}(s)$ makes up for a sizeable contribution in the coefficients $\bar{c}_{n,1}$ at the intermediate orders relevant for phenomenological analyses. In the context of this assumption it has already been shown in [119, 120], that the FOPT-CIPT discrepancy can be caused by the diverging Adler function series contributions given in $\delta \hat{D}_{4,0}(s)$.

Let us now turn to the construction of the renormalon-free (RF) gluon condensate scheme. The RF scheme only deals with the GC renormalon; all other renormalons are strictly unaltered. The starting point is by imposing that the order-dependence of $\langle \bar{G}^2 \rangle$ that compensates the factorial growth of the coefficients in equation (3.30) is made explicit, while maintaining the generic form of the GC OPE correction in equation (3.28). The relation between the original, order dependent, $\overline{\text{MS}}$ GC matrix element and a new renormalon-free GC matrix element, $\langle G^2 \rangle(R^2)$, is then

$$\langle \bar{G}^2 \rangle^{(n)} \equiv \langle G^2 \rangle(R^2) - R^4 \sum_{\ell=1}^{n} N_g \, r_\ell^{(4,0)} \, \bar{a}_R^\ell, \tag{3.31}$$

where $\bar{a}_R \equiv \beta_0\, \bar{\alpha_S}(R^2)/(4\pi)$ and the order dependence on the left-hand side has been made explicit. The term N_g is the universal GC renormalon norm, related to $N_{4,0}$ by $N_g = 3N_{4,0}/(2\pi^2)$. The condensate $\langle G^2\rangle(R^2)$ depends explicitly on the scale R, which sets its parametric size to be $\mathcal{O}(R^4)$ (instead of $\mathcal{O}(\Lambda^4_{\rm QCD})$ for the $\overline{\rm MS}$ GC $\langle \bar{G}^2\rangle^{(n)}$). The scale R plays the role of an IR factorization scale which can in principle be chosen arbitrarily. In practice, its value should be chosen smaller, but still of the order of, the typical dynamical scale of the observable of interest to avoid the appearance of (or, equivalently, to sum potentially) large logarithms. The dependence of $\langle G^2\rangle(R^2)$ on R is controlled by an R-evolution equation [153] (see [122] for its precise form).

From a practical perspective, the R dependence of $\langle G^2\rangle(R^2)$ is somewhat inconvenient. Therefore, in a second constructive step, a scale-invariant renormalon-free GC matrix element is defined. This is achieved by the addition of a function which obeys the same R-evolution equation as $\langle G^2\rangle(R^2)$. This is possible because the R-derivative of the subtraction series on the r.h.s. of equation (3.31) is convergent for $n \to \infty$. Such a function is obtained from the Borel sum of the subtraction series, defined through the principal value (PV) prescription:

$$\bar{c}_0(R^2) \equiv R^4\ \mathrm{PV}\int_0^\infty \frac{\mathrm{d}u}{(2-u)^{1+4\hat{b}_1}}\, e^{-\frac{u}{\bar{a}_R}}. \tag{3.32}$$

The result for $\bar{c}_0(R^2)$ can be given in closed analytic form [122]. Thus one can define a scale invariant renormalon-free GC matrix element, denoted as $\langle G^2\rangle^{\rm RF}$, by

$$\langle G^2\rangle(R^2) \equiv \langle G^2\rangle^{\rm RF} + N_g\, \bar{c}_0(R^2). \tag{3.33}$$

We denote as $\langle G^2\rangle^{\rm RF}$ the GC in the 'RF scheme'. The particular forms of the subtraction series in equation (3.31) and the function $c_0(R^2)$ are particular choices to define the RF scheme, but may in principle be chosen differently. In general, the subtraction must have the correct large order behavior to eliminate the factorial growth of the coefficients $r_n^{(4,0)}$, but could have additional convergent contributions. This would then imply a different form for $\bar{c}_0(R^2)$. Moreover, one could also add an additional constant to $\bar{c}_0(R^2)$. The RF scheme entails that the difference between the original $\overline{\rm MS}$ GC and the new scale-independent RF GC, $\langle G^2\rangle^{\rm RF}$, is formally $\mathcal{O}(\bar{a}_R^{n+1})$. In this sense, the modifications to the GC in our new RF scheme are minimal.

Using equations (3.33) and (3.28), it is straightforward to write down the resulting perturbation series for the Adler function in the RF GC scheme. Treating the term proportional to $\bar{c}_0(R^2)$, which is part of the definition of $\langle G^2\rangle^{\rm RF}$, like a tree-level contribution, the perturbation series has the form: ($\bar{c}_n \equiv 4\bar{c}_{n,1}/\beta_0$ for $n = 1, 2, \ldots$)

$$\begin{aligned}\hat{D}^{\rm RF}(s, R^2) = \tfrac{1}{s^2}&\left[1 - \frac{22}{81}\bar{a}(-s)\right] N_{4,0}\, \bar{c}_0(R^2) + \sum_{n=1}^{\infty} \bar{c}_n\, \bar{a}^n(-s)\\ &- \left[1 - \frac{22}{81}\,\bar{a}(-s)\right] N_{4,0}\, \frac{R^4}{s^2}\sum_{n=1}^{\infty} r_n^{(4,0)}\bar{a}_R^{\ell}.\end{aligned} \tag{3.34}$$

It is essential to reexpand and truncate the perturbative series terms (excluding the $\bar{c}_0$ term) coherently, using the strong coupling at a common renormalization scale. Only then the cancellation of the GC renormalon is realized is a consistent way. The treatment of the 'tree-level' term proportional to $\bar{c}_0(R^2)$ entails that the GC OPE correction retains its form of equation (3.28) with $\langle \bar{G}^2\rangle$ replaced by $\langle G^2\rangle^{\rm RF}$. Furthermore, it is possible to show that the Borel sum of the perturbation series for the RF scheme Adler function $\hat{D}^{\rm RF}(s, R^2)$ based on the PV prescription (as shown in equation (3.32)) remains the same as that of the original $\overline{\rm MS}$ scheme Adler function $\hat{D}(s) = \sum_{n=1}^{\infty} \bar{c}_n \bar{a}^n(-s)$ independently of the value of N_g (or $N_{4,0}$)

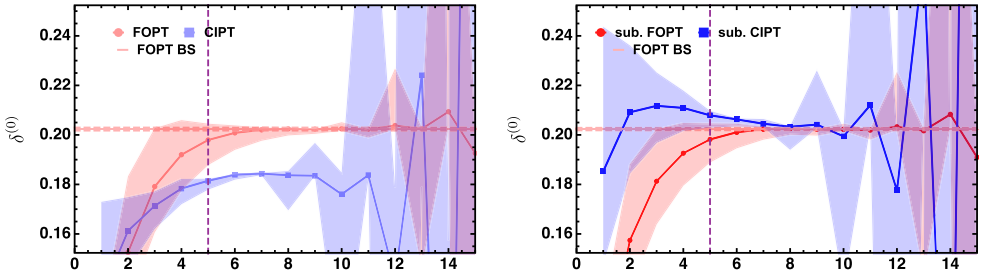

Figure 11. Left: series for the perturbative FOPT and CIPT expansions of the τ hadronic decay width order by order in full QCD in the $\overline{\text{MS}}$ GC scheme. The orders beyond 5 are obtained from a Borel model. Renormalization scale variations are indicated by the coloured bands. Right: corresponding series for FOPT and CIPT expansions for $\delta_W^{(0)}(m_\tau^2, R^2)$ in the RF GC scheme for $R = 0.8\, m_\tau$. The results are shown for $\alpha_S(m_\tau^2) = 0.315$ (in the $\overline{\text{MS}}$ scheme) and $N_\text{f} = 3$. The figures are taken from [122].

and the choice for R. Variations of R therefore vanish in the limit of larger-order truncations. The value of norm N_g is an input to the RF scheme that must be supplemented independently.

In [122], the effectiveness of the RF scheme for the perturbation series of the hadronic τ decay width has been demonstrated. In the following we quote some results given in [122], where the known QCD corrections up to $\mathcal{O}(\alpha_S^4)$ have been included and an estimate for the 6-loop coefficient $\bar{c}_{5,1}$, consistent with the values used in the recent analyses [104, 121, 132, 136] has been employed. In addition, corrections from beyond $\mathcal{O}(\alpha_S^5)$ were considered from a renormalon Borel model for the Adler function, based on the works of [117, 118], which has been shown there to be realistic within the first premise mentioned above. The model provides the concrete value $N_g = 0.64$, so that the decay width series in the RF scheme can be studied in a concrete way. In the left panel of figure 11, the results for FOPT (red) and CIPT (blue) are shown in the $\overline{\text{MS}}$ scheme for the GC. The vertical dashed line indicates the order up to which current state-of-the phenomenological analyses are carried out (including the concrete perturbative coefficients up to 6-loop), and for orders beyond the series relies on the renormalon model. The FOPT and CIPT series exhibit the well-known discrepancy at intermediate orders, which does not diminish with the successive inclusion of higher-order terms predicted by the model. In the context of the first premise, the results show that the discrepancy is systematic and not related to missing higher orders. The two series eventually run into the divergent behavior expected for asymptotic series. The right panel displays the results in the RF GC scheme for $R = 0.8\, m_\tau$. The FOPT series in the RF scheme is almost unaltered. This can be understood, since the decay width receives only a tiny contribution from the GC through the s-dependence of the Wilson coefficient's 1-loop correction and because the dominant part of the subtraction series in FOPT remains real-valued and factors out of the contour integral. The CIPT series, however, changes dramatically. This modification is by far larger than the tiny size of the GC OPE corrections itself. This is because the subtraction series needs to be expanded according to the CIPT prescription such that the contour integration modifies the contributions from the subtraction series in a non-trivial way. The fact that the resulting numerical effect is so large, corroborates the finding of [119, 120] that the CIPT series (in the $\overline{\text{MS}}$ GC scheme) is not compatible with the standard analytic form of OPE corrections shown in equation (3.27). Remarkably, in the RF GC scheme the discrepancy between the two series diminishes order by order and at $\mathcal{O}(\alpha_S^5)$ it is

already significantly reduced. For even higher orders (in the context of the Borel model), the two series become fully compatible and approach essentially the same value. The same observations are made for any other spectral function moment with a suppressed GC. At the same time, the convergence of the perturbation series for moments with an enhanced GC is substantially improved.

In [149] the practical value of the RF GC scheme in phenomenological analyses using the perturbative coefficients up to $\bar{c}_{5,1}$ was analyzed in detail. Is was shown that N_g can be determined with a relative uncertainty of 40%. Following the two recent state-of-the-art strong coupling determination analyses at $\mathcal{O}(\alpha_S^5)$ of [104] (in the tOPE approach) and [121] (in the DV-model approach) it was demonstrated that the RF GC scheme can successfully reconcile the extractions of $\alpha_S(m_\tau^2)$ based on CIPT and FOPT for both approaches to treat the non-perturbative corrections. The additional uncertainties that arise in the RF GC scheme due to variations of R and the uncertainty of N_g only lead to a small or moderate increase of the final uncertainty of $\alpha_S(m_\tau^2)$, and affect mainly the CIPT expansion results. The RF GC scheme thus constitutes a powerful new ingredient for future analyses of τ hadronic spectral function moments. Delicate issues such as the adequate treatment of nonperturbative corrections can now be studied without having to also deal with the CIPT-FOPT discrepancy problem.

Acknowledgments—DB and MJ would like to thank the Particle Physics Group of the University of Vienna for hospitality. We acknowledge partial support by the FWF Austrian Science Fund under the Doctoral Program 'Particles and Interactions' No. W1252-N27 and under the Project No. P32383-N27. DB's work was supported by the Coordenação de Aperfeiçoamento de Pessoal de Nível Superior—Brasil (CAPES)—Finance Code 001 and by the São Paulo Research Foundation (FAPESP) Grant No. 2021/06756-6.

4. $\alpha_S(m_Z^2)$ from DIS and parton densities

4.1. $\alpha_S(m_Z^2)$ through scheme-invariant evolution of N^{3}LO non-singlet structure functions[78]

We describe the measurement of the strong coupling constant $\alpha_S(m_Z^2)$ based on the scheme-invariant evolution of unpolarized and polarized flavour non-singlet structure functions at N^{3}LO accuracy with a precision at the subpercent level. Measurements of this kind can be performed at future facilities such as the EIC and LHeC, provided both proton and deuteron targets are used. The theory framework for this is already available. The measurement requires excellent control of the experimental systematics.

Currently, the values of the strong coupling constant $\alpha_S(m_Z^2)$ as determined in different classes of measurement, and even inside these classes, is obtained at different values differing by several standard deviations [154–156], reaching an individual accuracy of $\sim$1%. One reason for this lies in the experimental systematics but also in different theoretical approaches being applied. We will consider the measurement of $\alpha_S(m_Z^2)$ using deep-inelastic scattering (DIS) data. To minimize theoretical uncertainties, the measurement method has to be as simple as possible and widely free of effects that are difficult to control or are even widely unknown. Usually one performs mixed twist-2 flavour non-singlet/singlet analyses on a wide host of DIS and other hard scattering data, which are required because, besides the flavour non-singlet parton distribution functions, those of the different sea quark and gluon distributions are needed as well. Furthermore, the range of Q^2 usually includes also the region in which higher-twist contributions have to be fitted in addition. Also, the treatment of heavy-quark effects varies in the different approaches, although there is no such freedom in general.

[78] Authors: J Blümlein, M Saragnese (DESY).

Some of the cross sections used in the fits may not have the same higher-order correction as the massless DIS cross sections. The presence of all these different distribution functions will cost a large part of the statistics power to be determined and various parameter correlations, and potentially introduces theoretical biases [157, 158]. All this complicates the measurement of the strong coupling constant in using approaches of this kind.

The situation is completely different in the case of scheme-invariant flavour non-singlet evolution of the structure functions $F_2^{\rm NS}(x, Q^2)$ or $g_1^{\rm NS}(x, Q^2)$. The latter structure function usually needs a much higher luminosity, since in addition the longitudinal polarization difference has to be carried out. To form the corresponding data sets, DIS off proton and deuteron targets has to be measured and a reliable description of the deuteron wave function effects is needed. In both cases the input distribution is a measured structure function: $F_2^{\rm NS}(x, Q_0^2)$ or $g_1^{\rm NS}(x, Q_0^2)$, with experimental error bands. Both the shape of these quantities and their experimental uncertainties can be parameterized at sufficient precision, forming the input for the one-dimensional evolution equation [159]. What remains to be determined in the fit of the data for $Q^2 > Q_0^2$ is the strong coupling constant $\alpha_S(m_Z^2)$, the precision of which receives also contributions from the experimental uncertainty of the measured input distribution.

In the following we describe the theoretical basis of the scheme-invariant measurement of $\alpha_S(m_Z^2)$ and illustrate a few relevant aspects numerically, following [160], which may be performed in future experiments at EIC [161] or the LHeC [162]. We consider the combination of structure functions

$$F_2^{\rm NS}(x, Q^2) = F_2^p - \frac{1}{2}F_2^d = \frac{1}{6}xC_2^{\rm NS}(x, Q^2) \otimes v_3(x, Q^2), \tag{4.1}$$

where $\otimes$ denotes the Mellin convolution, $C_2^{\rm NS}(x, Q^2)$ is the corresponding unpolarized flavour non-singlet Wilson coefficient and

$$v_3(x, Q^2) = u_v(x, Q^2) - d_v(x, Q^2), \tag{4.2}$$

the difference of valence u- minus d-quark distributions. Nor the flavour singlet, gluon, or special sea-quark distributions enter the partonic input distribution. However, the different flavours contribute through virtual QCD corrections, including charm and bottom quarks.

The scale evolution of $F_2^{\rm NS}(x, Q^2)$ can be described by an evolution operator $E_{\rm NS}(x, Q^2)$

$$F_2^{\rm NS}(x, Q^2) = E_{\rm NS}(x, Q^2, Q_0^2; m_c, m_b) \otimes F_2^{\rm NS}(x, Q_0^2), \tag{4.3}$$

which reads in Mellin space

$$\begin{aligned}
E_{\rm NS}(Q^2, Q_0^2) = {} & \left(\frac{a}{a_0}\right)^{-\frac{P_0}{2\beta_0}}\Bigg\{1 + \frac{a - a_0}{2\beta_0^2} \\
& \times \Bigg\{[1 + a^2C_2^{Q^2} - a_0^2C_2^{Q_0^2}](2\beta_0^2C_1 - \beta_0P_1 + \beta_1P_0) - \frac{(a^2 - a_0^2)}{4\beta_0^3} \\
& \times (2\beta_0^2C_1 - \beta_0P_1 + \beta_1P_0)[2\beta_0^3C_1^2 + \beta_0^2P_2 - \beta_0\beta_1P_1 + (\beta_1^2 - \beta_0\beta_2)P_0] + \frac{(a^2 + aa_0 + a_0^2)}{3\beta_0^2} \\
& \times [2\beta_0^4C_1^3 - \beta_0^3P_3 + \beta_0^2\beta_1P_2 + (\beta_0^2\beta_2 - \beta_0\beta_1^2)P_1 + (\beta_0^2\beta_3 - 2\beta_0\beta_1\beta_2 + \beta_1^3)P_0] + \frac{a - a_0}{4\beta_0^2}(2\beta_0^2C_1 \\
& - \beta_0P_1 + \beta_1P_0)^2 + \frac{(a - a_0)^2}{24\beta_0^4}(2\beta_0^2C_1 - \beta_0P_1 + \beta_1P_0)^3 - \frac{a + a_0}{2\beta_0}[2\beta_0^3C_1^2 + \beta_0^2P_2 - \beta_0\beta_1P_1 \\
& + P_0(\beta_1^2 - \beta_0\beta_2)]\Bigg\} + a^2C_2^{Q^2} - a_0^2C_2^{Q_0^2} - C_1[a^3C_2^{Q^2} - a_0^3C_2^{Q_0^2}] + a^3C_3^{Q^2} - a_0^3C_3^{Q_0^2}\Bigg\}.
\end{aligned} \tag{4.4}$$

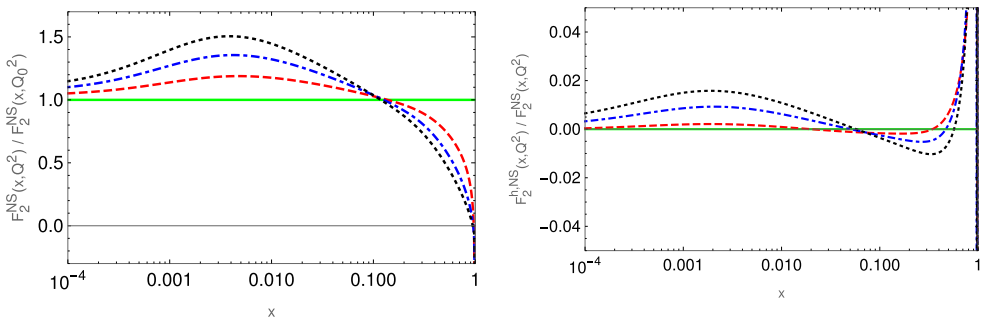

Figure 12. Left: evolution ratio of the structure function $F_2^{\rm NS}(x, Q^2)$. Right: relative contribution of the heavy flavour corrections in $F_2^{\rm NS}(x, Q^2)$. Dashed lines: $Q^2 = 10^2$ GeV^2, dash-dotted lines: $Q^2 = 10^3$ GeV^2, dotted lines: $Q^2 = 10^4$ GeV^2; from [160].

Here $a = a(Q^2)$ denotes the strong coupling constant and $a_0 = a(Q_0^2)$, P_i are the non-singlet splitting functions and $C_i = c_i + h_i$ the expansion coefficients of the Wilson coefficient, where c_i is the massless contribution and h_i the massive contribution, where $h_1 = 0$, $h_2 = h_2^c + h_2^b$ and $h_3 = h_3^c + h_3^b + h_3^{cb}$, i.e. there are mixed charm and bottom contributions from three-loops onward [160] for details. The dependence on the heavy-quark mass is logarithmic, with highest logarithmic powers $\ln^k(Q^2/m_h^2)$ for h_k. While the non-singlet splitting functions to three-loop order are known [163, 164], the four-loop non-singlet splitting function P_3 is not yet known, but it can be very well described by a Padé approximation. Eight Mellin moments are known, with the earliest calculation [165], and the presently available set [166]. The massless three-loop Wilson coefficients were calculated in [167] and the single and double mass three-loop heavy flavour corrections in [168]. At two-loop order the corrections are even available for the whole kinematic region [169, 170]. Different proposals to perform scheme-invariant evolution both in the non-singlet and singlet case have been made since 1979, see [92–100] of [160].

To illustrate the potential of the $\alpha_S(m_Z^2)$ measurement using the present method, we show in figure 12 (left) the ratio of $F_2^{\rm NS}(x, Q^2)$ to $F_2^{\rm NS}(x, Q_0^2)$ for $Q_0^2 = 10$ GeV^2 up to scales $Q^2 = 10^4$ GeV^2. In the lower x region positive corrections up to a factor of 1.5 are reached, while at large x the corrections are negative. In figure 12 (right) we illustrate the impact of the heavy flavour corrections due to charm and bottom quark effects. In the region below $x = 0.6$ they are bound to $\pm 1.5\%$ and grow for larger values of x. This shows their importance, because the future measurements will be performed at subpercent experimental accuracy. In [160] we also performed related studies for the case of the polarized structure function $g_1(x, Q^2)$.

A precision determination of the strong coupling constant $\alpha_S(m_Z^2)$ requires a high luminosity measurement of a sufficiently simple inclusive observable. The measurement must be carried out under stringent systematic control. Such a measurement would have been possible in the past, if the proposal [171] would have been carried out. It has not been possible at HERA, since deuterons have not been probed [172] and the reconstruction of a non-singlet structure function from charged current data has not been precise enough. Given a sufficient preparation, the measurement can be carried out at the EIC using proton and deuteron targets. LHeC may also perform such a measurement, provided also deuteron data will be available and the statistics for the non-singlet measurement is high enough. The theoretical analysis method is then scheme-invariant evolution in the flavour non-singlet case for the structure function $F_2^{\rm NS}(x, Q^2)$. Both the light and heavy flavour corrections for this

quantity are known at the level of the twist-2 approximation for $Q^2 \geqslant 10$ GeV^2, $W^2 \geqslant 15$ GeV^2 [173], to measure $\alpha_S(m_Z^2)$ at an accuracy well below the 1% level. This is one way to decide what is the correct value of $\alpha_S(m_Z^2)$.

To summarize, a high luminosity measurement of F_2^p and F_2^d at the EIC would allow to perform the N^{3}LO measurement of $\alpha_S(m_Z^2)$ using the scheme-invariant method discussed here.

Acknowledgments—Support from the European Union's Horizon 2020 research and innovation programme under the Marie Skłodowska-Curie grant agreement No. 764 850, SAGEX, is gratefully acknowledged.

4.2. $\alpha_S(m_Z^2)$ from DIS large-x structure function resummation[79]

We scrutinize the DIS $F_2(x, Q^2)$ structure functions (SFs) measured by the SLAC, NMC, and BCDMS experiments [174–179] at NNLO accuracy in massless perturbative QCD in order to extract $\alpha_S(m_Z^2)$. The so-called deep-inelastic scattering (DIS) scheme of the SFs [180] is considered, which leads to effective resummation of large-x logarithms into the Wilson coefficient function. The study presented here is a continuation of investigations carried out in closely related papers [181–185].

The function $F_2(x, Q^2)$ is represented as a sum of the leading twist (LT) $F_2^{\rm pQCD}(x, Q^2)$ and the twist-four terms (hereinafter, the superscripts pQCD and LT denote the twist-two approximation with and without target-mass corrections):

$$F_2(x, Q^2) = F_2^{\rm pQCD}(x, Q^2)\left(1 + \frac{\tilde{h}_4(x)}{Q^2}\right). \tag{4.5}$$

For large x values, gluons do not nearly contribute and the Q^2 evolution of the twist-two DIS $F_2(x, Q^2)$ SF is well determined by the so-called nonsinglet (NS) part. In this approximation, there is a direct relation between the moments of the DIS $F_2(x, Q^2)$ SF and the moments of the NS parton distribution function $\mathbf{f}(x, Q^2)$

$$M_n(Q^2) = \int_0^1 dx x^{n-2} F_2^{\rm LT}(x, Q^2), \quad \mathbf{f}(n, Q^2) = \int_0^1 dx x^{n-1}\, \mathbf{f}(x, Q^2) \tag{4.6}$$

which can be expressed as follows

$$M_n(Q^2) = R(f) \times C(n, a_s(Q^2)) \times \mathbf{f}(n, Q^2), \tag{4.7}$$

where the strong coupling constant

$$a_s(Q^2) = \frac{\alpha_S(Q^2)}{4\pi} \tag{4.8}$$

and the Wilson coefficient function is denoted as $C(n, a_s(Q^2))$. The constant $R(f) = 1/6$ for $f = 4$ [186].

4.2.1. Strong coupling constant derivation. The strong coupling constant is found from the corresponding renormalization group equation. At the NLO level, $a_s^{\rm NLO}(Q^2) \equiv a_1(Q^2)$, the latter looks like

[79] Authors: A V Kotikov, V G Krivokhizhin, B G Shaikhatdenov (JINR, Dubna).

$$\frac{1}{a_1(Q^2)} - \frac{1}{a_1(m_Z^2)} + b_1 \ln\left[\frac{a_1(Q^2)}{a_1(m_Z^2)}\frac{(1 + b_1 a_1(m_Z^2))}{(1 + b_1 a_1(Q^2))}\right] = \beta_0 \ln\left(\frac{Q^2}{m_Z^2}\right). \quad (4.9)$$

At NNLO level, $a_s^{\rm NNLO}(Q^2) \equiv a_2(Q^2)$, the strong coupling constant is derived from the following equation:

$$\frac{1}{a_2(Q^2)} - \frac{1}{a_2(m_Z^2)} + b_1 \ln\left[\frac{a_2(Q^2)}{a_2(m_Z^2)}\sqrt{\frac{1 + b_1 a_2(m_Z^2) + b_2 a_2^2(m_Z^2)}{1 + b_1 a_2(Q^2) + b_2 a_2(Q^2)}}\right] + \left(b_2 - \frac{b_1^2}{2}\right) \times (I(a_s(Q^2)) - I(a_s(m_Z^2))) = \beta_0 \ln\left(\frac{Q^2}{m_Z^2}\right). \quad (4.10)$$

The expression for I is

$$I(a_s(Q^2)) = \begin{cases} \dfrac{2}{\sqrt{\Delta}} \arctan \dfrac{b_1 + 2b_2 a_2(Q^2)}{\sqrt{\Delta}} & \text{for } f = 3, 4, 5; \quad \Delta > 0, \\ \dfrac{1}{\sqrt{-\Delta}} \ln\left[\dfrac{b_1 + 2b_2 a_2(Q^2) - \sqrt{-\Delta}}{b_1 + 2b_2 a_2(Q^2) + \sqrt{-\Delta}}\right] & \text{for } f = 6; \quad \Delta < 0, \end{cases}$$

where $\Delta = 4b_2 - b_1^2$ and $b_i = \beta_i/\beta_0$ are read off from the QCD β-function:

$$\beta(a_s) = -\beta_0 a_s^2 - \beta_1 a_s^3 - \beta_2 a_s^4 + \ldots.$$

The coefficient function $C(n, a_s(Q^2))$ is then expressed in terms of the coefficients $B_j(n)$, which are exactly known (for the odd n values, $B_j(n)$ and $Z_j(n)$ can be obtained by using the analytic continuation [187–189])

$$C(n, a_s(Q^2)) = 1 + a_s(Q^2) B_1(n) + a_s^2(Q^2) B_2(n) + \mathcal{O}(a_s^3). \quad (4.11)$$

The Q^2-evolution of the PDF moments can be calculated within the framework of perturbative QCD:

$$\frac{\mathbf{f}(n, Q^2)}{\mathbf{f}(n, Q_0^2)} = \left[\frac{a_s(Q^2)}{a_s(Q_0^2)}\right]^{\frac{\gamma_0(n)}{2\beta_0}} \times \frac{h(n, Q^2)}{h(n, Q_0^2)}, \quad (4.12)$$

where

$$h(n, Q^2) = 1 + a_s(Q^2) Z_1(n) + a_s^2(Q^2) Z_2(n) + \mathcal{O}(a_s^3), \quad (4.13)$$

and

$$Z_1(n) = \frac{1}{2\beta_0}[\gamma_1(n) - \gamma_0(n) b_1], \; Z_2(n) = \frac{1}{4\beta_0}[\gamma_2(n) - \gamma_1(n) b_1 + \gamma_0(n)(b_1^2 - b_2)] + \frac{1}{2} Z_1^2(n) \quad (4.14)$$

are combinations of the NLO and NNLO anomalous dimensions $\gamma_1(n)$ and $\gamma_2(n)$.

For large n (this corresponds to large x values), the coefficients $Z_j(n) \sim \ln n$ and $B_j(n) \sim \ln^{2j} n$. So, the terms $\sim B_j(n)$ can lead to potentially large contributions and, therefore, should be resummed.

4.2.2. Scale dependence. We are going to consider the dependence of the results on the factorization μ_F scale caused by the truncation of a perturbative series [181]. This way, equation (4.7) takes the form:

$$M_n(Q^2) = R(f) \times \hat{C}(n, a_s(k_F Q^2)) \times \mathbf{f}(n, k_F Q^2).$$

The function $\hat{C}$ is to be obtained from C by modifying the r.h.s. of equation (4.11) as follows:

$$a_s(Q^2) \to a_s(k_F Q^2), \quad B_1(n) \to B_1(n) + \frac{1}{2}\gamma_0(n)\ln k_F,$$
$$B_2(n) \to B_2(n) + \frac{1}{2}\gamma_1(n)\ln k_F + \left(\frac{1}{2}\gamma_0 + \beta_0\right)B_1 \ln k_F + \frac{1}{8}\gamma_0(\gamma_0 + 2\beta_0)\ln^2 k_F. \tag{4.15}$$

Taking a special form for the coefficient k_F, we can decrease contributions coming from the terms $\sim B_j(n)$. To accomplish this task, we consider the DIS-scheme [180], where the NLO corrections to the Wilson coefficients are completely cancelled by changes in the factorization scale.

In the NLO case

$$a_s(Q^2) \to a_s(k_{\rm DIS}(n)Q^2) \equiv a_n^{\rm DIS}(Q^2), \quad k_{\rm DIS}(n) = \exp\left(\frac{-2B_1(n)}{\gamma_0(n)}\right) = \exp\left(\frac{-r_1^{\rm DIS}(n)}{\beta_0}\right), \tag{4.16}$$

where

$$r_1^{\rm DIS}(n) = \frac{2B_1(n)\beta_0}{\gamma_0} \quad \text{and} \quad B_1(n) \to B_1^{\rm DIS} = 0. \tag{4.17}$$

The NLO coupling $a_n^{\rm DIS}(Q^2)$ obeys the following equation

$$\frac{1}{a_n^{\rm DIS}(Q^2)} - \frac{1}{a_1(m_Z^2)} + b_1 \ln\left[\frac{a_n^{\rm DIS}(Q^2)}{a_1(m_Z^2)}\frac{(1 + b_1 a_1(m_Z^2))}{(1 + b_1 a_n^{\rm DIS}(Q^2))}\right] = \beta_0 \ln\left(\frac{Q^2}{m_Z^2}\right) - r_1^{\rm DIS}(n). \tag{4.18}$$

In the NNLO case, in addition to equations (4.16) and (4.17), there is also the following modification

$$B_2(n) \to B_2^{\rm DIS}(n) = B_2(n) - \left(\frac{1}{2} + \frac{\beta_0}{\gamma_0(n)}\right)B_1^2(n) - \frac{\gamma_1(n)}{\gamma_0(n)}B_1(n), \tag{4.19}$$

that leads to the cancellation of the large terms $\sim \ln^4(n)$ in $B_1^{\rm DIS}(n)$.

The NNLO coupling $a_n^{\rm DIS}(Q^2)$ obeys the equation

$$\frac{1}{a_n(Q^2)} - \frac{1}{a_2(m_Z^2)} + b_1 \ln\left[\frac{a_n(Q^2)}{a_2(m_Z^2)}\sqrt{\frac{1 + b_1 a_2(m_Z^2) + b_2 a_2^2(m_Z^2)}{1 + b_1 a_n(Q^2) + b_2 a_n(Q^2)}}\right]$$
$$+ \left(b_2 - \frac{b_1^2}{2}\right) \times (I(a_n(Q^2)) - I(a_s(m_Z^2))) = \beta_0 \ln\left(\frac{Q^2}{m_Z^2}\right) - r_1^{\rm DIS}(n). \tag{4.20}$$

Table 7. Parameter values of the twist-four term in different cases obtained in the analysis of data (314 points: $Q^2 \geqslant 2$ GeV^2) carried out within VFNS (FFNS).

	NLO	NLO	NNLO	NNLO
x	$\overline{\text{MS}}$ scheme $\chi^2 = 246\,(259)$ $\alpha_S(m_Z^2) = 0.1195$ (0.1192)	DIS scheme $\chi^2 = 238\,(251)$ $\alpha_S(m_Z^2) = 0.1177$ (0.1179)	$\overline{\text{MS}}$ scheme $\chi^2 = 241\,(254)$ $\alpha_S(m_Z^2) = 0.1177$ (0.1170)	DIS scheme $\chi^2 = 242(249)$ $\alpha_S(m_Z^2) = 0.1178$ (0.1171)
0.275	−0.245 (− 0.264)	−0.187 (− 0.174)	−0.188 (− 0.204)	−0.141 (− 0.170)
0.35	−0.243 (− 0.252)	−0.111 (− 0.134)	−0.188 (− 0.193)	−0.133 (− 0.149)
0.45	−0.191 (− 0.187)	−0.040 (− 0.094)	−0.172 (− 0.158)	−0.110 (− 0.104)
0.55	−0.116 (0.096)	−0.106 (− 0.088)	−0.174 (− 0.137)	−0.121 (− 0.084)
0.65	0.054 (0.118)	−0.167 (− 0.094)	−0.145 (− 0.051)	−0.223 (− 0.100)
0.75	0.337 (0.477)	−0.568 (− 0.442)	0.115 (0.648)	−0.587 (− 0.314)

4.2.3. Fit results. Our analysis is carried out for the moments of the $F_2(x, Q^2)$ SF defined in equation (4.6). Then, for each Q^2, the $F_2(x, Q^2)$ SF is recovered using the Jacobi polynomial decomposition method [190–192]:

$$F_2(x, Q^2) = x^a(1 - x)^b \sum_{n=0}^{N_{\max}} \Theta_n^{a,b}(x) \sum_{j=0}^{n} c_j^{(n)}(\alpha, \beta) M_{j+2}(Q^2), \tag{4.21}$$

where $\Theta_n^{a,b}$ are the Jacobi polynomials, a, b are the parameters to be fit. The program MINUIT [193] is used to minimize the difference between experimental data and theoretical predictions for the $F_2(x, Q^2)$ SF.

We use free data normalizations for various experiments. As a reference set, the most stable data of hydrogen BCDMS are used at the value of the initial beam energy $E_0 = 200$ GeV. Contrary to previous analyses [181, 182], the cut $Q^2 \geqslant 2$ GeV^2 is used throughout, since for smaller Q^2 values equations (4.18) and (4.20) have no real solutions.

The starting point of Q^2-evolution is taken at $Q_0^2 = 90$ GeV^2. This value of Q_0^2 is close to the average values of Q^2 covering the corresponding data. Based on studies done in [184, 185], it is sufficient to take the maximum number of moments $N_{\max} = 8$, and the cut $0.25 \leqslant x \leqslant 0.8$ is applied on the data.

We work within the variable-flavour-number scheme (VFNS) [181]. To strengthen the effect of changing the sign of twist-four corrections, we also present results obtained in the fixed-flavour-number scheme with $N_{\text{f}} = 4$.

As one can see from table 7, the central values of $\alpha_S(m_Z^2)$ are mostly close to each other upon taking into account total experimental and theoretical errors [181, 182]:

$$\pm 0.0022 \quad \text{(total exp. error)}, \qquad \begin{cases} +0.0028 \\ -0.0016 \end{cases} \quad \text{(theor. error)}. \tag{4.22}$$

We plan to study these errors in more detail and present them in an upcoming publication.

From the table, it can also be seen that after resumming at large x values (i.e. in the DIS scheme), the twist-four corrections change sign at large values of x. Thus, unlike the standard analyses performed in [194], in this case, when twist-four corrections change the sign, (part of) the powerlike terms can be said to be swallowed up into a QCD analytic constant [195] just much like as it was observed at low-x values [196] in the framework of the so-called double asymptotic scaling approach [197, 198].

In previous papers [199, 200], where resummation at large values of x was performed within the framework of the Grunberg approach [201, 202], we saw only a decrease in the twist-four contribution, since the terms were not studied in detail. That is why we plan to include Grunberg's approach in an analysis similar to the present one and study in some detail the values of the twist-four corrections.

4.3. Strong coupling α_S in fits of parton distributions[80]

Data from deep-inelastic scattering (DIS) experiments collected during the last few decades contributes significantly to the knowledge about the structure of the proton and the extraction of parton distributions (PDFs). The theory description builds on QCD factorization, which allows to express the structure functions in the charged-lepton- (or neutrino-) proton hard scattering with large momentum transfer Q schematically as

$$F_a = f_i \otimes c_{a,i}, \qquad a = 2, 3, L, \tag{4.23}$$

where the process-dependent coefficient functions are denoted by $c_{a,i}$ and the PDFs for a given fraction of the proton momentum x by $f_i(x, \mu^2)$. Their dependence on the (renormalization and factorization) scale μ is governed by the well-known evolution equations

$$\frac{\partial}{\partial \ln \mu^2} f_i(x, \mu^2) = [P_{ik}(\alpha_S(\mu^2)) \otimes f_k(\mu^2)](x), \tag{4.24}$$

where the standard convolution is abbreviated by $\otimes$. Both, the splitting functions P_{ik} and the coefficient functions by $c_{a,i}$ are calculable in QCD perturbation theory in an expansion in powers of the strong coupling constant $a_s \equiv \alpha_S(\mu^2)/(4\pi)$,

$$P = a_s P^{(0)} + a_s^2 P^{(1)} + a_s^3 P^{(2)} + a_s^4 P^{(3)} + \ldots, \tag{4.25}$$

$$c_{a,i} = c_{a,i}^{(0)} + a_s c_{a,i}^{(1)} + a_s^2 c_{a,i}^{(2)} + a_s^3 c_{a,i}^{(3)} + \ldots. \tag{4.26}$$

Here, the first three terms define the NNLO predictions for DIS, which is currently the standard approximation [163, 203] for the splitting functions and [204–207] for the DIS coefficient functions at this accuracy. Form the perturbative expansion in equations (4.25) and (4.26) as well as from the PDF evolution in equation (4.24) it is obvious that there is, in general, significant correlation between the PDFs and the value of strong coupling constant $\alpha_S(m_Z^2)$ [158]. In the ABM PDF fits, this information can be obtained from the (positive-definite) covariance matrix [208].

Equation (4.23) holds up to power corrections suppressed by $1/Q^2$, and the accessible range of kinematics in the momentum transfer Q and Bjorken x requires careful considerations of the respective kinematic regions. Typical cuts in the application to DIS data restrict the invariant mass of the hadronic system $W^2 = m_p^2 + Q^2(1-x)/x$ (with the proton mass m_p) to $W^2 \geqslant 12.5\,\mathrm{GeV}^2$ and $Q^2 \geqslant 2.5$–$10\,\mathrm{GeV}^2$ [208]. Depending on these cuts, an improved theoretical description of $F_a x, Q^2$ to account for higher-twist and target-mass corrections becomes necessary. Higher-twist corrections arise from the infinite tower of power corrections $(1/Q^2)^n$, in the operator product expansion (with $n = 1, 2, 3, \ldots$). Higher-twist terms have a physical interpretation as multiparton correlations and modify the structure functions in equation (4.23) as

[80] Authors: S Moch (Hamburg Univ.).

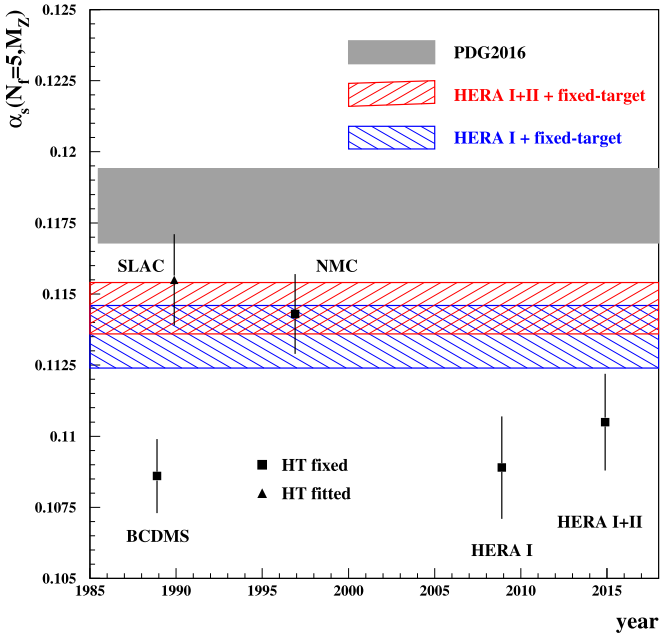

Figure 13. Value of $\alpha_S(m_Z^2)$ in the $\overline{\text{MS}}$ scheme for $N_\text{f} = 5$ flavours at NNLO in QCD preferred by individual data sets as a function of the year of their publication. Data from SLAC [211–213] (proton), BCDMS [177], NMC [176] (proton), the HERA run I [214] as well as the HERA run I+II combination [215] are considered in three variants for the treatment of the higher twist terms defined in equation (4.27): *(i)* the higher twist terms are set to zero (circles); (ii) they are fixed to the values obtained in the ABMP16 fit from considering all data sets (squares); (iii) they are fitted to the individual data set under study (triangles). The bands for $\alpha_S(m_Z^2)$ obtained by using the combination of the SLAC, BCDMS and NMC samples together with those from the HERA run I (left-tilted hatches) and the run I+II combination (right-tilted hatches). The 2016 PDG average [216] (shaded area) is shown for comparison. Plot from [208].

$$F_a^{\text{ht}}(x, Q^2) = F_a^{\text{TMC}}(x, Q^2) + \frac{H_a^{\tau=4}(x)}{Q^2}, \qquad a = 2, T, \tag{4.27}$$

where the additive terms $H_a^{\tau=4}(x)$ models the twist-four contribution and F_a^{TMC} denotes the leading-twist structure function with target mass corrections, which account for the finite nucleon mass [208].

Another important aspect in the theoretical description of the leading-twist structure functions from equation (4.23) entering in equation (4.27) concerns the active number of flavours and the treatment of DIS heavy quark production [209] A fixed-flavour number scheme and the use the standard decoupling relations for heavy quarks in QCD in the transition from $N_\text{f} = 3$ to $N_\text{f} = 5$ is justified given the currently available kinematics in x and Q for DIS charm quark data [158]. Variable-flavour-number schemes attempting the resummation of large logarithms in the ratio Q^2/m_h^2 with the heavy-quark mass squared m_h^2 introduce additional theoretical uncertainties from the matching, which manifest themselves predominantly at small Q^2 [210].

The impact of higher-twist terms and target-mass corrections in equation (4.27) on the extracted value of $\alpha_S(m_Z^2)$ to NNLO accuracy from world DIS data has been illustrated in

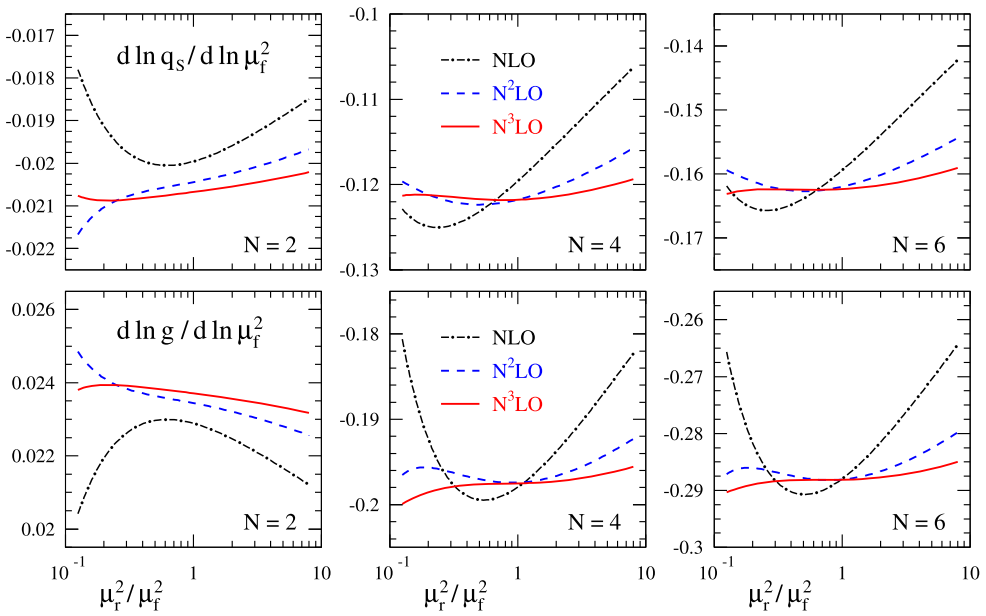

Figure 14. The dependence of the logarithmic factorization scale derivatives of the singlet PDFs on the renormalization scale μ_r at $N = 2$ (where the very small scaling violations of q_s and g are related by the momentum sum rule), $N = 4$ and $N = 6$ for $\alpha_S(\mu_0^2) = 0.2$ and $N_f = 4$ and initial distributions of the form $xq_s = 0.6\, x^{-0.3}(1-x)^{3.5}(1+5.0\, x^{0.8})$ and $xg = 1.6\, x^{-0.3}(1-x)^{4.5}\,(1-0.6\, x^{0.3})$ at the standard scale $\mu_r = \mu_f$. Plot from [217].

figure 13, where it is shown that variants of the fits with no higher twist lead to systematically larger values of $\alpha_S(m_Z^2)$. The combined fit of PDFs and $\alpha_S(m_Z^2)$ to the world data shown in figure 13 delivers in the ABMP16 analysis at NNLO in QCD the value of [208]

$$\alpha_S(m_Z^2) = 0.1145 \pm 0.0009 \qquad \text{for } N_f = 5, \tag{4.28}$$

while the full ABMP16 analysis (also including LHC data on top-quark hadroproduction) finds the value

$$\alpha_S(m_Z^2) = 0.1147 \pm 0.0008 \qquad \text{for } N_f = 5. \tag{4.29}$$

Higher-order QCD corrections beyond NNLO become important whenever high precision is needed for benchmark processes at the LHC and for the novel accurate DIS measurements expected at the future Electron Ion Collider (EIC). Then, determinations of PDFs and α_S at N^{3}LO accuracy requires the calculation of the N^{3}LO corrections in equations (4.25) and (4.26). Those for the DIS coefficient functions are already available [167, 218–220], including effects of massive quarks [168]. Work on the four-loop splitting functions in equation (4.25) to ensure QCD evolution equations at N^{3}LO accuracy is ongoing [166, 217, 221] and the gain in the theoretical accuracy in the solution of equation (4.24) for the evolution of the PDFs is illustrated in figure 14 for a number of Mellin moments ($N = 2$ to $N = 6$) available from [217]. With the full N^{3}LO contributions to DIS the residual theoretical uncertainty due the scale variation and the truncation of the perturbative series will be limited to 1% in the range of parton kinematics relevant for the current world DIS data and

the EIC. With respect to the theory error, inclusive DIS data offer the most precise method to measure $\alpha_S(m_Z^2)$.

4.4. Strong coupling determination in the CT18 global analyses[81]

The CT18 global QCD analysis [222] updates the previous CTEQ-TEA PDFs, CT14 [223] and CT14HERA2 [224], adding a variety of high-precision data from the Large Hadron Collider (LHC). New measurements of single-inclusive jet production, Drell–Yan lepton pairs, top-quark pairs, as well as high transverse momentum (p_T) Z bosons from ATLAS, CMS and LHCb, at the center-of-mass energies of 7 and 8 TeV, provide significant additional sensitivity to the PDF determination. A new family of PDF sets, CT18, CT18A, CT18X, and CT18Z, are released at both NLO and NNLO. The nominal PDF set, CT18, is recommended for general collider phenomenology studies, while CT18A includes an additional ATLAS 7 TeV W/Z precision data set [225], which is found to be in tension with other data sets in the global fit. An alternative PDF set, CT18X, has adopted an x-dependent DIS scale, which captures the small-x behavior at low Q^2 and improves the QCD description of HERA DIS data. The CT18Z PDF set includes the features of CT18A and CT18X, in addition to having a slightly larger charm pole mass, $m_c = 1.4$ GeV versus $m_c = 1.3$ GeV. CT18Z maximizes the difference from CT18 PDFs, but preserves a similar goodness-of-fit. More details can be found in [222].

The final product—the published error PDF sets such as CT18—takes the strong coupling at a scale m_Z as the world average value $\alpha_S(m_Z^2) = 0.118$ [226]. Alternative error PDF sets are produced with a series of fixed $\alpha_S(m_Z^2)$ values for the use in the estimation of combined PDF+α_S uncertainties. As shown in CT10 [227], a change in α_S is partially compensated by changes in the PDF parameters. An α_S uncertainty can be defined, which quantifies the allowed variation of α_S when allowed to be freely varied in the PDF fit. In general, the $\alpha_S(m_Z^2)$ sensitivity to a specific data set is introduced either through radiative corrections, such as in the Drell–Yan pair production, or through scaling violations, such as in DIS.

Simultaneous fits of the α_S and PDFs were also performed during the CT18 study. An optimal way to explore experimental constraints on $\alpha_S(m_Z^2)$ is to examine the corresponding χ^2 variations with the Lagrangian multiplier (LM) technique [228]. In figures 15, 16 and 17, we adapt this technique to plot a a series of curves for $\Delta\chi^2 = \chi^2(\alpha_S) - \chi^2(\alpha_{S,0})$ for CT18 NNLO, CT18NLO, and CT18Z NNLO, respectively, where $\alpha_{S,0}$ corresponds to the global χ^2 minimum in the PDF+α_S fit. The black solid curves are for the total $\Delta\chi^2$, and the other curves are for $\Delta\chi^2$ from the individual experiments with the highest sensitivities to α_S. From the figures, it is clear that the data sets and even groups of data sets have different preferences to $\alpha_S(m_Z^2)$ in terms of both the central values and uncertainties. The spread of the pulls on α_S by the data sets is broader than it would be normally expected from random fluctuations of data around theory, suggesting that a more conservative prescription for the estimation of the α_S uncertainty is necessary than the straightforward averaging over the data sets [229].

From the figures, we see that the HERA I and II combined DIS data [215] provide the strongest constraints on $\alpha_S(m_Z^2)$ in CT18 at both NLO and NNLO. The BCDMS proton data [177] play a slightly stronger role in the CT18Z PDF fit. These two DIS data sets prefer a lower value of $\alpha_S(m_Z^2)$ than the world average, with a value about 0.114−0.116, but with larger uncertainties. On the other hand, we see that the hadron collider data, such as inclusive jet, top-quark pairs, and Drell–Yan production, pull the $\alpha_S(m_Z^2)$ value higher, with a preferred

[81] Authors: J Huston (MSU, East Lansing), P Nadolsky (Southern Methodist Univ., Dallas), K. Xie (Univ. of Pittsburgh), on behalf of the CTEQ-TEA Collaboration.

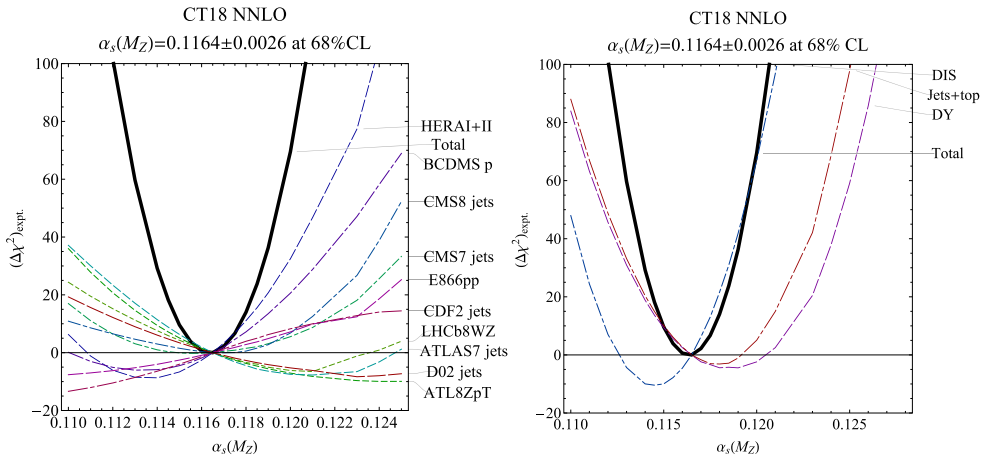

Figure 15. The log-likelihood χ^2 in the CT18 NNLO global PDF analysis as a function the strong coupling at scale m_Z, plotted for the total fitted data set and the most sensitive experiments. Adapted from [222].

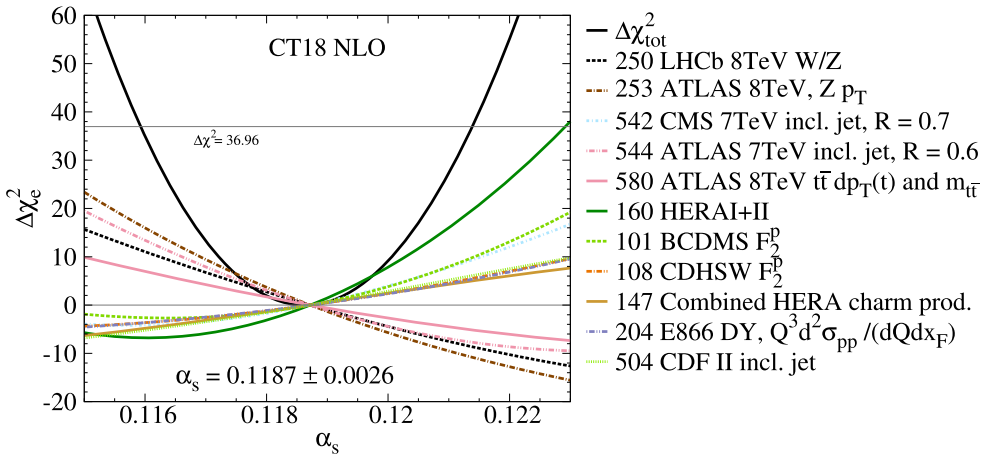

Figure 16. Same as figure 15, but now for the $\alpha_S(m_Z^2)$ dependence of χ^2 in the CT18 NLO fit. Adapted from [222].

value of 0.117−0.119 for the CT18 NNLO case. The strongest pull comes ATLAS 8 TeV Z p_T data [230], followed by the LHCb 8 TeV W/Z measurement [231]. We also see significant pulls from inclusive jet production at ATLAS 7 TeV [232] and D0 Run II [233], as well as the measurements of the p_T^t and $m_{t\bar{t}}$ distributions in top-quark pair production at ATLAS 8 TeV [234]. In contrast to the ATLAS case, the CMS measurements of inclusive jet production at both 7 TeV [235] and 8 TeV [236] prefer a smaller $\alpha_S(m_Z^2)$, reflecting a tension between these measurements from the two experiments.

Within the 68% probability level, the global average values are

$$\alpha_S(m_Z^2)_{\rm NNLO} = 0.1164 \pm 0.0026, \quad \alpha_S(m_Z^2)_{\rm NLO} = 0.1187 \pm 0.0026, \tag{4.30}$$

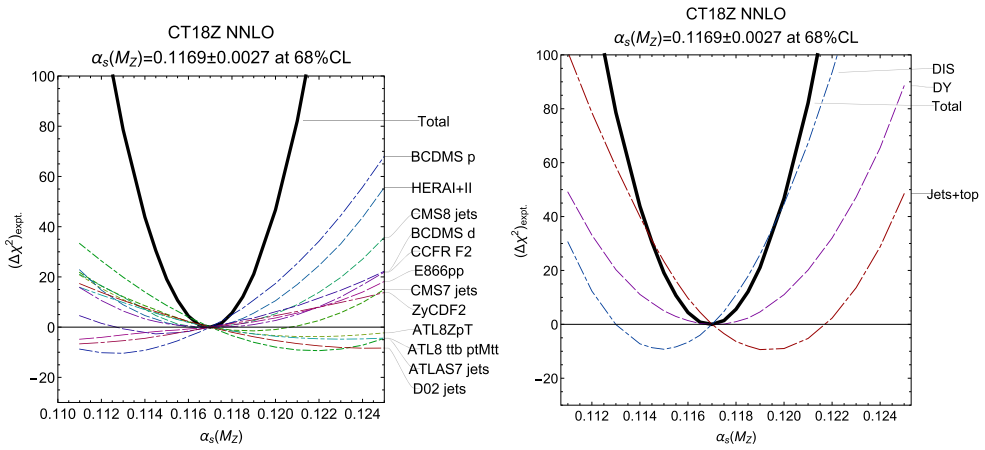

Figure 17. Same as figure 15, but for the CT18Z NNLO fit. Adapted from [222].

while CT18Z NNLO gives 0.1169 ± 0.0027, all consistent with the world average [226]. In comparison with the CT14 global fit [223], the CT18 data sets prefer a larger central $\alpha_S(m_Z^2)$ with a marginally smaller uncertainty. Note that the uncertainties quoted here are larger than those in the contemporary analyses done by other two groups, MSHT and NNPDF. This is primarily a result of a more conservative prescription for the uncertainty adopted in CT18, despite similar constraining power of the experiments included by the three groups. The CT18 prescription reflects in part some inconsistency between the fitted data sets, as discussed above. In the presence of such inconsistencies due to unidentified systematic effects, which would lead to enlarged variations in α_S when the selection of experimental data sets is varied, the final uncertainty should be generally increased [237]. In addition, the CT18 uncertainty incorporates outcomes from the fits with comparable χ^2 that are obtained with more than 250 alternative functional forms of the PDFs and with alternative QCD scale choices in inclusive jet and high-p_T production. To achieve this, the α_S and PDF uncertainties are estimated using the tolerance chosen so as to cover a large number of candidate fits that are made with such alternative choices and pass the goodness-of-fit criteria accepted for the final fit [229, 238].

Acknowledgments—The work of KX is supported by the US Department of Energy, under Grant No. DE-SC0007914, U.S. National Science Foundation under Grant No. PHY-2112829, and in part by the PITT PACC. The work of PN is supported by U.S. Department of Energy under Grant No. DE-SC0010129.

4.5. NNLO $\alpha_S(m_Z^2)$ determination from HERA inclusive and jet data[82]

Deep inelastic scattering (DIS) of electrons on protons, e–p, at centre-of-mass energies of up to $\sqrt{s} \approx 320$ GeV at HERA has been central to the exploration of proton structure and quark–gluon dynamics as described by perturbative Quantum Chromodynamics (pQCD). The combination of H1 and ZEUS data on inclusive e–p scattering and the subsequent pQCD analysis, introducing the family of parton density functions (PDFs) known as HERAPDF2.0 [215], was a milestone for the exploitation of the HERA data. The work presented here represents a completion of the HERAPDF2.0 family with a fit at NNLO to HERA combined inclusive data and jet production data published separately by the ZEUS and H1

[82] Authors: A M Cooper-Sarkar (Univ. of Oxford), on behalf of H1 and ZEUS collaborations.

collaborations. This was not possible at the time of the original introduction of HERAPDF2.0 because a treatment at NNLO of jet production in e−p scattering was not available then.

The name HERAPDF stands for a pQCD analysis within the DGLAP formalism [239–241], where predictions from pQCD are fitted to data. These predictions are obtained by solving the DGLAP evolution equations at NNLO in the $\overline{\text{MS}}$ scheme. The inclusive and dijet production data which were already used for HERAPDF2.0Jets NLO were again used for the analysis presented here. A new data set [242] published by the H1 collaboration on jet production in low Q^2 events, where Q^2 is the four-momentum-transfer squared, was added as input to the fits.

The fits presented here were done in the same way as for all other members of the HERAPDF2.0 family, for full details see [243] and references therein. All parameter settings were the same as for the HERAPDF2.0Jets NLO fit, with the exception of the heavy quark masses m_c and m_b and their uncertainty ranges, which were reevaluated using the recently published HERA combined charm and beauty data [244]. The default minimum Q^2 of data entering the fit is $Q^2 = 3.5$ GeV^2 and the starting scale for DGLAP evolution is $Q_0^2 = 1.9$ GeV^2. Note that all HERA data are at very large W so that higher twist effects at small Q^2 and large x are not relevant.

As for previous HERAPDF analyses, model and parametrization uncertainties were evaluated. For the present analysis the uncertainties on the hadronization corrections for the jet data were included as systematic uncertainties, 50% correlated and 50% uncorrelated, together with the experimental systematic uncertainties.

The jet data were included in the fits at NNLO by calculating predictions for the jet cross sections using the NNLOJet [245] extension of NLOjet++ interfaced to the Applfast framework in order to achieve the speed necessary for iterative PDF fits. The predictions were supplied with uncertainties which were also input to the fit as 50% correlated and 50% uncorrelated systematic uncertainties.

The NNLO analysis of the jet data was applied to a slightly reduced phase space compared to HERAPDF2.0NLOJets. All data points with $\sqrt{\langle p_{\text{T}}^2\rangle + Q^2} \leqslant 10$ GeV were excluded to keep the level of scale uncertainties in the predictions for the data points to $\lesssim$10%. Six data points, the lowest $\langle p_{\text{T}}\rangle$ bin for each Q^2 region, were excluded from the ZEUS dijet data set because predictions for these points were not fully NNLO. The trijet data which were used as input to HERAPDF2.0NLOJets had to be excluded as their treatment at NNLO is not available. In addition six extra data points for H1 inclusive jet data at high Q^2 but low p_{T}, which were published more recently [242], were included.

The choice of scales was also adjusted for the NNLO analysis. At NLO, the factorization scale was chosen as $\mu_{\text{f}}^2 = Q^2$, while the renormalization scale was linked to the transverse momenta, p_{T}, of the jets by $\mu_{\text{r}}^2 = (Q^2 + p_{\text{T}}^2)/2$. For the NNLO analysis, $\mu_{\text{f}}^2 = \mu_{\text{r}}^2 = Q^2 + p_{\text{T}}^2$, was chosen for both factorization and renormalization scales.

Jet production data are essential for the determination of the strong coupling constant, $\alpha_S(m_Z^2)$. In pQCD fits to inclusive DIS data alone the value of $\alpha_S(m_Z^2)$ is strongly correlated to the shape of the gluon PDF. Data on jet production cross sections provide an independent constraint on the gluon distribution since inclusive jet and dijet production are directly sensitive to $\alpha_S(m_Z^2)$. Thus such data allow for an accurate simultaneous determination of $\alpha_S(m_Z^2)$ and the PDFs.

The HERAPDF2.0Jets NNLO fit with free $\alpha_S(m_Z^2)$ and $Q_{\text{min}}^2 = 3.5$ GeV^2 gives a value of

$$\alpha_S(m_Z^2) = 0.1156 \pm 0.0011\,(\text{exp})^{+0.0001}_{-0.0002}\,(\text{model/parameterization}) \pm 0.0029\,(\text{scale}).$$

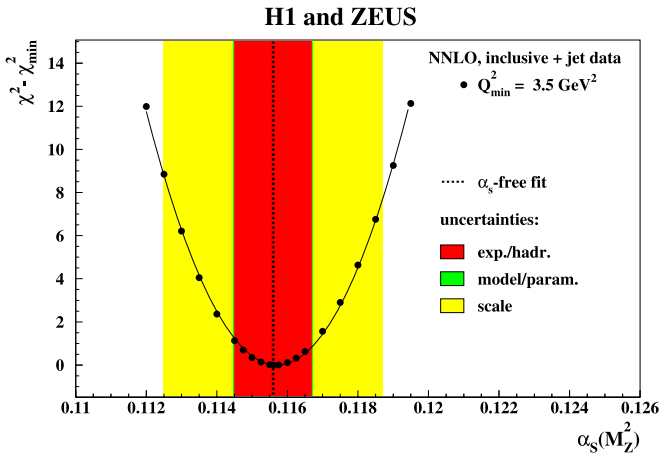

Figure 18. Distribution of $\Delta\chi^2 = \chi^2 - \chi^2_{\text{min}}$ versus $\alpha_S(m_Z^2)$ for HERAPDF2.0NNLOJets fits with fixed $\alpha_S(m_Z^2)$ values. Experimental, model/parametrization, and scale uncertainties are illustrated (figure from [243]).

Note that the the label experimental uncertainty covers the full experimental uncertainties of the simultaneous PDF and free $\alpha_S(m_Z^2)$ fit, which thus includes contributions from the PDF parametrization, the uncertainty on the hadronization corrections and the small uncertainties on the theoretical predictions. Additional model uncertainties come from variation of the input assumptions such as the the value of Q_0^2, the starting scale for QCD evolution, the value of the minimum Q^2 of data entering the fit and the values of heavy quark masses. Additional parametrization uncertainties come from the consideration of fits which have additional parameters that do not change the χ^2 of the fit significantly, but which can sometimes alter PDF shape. A further cross-check on the parametrization comes from modifying the gluon parametrization such that it must remain positive definite even at very low-x, $x < 10^{-4}$, and Q^2 below 2 GeV^2. The largest uncertainty comes from the scale uncertainty, as discussed later.

The HERAPDF2.0Jets NNLO fit with free $\alpha_S(m_Z^2)$ uses 1363 data points and has a goodness-of-fit per degree of freedom of $\chi^2/n_{\text{dof}} = 1614/1348 = 1.197$. This can be compared to the $\chi^2/n_{\text{dof}} = 1363/1131 = 1.205$ for HERAPDF2.0 NNLO based on inclusive data only. The similarity of the χ^2/n_{dof} values indicates that the data on jet production do not introduce any tension. Data/fit comparisons are shown in [243].

A scan of the fit χ^2 for fits with varying $\alpha_S(m_Z^2)$ shown in figure 18 and confirms the value of $\alpha_S(m_Z^2)$ and its experimental uncertainty found in the simultaneous $\alpha_S(m_Z^2)$ and PDF fit. The model, parameterization and scale uncertainties are also shown in the figure. The PDFs associated with this NNLO analysis are described in [243], the input of the jet data reduces the gluon PDF uncertainties.

The question whether data with relatively low Q^2 bias the determination of $\alpha_S(m_Z^2)$ arises in the context of the HERA data analysis for which low Q^2 is also low x. A treatment beyond DGLAP may be necessary because of low-x higher-twist terms, $\ln(1/x)$ terms or even parton saturation. To check for such bias the minimum Q^2 entering the fit was varied to $Q^2_{\text{min}} = 10$ and 20 GeV^2. Thus the HERAPDF analysis considers the possible impact of nonperturbative and beyond DGLAP effects on the result for $\alpha_S(m_Z^2)$. These variations do not alter the value of $\alpha_S(m_Z^2)$ obtained significantly, the value of $\alpha_S(m_Z^2)$ obtained for $Q^2_{\text{min}} = 10$ GeV^2 is

$\alpha_S(m_Z^2) = 0.1156 \pm 0.0011\,(\text{exp}) \pm 0.0002\,(\text{model/parameterization}) \pm 0.0021\,(\text{scale})$.

The scale uncertainty is reduced with this harder cut on Q^2 but the largest uncertainty still comes from the scale uncertainty.

The scale uncertainty was evaluated by varying the renormalization and factorization scales by a factor of two, both separately and simultaneously (7-point variation), and taking the maximal positive and negative deviations. Scale uncertainties were assumed to be 100% correlated between bins and data sets.

A strong motivation to determine $\alpha_S(m_Z^2)$ at NNLO was the hope to substantially reduce scale uncertainties from those determined at NLO. However, for our previous NLO result we had treated scale uncertainties as 50 % correlated and 50 % uncorrelated. If we repeat this treatment then the scale uncertainty for the present NNLO analysis (with $Q^2_{\text{min}} = 3.5\ \text{GeV}^2$, comparable to the NLO analysis) would be ± 0.0022, very significantly lower than the $+0.0037, -0.0030$ previously observed for the HERAPDF2.0NLOJets analysis. The absolute value of $\alpha_S(m_Z^2)$ at NNLO $\alpha_S(m_Z^2) = 0.1156$ is also lower than that observed at NLO $\alpha_S(m_Z^2) = 0.1183$. However, the analyses were done at different scales and with somewhat different data sets. In fact, if these choices were harmonized, the difference in the values of $\alpha_S(m_Z^2)$ would be even greater: at NLO $\alpha_S(m_Z^2) = 0.1186 \pm 0.0014$ (exp) and at NNLO $\alpha_S(m_Z^2) = 0.1144 \pm 0.0013$ (exp), where the scale choices are both $Q^2 + p_{\text{T}}^2$, the cuts on the data sets for both orders are the harder cuts introduced for the present analysis and the H1 low Q^2 jet data set [242] is excluded (this choice is made because these data cannot be well fitted at NNLO). The main reason for the decrease in the central value at NNLO is exclusion of these low-Q^2 H1 inclusive and dijet data.

It is clear that the main limiting factor today is the theoretical uncertainty, which we estimate from the scale uncertainty. The decrease in scale uncertainty between NLO and NNLO gives some hope for an increase in precision at N^{3}LO. Once theoretical uncertainties are reduced, the experimental uncertainty will need to be reduced. One may hope for progress from analyses at future e−p colliders such as the EIC/LHeC/FCC-eh. Experimental accuracy on $\alpha_S(m_Z^2) \sim 0.0001$ is projected at the LHeC [246].

Acknowledgments—AMC-S would like to thank the Leverhulme Trust.

4.6. Determination of the strong coupling $\alpha_S(m_Z^2)$ in the MSHT20 NNLO PDF fit[83]

MSHT20 [247] represented a significant step forward in the global determination of PDFs within the MSHT collaboration (previously MRST/MSTW/MMHT), with more data of greater precision across more channels and more differential in nature now incorporated alongside the inclusion of full NNLO QCD theoretical predictions (and NLO EW corrections where relevant [248]). This has been further complemented by progress on the methodological side, including in particular the extension of the PDF parameterization. The overall result was a significant improvement in our knowledge of the PDFs, including the central values and a general reduction of the PDF uncertainties. Within this context we undertook a follow-up study [249] examining the effects of varying the strong coupling and heavy quark masses within the global fit. This updated previous work with MMHT14 [250]. As a result of this new analysis we determined the preferred value of $\alpha_S(m_Z^2)$ and its associated uncertainty and we report on this in this brief review.

The default PDFs within MSHT are provided at $\alpha_S(m_Z^2) = 0.118$ at NNLO in order to provide a common value between different PDF fitting groups which is also consistent with the world average value of $\alpha_S(m_Z^2) = 0.1179 \pm 0.0009$ [251]. However, $\alpha_S(m_Z^2)$ can also be

[83] Authors: T Cridge (UCL, London) on behalf of the MSHT Collaboration.

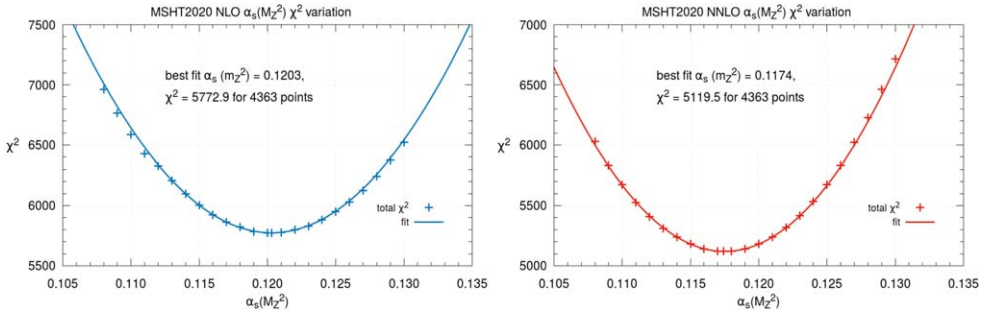

Figure 19. The plots show the total χ^2 as a function of $\alpha_S(m_Z^2)$ for NLO (left) and NNLO (right) MSHT20 fits respectively. Figure originally from [249].

left as a free parameter and fit alongside the PDFs, we are then able to utilize the global nature of the PDF fits to extract $\alpha_S(m_Z^2)$. Performing the fit with $\alpha_S(m_Z^2)$ free within MSHT20 at NLO and NNLO obtains the best fit values of 0.1203 and 0.1174 respectively, with the excellent quadratic χ^2 profiles shown in figure 19, demonstrating the clear sensitivity at the global fit level.

Nonetheless, performing such a fit simply extracts the best fit value of the strong coupling, in reality we wish to determine a value of the uncertainty arising on this value from the PDF fit. In order to do this, we utilize the dynamical tolerance method [247, 252, 253] which enables the determination of the 68% confidence level interval for the uncertainties on $\alpha_S(m_Z^2)$ by obtaining a 'tolerance' $\Delta\chi^2$ increase from the best fit value for a particular dataset. Once this is exceeded, it sets the upper and lower bound on a dataset-by-dataset level for the strong coupling. It should be noted this is the same method applied to the determination of the PDF uncertainties. Performing this across the vast array of datasets in MSHT20 one obtains bounds from each dataset on $\alpha_S(m_Z^2)$, the most relevant of which are presented in figure 20 for the MSHT20 NNLO fit, further details can be found in [249].

As can be observed, different datasets may prefer significantly different values of $\alpha_S(m_Z^2)$ within the context of the global PDF fit and correspondingly offer different bounds. Nonetheless, several general comments can be made. The fixed target and DIS data, and in particular the BCDMS and SLAC proton data, have a preference for lower values of the strong coupling (albeit not universally) in order to slow the fall of the structure function with Q^2. These represent relatively clean means of determining $\alpha_S(m_Z^2)$ through their high x nature meaning they are dominantly non-singlet. On the other hand, the HERA deep inelastic scattering data has relatively limited sensitivity compared to its large number of points in the fit, this is a reflection of its significant pull on the central values of the PDFs, meaning it naturally sits near the minimum of the profiles. The inclusive jets and Z p_{T} data from the LHC have direct sensitivity to $\alpha_S(m_Z^2)$ and are seen to generally prefer lower values of the strong coupling within the fit. This is also observed for the top data, certainly at NNLO, however the differential data are dropped from the determination of the global $\alpha_S(m_Z^2)$ bounds due to the fixed top mass available in the theoretical prediction grids utilized, which restricts their utility for the uncertainty determination. Finally, whilst the high precision W, Z data from the LHC have only indirect sensitivity to the strong coupling, these datasets are often still able to provide bounds on $\alpha_S(m_Z^2)$, and are generally seen to favour higher values of $\alpha_S(m_Z^2)$, albeit again not universally.

Examining these bounds on $\alpha_S(m_Z^2)$ across the whole fit, we can then extract the global upper and lower bounds on our strong coupling determinations. At NNLO the BCDMS

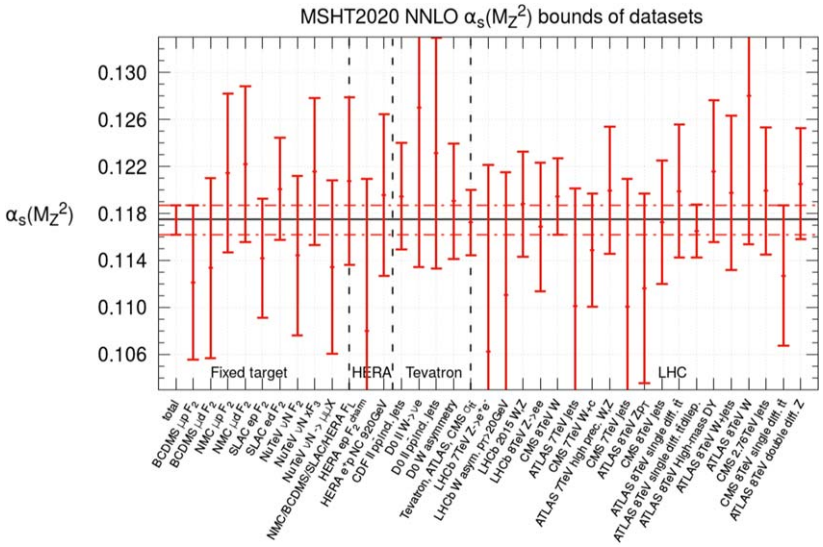

Figure 20. The plot shows the value of $\alpha_S(m_Z^2)$ corresponding to the best fit, together with the upper and lower 1σ constraints on $\alpha_S(m_Z^2)$ from the more constraining data sets at NNLO. The overall upper and lower bounds taken are given by the horizontal dashed red lines. Figure originally from [249].

proton data provides the tightest upper bound, reflecting its preference for a lower $\alpha_S(m_Z^2)$, its $\Delta\chi^2$ rises rapidly as the strong coupling is increased and therefore bounds the upward variation of $\alpha_S(m_Z^2)$. On the other hand, the CMS 8 TeV W data provides the most stringent lower bound, fitting with the general trend of the W, Z data favouring larger $\alpha_S(m_Z^2)$ values. Nonetheless, several other datasets would provide only slightly weaker bounds including the SLAC proton data in the upwards direction and the ATLAS 8 TeV Z and high mass Drell–Yan data in the downwards direction. Overall, a symmetrized uncertainty on the strong coupling is obtained of 0.0013, corresponding to a change of $\Delta\chi^2_{\text{global}} = 17$, a similar change in fit quality to that observed for changing the PDFs by their uncertainty in an eigenvector direction. A similar analysis can be performed at NLO, for which the BCDMS proton data again provides the tightest upper bound (followed by the ATLAS 8 TeV Z p_{T} and ATLAS 7 TeV inclusive jets data, demonstrating their preference for lower $\alpha_S(m_Z^2)$) whilst the LHCb 7 and 8 TeV W, Z data provides the lower bound (closely followed by the SLAC deuterium data). Overall the best fit values and uncertainties on $\alpha_S(m_Z^2)$ within MSHT at NLO and NNLO respectively are determined to be as follows and the NNLO result is consistent with the PDG world average[84]:

$$\alpha_S(m_Z^2)_{\text{NNLO}} = 0.1174 \pm 0.0013, \qquad \alpha_S(m_Z^2)_{\text{NLO}} = 0.1203 \pm 0.0015.$$

One of the benefits of performing such analyses within the context of global PDF fits, is the incorporation of correlations between the PDFs and the strong coupling, this is investigated in [249] and the standard method of treating the $\alpha_S(m_Z^2)$ uncertainty as an additional eigenvector in the fit and combining it in quadrature with the PDF uncertainty to obtain the total PDF + $\alpha_S(m_Z^2)$ uncertainty is demonstrated. Given these correlations, there are both

[84] It should be noted that the uncertainties given here are experimental in nature, propagated through the PDF fit, the theoretical uncertainties are not included within the global PDF fit at this stage.

direct contributions to the total uncertainty on an observable from the strong coupling change, but also indirect contributions from the associated correlated changes in the PDFs. The latter can partially cancel the direct $\alpha_S(m_Z^2)$ contribution to the uncertainty, for example by probing the gluon below $x \lesssim 0.1$ where it is anticorrelated with the value of the strong coupling. Studies of the heavy quark masses and their correlation with $\alpha_S(m_Z^2)$ were also performed for $m_{\rm charm}$ and demonstrated only limited correlation, with the value of $\alpha_S(m_Z^2)$ extracted rising slightly with the charm quark mass utilized.

The various PDF sets determined within this work are provided for public use on the MSHT website and the LHAPDF repository [254]. In particular, of relevance for this review are the sets provided at NLO and NNLO at fixed $\alpha_S(m_Z^2)$ in steps of 0.001 for the range $0.108 \leqslant \alpha_S(m_Z^2) \leqslant 0.130$, moreover the $\Delta\chi^2_{\rm global}$ in the PDF global fit at each fixed different value of $\alpha_S(m_Z^2)$ in these sets are provided [249].

Looking into the future, there are several developments which would facilitate improvements in $\alpha_S(m_Z^2)$ extractions from global PDF fits of deep inelastic scattering and collider data. Firstly, there are questions of the means to incorporate estimates of the theoretical uncertainties into the $\alpha_S(m_Z^2)$ extractions in global PDF fits (beyond relating it to (half) the difference of NLO and NNLO), this is being actively investigated by the various groups and progress is to be expected on this front. Meanwhile, the current uncertainties are limited by the experimental data available, as well as perhaps our understanding of its treatment. The measurements from the LHC in recent years of gluon-sensitive processes, such as inclusive jets and top processes have enabled improvements of our constraints on the PDFs and, in some cases also of $\alpha_S(m_Z^2)$. The rapid availability of grids for theoretical predictions for inclusion in PDFs for $\alpha_S(m_Z^2)$ sensitive processes, such as triple differential jet data, would enable further progress here and this could be complemented by the inclusion of deep inelastic scattering jet data from HERA. The ability to account for the top quark mass dependence in the top differential data would also certainly represent a step forward but is reliant on the provision of theoretical grids at different fixed values, we hope these can be provided in the short term. There is also the possibility of utilising ratios to provide particular sensitivity to $\alpha_S(m_Z^2)$, e.g. the ratio of the inclusive 3- and 2-jet cross-sections [255], in which the quantities involved are highly correlated (both experimentally and theoretically), these could further supplement the $\alpha_S(m_Z^2)$ sensitivity of the PDFs if included into the global fits. However, more analysis than simply providing the experimental data and corresponding theoretical predictions in a form suitable for inclusion in the PDFs is required. As precision has increased and statistical uncertainties have reduced, systematic uncertainties and their correlations have come to dominate in precision measurements. Correspondingly, increasingly global PDF fits have run into issues with such correlated systematic uncertainties and an improved understanding of such correlations would likely also benefit $\alpha_S(m_Z^2)$ extractions simultaneously to PDF extractions. More broadly, this study emphasizes the array of datasets with sensitivity to the strong coupling through the global PDF fits, with older fixed target data providing the tightest bounds in some places and newer LHC inclusive jet and high precision Drell–Yan data providing bounds in others. Therefore the continual evolution of the number and breadth of datasets included, along with their individual precisions, is important for further reducing these uncertainties, and we look forward to further data from the LHC and elsewhere in this regard.

Acknowledgments—TC would like to thank the Science and Technology Facilities Council (STFC) for support via grant awards ST/P000274/1 and ST/T000856/1.

4.7. Strong coupling determinations from the NNPDF global analyses[85]

The model-independent approach based on machine learning that is adopted by the NNPDF Collaboration is specially suitable for the simultaneous extraction of parton distributions together with SM parameters, such as the strong coupling $\alpha_S(m_Z^2)$, the heavy quark masses, and the CKM matrix elements [256] as well as BSM parameters such as Wilson coefficients in the Standard Model Effective Field Theory [257–259]. In this contribution, we briefly review studies of $\alpha_S(m_Z^2)$ fits in the context of the NNPDF global analyses, and outline ongoing studies in the framework of the NNPDF4.0 determination [260, 261].

The first determination of the strong coupling in the NNPDF framework was presented in [262] at NLO and updated in [263] to NNLO, in both cases based on the NNPDF2.1 dataset and fitting methodology [264, 265]. This dataset contained fixed-target DIS and Drell–Yan data, HERA collider DIS, and gauge boson and jet production measurements from the Tevatron, and hence was devoid of LHC data. A parabolic fit to the $\chi^2(\alpha_S)$ profile constructed from a large number of uncorrelated Monte Carlo replicas led to a value of the strong coupling

$$\alpha_S(m_Z^2) = 0.1173 \pm 0.0007_{\rm pdf} \pm 0.0009_{\rm mhou}, \tag{4.31}$$

at NNLO, where the missing higher order uncertainties (MHOUs) were estimated using the Cacciari–Houdeau method [266]. The stability of this determination with respect to the number of replicas was assessed, and the distribution of pulls from individual datasets was found consistent with statistical expectations.

The extraction of $\alpha_S(m_Z^2)$ within the NNPDF framework was subsequently revisited in [267], an analysis based on the NNPDF3.1 settings [268]. In order to fully account for the PDF- and data-induced correlations on $\alpha_S(m_Z^2)$, a new methodology denoted as the 'correlated replica (c-replica) method' was developed. In this approach, one also produces variants of the global fit for different $\alpha_S(m_Z^2)$ values, but in a manner that one has used correlated data- and PDF-replicas which are identical in all settings except for the value of the strong coupling itself. The correlated replica method makes possible a more robust estimate of the methodological uncertainties associated to the $\alpha_S(m_Z^2)$ extraction, at the price of a high computational cost since the number of replicas that need to be generated in this way is $\mathcal{O}(10^4)$.

Figure 21 (left) displays the NNPDF2.1- and NNPDF3.1-based NNLO determinations of $\alpha_S(m_Z^2)$, compared with the results from the corresponding MMHT14 and ABMP16 analyses as well as to the 2017 PDG average. The thicker error bars correspond to the PDF uncertainties, while the thinner ones indicate the addition in quadrature of PDF and MHO uncertainties. The latter are estimated as half the difference between the NNLO and NLO results. The NNPDF3.1-based NNLO result is found to be

$$\alpha_S(m_Z^2) = 0.1185 \pm 0.0005_{\rm pdf} \pm 0.0001_{\rm meth} \pm 0.0011_{\rm mhou}. \tag{4.32}$$

One can observe the good consistency between the two NNPDF determinations as well as among them and the MMHT14 the PDG average results. It is also clear how, specially for the NNPDF3.1-based analysis, MHOUs are currently the limiting factor in strong coupling determinations from global PDF fits. The methodological uncertainties, associated to e.g. the finite number of replicas, are found to be negligible in comparison to both the data and the MHO uncertainties. The role of the choice of figure of merit χ^2 was also explored, showing that the frequently used experimental definition leads to a downwards D'Agostini bias which is avoided with the t_0 definition [269, 270].

[85] Authors: J Rojo (NIKHEF and VU Amsterdam) on behalf of the NNPDF Collaboration.

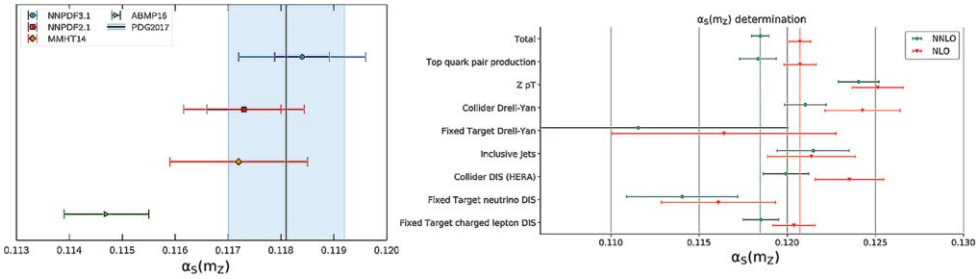

Figure 21. Left: NNPDF2.1- and NNPDF3.1-based NNLO determinations of $\alpha_S(m_Z^2)$, compared with the corresponding results from the MMHT14 and ABMP16 analyses as well as to the 2017 PDG average. The thicker error bars correspond to the PDF uncertainties, while the thinner ones indicate the addition in quadrature of PDF and MHO uncertainties. Right: central values and 68% CL uncertainties on $\alpha_S(m_Z^2)$ in the NNPDF3.1 NLO and NNLO analyses, comparing the baseline results with those obtained from the partial $\chi^2_p(\alpha_S)$ restricted to the specific subsets of processes indicated.

One issue that is frequently raised in the context of PDF-based α_S extractions is that of the interplay between the various types of processes that enter the global fit, and whether or not their relative pulls are overall consistent with the global determination. One possible strategy to gain some insight on this is provided by repeating the $\alpha_S(m_Z^2)$ extraction but now using the partial, $\chi^2_p(\alpha_S)$, rather than global, $\chi^2_{\rm tot}(\alpha_S)$, profiles. Hence in this case $\alpha_S(m_Z^2)$ is extracted from a $\chi^2_p(\alpha_S)$ profile restricted to the contribution of specific groups of processes, i.e. top quark or jet data. It should be emphasized, that, as discussed in detail in [271], it would not be correct to interpret these results as the value of α_S preferred by, say, top or jet data: such value could only be determined from a PDF fit based exclusively on this specific group of processes. With this caveat, figure 21 (right) displays the central values and 68% CL uncertainties on $\alpha_S(m_Z^2)$ in the NNPDF3.1 NLO and NNLO analyses, comparing the baseline results with those obtained from the partial $\chi^2_p(\alpha_S)$ restricted to the specific subsets of processes listed. One can observe that collider processes (jets, Z $p_{\rm T}$, Drell–Yan) tend to favour a larger $\alpha_S(m_Z^2)$ value as compared to the global fit result, while the opposite is found for most fixed-target measurements. The best-fit values from $\chi^2_p(\alpha_S)$ for top quark pair production and neutral-current DIS structure functions are similar to the global fit result.

Work in progress aims to revisit these $\alpha_S(m_Z^2)$ extractions now based on the recent NNPDF4.0 [260, 261] analysis. NNPDF4.0 benefits from a number of methodological improvements as well as from the addition of several gluon-sensitive measurements, such as dijets [272], direct photon production [273], and several new top quark production datasets, which in turn provide novel handles on the α_S value. The left panel of figure 22 compares the gluon-gluon PDF luminosity at the LHC $\sqrt{s} = 14$ TeV between the NNPDF3.1 and NNPDF4.0 NNLO fits, highlighting the impact of the new gluon-sensitive measurements both in terms of uncertainty reduction as well as in the shift in central values. The right panel of figure 22 displays the percentage PDF uncertainties in the double-differential gluon-gluon luminosity as a function of m_X and the rapidity y in NNPDF4.0 NNLO, showing how uncertainties are at the 1% level for most of the kinematic range accessible at the LHC. In order to fully exploit the uncertainty reduction in the PDF determination observed in NNPDF4.0, it will be crucial to assess carefully all other sources of uncertainty that impact

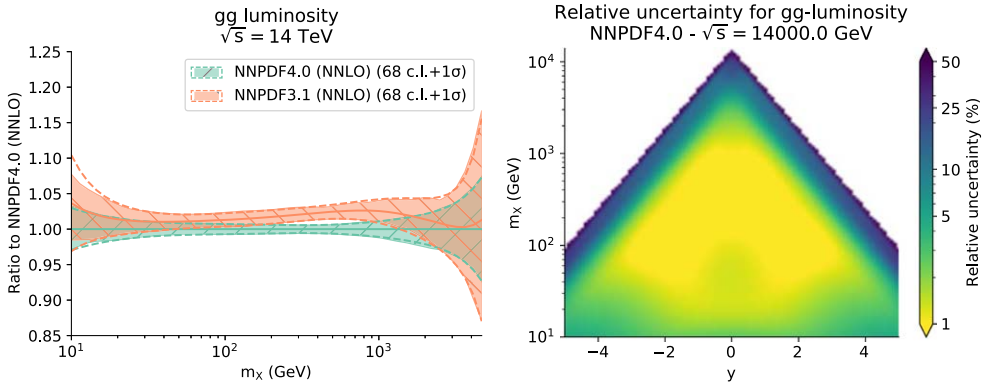

Figure 22. Left: comparison of the gluon-gluon PDF luminosities at the LHC $\sqrt{s} = 14$ TeV as a function of the invariant mass m_X between the NNPDF3.1 and NNPDF4.0 NNLO fits, highlighting the impact of the new gluon-sensitive measurements. Right: relative PDF uncertainties in the double-differential gluon-gluon luminosity as a function of m_X and the rapidity y in NNPDF4.0.

the α_S extraction of global PDF fits, in particular those associated with MHOUs, which will be tackled using the strategy laid out in [274, 275].

Future work by the NNPDF collaboration will focus on extending the correlated replica method to the NNPDF4.0 fits and update the determination of the strong coupling constant. Another option that is being considered is the recently developed SIMUNET methodology [257], based on an extension of the NNPDF4.0 neural network architecture with an extra layer to simultaneously determine PDFs alongside an arbitrary number of SM and BSM parameters from the direct joint minimization of the χ^2 figure of merit. The main advantage of SIMUNET would be to bypass the need of running a very large number of MC replicas, since the simultaneous extraction of $\alpha_S(m_Z^2)$ together with the PDFs would only require $N_{\rm rep} = \mathcal{O}(100)$ replicas as in standard NNPDF fits. Results for the determination of $\alpha_S(m_Z^2)$ from NNPDF4.0 using both SIMUNET and the correlated replica method will be presented in the near future.

4.8. Measurements of α_S from spin structure functions[86]

In this section, we discuss the extraction of α_S from nucleon spin structure data. The information is obtained from the cross-section asymmetry of Deep Inelastic scattering (DIS). The cross-section for inclusive lepton scattering is:

$$\frac{d\sigma}{d\Omega\, dx} = \sigma_{\rm Mott}[aF_1(x, Q^2) + bF_2(x, Q^2) + cg_1(x, Q^2) + dg_2(x, Q^2)], \tag{4.33}$$

where Ω is the solid angle, and $\sigma_{\rm Mott}$, a, b, c and d are kinematic factors (see e.g. [276] for their explicit expressions). In particular, $\sigma_{\rm Mott}$ is the Mott cross-section for scattering off a point-like target. The information on the nucleon structure is contained in the four structure functions $F_1(x, Q^2)$, $F_2(x, Q^2)$, $g_1(x, Q^2)$ and $g_2(x, Q^2)$. The unpolarized structure functions F_1 and F_2 are obtained with unpolarized beam and/or target and are kinematically separated by varying a and b. The spin structure functions g_1 and g_2 arise when beam and target are both polarized. One accesses g_1 and g_2 by measuring beam spin asymmetries. Varying the target polarization direction allows to separate g_1 from g_2. One can extract α_S from g_1 (g_2 is harder

[86] Author: A Deur (JLAB).

to measure and without simple partonic interpretation) by performing a global fit of its Q^2-evolution, see e.g. [277]. This is a thorough but complex method, and modeled nonperturbative inputs (quark and gluon PDFs and possibly higher twists) are required. Alternatively, the Q^2-evolution of the moment $\Gamma_1(Q^2) \equiv \int_0^1 g_1(x, Q^2)dx$ can be used. The method is much simpler since there is no x-dependence, and the nonperturbative inputs are the more-or-less well-measured axial charges a_0, a_3 and a_8 [276] (and higher-twists if low-Q^2 data are used). The difficulty is that the low-x contribution to a moment cannot be measured, as it would require infinite beam energy. Furthermore, a_0, which is the quark spin contribution to the nucleon spin, is Q^2-dependent and in some renormalization schemes may receive a contribution from the polarized gluon PDF ΔG. Extracting α_S is further simplified when the isovector component of Γ_1 is used, *viz*, $\Gamma_1^p - \Gamma_1^n \equiv \Gamma_1^{p-n}$. The relevant axial charge is precisely measured ($a_3 = g_A = 1.2762(5)$) [251], the Q^2-evolution of Γ_1^{p-n} is known to higher order than $\Gamma_1^{p,n}$ or g_1 [278–280], and there is no gluon contribution. On the other hand, the low-x issue remains and Γ_1^{p-n} measurements are demanding since polarized proton and neutron data are needed. We will focus here on using Γ_1^{p-n}.

The Bjorken sum rule [281, 282] generalized to finite Q^2 by including QCD radiative and power corrections is [278–280]:

$$\Gamma_1^{p-n}(Q^2) = \frac{g_A}{6}\left[1 - \frac{\alpha_S}{\pi} - 3.58\left(\frac{\alpha_S}{\pi}\right)^2 - 20.21\left(\frac{\alpha_S}{\pi}\right)^3 - 175.7\left(\frac{\alpha_S}{\pi}\right)^4 - \sim 893\left(\frac{\alpha_S}{\pi}\right)^5 + \mathcal{O}(\alpha_S^6)\right] + \frac{M^2}{Q^2}(a_2 + 4d_2 + 4f_2) + \mathcal{O}(1/Q^4), \tag{4.34}$$

where the series coefficient values are for $\overline{\text{MS}}$ and $N_\text{f} = 3$. Here, M^2 is nucleon mass, $a_2(Q^2)$ and $d_2(Q^2)$ are the twist-2 and 3 target mass corrections, respectively, and $f_2(Q^2)$ is the dynamical twist-4 correction. The higher twist coefficients are also subject to QCD radiative corrections and thus depend on α_S, i.e. Q^2. To extract α_S, one can either solve equation (4.34) for α_S or fit the Q^2-dependence of equation (4.34). The latter method is more accurate because it suppresses systematic uncertainties affecting the magnitude of Γ_1^{p-n} [283]. Such analysis was performed on the data of the Jefferson Lab (JLab) experiment EG1dvcs [284, 285]. The experiment took data during the 6 GeV era of JLab and used the CEBAF Large Acceptance Spectrometer (CLAS) together with polarized NH_3 (for proton) and ND_3 (for neutron) targets and the JLab polarized electron beam. Since EG1dvcs was dedicated to exclusive measurements (DVCS process) it provides inclusive data with very high statistics. Only EG1dvcs data were used to avoid uncorrelated systematics between different experiments since, in contrast to point-to-point correlated systematics (e.g. from polarimetries), uncorrelated errors are not suppressed in the extraction of α_S. Furthermore, since the EG1dvcs data largely dominate the world data in terms of statistics, including other experiments would only increase the systematic uncertainty on the extraction without being balanced by the gains in Q^2 leverage and statistics. However, one must recognize that the availability of polarized g_1 data from higher energy experiments [286–289, 290–304] is crucial for this analysis since it allows to control the low-x extrapolation necessary to complement Γ_1^{p-n}. The EG1dvcs data used cover $Q^2 > 2.32$ GeV^2 and are comprised of five data points. The statistical uncertainty is negligible for this analysis. The point-to-point correlated uncertainty was separated from the point-to-point uncorrelated one using the *unbiased estimate* prescription [251, 305], and the uncertainties on the low-x extrapolation were approximately separated into Q^2-dependent and independent parts. Thus, a large fraction of the uncertainties is suppressed in the extraction of α_S. The dominant errors are the point-to-point uncorrelated (4.4%) and correlated (3.3%) uncertainties. The others are

negligible (power corrections: <0.1 %; equation (4.34) truncation: 1.3%; truncation of the β-series needed to evolve α_S to m_Z: 0.1%). In all the analysis provided $\alpha_S(m_Z^2) = 0.1123 \pm 0.0061$ [306] at N^{3}LO with an N^{4}LO correction estimate, see equation (4.34).

This analysis can be repeated with better precision in the future thanks to two developments. The first is experiment EG12 using CLAS12 with the JLab 11-GeV beam and scheduled for June 2022. The expected precision is similar to EG1dvcs, but with a Q^2 reach of up to 6 GeV and better low-x coverage. The second is the EIC [307], which will now be summarily described.

The optimal Q^2 range to extract α_S from Γ_1^{p-n} at EIC is $1 \lesssim Q^2 \lesssim 50$ GeV^2. Below, power corrections could be an issue and above, the unmeasured low-x part of Γ_1^{p-n} becomes large ($\gtrsim$15%. Since for EIC there will be no higher energy data to guide the low-x extrapolation, it must be kept small). Assuming a luminosity of 2×10^{33} cm^{-2}s^{-1} and an electron (nucleus) beam polarization of 50% (60%), a year of data taking yields statistical uncertainties ranging from $\Delta\Gamma_1^{p-n} = 0.5\%$ for $Q^2 = 3$ GeV^2 to 0.05% for $Q^2 = 15$ GeV^2. For systematics, we assume 4% for deuteron's nuclear corrections or negligible if the associated proton can be tagged, 100% on the low-x extrapolation, 3% on beam polarimetries, 6% on radiative corrections, 2.5% on the F_1 structure function necessary to form g_1 from the measured A_1 asymmetry [276] (specifically, we assumed 2% on F_2 and 10% on the R ratio). Since g_2 will be measured at the EIC, correcting for it to obtain A_1 from the experimental asymmetry $A_{||}$ will not add significant uncertainties. We neglected the contamination from particle misidentification. Detector/trigger efficiencies, acceptance, beam currents uncertainties are negligible for asymmetry measurements. Finally, we assumed that 60% of the systematic is point-to-point uncorrelated, as found for the EG1dvcs data. Fitting the simulated pseudodata yields $\Delta\alpha_S(m_Z^2) = \pm 0.0033 \pm 0.0005$, where the first (second) uncertainty is point-to-point uncorrelated (correlated). The fit was performed over $1.5 \leqslant Q^2 \leqslant 15$ GeV^2. Adding a higher Q^2 data point only reduces marginally the point-to-point uncorrelated error while significantly increasing the correlated one: $\Delta\alpha_S(m_Z^2) = \pm 0.0030 \pm 0.0021$. Increasing the statistics by a factor of 10 and assuming that the proton of the deuteron can be tagged yields $\Delta\alpha_S(m_Z^2) = \pm 0.0016 \pm 0.0003$. This simple exercise suggests that an accurate measurement of acceptable precision is possible at EIC, warranting to investigate more seriously the possibility. A more thorough investigation is currently being performed by the EIC structure function working group.

Another method has been used to extract α_S from Γ_1^{p-n} at low Q^2. It is based on the gauge-gravity duality, specifically LFHQCD [308], a model closely tied to QCD. The Lagrangian of LFHQCD is that of QCD quantized on the light-front, a completely rigorous procedure. The only unknown is the interaction part of the Lagrangian. It can be determined by imposing the approximate chiral symmetry of QCD. Alternatively, one can require QCD's approximate conformal symmetry and apply de Alfaro–Fubini–Furlan procedure [309], or require that the light-front potential transformed to the traditional instant-form produces the Cornell potential in the heavy quark case [310]. The three methods lead to the same semiclassical potential that effectively accounts for the action of the gluons. Imposing upon LFHQCD a nearly exact QCD symmetry to determine the full Lagrangian is the same procedure as used for chiral perturbation theory to determine its Lagrangian. However, contrary to the latter, no counterterms determined from phenomenology are required for LFHQCD since renormalization is unnecessary for nonperturbative frameworks. In fact, LFHQCD has in principle a single free parameter, determined e.g. from a hadron mass or a fit to the $\Gamma_1^{p-n}(Q^2)$ data at low Q^2. (One free parameter is always needed to set units since they are arbitrary human conventions.) In practice, LFHQCD has a few additional parameters to account for hadronic higher Fock

states. They are however of secondary importance and do not enter the determination of α_S discussed here. LFHQCD provides a wide range of results that agree with experiments, including hadron spectroscopy [311], form factors [312], polarized and unpolarized PDFs and GPDs [313–315] and $\alpha_S(Q^2)$ [316]. The latter is obtained by forming the effective charge [201, 202, 317] characterizing $\Gamma_1^{p-n}(Q^2)$ and calculating it with LFHQCD. The obtained effective charge, straightforwardly related to α_S, is valid over the $0 \leqslant Q^2 \lesssim 2$ GeV^2 domain. Thus, LFHQCD and pQCD share a domain of applicability over $1 \lesssim Q^2 \lesssim 2$ GeV^2. Using the analytical expressions of α_S from LFHQCD and pQCD one can then deduce the relation between Λ_s and the LFHQCD scale parameter [318, 319]. The procedure yields $\alpha_S(m_Z^2) = 0.1190 \pm 0.0006$ (N^{3}LO). The uncertainty, which is comparable to that of the best lattice results, comes from uncertainties on the LFHQCD scale, on the chiral limit approximation and on the truncations of the Bjorken and α_S pQCD series.

To summarize, two determinations of α_S using the Bjorken sum Γ_1^{p-n} were reviewed. The first yields $\alpha_S = 0.1123 \pm 0.0061$ (N^{3}LO) [306] and is based on a fit to the JLab EG1dvcs data. A similar analysis of the expected EIC data may reduce the uncertainty to $\Delta\alpha_S \simeq \pm 0.0016$. The second determination, $\alpha_S = 0.1190 \pm 0.0006$ (N^{3}LO) [319], is obtained by matching the pQCD expression of α_S to that from LFHQCD in the domain of validity common to the two approaches.

Acknowledgments—This material is based upon work supported by the U.S. Department of Energy, Office of Science, Office of Nuclear Physics under contract DE-AC05-06OR23177.

4.9. $\alpha_S(m_Z^2)$ from a combined NNLO analysis of normalized jet cross sections and DIS data[87]

The H1 and NNLOJET Collaborations have performed a simultaneous determination of PDFs and $\alpha_S(m_Z^2)$ using the entire set of inclusive neutral-current and charged-current (NC and CC) DIS data from H1 together with all of H1's normalized inclusive jet and dijet cross section data [320]. The methodology of the analysis follows closely the well-established formalism of PDF determinations at HERA, as it was previously employed for HERAPDF-style or H1PDF-style fits [215, 321, 322], but additionally $\alpha_S(m_Z^2)$ is further considered as a free parameter in the fit.

The α_S sensitivity in the analysis is obtained by exploiting H1's normalized inclusive jet and dijet cross sections that were published previously [242, 323, 324]. These jet measurements were performed double-differentially as functions of Q^2 and p_T (where p_T denotes the transverse momenta of a single jet for inclusive jets, and the average p_T of the dijet system). The data were taken during the HERA-I [323] and HERA-II [242, 324] running periods and for Q^2 values lower than 100 GeV^2 [242] or above [323, 324], and jets were measured in the Breit frame in the range of about $4.5 < p_T < 50$ GeV. Differently than absolute jet cross sections, normalized jet cross are measured as the ratio of absolute jet cross sections to the bin-integrated inclusive NC DIS cross section in the respective Q^2 interval. Thus, some experimental uncertainties are reduced or cancel (like normalization uncertainties), and since the inclusive DIS data themselves are used in the fit, the correlations of the uncertainties between different data sets are correctly treated in the fit. It is also hoped that the PDF-dependence cancels out to some extent. Since jet cross sections in the Breit frame are proportional to $\mathcal{O}(\alpha_S^1)$ in leading-order pQCD, while inclusive DIS is of $\mathcal{O}(\alpha_S^0)$, the α_S dependence is preserved but smaller experimental uncertainties are achieved, when compared to absolute jet cross sections.

[87] Authors: D Britzger (MPI Munich) on behalf of the H1 Collaboration.

The selected inclusive DIS data comprise the full set of H1's inclusive NC and CC DIS data, and makes particularly use of the combined low-Q^2 data from HERA-I [325] and high-Q^2 data with polarized lepton beams from HERA-II [322]. The x-dependence of five orthogonal PDFs (g, $\bar{u}$, $\bar{d}$, $\bar{U}$, $\bar{D}$) are parameterized at a scale of $\sqrt{1.9}$ GeV using a common HERAPDF-style parameterization. The inclusive DIS data is restricted to $Q^2 > 12$ GeV^2, to reduce effects from heavy-quark masses and low-x effects [326]. Since the α_S-sensitivity arises from the matrix elements of the jet data, the α_S results are rather insensitive to the exact parameterization of the PDFs. The PDF evolution and structure function calculation is performed using the program QCDNUM [327] in the ZM-VFNS scheme.

The jet data are confronted for the first time with NNLO predictions [328, 329] from NNLOJET [330] with five massless flavours and interfaced to fastNLO [331], and the denominator of the normalized jet cross sections is calculated in NNLO using QCDNUM. Similarly as inclusive DIS data, also jet data are restricted to scales that are two times higher than the b-quark mass in order to reduce the impact from heavy quark masses. The renormalization and factorization scales are identified with $\mu^2 = Q^2 + p_{\mathrm{T}}^2$. The NNLO predictions are corrected for hadronization effects using multiplicative correction factors, which were derived using the MC event generators Djangoh [332] and Rapgap [333].

The fit minimizes a χ^2 quantity based on log-normal probability distribution functions. At the minimum $\chi^2/n_{\mathrm{dof}} = 1.0$ for $n_{\mathrm{dof}} = 1516$ degrees of freedom is found, which is an excellent data-to-theory agreement. The value of $\alpha_S(m_Z^2)$ is determined in the PDF+$\alpha_S(m_Z^2)$ fit to [320]

$$\alpha_S(m_Z^2) = 0.1147(11)_{\mathrm{exp,had,PDF}}(2)_{\mathrm{mod}}\,(3)_{\mathrm{par}}(23)_{\mathrm{scale}}, \tag{4.35}$$

where the first uncertainty denotes the *fit* uncertainty, the second and third component is obtained from variations of model (mod) or parameterization (par) assumptions of the PDF. The last uncertainty denotes scale uncertainties which are obtained from repeating the fit with scale-factors of 0.5 and 2. The α_S value is found to be consistent with a determination from non-normalized jet cross sections (section 8). The resulting PDF is denoted H1PDF2017nnlo and is found to be somewhat compatible with NNPDF3.1 [268] and in good consistency with NNPDF3.1sx [326].

In a PDF+$\alpha_S(m_Z^2)$ fit to inclusive DIS data alone, large uncertainties in $\alpha_S(m_Z^2)$ are obtained, and it was shown that the inclusion of normalized jet data reduces the correlation of $\alpha_S(m_Z^2)$ and the gluon density in the PDF+α_S fit [320]. It can be concluded that the sensitivity to $\alpha_S(m_Z^2)$ arises exclusively from the jet data, but not from the inclusive DIS data, which is also seen from the small (mod) and (par) uncertainties in equation (4.35).

A recent reanalysis of the selected H1's normalized jet cross section data from the H1PDF2017nnlo analysis by a somewhat different author group [243] exploits the same NNLO predictions. Differences are in the selection of the DIS data, and the addition of further non-normalized DIS jet data. That analysis finds a consistent result for $\alpha_S(m_Z^2)$, equal-sized experimental uncertainties, and also scale uncertainties of comparable size (albeit a bit higher). It is concluded, that the superior sensitivity of H1's normalized jet data to $\alpha_S(m_Z^2)$ makes the $\alpha_S(m_Z^2)$ result from the PDF+α_S fit rather insensitive to changes in the inclusive DIS data, or to the addition of further, absolute, jet cross sections from HERA. The scope of [243] focuses on different QCD aspects, like PDFs, but it does not supersede the original α_S analysis [320], since it does not employs improved predictions, or achieves smaller uncertainties in $\alpha_S(m_Z^2)$. Therefore, the present α_S from HERA (normalized) jet data from PDF+α_S analyses remains is quoted in [320], and equation (4.35). Future uncertainty reductions can be

achieved with improved predictions, like N^{3}LO, or by adding normalized jet data from more experiments.

5. $\alpha_S(m_Z^2)$ from electroweak data

The present QCD coupling world average [251] contains an 'electroweak precision fit' category where an $\alpha_S(m_Z^2) = 0.1208 \pm 0.0028$ value is determined from the average of two results: (i) a global fit of multiple SM electroweak and Higgs observables with the QCD coupling constant left as single free parameter, yielding $\alpha_S(m_Z^2) = 0.1194 \pm 0.0029$ [334], and (ii) a fit of three hadronic pseudoobservables measured at LEP and SLC in e^+e^- collisions at the Z mass pole [335], resulting in $\alpha_S(m_Z^2) = 0.1221 \pm 0.0027$. More recently, [336] has improved both Z-boson-based determinations by incorporating higher-order theoretical corrections [337–339] and an experimental update of the LEP luminosity corrections [340]. In addition, it has been shown that similar future high-precision measurement of W boson hadronic decays [336, 341] will also provide competitive $\alpha_S(m_Z^2)$ determinations. The results of these two latest $\alpha_S(m_Z^2)$ extractions from Z and W boson decays are summarized below.

5.1. Strong coupling from electroweak boson decays at N^{3}LO accuracy[88]

The $\alpha_S(m_Z^2)$ value can be neatly extracted from various electroweak-boson hadronic pseudoobservables that can be accurately measured in high-energy e^+e^- collisions, such as:

1. The W and Z hadronic widths, computable theoretically through the expression

$$\Gamma^{\rm had}_{\rm W,Z}(Q) = \Gamma^{\rm Born}_{\rm W,Z}\left(1 + \sum_{i=1}^{4} a_i(Q)\left(\frac{\alpha_S(Q)}{\pi}\right)^i + \mathcal{O}(\alpha_S^5) + \delta_{\rm EW} + \delta_{\rm mix} + \delta_{\rm np}\right), \tag{5.1}$$

   where the Born width $\Gamma^{\rm Born}_{\rm W,Z} = f(G_{\rm F}, m^3_{\rm W,Z}, N_{\rm C}; \sum |{\rm V}_{ij}|^2)$ depends on the Fermi constant G_F, the cube of the EW boson mass, the number of colours N_C, and, in the W case, also on the sum of CKM matrix elements $|{\rm V}_{ij}|^2$. The $a_i(Q)$ and $\delta_{\rm EW,mix,np}$ terms are, respectively, higher-order pQCD, EW, mixed, and non-pQCD corrections discussed below. Since the total W and Z widths—given by the sum of hadronic and leptonic partial widths $\Gamma^{\rm tot}_{\rm W,Z} = \Gamma^{\rm had}_{\rm W,Z} + \Gamma^{\rm lep}_{\rm W,Z}$—have smaller experimental uncertainties than the hadronic ones alone, and since $\Gamma^{\rm lep}_{\rm W,Z}$ can be both accurately measured and computed, the value of $\Gamma^{\rm tot}_{\rm W,Z}$ is often directly used to determine $\alpha_S(m_Z^2)$.
2. The ratio of W, Z hadronic-to-leptonic widths, defined theoretically as

$$R_{\rm W,Z}(Q) = \frac{\Gamma^{\rm had}_{\rm W,Z}(Q)}{\Gamma^{\rm lep}_{\rm W,Z}(Q)} = R^{\rm EW}_{\rm W,Z}\left(1 + \sum_{i=1}^{4} a_i(Q)\left(\frac{\alpha_S(Q)}{\pi}\right)^i + \mathcal{O}(\alpha_S^5) + \delta_{\rm mix} + \delta_{\rm np}\right), \tag{5.2}$$

   where the $R^{\rm EW}_{\rm W,Z} = f(\alpha, \alpha^2, ...)$ prefactor, which depends on the fine structure constant α, accounts for the purely electroweak dependence of the calculation. Experimentally, in the W boson case the denominator of the R_W ratio represents the *sum* of all leptonic decays, which can be accurately determined from the ratio of hadronic over leptonic decay branching ratios: $R_{\rm W} = \mathcal{B}^{\rm had}_{\rm W}/\mathcal{B}^{\rm lep}_{\rm W} = 2.0684 \pm 0.0254$ [251]. However, in the Z boson case the denominator of R_Z (often labeled R^0_ℓ) is the average width over the three charged lepton species, i.e. $R_{\rm Z} = \Gamma^{\rm had}_{\rm Z}/\Gamma^{\ell}_{\rm Z} = 20.767 \pm 0.025$ [251] with $\Gamma^{\ell}_{\rm Z} = \frac{1}{3}(\Gamma^{\rm e}_{\rm Z} + \Gamma^{\mu}_{\rm Z} + \Gamma^{\tau}_{\rm Z})$, which can be more precisely measured.

[88] Authors: D d'Enterria (CERN).

3. In the Z boson case, the hadronic cross section at the resonance peak in e^+e^- collisions, theoretically given by

$$\sigma_{\rm Z}^{\rm had} = \frac{12\pi}{m_{\rm Z}} \cdot \frac{\Gamma_{\rm Z}^{e}\,\Gamma_{\rm Z}^{\rm had}}{(\Gamma_{\rm Z}^{\rm tot})^2}, \tag{5.3}$$

where $\Gamma_{\rm Z}^{e}$ is its electronic width. This quantity is also useful because $\sigma_{\rm Z}^{\rm had}$ can be measured with small experimental uncertainties in the $e^+e^- \to {\rm Z} \to$ hadrons process, independently of any of the $\Gamma_{\rm Z}^{\rm e,had,tot}$ widths appearing in the theoretical equation.

In [336], two new determinations of the QCD coupling constant at the Z pole have been carried out from detailed comparisons of inclusive W and Z hadronic decays data to state-of-the-art pQCD calculations at next-to-next-to-next-to-leading order (N^3LO) accuracy, incorporating the latest experimental and theoretical developments. In the W boson case, the total width computed at N^3LO has been used for the first time in the extraction. For the Z boson pseudoobservables, the N^3LO results have been complemented with the full two- and partial three-loop EW corrections recently made available, and the experimental values have been updated to account for newly estimated LEP luminosity biases. A combined reanalysis of the Z boson data yields $\alpha_S(m_Z^2) = 0.1203 \pm 0.0028$, with a 2.3% uncertainty reduced by about 7% compared to the previous state-of-the-art. From the combined W boson data, a value of $\alpha_S(m_Z^2) = 0.107 \pm 0.035$ is extracted, with still large experimental uncertainties but also reduced compared to previous works. The levels of theoretical and parametric precision required in the context of QCD coupling determinations with permil uncertainties from high-statistics W and Z boson samples expected at future e^+e^- colliders, such as the FCC-ee, are discussed.

5.1.1. $\alpha_S(m_Z^2)$ from W boson decays. The state-of-the-art analytic unintegrated expressions for the leptonic and hadronic W boson decay widths [342, 343] have been integrated out, and convenient parametrizations of all quantities of interest ($\Gamma_{\rm W}^{\rm lep,had,tot}$ and R_W) have been derived for the subsequent $\alpha_S(m_Z^2)$ fitting procedure. The parametrizations of all the W boson observables include the full-N^3LO QCD $\mathcal{O}(\alpha_S^4)$, the leading EW $\mathcal{O}(\alpha)$, and mixed QCD+EW $\mathcal{O}(\alpha_S\alpha)$ corrections. The value of $\alpha_S(m_Z^2)$ is then obtained by a combined fit of the theoretical expressions for $\Gamma_{\rm W}^{\rm tot}$ and R_W to the experimental data: $\Gamma_{\rm W}^{\rm tot} = 2085 \pm 42$ and $R_{\rm W} = 2.0684 \pm 0.0254$ (combining the three leptonic decays, assuming lepton universality). The relative experimental uncertainties of $\Gamma_{\rm W}^{\rm tot}$ and R_W are 2% and 1.2%, respectively, and combining both observables in the fit, assuming them to be fully uncorrelated [226, 344], provides some improvement in the final $\alpha_S(m_Z^2)$ precision. The derived $\alpha_S(m_Z^2)$ values are tabulated in table 8, and the corresponding goodness-of-fit $\Delta\chi^2$ scans are plotted in figure 23 (left). Without imposing CKM unitarity, the fitted QCD coupling constant is left basically unconstrained: $\alpha_S(m_Z^2) = 0.042 \pm 0.052$, due to the large dominant parametric uncertainties of the theoretical $\Gamma_{\rm W}^{\rm tot}$ and R_W calculations. Imposing unitary of the CKM matrix leads to an extraction with ∼30% uncertainty of experimental origin. The obtained value of $\alpha_S(m_Z^2) = 0.107 \pm 0.035$ (with comparatively negligible parametric and theoretical uncertainties) is obviously, within its large uncertainties, in perfect accord with the current world average (orange band in figure 23). With respect to the previous NNLO extraction, $\alpha_S(m_Z^2) = 0.117 \pm 0.042$ based on R_W alone [341], our new calculation leads to a ∼10% relative improvement in the experimental (as well as more accurate N^3LO theoretical and parametric) uncertainties.

Achieving a truly competitive $\alpha_S(m_Z^2)$ determination from the W decay data, with propagated experimental uncertainties reduced by a factor of ×30 at least (i.e. below the 1%

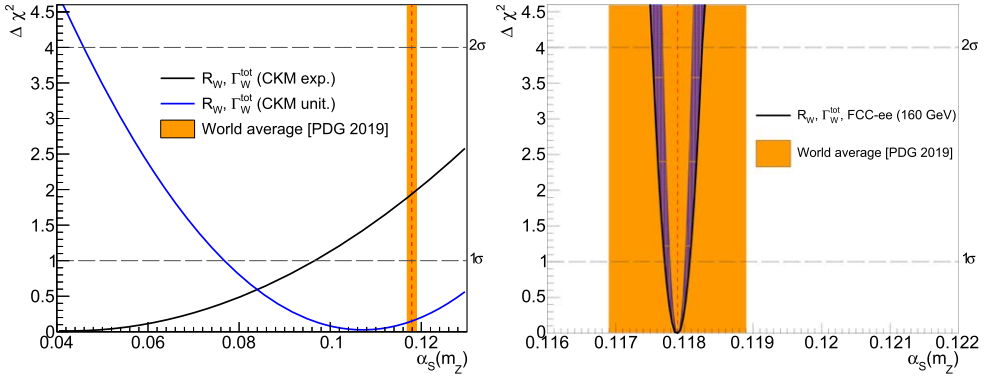

Figure 23. $\Delta\chi^2$ fit profiles of the $\alpha_S(m_Z^2)$ determined from the combined N^{3}LO analysis of the total W width and R_W ratio, compared to the 2019 $\alpha_S(m_Z^2)$ world average (vertical orange band). Left: extraction with the present W data assuming (blue curve) or not (black curve) CKM unitarity. Right: extraction expected at the FCC-ee, with the total (experimental, parametric, and theoretical, added in quadrature) uncertainties (outer parabola) and with the experimental uncertainties alone (inner parabola).

Table 8. Values of $\alpha_S(m_Z^2)$ extracted from the combined Γ_W^{tot} and R_W measurements compared to the corresponding N^{3}LO theoretical calculations, assuming or not CKM unitarity, with the breakdown of propagated experimental, parametric, and theoretical uncertainties. The last row lists the $\alpha_S(m_Z^2)$ result expected in e^+e^- collisions at the FCC-ee.

W boson observables	$\alpha_S(m_Z^2)$	$\alpha_S(m_Z^2)$ uncertainties		
		exp.	param.	theor.
Γ_W^{tot}, R_W (exp. CKM)	0.042 ± 0.052	± 0.027	± 0.045	(± 0.0014)
Γ_W^{tot}, R_W (CKM unit.)	0.107 ± 0.035	± 0.035	(± 0.0002)	(± 0.0016)
Γ_W^{tot}, R_W (FCC-ee, CKM unit.)	0.11790 ± 0.00023	± 0.00012	± 0.00004	± 0.00019

level), requires much larger data samples than those collected in e^+e^- collisions at LEP-2 (about 40 000 events). This can be reached at a future machine such as the FCC-ee, where the total W width can be accurately measured through a threshold $e^+e^- \to W^+W^-$ scan around $\sqrt{s} = 2m_W$ center-of-mass energies [139], and where the R_W ratio will benefit from the huge sample of $5 \cdot 10^8$ W bosons collected (about 12 000 times larger at LEP-2) . Without parallel progress in the measurements of $|V_{cs}|$, $|V_{cd}|$, and m_W, the parametric uncertainty would then largely dominate the precision of any $\alpha_S(m_Z^2)$ extraction, as it is the case today when CKM unitarity is not enforced. However, both CKM elements will be also accurately determined at the FCC-ee by exploiting (i) the huge $\mathcal{O}(10^{12})$ and clean samples of charmed mesons available in runs at the Z pole, and (ii) an experimental precision of 0.5 (1.2) MeV for the W mass (width) within reach with 12 ab^{-1} accumulated at the W W production threshold.

To assess the ultimate precision achievable from W-boson data, we run a combined $\alpha_S(m_Z^2)$ fit with our N^{3}LO setup employing the following experimental values expected at the FCC-ee of the W observables and all other relevant parameters: (i) $\Gamma_W^{tot} = 2089.5 \pm 1.2$ MeV (to be compared to 2085 ± 42 today) and (ii) $R_W = 2.07570 \pm 0.00008$ (instead of the

current 2.068 ± 0.0025 value), (iii) CKM unitarity (or, equivalently, $|V_{cs}|$ and $|V_{cd}|$ uncertainties at the level of 10^{-5}), and (iv) a W mass with $m_W = 80.3800 \pm 0.0005$ GeV precision, leads to ∼0.1% uncertainties in $\alpha_S(m_Z^2)$ (last row of table 8). At such high level of experimental and parametric precision, the present propagated theoretical uncertainties would be about ten times larger than the former, although theory improvements are also expected in the coming years [5]. The theoretical effort should focus at computing the missing two- and three-loop $\mathcal{O}(\alpha^2, \alpha^3)$ EW, N^{4}LO QCD, as well as the mixed QCD+EW $\mathcal{O}(\alpha\alpha_S^2, \alpha\alpha_S^3, \alpha^2\alpha_S)$ corrections, which are all of about the same size and yield today a relative theoretical uncertainty of $\sim 3.5 \cdot 10^{-4}$ in the W boson observables. With a factor of 10 reduction of the theory uncertainties, a final QCD coupling extraction at the FCC-ee with a 2-permil total uncertainty is possible: $\alpha_S(m_Z^2) = 0.11790 \pm 0.00012_{\text{exp}} \pm 0.00004_{\text{par}} \pm 0.00019_{\text{th}}$ (table 8, last row), where the central value quoted is arbitrarily set at the world average. Figure 23 (right) shows the corresponding $\Delta\chi^2$ parabola for the $\alpha_S(m_Z^2)$ determination expected at the FCC-ee compared to the 2019 world average (orange band), with the dashed band covering the range between taking into account all uncertainties (outer curve) or only experimental uncertainties (inner curve).

5.1.2. $\alpha_S(m_Z^2)$ from Z boson decays. For the Z boson case, we incorporate into the GFITTER v2.2 code [334] all parametrizations of the partial and total Z widths, including the full two-loop $\mathcal{O}(\alpha^2)$ electroweak terms given in [337], plus the leading fermionic three-loop $\mathcal{O}(\alpha^3)$ EW corrections of [339]. These 2-loop (leading fermionic 3-loop) EW corrections increase the theoretical predictions for Γ_Z^{tot} by +0.83 MeV (+0.33 MeV), R_Z by +0.0186 (−0.0037), and σ_Z^{had} by +1 pb. The theoretical errors from missing higher-order $\mathcal{O}(\alpha^3)$ EW, $\mathcal{O}(\alpha^5)$ QCD, and $\mathcal{O}(\alpha\alpha_S^2, \alpha\alpha_S^3, \alpha^2\alpha_S)$ mixed corrections estimated in [337, 339] are of relative size of $\sim 1.5 \cdot 10^{-4}$ for Γ_Z^{tot} and σ_Z^{had}, and $\sim 2.5 \cdot 10^{-4}$ for R_Z, i.e. they are about a factor of two better than the corresponding theoretical calculations for the W boson pseudoobservables, as expected since the EW accuracy of the latter is only $\mathcal{O}(\alpha)$ today.

On the experimental data, new studies [340, 345] have updated the LEP luminosity corrections at and off the resonance peak that modify the PDG results for the Z boson pseudoobservables Γ_Z^{tot} and σ_Z^{had}. The change in Γ_Z^{tot} is of +0.012%. The impact on σ_Z^{had} is the largest of all pseudoobservables, with a 0.144% reduction of the hadronic cross section at the Z peak that brings the data very close to the theoretical prediction. The central R_Z ratios have not changed, but an extra precision digit is added now. The experimental uncertainties today (∼0.1%) are about a factor of four larger than their theoretical or parametric counterparts (∼0.025%). Matching the uncertainties of the current theory state-of-the-art calls for higher precision measurements in e^+e^- collisions at the Z pole with, at least, 20 times larger data samples than those collected at LEP.

The extraction of $\alpha_S(m_Z^2)$ is carried out with 1-D scans of this variable as a free parameter using single and combined observables with our updated version of GFITTER 2.2. The results from these fits are listed in table 9, and the corresponding $\Delta\chi^2$ profiles are plotted in figure 24. The solid lines represent the results of the present improved calculations and data, whereas the dashed lines are those obtained with GFITTER in 2018 [334]. All new QCD couplings are clustered around $\alpha_S(m_Z^2) = 0.1200$, whereas previously the extraction from σ_Z^{had} was about 2σ lower (and also had larger uncertainties) than the average of the three, and that from R_Z was 1σ above it. Among $\alpha_S(m_Z^2)$ extractions, the most precise is that from R_Z (3.4% uncertainty), followed by the ones from Γ_Z^{tot} (3.9% uncertainty) and σ_Z^{had} (5.6% uncertainty). The precision did not change appreciably compared to the previous Γ_Z^{tot} and R_Z results, but the extraction from the hadronic Z cross section has been improved by about 20%

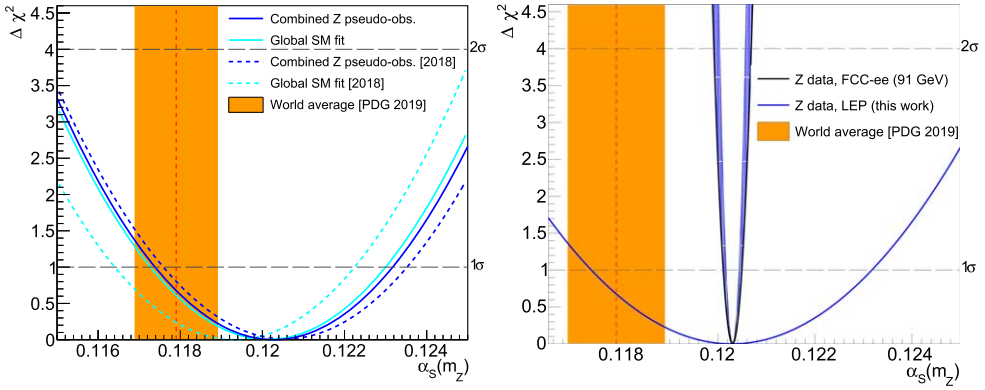

Figure 24. $\Delta\chi^2$ fit profiles of $\alpha_S(m_Z^2)$ determined from the combined Z boson pseudoobservables analysis and/or the global SM fit compared to the 2019 world average (orange band). Left: current results (solid lines) compared to the previous 2018 fit (dashed lines). Right: extraction expected at the FCC-ee –with central value arbitrarily set to $\alpha_S(m_Z^2) = 0.12030$ and total (experimental, parametric, and theoretical, added in quadrature) uncertainties (outer parabola) and experimental uncertainties alone (inner parabola)–compared to the present one from the combined Z data (blue line).

Table 9. Values of $\alpha_S(m_Z^2)$ determined at N^{3}LO accuracy from $\Gamma_Z^{\rm tot}$, R_Z, and $\sigma_Z^{\rm had}$ individually, combined, as well as from a global SM fit, with propagated experimental, parametric, and theoretical uncertainties broken down. The last two rows list the expected values at the FCC-ee from all Z pseudoobservables combined and from the corresponding SM fit.

Observable	$\alpha_S(m_Z^2)$	Uncertainties		
		exp.	param.	theor.
$\Gamma_Z^{\rm tot}$	0.1192 ± 0.0047	± 0.0046	± 0.0005	± 0.0008
R_Z	0.1207 ± 0.0041	± 0.0041	± 0.0001	± 0.0009
$\sigma_Z^{\rm had}$	0.1206 ± 0.0068	± 0.0067	± 0.0004	± 0.0012
All above combined	0.1203 ± 0.0029	± 0.0029	± 0.0002	± 0.0008
Global SM fit	0.1202 ± 0.0028	± 0.0028	± 0.0002	± 0.0008
All combined (FCC-ee)	0.12030 ± 0.00026	± 0.00013	± 0.00005	± 0.00022
Global SM fit (FCC-ee)	0.12020 ± 0.00026	± 0.00013	± 0.00005	± 0.00022

thanks mostly to the updated LEP data. When combining various Z observables, their associated correlation matrix is used in the fit. Table 9 lists all results with their propagated uncertainties broken down into experimental, parametric, and theoretical sources. Our final values, $\alpha_S(m_Z^2) = 0.1203 \pm 0.0028$ from the combined Z boson data, and $\alpha_S(m_Z^2) = 0.1202 \pm 0.0028$ from the full SM fit, and the PDG electroweak fit result ($\alpha_S(m_Z^2) = 0.1203 \pm 0.0028$) [251] are all virtually identical now.

At the FCC-ee, combining the $3{\cdot}10^{12}$ Z bosons decaying hadronically at the Z pole, and the $\mathcal{O}$(tens of keV)-accurate $\sqrt{s}$ calibration obtained using resonant depolarization [346], will

provide measurements with unparalleled precision. The statistical uncertainties in the Z mass and width, today of ±1.2 MeV and ±2 MeV (dominated by the LEP beam energy calibration), will be reduced to below ±4 keV and ±7 keV respectively. Similarly, the statistical uncertainty in R_Z^{exp} will be negligible and the measurement in the $Z \to \mu^+\mu^-$ final state alone, yielding an experimental precision of 0.001 from the knowledge of the detector acceptance, will suffice to reach an absolute (relative) uncertainty of 0.001 ($5{\cdot}10^{-5}$) on the ratio of the hadronic-to-leptonic partial Z widths. Thus, accounting for the dominant experimental systematic uncertainties at the FCC-ee, we expect: δm_Z = 0.025–0.1 MeV, $\delta\Gamma_Z^{tot}$ = 0.1 MeV, $\delta\sigma_Z^{had}$ = 4.0 pb, and $\delta R_Z = 10^{-3}$ relative uncertainties [139]. In addition, the QED coupling at the Z peak will be measured with a precision of $\delta\alpha = 3 \cdot 10^{-5}$ [347], thereby also reducing the corresponding propagated parametric uncertainties. Implementing the latter uncertainties into our updated GFITTER setup, namely taking $\Gamma_Z^{tot} = 2495.2 \pm 0.1$ MeV, $\sigma_Z^{had} = 41\,494 \pm 4$ pb, and $R_Z = 20.7500 \pm 0.0010$, as well as $m_Z = 91.18760 \pm 0.00001$ GeV, and $\delta\alpha_{had}^{(5)}(m_Z) = 0.0275300 \pm 0.0000009$, we derive the results listed in the last two rows of table 9 where, the central $\alpha_S(m_Z^2)$ value is arbitrarily set at the current SM global fit extraction. The final uncertainties in the QCD coupling constant are reduced to the ∼0.1% level, namely about three times smaller than the propagated theoretical uncertainties today. Theoretical developments in the years to come should further bring down the latter by a factor of four [5]. A final QCD coupling constant extraction at the FCC-ee with a two-permil total uncertainty is thereby reachable: $\alpha_S(m_Z^2) = 0.12030 \pm 0.00013_{exp} \pm 0.00005_{par} \pm 0.00022_{th}$ (table 9). Figure 24 (right) shows the $\Delta\chi^2$ parabola for the $\alpha_S(m_Z^2)$ extraction from the Z boson data (or from the SM fit that is almost identical) expected at the FCC-ee (with the central value arbitrarily set to its present result), compared to the same extraction today (blue parabola) and to the 2019 world average (orange band). The large improvement, by more than a factor of ten, in the FCC-ee extraction of $\alpha_S(m_Z^2)$ from the Z boson data (and its comparison to the similar extraction from the W boson, figure 23 right) will enable searches for small deviations from the SM predictions that could signal the presence of new physics contributions.

6. $\alpha_S(m_Z^2)$ from hadronic final-states in e^+e^- collisions

6.1. Hadronic vacuum polarization function, R-ratio, and the strong coupling[89]

The process of electron–positron annihilation into hadrons plays a distinctive role in elementary particle physics. This is primarily caused by the remarkable fact that its theoretical description requires no phenomenological models of hadronization, which forms the experimentally detected final-state particles. In turn, this feature makes it possible to extract the key parameters of the theory from pertinent experimental data in a model-independent way, thereby constituting one of the cleanest methods of their determination.

In the theoretical studies of e^+e^- annihilation into hadrons, one needs to operate with the physical observable that depends on the timelike kinematic variable (namely, the center-of-mass energy squared $s = q^2 > 0$), whereas such basic tools as the perturbative technique and the renormalization group (RG) method are directly applicable only to quantities that depend on the spacelike kinematic variable $Q^2 = -q^2 > 0$. The proper description of the strong interactions in the timelike domain substantially relies on the corresponding dispersion relations, which provide the physically consistent way to interrelate the 'timelike' experimentally measurable observables (such as the *R*-ratio of e^+e^- annihilation into hadrons) with

[89] Author: A V Nesterenko (JINR, Dubna).

the 'spacelike' theoretically computable quantities (such as the hadronic vacuum polarization function and the Adler function), see, e.g. [348] and references therein for details.

The hadronic vacuum polarization function $\Pi(q^2)$ is defined as the scalar part of the hadronic vacuum polarization tensor

$$\Pi_{\mu\nu}(q^2) = i\int d^4x\, e^{iqx}\langle 0|\, T\{J_\mu(x)J_\nu(0)\}|0\rangle = \frac{i}{12\pi^2}(q_\mu q_\nu - g_{\mu\nu}q^2)\Pi(q^2), \qquad q^2 < 0. \tag{6.1}$$

The physical kinematic restrictions on the process on hand define the location of the cut of the function $\Pi(q^2)$ in the complex q^2-plane, that enables one to write down the corresponding dispersion relation. In particular, as discussed in, e.g. [349], for the processes involving final state hadrons the function $\Pi(q^2)$ (6.1) possesses the only cut along the positive semiaxis of real q^2 starting at the hadronic production threshold $q^2 \geqslant 4m_\pi^2$, that implies

$$\Pi(q^2) - \Pi(q_0^2) = (q^2 - q_0^2)\int_{4m_\pi^2}^{\infty} \frac{R(\sigma)}{(\sigma - q^2)(\sigma - q_0^2)}\, d\sigma, \tag{6.2}$$

where

$$R(s) = \frac{1}{2\pi i}\lim_{\varepsilon\to 0_+}\big[\Pi(s + i\varepsilon) - \Pi(s - i\varepsilon)\big] = \frac{1}{\pi}\,\mathrm{Im}\lim_{\varepsilon\to 0_+}\Pi(s + i\varepsilon). \tag{6.3}$$

The function $R(s)$ (6.3) is commonly identified with the so-called R-ratio of e^+e^- annihilation into hadrons $R(s) = \sigma(e^+e^- \to \text{hadrons}; s)/\sigma(e^+e^- \to \mu^+\mu^-; s)$. For the practical purposes it proves to be convenient to deal with the Adler function [350]

$$D(Q^2) = -\frac{d\,\Pi(-Q^2)}{d\ln Q^2}, \qquad Q^2 = -q^2 > 0. \tag{6.4}$$

The corresponding dispersion relation [350]

$$D(Q^2) = Q^2\int_{4m_\pi^2}^{\infty} \frac{R(\sigma)}{(\sigma + Q^2)^2}\, d\sigma \tag{6.5}$$

directly follows from equations (6.2) and (6.4) and enables one to extract the experimental prediction for the Adler function from the respective data on the R-ratio. In turn, the theoretical expression for the function $R(s)$ can be obtained by integrating equation (6.4) in finite limits, namely [351, 352]

$$R(s) = \frac{1}{2\pi i}\lim_{\varepsilon\to 0_+}\int_{s+i\varepsilon}^{s-i\varepsilon} D(-\zeta)\frac{d\zeta}{\zeta}, \tag{6.6}$$

where the integration contour in the complex ζ-plane lies in the region of analyticity of the integrand. At the same time, equation (6.4) additionally provides the relation that expresses the hadronic vacuum polarization function in terms of the Adler function, specifically [353–356]

$$\Pi(-Q^2) - \Pi(-Q_0^2) = -\int_{Q_0^2}^{Q^2} D(\zeta)\frac{d\zeta}{\zeta}, \tag{6.7}$$

where $Q^2 = -q^2 > 0$ and $Q_0^2 = -q_0^2 > 0$ denote, respectively, the spacelike kinematic variable and the subtraction point.

Basically, equations (6.2)–(6.7) constitute the complete set of relations, which mutually express the functions $\Pi(q^2)$, $D(Q^2)$, and $R(s)$ in terms of each other. The derivation of the foregoing relations, being based only on the kinematics of the process on hand, requires

neither additional approximations nor model-dependent phenomenological assumptions. It is worthwhile to note also that the dispersion relations (6.2)–(6.7) impose a number of stringent physical intrinsically nonperturbative constraints on the functions $\Pi(q^2)$, $D(Q^2)$, and $R(s)$, that should definitely be accounted for when one reaches the limits of applicability of the perturbative approach, see, in particular, [348, 357, 358] for a detailed discussion of this issue. The nonperturbative aspects of the strong interactions will be disregarded hereinafter and the massless limit $m_\pi = 0$ will be assumed in what follows.

To calculate the R-ratio of e^+e^- annihilation into hadrons one usually starts with the perturbative expression for the hadronic vacuum polarization function

$$\Pi^{(\ell)}(q^2, \mu^2, a_s) = \sum_{j=0}^{\ell} [a_s^{(\ell)}(\mu^2)]^j \sum_{k=0}^{j+1} \Pi_{j,k} \ln^k\left(\frac{\mu^2}{-q^2}\right), \qquad q^2 \to -\infty. \tag{6.8}$$

In this equation ℓ specifies the loop level, $q^2 < 0$ denotes the spacelike kinematic variable, $\mu^2 > 0$ is the renormalization scale, $\alpha_s = g^2/(4\pi)$ stands for the strong coupling, $a_s^{(\ell)}(\mu^2) = \alpha_s^{(\ell)}(\mu^2)\beta_0/(4\pi)$, $\beta_0 = 11 - 2N_f/3$ denotes the one-loop β function perturbative expansion coefficient, N_f is the number of active flavours, and the common prefactor $N_c\sum_{f=1}^{N_f} Q_f^2$ is omitted throughout, where $N_c = 3$ stands for the number of colours and Q_f denotes the electric charge of f-th quark. In particular, at the one-loop level ($\ell = 1$) equation (6.8) reads

$$\Pi^{(1)}(q^2, \mu^2, a_s) = \frac{5}{3} + \ln\left(\frac{\mu^2}{-q^2}\right) + a_s^{(1)}(\mu^2)\left(\frac{4}{\beta_0}\right)\left[\frac{55}{12} - 4\zeta(3) + \ln\left(\frac{\mu^2}{-q^2}\right)\right], \qquad q^2 \to -\infty. \tag{6.9}$$

As mentioned earlier, in practice it is convenient to employ the Adler function (6.4), which, contrary to the hadronic vacuum polarization function (6.1), is an RG-invariant quantity. Specifically, equations (6.4) and (6.8) imply that at the ℓ-loop level the perturbative expression for the Adler function reads

$$D^{(\ell)}(Q^2, \mu^2, a_s) = \sum_{j=0}^{\ell} [a_s^{(\ell)}(\mu^2)]^j \sum_{k=0}^{j+1} k\Pi_{j,k} \ln^{k-1}\left(\frac{\mu^2}{Q^2}\right), \qquad Q^2 \to \infty. \tag{6.10}$$

Note that the hadronic vacuum polarization function (6.1) and the Adler function (6.4) satisfy, respectively, the inhomogeneous and homogeneous RG equations, which, in turn, enable one to express the higher-order coefficients $\Pi_{j,k}$ entering equations (6.8) and (6.10) in terms of the lower-order ones. In particular, such RG relations have been obtained at the first few loop levels in [360, 117, 359], at the higher loop levels in [361], and at an arbitrary loop level (in a compact recurrent and unfolded explicit forms) in [362].

The native choice of the renormalization scale $\mu^2 = Q^2$ (that amounts to the RG summation in the spacelike domain) casts the Adler function (6.10) to a well-known form ($\Pi_{0,1} = 1$)

$$D^{(\ell)}(Q^2) = \sum_{j=0}^{\ell} \Pi_{j,1}[a_s^{(\ell)}(Q^2)]^j = 1 + d^{(\ell)}(Q^2), \;\; d^{(\ell)}(Q^2) = \sum_{j=1}^{\ell} d_j[a_s^{(\ell)}(Q^2)]^j, \;\; \Pi_{j,1} = d_j. \tag{6.11}$$

It is worthwhile to note here that a general choice of the renormalization scale $\mu^2 = c\,Q^2$ (with $c \neq 1$ being a positive constant) retains in the resulting expression for the Adler function $D^{(\ell)}(Q^2)$ all the terms proportional to the higher-order coefficients $\Pi_{j,k}$ appearing on the right-hand side of equation (6.10). The function $a_s^{(\ell)}(Q^2)$ entering equation (6.11) can be represented as the double sum

$$a_{\rm s}^{(\ell)}(Q^2) = \sum_{n=1}^{\ell}\sum_{m=0}^{n-1} b_n^m \,\frac{\ln^m(\ln z)}{\ln^n z}, \qquad z = \frac{Q^2}{\Lambda^2}, \tag{6.12}$$

where Λ is the QCD scale parameter and b_n^m (the integer superscript m is not to be confused with a respective power) stands for the combination of the β function perturbative expansion coefficients (in particular, $b_1^0 = 1$, $b_2^0 = 0$, $b_2^1 = -\beta_1/\beta_0^2$, see, e.g. appendix A of [348]). For example, at the one-loop level ($\ell = 1$) the Adler function (6.11) takes a quite simple form

$$D^{(1)}(Q^2) = 1 + d_1 a_{\rm s}^{(1)}(Q^2), \qquad a_{\rm s}^{(1)}(Q^2) = \frac{1}{\ln(Q^2/\Lambda^2)}, \qquad d_1 = \frac{4}{\beta_0}. \tag{6.13}$$

The Adler function perturbative expansion coefficients d_j entering equation (6.11) were calculated up to the fourth order in the strong coupling ($1 \leqslant j \leqslant 4$), see [100, 280, 363] and references therein, whereas the β function perturbative expansion coefficients β_j appearing in equation (6.12) are available up to the five-loop level ($0 \leqslant j \leqslant 4$), see [364–367] and references therein.

In turn, the dependence of the hadronic vacuum polarization function (6.8) on the renormalization scale can be eliminated in the following way (see, in particular, [353–355]). Namely, for this purpose one first calculates the corresponding Adler function (6.4), then performs the RG summation, and then employs the relation (6.7), that yields at the one-loop level [353–356, 358]

$$\Pi^{(1)}(-Q^2) - \Pi^{(1)}(-Q_0^2) = -\ln\left(\frac{Q^2}{Q_0^2}\right) - d_1 \ln\left[\frac{a_{\rm s}^{(1)}(Q_0^2)}{a_{\rm s}^{(1)}(Q^2)}\right], \quad Q^2 = -q^2 > 0, \quad Q_0^2 = -q_0^2 > 0, \tag{6.14}$$

where $a_{\rm s}^{(1)}(Q^2)$ and d_1 are given in equation (6.13). At an arbitrary loop level the corresponding expression for the hadronic vacuum polarization function has been obtained in [361]:

$$\Pi^{(\ell)}(-Q^2) - \Pi^{(\ell)}(-Q_0^2) = -\ln\left(\frac{Q^2}{Q_0^2}\right) + \sum_{j=1}^{\ell} d_j [p_j^{(\ell)}(Q^2) - p_j^{(\ell)}(Q_0^2)], \tag{6.15}$$

where

$$p_j^{(\ell)}(Q^2) = \sum_{n_1=1}^{\ell} \ldots \sum_{n_j=1}^{\ell}\sum_{m_1=0}^{n_1-1} \ldots \sum_{m_j=0}^{n_j-1} \left(\prod_{i=1}^{j} b_{n_i}^{m_i}\right) J\left(Q^2, \sum_{i=1}^{j} n_i, \sum_{i=1}^{j} m_i\right), \tag{6.16}$$

$$J(Q^2, n, m) = \begin{cases} -\dfrac{\ln^{m+1}(\ln z)}{m+1}, & \text{if} \quad n = 1, \\ \displaystyle\sum_{k=0}^{m} \frac{m!}{k!}(n-1)^{k-m-1} \frac{\ln^k(\ln z)}{\ln^{n-1} z}, & \text{if} \quad n \geqslant 2, \end{cases} \tag{6.17}$$

$z = Q^2/\Lambda^2$, and the coefficients d_j and b_n^m are specified in equations (6.11) and (6.12), respectively, see [361] for the details.

At this point there are two equivalent methods to calculate the R-ratio of $\mathrm{e}^+\mathrm{e}^-$ annihilation into hadrons. Specifically, the first one consists in applying the relation (6.6) to the Adler function $D(Q^2)$ (6.11). This method eventually leads to an integral representation for the function $R(s)$, which involves the so-called spectral function, the latter being the discontinuity of the strong correction to the Adler function $d(Q^2)$ (6.11) across the physical cut $Q^2 < 0$. In turn, the second method to calculate the R-ratio consists in applying the relation (6.3) to the hadronic vacuum polarization function (6.15). At the one-loop level the R-ratio of $\mathrm{e}^+\mathrm{e}^-$

annihilation into hadrons takes the following form (note that this expression first appeared in [368] and only afterwards was derived in [351, 356, 369–371]):

$$R^{(1)}(s) = 1 + d_1 A^{(1)}_{\mathrm{TL},1}(s), \qquad A^{(1)}_{\mathrm{TL},1}(s) = \frac{1}{2} - \frac{1}{\pi}\arctan\left(\frac{\ln w}{\pi}\right), \quad w = \frac{s}{\Lambda^2}, \tag{6.18}$$

where the coefficient d_1 is given in equation (6.13) and it is assumed that $\arctan(x)$ is a monotonic nondecreasing function of its argument [namely, $-\pi/2 \leqslant \arctan(x) \leqslant \pi/2$ for $-\infty < x < \infty$].

Basically, the first method of calculation of the R-ratio becomes somewhat inconvenient at the higher-loop levels. In particular, since the required spectral function turns out to be rather cumbrous beyond the one-loop level, its integration can, in general, be performed only by making use of numerical methods. Moreover, at the higher-loop levels the explicit calculation of the spectral function represents a rather demanding task, whereas its numerical evaluation needs a lot of computation resources and essentially slows down the overall computation process. Nonetheless, the required spectral function has explicitly been calculated at the first few loop levels in, e.g. [372–374] and at an arbitrary loop level in [348, 375], that, in turn, facilitates the numerical calculation of the R-ratio within the first method.

The explicit expression for the R-ratio of $\mathrm{e}^+\mathrm{e}^-$ annihilation into hadrons, which properly accounts for all the effects due to continuation of the spacelike perturbative results into the timelike domain, has recently been obtained at an arbitrary loop level within the second method in [361], namely

$$R^{(\ell)}(s) = 1 + r^{(\ell)}(s), \qquad r^{(\ell)}(s) = \sum_{j=1}^{\ell} d_j\, A^{(\ell)}_{\mathrm{TL},j}(s). \tag{6.19}$$

In this equation d_j stand for the Adler function perturbative expansion coefficients (6.11),

$$A^{(\ell)}_{\mathrm{TL},j}(s) = \sum_{n_1=1}^{\ell} \ldots \sum_{n_j=1}^{\ell} \sum_{m_1=0}^{n_1-1} \ldots \sum_{m_j=0}^{n_j-1} \left(\prod_{i=1}^{j} b_{n_i}^{m_i}\right) T\left(s, \sum_{i=1}^{j} n_i, \sum_{i=1}^{j} m_i\right) \tag{6.20}$$

denotes the ℓ-loop j-th order 'timelike' effective expansion function (which constitutes the corresponding continuation of the j-th power of ℓ-loop function $[a_{\mathrm{s}}^{(\ell)}(Q^2)]^j$ from spacelike into the timelike domain), the coefficients b_n^m are specified in equation (6.12),

$$T(s, n, m) = \begin{cases} -V_0^1(s), & \text{if } n = 1 \quad \text{and} \quad m = 0, \\ \displaystyle\sum_{k=0}^{m} \frac{m!}{k!}(n-1)^{k-m-1}\, V_{n-1}^k(s), & \text{if } n \geqslant 2, \end{cases} \tag{6.21}$$

$$V_n^m(s) = \begin{cases} 0, & \text{if } n = 0 \quad \text{and} \quad m = 0, \\ v_0^m(s), & \text{if } n = 0 \quad \text{and} \quad m \geqslant 1, \\ v_n^0(s), & \text{if } n \geqslant 1 \quad \text{and} \quad m = 0, \\ v_n^0(s) u_0^m(s) + u_n^0(s) v_0^m(s), & \text{if } n \geqslant 1 \quad \text{and} \quad m \geqslant 1, \end{cases} \tag{6.22}$$

$$v_0^m(s) = \sum_{k=0}^{K(m)} \binom{m}{2k+1} (-1)^{k+1} \pi^{2k} [L_1(y)]^{m-2k-1} [L_2(y)]^{2k+1}, \tag{6.23}$$

$$v_n^0(s) = \frac{1}{(y^2+\pi^2)^n} \sum_{k=0}^{K(n)} \binom{n}{2k+1} (-1)^k \pi^{2k} y^{n-2k-1}, \tag{6.24}$$

$$u_0^m(s) = \sum_{k=0}^{K(m+1)} \binom{m}{2k} (-1)^k \pi^{2k} [L_1(y)]^{m-2k} [L_2(y)]^{2k}, \tag{6.25}$$

$$u_n^0(s) = \frac{1}{(y^2 + \pi^2)^n} \sum_{k=0}^{K(n+1)} \binom{n}{2k} (-1)^k \pi^{2k} y^{n-2k}, \tag{6.26}$$

$$L_1(y) = \ln\sqrt{y^2+\pi^2}, \;\; L_2(y) = \frac{1}{2} - \frac{1}{\pi}\arctan\left(\frac{y}{\pi}\right), \;\; \binom{n}{m} = \frac{n!}{m!(n-m)!}, \;\; K(n) = \frac{n-2}{2} + \frac{n \bmod 2}{2}, \tag{6.27}$$

($n \bmod m$) denotes the remainder on division of n by m, and $y = \ln(s/\Lambda^2)$, see [361, 375] for the details.

It is worthwhile to note that a commonly employed way of calculation of the R-ratio of e^+e^- annihilation into hadrons, being different from the two equivalent methods described above, leads to an incomplete result for the function $R(s)$. In particular, here one applies the relation (6.3) directly to equation (6.8) and then assigns the renormalization scale $\mu^2 = |s|$ (that factually amounts to an incomplete RG summation in the timelike domain, see, e.g. [353–356, 361, 362, 375] and references therein), that yields [92]

$$R^{(\ell)}_{\rm appr}(s) = 1 + r^{(\ell)}_{\rm appr}(s), \qquad r^{(\ell)}_{\rm appr}(s) = \sum_{j=1}^{\ell} r_j [a_{\rm s}^{(\ell)}(|s|)]^j, \qquad r_j = d_j - \delta_j. \tag{6.28}$$

In this equation the function $a_{\rm s}^{(\ell)}(|s|)$ is given in equation (6.12), d_j stand for the Adler function perturbative expansion coefficients (6.11), and δ_j embody the contributions of the so-called π^2-terms, which play a significant role in the studies of the process on hand [376]. At the first two loop levels the coefficients δ_j (6.28) vanish ($\delta_1 = \delta_2 = 0$) and the first several non-vanishing coefficients δ_j were reported in [143, 348, 361, 375–377]. The explicit expression for the coefficients δ_j (6.28) has recently been obtained at an arbitrary loop level in [362]:

$$\begin{aligned}\delta_j = -\sum_{k=1}^{K(j)} \frac{(-2\pi^2)^k}{(2k+1)!} \sum_{i_1=2(k-1)+1}^{j-2} \underbrace{\sum_{i_2=2(k-2)+1}^{i_1-2} \ldots \sum_{i_n=2(k-n)+1}^{i_{n-1}-2} \ldots \sum_{i_k=1}^{i_{k-1}-2}}_{(k-1)\text{ sums}} (j+i_1) i_1 \\ \times \underbrace{(i_1+i_2) i_2 \times \ldots \times (i_{n-1}+i_n) i_n \times \ldots \times (i_{k-1}+i_k) i_k}_{(k-1)\text{ products}} \\ \times \mathfrak{B}_{j-i_1-2} \underbrace{\mathfrak{B}_{i_1-i_2-2} \ldots \mathfrak{B}_{i_{n-1}-i_n-2} \ldots \mathfrak{B}_{i_{k-1}-i_k-2}}_{(k-1)\text{ terms}} d_{i_k}, \;\; \mathfrak{B}_n = \frac{1}{4}\sum_{i=0}^{n} B_i B_{n-i}, \;\; B_i = \frac{\beta_i}{\beta_0^{i+1}}, \;\; j \geqslant 3,\end{aligned} \tag{6.29}$$

where the coefficients d_j are specified in equation (6.11), β_j denote the β function perturbative expansion coefficients, and the function $K(n)$ is defined in equation (6.27), see [362] for the details.

It is necessary to emphasize that, as argued in, e.g. [353–356], the effects due to continuation of the spacelike perturbative results into the timelike domain are only partially accounted for in equation (6.28) by the coefficients δ_j, whereas the ignorance (complete or partial) of such effects may yield misleading results. In particular, it was shown [361, 362, 375] that the approximation $R_{\rm appr}(s)$ (6.28) factually constitutes the truncated re-expansion of the proper expression $R(s)$ (6.19) at high energies and the validity range of such re-expansion is strictly limited to $\sqrt{s} > \Lambda\exp(\pi/2) \simeq 4.81\,\Lambda$. Moreover, the contribution of a given order to the proper expression for the R-ratio (6.19) appears to be redistributed over the higher-order terms in its approximate form (6.28), thereby substantially amplifying them. In turn, this makes the loop convergence of a commonly employed approximation of the

R-ratio (6.28) much worse than that of its proper form (6.19) and increases the resulting theoretical uncertainty of the strong coupling and the QCD scale parameter associated with the higher-loop perturbative corrections disregarded in equation (6.28). Basically, the aforementioned truncation of the re-expansion of the proper expression for the R-ratio (6.19) neglects all the higher-order π^2-terms in equation (6.28), though the latter may not necessarily be small enough to be safely neglected. Specifically, it was shown that the higher-order π^2-terms omitted in a commonly employed approximation $R_{\rm appr}(s)$ (6.28) can produce a considerable effect on the determination of the strong coupling and the QCD scale parameter from the experimental data on the R-ratio, see [361, 362, 375] and references therein for the details.

6.2. $\alpha_S(m_Z^2)$ from soft parton fragmentation functions[90]

We summarize a derivation of the QCD coupling α_S from the energy evolution of the moments of the parton-to-hadron fragmentation functions (FFs) at low hadron Feynman momentum fraction z. In [378–382], the energy evolution of the moments of the parton-to-hadron FFs were computed up to approximate next-next-to-leading-order (NNLO*) fixed-order including next-to-next-to-leading-log (NNLL) resummation corrections. A fit to the corresponding experimental jet data from e^+e^- and deep-inelastic $e^\pm$, ν-p collisions, to the NNLO*+NNLL predictions yields $\alpha_S(m_Z^2) = 0.1205 \pm 0.0010\,(\rm exp) \pm 0.0022\,(\rm th)$, in good agreement with the current α_S world average. Forthcoming prospects based on full-NNLO calculations are discussed.

The conversion of a quark and gluon (collectively called partons) into a final jet of hadrons is driven by soft and collinear gluon bremsstrahlung [383] followed by the final transformation into hadrons of the last partons produced in the QCD shower at nonperturbative scales approaching $\Lambda_{\rm QCD}$. The distribution of hadrons inside a jet is described by its fragmentation function, $D_{a\to h}(z, Q)$, that encodes the probability that an initial parton a eventually fragments into a hadron h carrying a fraction $z = p_{\rm hadron}/p_{\rm parton}$ of the parent parton's momentum. Starting with a parton at a given δ-function energy Q, its evolution to any other lower energy scale Q' is driven by a branching process of parton radiation and splitting, $a \to b\,c$, that can be perturbatively computed. At large $z \gtrsim 0.1$ one uses the DGLAP evolution equations [239–241], whereas the Modified Leading Logarithmic Approximation (MLLA) [384], resumming soft (along with hard) and collinear logs, provides an appropriate theoretical framework at small z. In this latter approach, one writes the FF as a function of the log of the inverse of z, i.e. $\xi = \ln(1/z)$, in order to describe the region of low hadron momenta that dominates the jet fragments. Due to colour coherence and interference in gluon radiation (angular ordering), not the softest partons but those with intermediate energies multiply most effectively in QCD cascades, leading to a final FF with a typical 'hump-backed plateau' (HBP) shape as a function of ξ (figure 25, left). Such a shape can be perfectly reproduced by a distorted Gaussian (DG, [385]) parametrized in terms of the hadron multiplicity $\mathcal{N}$ (giving the integral, and thereby the normalization, of the DG), the mean peak position $\bar{\xi}$, the dispersion σ, the skewness s, and kurtosis k of the distribution.

In [379], we described a new approach that solves the set of integro-differential equations for the FF evolution combining both DGLAP and MLLA corrections. This is done by expressing the Mellin-transformed hadron distribution in terms of the anomalous dimension γ: $D \simeq C\,(\alpha_S(t))\exp\left[\int^t \gamma\,(\alpha_S(t'))dt\right]$ where $t = \ln Q$ is the 'time' evolution variable in QCD parton showers. The analysis leads to a series in half powers of α_S:

[90] Authors: R Perez-Ramos (DRII-IPSA and LPTHE, Paris), D d'Enterria (CERN).

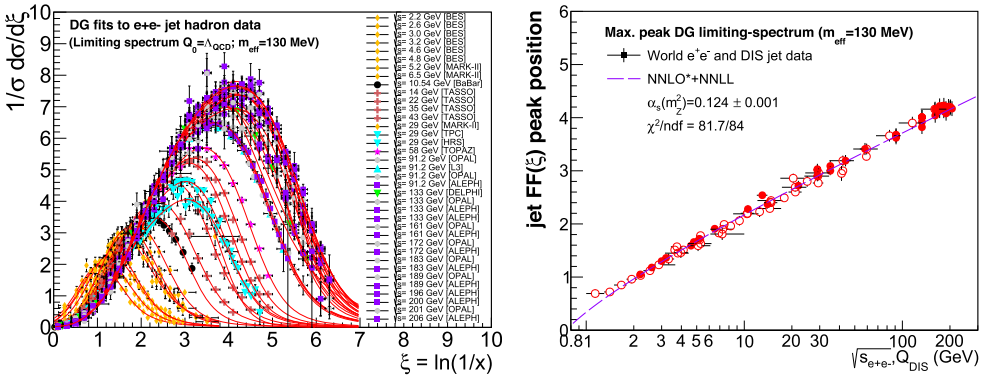

Figure 25. Left: HBP charged-hadron spectra in jets as a function of $\xi = \ln(1/z)$ measured in e^+e^- at $\sqrt{s} \approx$ 2–200 GeV, fitted to a DG distribution. Right: energy evolution of the peak position of the DG measured in e^+e^- and DIS data (open and closed symbols) fitted to the NNLO*+NNLL predictions (dashed curve).

$\gamma \sim \mathcal{O}(\alpha_S^{1/2}) + \mathcal{O}(\alpha_S) + \mathcal{O}(\alpha_S^{3/2}) + \mathcal{O}(\alpha_S^{2}) + \mathcal{O}(\alpha_S^{5/2}) + \cdots$, where integer powers of α_S correspond to fixed-order corrections, and half-integer terms can be identified with increasingly accurate resummations of soft and collinear logarithms. The full set of NLO $\mathcal{O}(\alpha_S^2)$ terms for the anomalous dimension, including the one-loop splitting functions $P_{ac}^{(1)}$ and the two-loop running of α_S, plus a fraction of the $\mathcal{O}(\alpha_S^{5/2})$ terms, coming from the NNLO expression of α_S have been computed [386]. Upon inverse-Mellin transformation, one can derive the analytical expressions for the energy evolution of the FF, and its associated moments, as a function of $Y = \ln(E/\Lambda_{\rm QCD})$, for an initial parton energy E, down to a shower cutoff scale $Q_0 > \Lambda_{\rm QCD}$ for $N_f = 3, 4, 5$ quark flavours. By introducing $\lambda = \ln(Q_0/\Lambda_{\rm QCD})$, the resulting formulas for the energy evolution of the moments depend on $\Lambda_{\rm QCD}$ as a *single* free parameter. Simpler expressions can be further obtained for $Q_0 \to \Lambda_{\rm QCD}$ (limiting spectrum) motivated by the 'local parton-hadron duality' hypothesis for inclusive-enough observables. Thus, by fitting to the distorted Gaussian, the measured HBP at various energies, one can determine α_S from the corresponding jet energy-dependence of the FF moments $\mathcal{N}$, $\bar{\xi}$, σ, s, and k.

In the phenomenological analysis, we first start by fitting to the DG all existing jet FF data measured in e^+e^- and $e^\pm$, ν-p collisions over $\sqrt{s} \approx$ 1–200 GeV, and thereby derive the corresponding FF moments at each jet energy [387]. The overall normalization of the HBP spectrum ($\mathcal{K}_{\rm ch}$), which determines the average charged-hadron multiplicity of the jet (i.e. the zeroth moment of the FF), is an extra free parameter in the DG fit which, nonetheless, plays no role in the finally derived $\Lambda_{\rm QCD}$ value since the latter is *solely* dependent on the relative evolution of the multiplicity, and not on its absolute value at any given jet energy. The impact of finite hadron-mass effects in the DG fit are taken into account through a rescaling of the theoretical (massless) parton momenta with an effective mass $m_{\rm eff} \approx m_\pi$. Varying such effective mass from zero to a few hundred MeV, results in small propagated uncertainties into the final extracted $\Lambda_{\rm QCD}$ (and associated $\alpha_S(m_Z^2)$) value, as discussed in [379].

Once the energy evolution of all FF moments has been obtained from the individual experimental measurements, one can perform a combined fit of them as a function of the original parton energy. In the case of e^+e^- collisions, the latter corresponds to half the centre-of-mass energy $\sqrt{s}/2$ whereas, for DIS, the invariant four-momentum transfer $Q_{\rm DIS}$ is used. The experimental and theoretical evolutions of the hadron multiplicity and FF peak position

as a function of jet energy are shown in [387]. The hadron multiplicities measured in DIS jets appear somewhat smaller (especially at high energy) than those from e^+e^- collisions, due to limitations in the FF measurement only in half (current Breit) $e^{\pm}$-p hemisphere and/or in the determination of the relevant Q scale [379]. The NNLO*+NNLL limiting-spectrum ($\lambda = 0$) predictions for $N_f = 5$ active quark flavours (the moments of the lowest-$\sqrt{s}$ data have a few-percent correction applied in order to account for the slightly different ($N_f = 3, 4$) evolutions below the charm and bottom production thresholds), leaving $\Lambda_{\rm QCD}$ as a free parameter, reproduce very well the data. Fit results for the rest of the FF moments can be found in [379]. Figure 25 (right) shows the result of the peak position fit. Among FF moments, the peak position $\xi_{\rm max}$ appears as the most 'robust' for the determination of $\Lambda_{\rm QCD}$, being relatively insensitive to most of the uncertainties associated with the extraction method (DG fits, energy evolution fits, finite-mass corrections, ...) as well as to higher-order corrections [387]. Finally, the energy evolution of all or a fraction of HBP moments can be simultaneously fitted to the corresponding theoretical predictions in the limiting-spectrum case with just $\Lambda_{\rm QCD}$ as single free parameter.

The QCD coupling obtained from the combined fit of the multiplicity and peak position is $\alpha_S(m_Z^2) = 0.1205 \pm 0.0010(\text{exp}) \pm 0.0022(\text{theo})$, where the first uncertainty includes all experimentally-related sources discussed in [379], and the second one is a theoretical scale uncertainty derived at NLO by stopping the parton evolution of the FFs at $Q_0 = 1$ GeV rather than at the limiting spectrum value $Q_0 = \Lambda_{\rm QCD}$. Our extracted $\alpha_S(m_Z^2)$ value is consistent with all other NNLO results from the latest PDG compilation [251], as well as with other determinations with a lower degree of theoretical accuracy [388]. The precision of our result ($\pm 2\%$) is competitive with the other extractions, with a totally different set of experimental and theoretical uncertainties.

Outlook: Given the robustness of the observables chosen, energy evolution of FF moments, the purely experimental uncertainties of our $\alpha_S(m_Z^2)$ extraction are small, $\sim$0.8%, and will be eventually negligible with the large jet data samples, orders of magnitude larger than those at LEP, expected to be collected at future e^+e^- machines [139, 389]. Thus, the main source of imprecision is of theoretical origin. The main theoretical challenges of the approach presented here are to match the MLLA anomalous dimension to the $\overline{\rm MS}$ anomalous dimension and to reach full-NNLO pQCD accuracy. It is known that the MLLA anomalous dimension obtained within the massive gluon (MG) regularization scheme [390] turns out to be inconsistent with the expected N^{4}LL+NNLO result in the $\overline{\rm MS}$ scheme. For instance, the inconsistency between NNLO DLs terms to the anomalous dimension calculated in [390] and those calculated in [391] can be explained from the use of different regularization and factorization schemes [392]. More recently, it has been noticed that the main difference is entirely due to running coupling effects being truncated in a quite severe way [393]. In addition, in order to extract a coupling constant with NNLO fixed-order accuracy from the moments of the FFs, the diagonalization of the matrix elements (i.e. the splitting functions) beyond the $\mathcal{O}(\alpha_S^{5/2})$ order is a crucial step forwards. The diagonalization method to be adopted was considered a major technical challenge since the splitting functions do not commute beyond leading order. However, it becomes now possible thanks to the recent work by Kotikov and Teryaev [394]. To conclude, the implementation of the approach used in [394] and the change from the MG regularization scheme to the $\overline{\rm MS}$ scheme may make it possible to complete the present programme on the full-NNLO extraction of $\alpha_S(m_Z^2)$ from the moments of FFs.

6.3. Power corrections to event-shape distributions and impact on α_S extractions[91]

In this brief note we discuss some recent developments on the fits of α_S from event-shape distributions at lepton colliders. These determinations rely on the fact that event shape variables that vanish in the two-jet limit are directly sensitive to the QCD $q\bar{q}g$ vertex, and thus arguably offer one of the simplest frameworks to extract the strong coupling constant. The present status of these measurements as reported in the Particle Data Group (PDG) [226, 251] is not very satisfactory. In particular, determinations in which nonperturbative corrections are estimated via analytic models tend to give values for the strong coupling which are systematically smaller than those obtained using Monte Carlo generators to correct for nonperturbative effects. Specifically, some of the most precise $\alpha_S(m_Z^2)$ determinations obtained with analytical nonperturbative models ($\alpha_S(m_Z^2) = 0.1135 \pm 0.0010$ [395] from fitting thrust data, and $\alpha_S(m_Z^2) = 0.1123 \pm 0.0015$ [396] from C-parameter data), are in tension with the world average of 0.1179 ± 0.0010 and from other individual precise extractions, such as 0.1185 ± 0.0008 from lattice step scaling [18] and 0.1188 ± 0.0013 from jet rates [397]. A similar extraction, that of [398], uses the thrust distribution and an analytical hadronization model and returns a value for $\alpha_S(m_Z^2)$ compatible with those of [395, 396], although with larger uncertainties.

A feature common to analytic approaches to nonperturbative corrections (see e.g. [395, 396, 398–411]) is that their application to event shapes relies upon a power series in $1/Q$ (with Q being the centre-of-mass energy of the e^+e^- collision), of which only the leading (linear) term is retained. This linear power correction is proportional to a nonperturbative parameter (that is extracted together with α_S) via a calculable, observable-dependent coefficient. Furthermore, this coefficient is commonly calculated in the 2-jet limit, in general supplementing a Sudakov resummation of logarithmic corrections assuming that the above coefficient remains constant across the fit range, which instead covers both 2- and 3-jet configurations (see e.g. [395, 396, 398, 410, 411]). This assumption has recently been questioned in [412, 413], where the first calculations of the nonperturbative correction in three-jet configurations have appeared.

In this note, we briefly discuss the calculation of the leading power correction reported in [412, 413]. We start by recalling how the calculation is performed in the two-jet limit, and then we outline how it can be performed in the symmetric three-jet limit, as well as in a generic three-jet configuration. Finally, we present some phenomenological considerations on the impact on α_S fits, and discuss future developments.

6.3.1. Definition of the observable. Here we limit our discussion to the C-parameter, but analogous considerations apply to other shape variables such as thrust [414]. The C-parameter variable for a hadronic final state in e^+e^- annihilation is defined as follows [415],

$$C = 3(\lambda_1\lambda_2 + \lambda_2\lambda_3 + \lambda_3\lambda_1), \tag{6.30}$$

in terms of the eigenvalues λ_i of the linearized momentum tensor $\Theta^{\alpha\beta}$ [416, 417],

$$\Theta^{\alpha\beta} = \frac{1}{\sum_i |\vec{p}_i|} \sum_i \frac{\vec{p}_i{}^{\alpha}\vec{p}_i{}^{\beta}}{|\vec{p}_i|}, \tag{6.31}$$

where $|\vec{p}_i|$ is the modulus of the three momentum of particle i and $\vec{p}_i{}^{\alpha}$ is its momentum component along spatial dimension α ($\alpha = 1, 2, 3$). In events where all particles are massless, this can also be written as

[91] Authors: P F Monni (CERN), P Nason (MPI Munich, INFN and Univ. Milano).

$$C = 3 - \frac{3}{2}\sum_{i,j}\frac{(p_i \cdot p_j)^2}{(p_i \cdot Q)(p_j \cdot Q)} = \frac{3}{8}\sum_{i,j} x_i x_j \sin^2\theta_{ij}, \tag{6.32}$$

where Q is the centre-of-mass energy, p_i denotes the four-momentum of particle i, $x_i = 2(p_i \cdot Q)/Q^2$, and θ_{ij} is the angle between particles i and j. We consider the calculation of the linear power correction in the context of the so-called dispersive model [404], which postulates that the leading power correction to the cumulative distribution of the event shape, i.e.

$$\Sigma(C) \equiv \int_0^C dC' \frac{d\sigma}{dC'}, \tag{6.33}$$

is due to the radiation of a soft and nonperturbative system with gluon quantum numbers, i.e. a *gluer*. Starting from a Born configuration of final state momenta $\{\tilde{p}\}$ (e.g. at the leading order $\{\tilde{p}\} \equiv \{\tilde{p}_q, \tilde{p}_{\bar{q}}\}$ in the two-jet limit and $\{\tilde{p}\} \equiv \{\tilde{p}_q, \tilde{p}_{\bar{q}}, \tilde{p}_g\}$ in the three-jet limit), $\Sigma(C)$ schematically reads

$$\Sigma(C) = \sigma - \left\{\int d\sigma(\{\tilde{p}\})\Theta(C(\{\tilde{p}\}) - C) + \int d\sigma(\{p\}, k)\Theta(C(\{p\}, k) - C)\right\}, \tag{6.34}$$

where σ is the total cross section (in which the radiation of the gluer k does not generate any linear correction [404]), $d\sigma(\{\tilde{p}\})$ includes also the contribution in which the gluer is virtual, and $d\sigma(\{p\}, k)$ encodes the one in which the gluer is real. In the latter term, we have denoted with $(\{p\}, k)$ the set of hard momenta $\{p\}$ ($\neq\{\tilde{p}\}$ due to kinematic recoil) and the collective set of soft particles (k) constituting the gluer system.

6.3.2. Schematic illustration of the calculation. We now focus our discussion on the two-jet limit, i.e. $\{\tilde{p}\} \equiv \{\tilde{p}_q, \tilde{p}_{\bar{q}}\}$. Here the value of C approaches zero (i.e. $C(\{\tilde{p}\}) = 0$) as

$$C(\{p\}, k) \sim \mathcal{O}(k). \tag{6.35}$$

Quadratic corrections to the above equation (e.g. due to the recoil of the hard partons against k) can be safely ignored if one is interested in the computation of the linear power correction $\mathcal{O}(1/Q)$. In order to single out the linear contribution $\mathcal{O}(1/Q)$, we can therefore recast equation (6.34) as

$$\Sigma(C) = \sigma - \left\{\int d\sigma(\{\tilde{p}\}) + d\sigma(\{p\}, k)\Theta(C(\{\tilde{p}\}) - C) + \int d\sigma(\{p\}, k)\Theta(C(\{p\}, k) - C) - \Theta(C(\{\tilde{p}\}) - C)\right\}. \tag{6.36}$$

The first line in the r.h.s. of equation (6.36) reduces to the total cross section, which is well known to be free from linear corrections. Therefore, the second line in the r.h.s. of equation (6.36) is the only source of linear power corrections. Because of the linear suppression (6.35), this can be computed in the soft approximation along the lines of [403, 418, 419].

The C parameter is special in that it has two singular points which feature a scaling of the type 6.35. One of them is the two-jet limit discussed in the previous section (i.e. $C = 0$) and the second is the symmetric three-jet configuration (i.e. $C = 3/4$) at which the distribution features a *Sudakov shoulder* [418, 420]. Due to this property, the value of the C parameter is nearly constant (i.e. up to quadratic corrections) near the symmetric three-jet limit, and the same considerations used for the two-jet case apply also here. One can therefore apply equation (6.36) by considering only the contribution of the second line and restricting the calculation to the soft approximation as done in [412].

In between the two- and symmetric three-jet configurations (i.e. $0 < C < 3/4$), the simplifications derived in the above sections do not apply trivially. To simplify the discussion, let us consider for simplicity the radiation of the gluer k off a single colour dipole (the final result is simply obtained by summing over all possible dipoles). Let us assume the existence of a mapping $p \equiv p(\{\tilde{p}\}, k)$ that is collinear safe in the limit where the system k is collinear to the ends of the radiating dipole, and such that in the soft limit one has (schematically)

$$p(\{\tilde{p}\}, k) = \tilde{p} + \mathcal{M}(\{\tilde{p}\}) \sum_i k_i + \mathcal{O}(k^2), \tag{6.37}$$

where the sum runs over all constituents k_i of the gluer, and the tensor $\mathcal{M}$ only depends on $\{\tilde{p}\}$. The master formula (6.36) can be rewritten as

$$\Sigma(C) = \sigma - \left\{ \int [d\sigma(\{\tilde{p}\}) + d\sigma(\{p(\{\tilde{p}\}, k)\}, k)] \Theta(C(\{\tilde{p}\}) - C) + \int d\sigma(\{p(\{\tilde{p}\}, k)\}, k) [\Theta(C(\{p(\{\tilde{p}\}, k)\}, k) - C) - \Theta(C(\{\tilde{p}\}) - C)] \right\}. \tag{6.38}$$

The first line of equation (6.38) represents a cross section that is integrated inclusively over k at fixed $\{\tilde{p}\}$ according to a mapping of the form (6.37). According to the finding of [413], such cross section is free of linear power corrections, and therefore the only linear contribution comes from the second line as in the previous cases. Moreover, the expression in squared brackets of the second line of equation (6.38) is suppressed in the soft limit so that one can once again compute the linear contribution in the soft approximation.

6.3.3. Results and impact on α_S fits. One finds that the leading power correction can be parametrized as

$$\Sigma(C) = \Sigma^{\text{pert}} \left(C - \zeta(C) \frac{\alpha_0(\mu_I^2)}{Q} \Delta^{\text{NP}} \right), \tag{6.39}$$

where the quantity Δ^{NP} does not depend on C, and Σ^{pert} denotes the perturbative cumulative distribution. The parameter $\alpha_0(\mu_I^2)$ is a nonperturbative quantity related to the mean value of the strong coupling constant in a physical scheme at scales smaller than μ_I [404]. It is commonly extracted from fits to experimental data together with α_S. The entire dependence of the leading power correction on C is encoded in the function $\zeta(C)$, which can be extracted directly from the calculations outlined in the above sections. Specifically, [412] obtains that $\zeta(3/4)/\zeta(0) \simeq 0.476$, i.e. the nonperturbative correction in the three-jet limit is about a factor of two smaller than the result in the two-jet limit.

In order to study the intermediate region $0 < C < 3/4$, [412] considered a set of possible functional forms for the function $\zeta(C)$, with which a fit of the strong coupling constant from a differential distribution of the C parameter was performed. This relies on a NNLO+NNLL perturbative calculation obtained with the results of [421–423] and experimental data from [424, 425] (we refer to [412] for the technical details). This study reveals that the variation of the functional form of $\zeta(C)$ can impact the extracted value of the strong coupling at the $\sim$4% level. In particular, the standard assumption $\zeta(C) = \zeta(0)$ used in past extractions leads to the following values of $\alpha_S(m_Z^2)$ and $\alpha_0(\mu_I^2)$

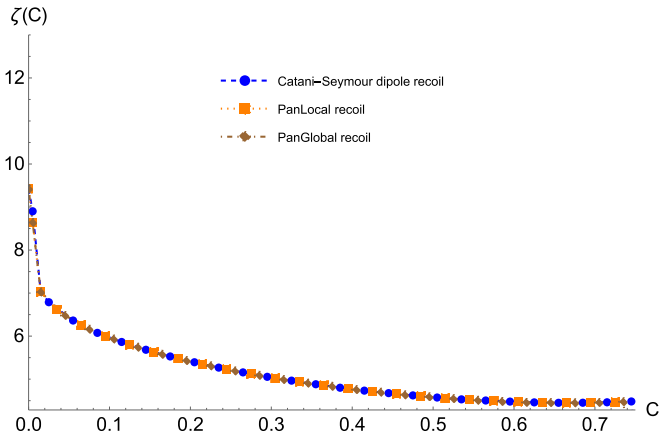

Figure 26. Fixed order calculation of $\zeta(C)$ with different recoil schemes [412].

$$\alpha_S(m_Z^2) = 0.1121^{+0.0024}_{-0.0016}, \quad \alpha_0(\mu_I^2) = 0.53^{+0.07}_{-0.05},$$

and agrees well with that of [396] (albeit with larger uncertainties, in part due to the use of NNLL+NNLO theory in [412] rather than N^{3}LL+NNLO [426] as in [396]). Conversely, several of the assumed $\zeta(C)$ scalings lead to a χ^2 value that is the same as, or smaller than, that for the fit within the $\zeta(C) = \zeta(0)$ assumption. In particular, one of the considered models returns

$$\alpha_S(m_Z^2) = 0.1163^{+0.0028}_{-0.0018}, \quad \alpha_0(\mu_I^2) = 0.51^{+0.06}_{-0.04},$$

with a χ^2 that is similar to that of the previous fit. This corresponds to a potential additional uncertainty in $\alpha_S(m_Z^2)$ due to nonperturbative corrections of about 3.7%. With this uncertainty taken into account, the extracted values of α_S become compatible with the world average $\alpha_S(m_Z^2) = 0.1179 \pm 0.0010$ [427].

With the above conclusions, an important question is whether one can calculate $\zeta(C)$ between the two-jet and three-jet limits. As discussed in section 6.3.2, [413] demonstrates that such a calculation can be performed in the soft approximation provided certain regularity conditions (6.37) are met by the kinematic map used to share the recoil due to the radiation of the gluer among the three hard particles in the event. Figure 26 shows the results of a calculation of this type performed in [412], where it was observed that the displayed $\zeta(C)$ scaling obtained with three commonly used recoil schemes [428, 429] yielded identical results. Later, in [413] it was shown that (in a simplified theoretical framework, described in detail in that reference) one obtains the correct power correction if the recoil scheme satisfies scalings of the kind given in equation (6.37). Specifically, as shown in [430], the three recoil schemes considered in figure 26 do satisfy an appropriate scaling.

A precise extraction of α_S with the above $\zeta(C)$ profile and further in depth studies of the interplay of the nonperturbative corrections discussed in this note with perturbative aspects of the calculation at higher orders are still necessary in order to make conclusive statements on the impact of the developments discussed in this note. Furthermore, similar studies for other event shape observables such as thrust (also addressed in [413]) will be essential to shed more light on the current discrepancies among the different event-shape based extractions of α_S considered in the world average [427].

6.4. The strong coupling from groomed event shapes[92]

Event-shape variables such as thrust have been measured with high precision by the LEP experiments. These observables have played and continue to play an important role in the determination of the value of the strong coupling, see for instance [395, 398, 411, 431–436], as well as the discussion in this report. While event shapes can be calculated with astonishing precision within perturbative QCD, both at fixed-order and resummed levels, nonperturbative contributions in particular due to hadronization can be sizable and thus affect the ultimate precision achievable. In the context of jet-substructure analyses of final states produced in hadronic collisions the soft-drop grooming technique offers a handle to reduce nonperturbative corrections [437]. This idea can be transferred to (global) event shapes in lepton [438] and hadron [439] collisions. With a possibly reduced impact of nonperturbative contributions, this can offer an improved precision in extractions of α_S. In [440] this has been explored for the soft-drop version of thrust in e^+e^- collisions at $\sqrt{s} = m_Z$.

The soft-drop variant of thrust (and similarly for other event shapes) is defined by first determining the conventional thrust axis and accordingly separating a given event into two hemispheres. The soft-drop procedure is then applied to both hemispheres independently. Soft-drop thrust is calculated based on the remaining constituents of both hemispheres, according to

$$\tau_{\mathrm{SD}} = \frac{\sum_{i\in\mathcal{E}_{\mathrm{SD}}}|\vec{p}_i|}{\sum_{i\in\mathcal{E}}|\vec{p}_i|}\left[1 - \frac{\sum_{i\in\mathcal{H}^L_{\mathrm{SD}}}|\vec{n}_L\cdot\vec{p}_i| + \sum_{i\in\mathcal{H}^R_{\mathrm{SD}}}|\vec{n}_R\cdot\vec{p}_i|}{\sum_{i\in\mathcal{E}_{\mathrm{SD}}}|\vec{p}_i|}\right], \tag{6.40}$$

where $\vec{n}_{L/R}$ denote the axes for the left and the right hemispheres, respectively, and the sums extend over all particles in the full event ($\mathcal{E}$), the soft-dropped event ($\mathcal{E}_{\mathrm{SD}}$) or the left and right hemispheres ($\mathcal{H}^{L/R}$). Thereby, the e^+e^- version of soft drop operates on the hemispheres defined by the thrust axis, reclusters them using the Cambridge–Aachen algorithm and discards soft subjets failing the criterion

$$\frac{\min(E_i, E_j)}{E_i + E_j} > z_{\mathrm{cut}}(1 - \cos\theta_{ij})^{\beta/2}\,. \tag{6.41}$$

While the parameter z_{cut} determines how stringent the cut on the subjet energies is, β provides an angular suppression to grooming.

Though originally designed to reduce nonperturbative effects like what is usually accounted for in multiple parton interaction (MPI) and underlying event (UE) simulations at hadron colliders [441], soft drop has been shown to also significantly reduce the impact of hadronization corrections in event shapes and jet observables at lepton colliders [438]. The viability of using soft-drop thrust in fits of α_S was studied in detail in [440]. Theoretical predictions computed at NLO+NLL′ accuracy were employed in fits to hadron-level pseudodata generated with SHERPA [442] based on merging the NLO pQCD matrix elements for $e^+e^- \to 2, 3, 4, 5$ partons with the dipole shower [443], using a nominal value of $\alpha_S(m_Z^2) = 0.117$, and the cluster-fragmentation model [444]. The main results of this study are summarized in figure 27.

Firstly, the results obtained from fitting α_S in the NLO+NLL′ prediction for the soft-drop thrust distribution depend less strongly on nonperturbative effects than for plain thrust when using the same Monte Carlo (MC) pseudodata. This is illustrated in the left plot of figure 27. While the best-fit α_S values obtained from plain thrust change significantly when going from

[92] Authors: S Marzani (INFN and Univ. Genova), D Reichelt (Durham), S Schumann (Univ. Göttingen), G Soyez (CEA-Saclay).

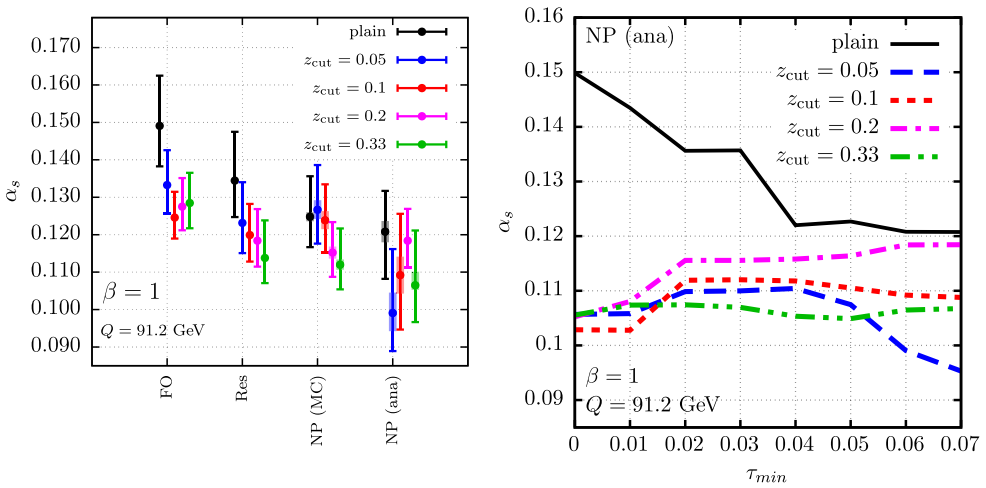

Figure 27. Results of [440] illustrating the advantages of using soft-drop thrust in fits of α_S. Both are based on fits to pseudodata generated with SHERPA. Left: dependence of the results on the effects included in the calculation, starting from only fixed order, i.e. NLO QCD, on the left and including effects of resummation, corresponding to NLO +NLL′ accuracy, and upon including nonperturbative effects in two different approaches. Right: dependence of the α_S best-fit value on the range of (soft-drop) thrust included in the fit.

using fixed-order (FO) results to including resummation effects (Res) and again when including nonperturbative (NP) effects, either extracted from MC simulations or from an analytic model (ana). This change is reduced when considering soft-drop thrust, shown in figure 27 for $\beta = 1$ and a variety of $z_{\rm cut}$ values. Note, in [440] also the cases $\beta = 0$ and $\beta = 2$ have been considered.

Secondly, for soft-drop thrust the value of α_S obtained from the fits is less affected by the choice of the considered observable range. This is illustrated in the right plot of figure 27. The minimal observable value $\tau_{\rm min}$ included in the fit is lowered from the default value $\tau_{\rm min} = 0.07$. The upper boundary is thereby kept fixed at $\tau_{\rm max} = 0.25$. For plain thrust, this results in dramatic changes due to increasing and severe hadronization corrections. Consequently, for plain thrust this additional observable range, i.e. phase-space region, cannot be reliably used in an α_S extraction. However, the results obtained from soft-drop thrust, with the various choices of $z_{\rm cut}$, are significantly more stable and the fit range could be extended into those areas.

From an experimental point of view, an obvious problem is that soft-drop event shapes have not been measured by the LEP experiments. However, their data are preserved and have recently been reanalysed for other observables [445–448]. Thus, we believe, it would be very interesting to measure soft-drop event shapes, as well as broader families of (groomed) substructure observables like angularities or energy correlation functions, on archived LEP data and use them to perform novel fits of the strong coupling. On the other hand, soft-drop groomed event shapes can also be studied in hadron collisions [439], so analogous analyses could be performed at the currently running LHC experiments. The same comment applies to analyses of soft-drop groomed jet substructure observables, see for example [449–455] for recent theoretical and experimental results. However, it should be noted that the study in [456] identified a strong correlation between α_S and the overall structure of the hard collision,

in particular the fraction of quarks and gluons that enter the calculation, as one of the main challenges for extractions of α_S from jet-shape measurements in proton-proton collisions. Thus, in this context, it would be important to find observables that can break this degeneracy.

On the theory side, we also anticipate that higher-accuracy calculations will be necessary to be competitive with fits using traditional event shapes. At fixed order, NNLO accurate predictions are in principle available [457]. Furthermore, resummed predictions for soft-drop observables have been obtained at NNLL [458] and some results are available even at N^3LL [459]. Regarding all-orders soft-gluon effects, a crucial ingredient is an improved understanding of the transition region where emissions soft enough to be groomed become important for the distribution. The resummed calculations like the ones used in [440] are performed in the strict $\tau \ll z_{\rm cut} \ll 1$ limit. However, judging from the ranges where α_S has been extracted from LEP data of the thrust distribution, and assuming a traditional choice of $z_{\rm cut} \sim \mathcal{O}(0.1)$, it seems however inevitable that a fit would also rely on the region $\tau \lesssim z_{\rm cut}$ or even $\tau \sim z_{\rm cut}$. Extending calculations to this region has been discussed recently in [460]. With this, NNLL accuracy appears to be achievable over the whole range, however still limited to the assumption $z_{\rm cut} \ll 1$. A better understanding of those power corrections in $z_{\rm cut}$ is still a missing ingredient to date.

Finally, despite the fact that soft drop successfully reduces the sensitivity to nonperturbative effects, calculations aimed at precision determinations of the strong coupling cannot neglect them. In this context, significant improvement has been recently achieved, both in the analytic and MC approaches. Using effective field theory techniques, a more detailed understanding of power corrections due to hadronization in the presence of soft-drop grooming has been achieved in [461, 462]. The Monte Carlo approach has also been improved thanks to the implementation of so-called transfer matrices [454]. This method allows us to better model the effect that the hadronization process has on the event kinematics, although it was shown in [440] to not significantly alter the effect of nonperturbative corrections in the range of soft-drop thrust used for the central fits, like the ones in the left plot of figure 27. However, outside of this range, differences might be sizable. In this context, it would be interesting to compare this improved numerical model with the aforementioned first-principle analysis.

7. $\alpha_S(m_Z^2)$ from hadronic final-states in e−p and p−p collisions[93]

7.1. α_S from jet-production cross sections in neutral-current DIS using NNLO predictions

The measurements of jet-production cross sections in neutral-current deep-inelastic scattering (NC DIS) are performed at HERA in the Breit frame of reference and provide clean and precise measurements. The Breit frame is defined as a brick-wall frame, where in leading-order NC DIS the incoming parton, literally, bounces back from the photon wall. Consequently, once the outgoing partons have significant transverse momenta, the process is described by a $2 \to 2$ photon-parton scattering process in pQCD and is proportional to $\mathcal{O}(\alpha_S)$ in leading order. Progress in the antenna subtraction formalism enabled to perform predictions for single-inclusive jet and dijet production cross sections up to next-to-next-to-leading order (NNLO) in pQCD [328, 329]. Several measurements of inclusive jet and dijet cross section measurements from the H1 and ZEUS collaborations, from different run-periods and different kinematic ranges in Q^2, were already exploited for the determination of α_S.

[93] Authors: D Britzger (MPI Munich).

a. Methodology. The value of $\alpha_S(m_Z^2)$ is determined from HERA jet cross sections in a χ^2-minimization procedure of NNLO predictions to data. Following the application of the factorization theorem, the pQCD predictions for jet cross sections are

$$\sigma = \sum_{k=q,\bar{q},g} \int \mathrm{d}x f_k(x) \hat{\sigma}_k(x) \cdot c_{\mathrm{had}}, \tag{7.1}$$

where f_k denotes the parton-distribution functions, $\hat{\sigma}$ the partonic NNLO cross section, and c_{had} nonperturbative correction factors which account for hadronization effects. Both components at the hard scale, f_k and $\hat{\sigma}_k$, exhibit a sensitivity to $\alpha_S(m_Z^2)$, which can directly be seen when calculating the partial derivative $\frac{\partial \sigma}{\partial \alpha_S(m_Z^2)}$. In order to account for both α_S-sensitive terms, a constant *starting scale* μ_0 is introduced, similarly as in DGLAP-based PDF-fits, and consequently the PDFs f_k are defined through their x-dependence at μ_0 and *evolved* to the factorization scale using the DGLAP formalism, where also the α_S-sensitivity in the DGLAP kernels is exploited in the fitting procedure. The evolution starting scale is chosen to be $\mu_0 = 20\,\mathrm{GeV}$. In a study by H1, it was observed that the extracted values of $\alpha_S(m_Z^2)$ are rather insensitive to the exact choice of the starting scale, and that the predominant sensitivity to $\alpha_S(m_Z^2)$ arises from the NNLO coefficients $\hat{\sigma}$. The value of $\alpha_S(m_Z^2)$ is then determined by minimizing the χ^2 expression based on log-normal probability distribution functions

$$\chi^2 = \boldsymbol{r}^T (V_{\mathrm{exp}} + V_{\mathrm{had}} + V_{\mathrm{PDF}})^{-1} \boldsymbol{r} \quad \text{using} \quad r_i = \log \sigma_{\mathrm{data},i} - \log \sigma_{\mathrm{pred.},i}, \tag{7.2}$$

where the covariance matrices are calculated from relative uncertainties of the data (V_{exp}), the hadronization factors (V_{had}) and the PDFs (V_{PDF}) and the cross sections $\sigma_{\mathrm{data},i}$ and $\sigma_{\mathrm{pred.},i}$ refer to data and the NNLO predictions (pred.) in a bin i, respectively. The PDF uncertainties are calculated from the eigenvectors or replicas of a given PDF set from an external analysis. Note that, by including the PDF uncertainties in the χ^2 expression, the fit exploits the same degrees of freedom as the respective PDF fit, and the PDFs become *profiled* in the minimization procedure. This procedure is de-facto equivalent to adding the HERA jet to the PDF fit, while contrary the $\alpha_S(m_Z^2)$ inference exploits exclusively the jet data and thus ensures a theoretically and experimentally cleaner determination of $\alpha_S(m_Z^2)$ than PDF fits, which mix different predictions and processes.

The NNLO predictions are obtained using the program NNLOJET [329], which is interfaced [245] to fastNLO [331] and Applgrid [463] to enable repeated calculations with differing values for $\alpha_S(m_Z^2)$ and differing PDFs. The DGLAP evolution is done with QCDNUM [327] or Apfelxx [464], and the hadronization correction factors are provided by the experimental collaborations together with the data and are commonly determined using the MC event generators Djangoh [332] or Rapgap [333]. The PDFs are obtained from NNPDF3.1 [268] and further PDF sets are studied [208, 215, 223, 252] and are used to define a so-called PDFset uncertainty. The renormalization and factorization scales are identified with $\mu^2 = Q^2 + p_{\mathrm{T}}^2$, where p_{T} is identified with the single-jet transverse momentum in case of inclusive jets, and with the average p_{T} of the two leading jets in case of dijet cross sections.

b. α_S from single-jet inclusive cross sections. The value of $\alpha_S(m_Z^2)$ was determined from inclusive jet cross sections from previously published data by H1 in [320], and from H1 and ZEUS inclusive jet cross sections in [245]. Both experiments employ the k_t jet-algorithm with a distance measure $R = 1.0$ and provide double-differential cross section data as functions of Q^2 and jet transverse momenta $p_{\mathrm{T}}^{\mathrm{jet}}$. The combined analysis of the H1 data using NNLO predictions exploits five independent cross section measurements [242, 321, 324, 465, 466] in the kinematic range of $5 < Q^2 < 15\,000\ \mathrm{GeV}^2$ and $4.5 < p_{\mathrm{T}}^{\mathrm{jet}} < 50\,\mathrm{GeV}$ and yields a value

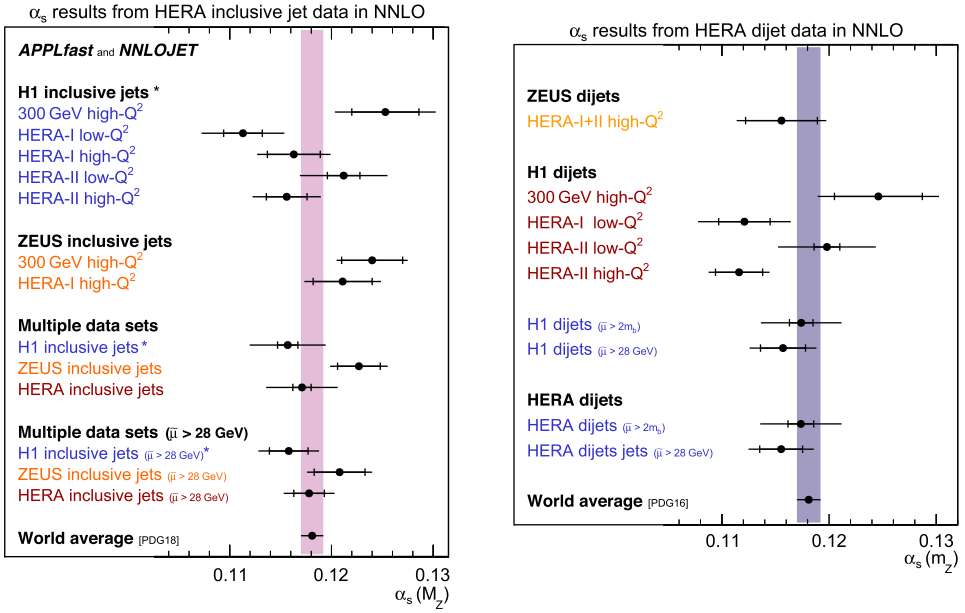

Figure 28. Strong coupling $\alpha_S(m_Z^2)$ determined from HERA inclusive jet (left) and dijet (right) cross section measurements using NNLO pQCD predictions (left). The vertical bands indicate the 2019 world average.

of $\alpha_S(m_Z^2) = 0.1157(10)_{\text{exp}}(36)_{\text{th}}$ [320], where the first uncertainty comprises experimental uncertainties, and the second collects theoretical uncertainties from PDFs, hadronization, and missing higher orders. The analysis of ZEUS inclusive jet cross sections exploits two data sets from the HERA-I running period [467, 468] in the kinematic range $120 < Q^2 < 20\,000\,\text{GeV}^2$ and yields $\alpha_S(m_Z^2) = 0.1227(21)_{\text{exp}}(19)_{\text{th}}$ [245]. Since H1 provides more data, and data at lower scales μ, their experimental uncertainty is smaller as compared to the ZEUS result, while contrary the highly-sensitive low-scale data results in increased scale uncertainties.

The combined analysis of H1 and ZEUS inclusive jet data yields the most precise result of [245]

$$\alpha_S(m_Z^2) = 0.1178(15)_{\text{exp}}\,(21)_{\text{th}}, \tag{7.3}$$

which is obtained by restricting the selected data to $\mu > 28$ GeV (figure 28, left). The NNLO predictions provide an excellent description of the data in all aspects and the value of χ^2/n_{dof} is found to be $79.2/104$. The dominant uncertainty arises from scale variations of the NNLO predictions, while several PDF-related uncertainties are found to be (negligibly) small. Future improved predictions may exploit these low-μ data and may achieve total uncertainties of less than ± 0.002.

c. α_S from di-jet cross sections. A determination of $\alpha_S(m_Z^2)$ from dijet cross sections in NC DIS was performed by H1. Four previously published double-differential dijet cross section measurements as a function of Q^2 and the average transverse momenta of the two leading jets in the Breit frame $\langle p_T \rangle$ were analyzed using NNLO pQCD predictions. The data were taken during different HERA run-periods, at different $e^{\pm}$-p center-of-mass energies and different kinematic regions in Q^2. From all four dijet data sets together a value of [320]

$$\alpha_S(m_Z^2) = 0.1157(22)_{\text{exp}}\,(23)_{\text{th}} \tag{7.4}$$

is determined, and the fit exhibits an excellent quality with $\chi^2/n_{\text{dof}} = 31.6/43$. While the above value is restricted to data with $\mu > 28$ GeV, a determination from all dijet data yields $\alpha_S(m_Z^2) = 0.1174(10)_{\text{exp}}(36)_{\text{th}}$ (figure 28, right). Hence, the experimental uncertainty would significantly be reduced, but contrary the theoretical uncertainties increase overly, which is due to enhanced sensitivity to $\alpha_S(m_Z^2)$ of data at lower scales and thus increased scale uncertainties.

An analysis of dijet cross section measurements from ZEUS exploits a single double-differential measurement [469], as a function of Q^2 and $\langle p_{\text{T}} \rangle$, where data were taken during HERA-I and HERA-II. However, its sensitivity to $\alpha_S(m_Z^2)$ is somewhat reduced, since the most sensitive data at low $\langle p_{\text{T}} \rangle$ have to be omitted since the definition of the dijet observable causes instabilities of the pQCD predictions because of symmetric cuts on the two jets [329, 469]. The ZEUS dijet cross sections yield a value

$$\alpha_S(m_Z^2) = 0.1156(34)_{\text{exp}}\,(25)_{\text{th}}. \tag{7.5}$$

Due to the limited sensitivity of the ZEUS dijet cross sections to $\alpha_S(m_Z^2)$, a combined analysis with H1 data does not improve over the H1 only result. For the future, a reanalysis of these data would be desirable, such that they can have a relevant impact on $\alpha_S(m_Z^2)$, and the analysis would profit from uncorrelated experimental uncertainties of the two independent experiments and high statistics.

d. α_S from jet cross sections of the H1 Collaboration. The H1 Collaboration performed a determination of $\alpha_S(m_Z^2)$ from inclusive jet and dijet data simultaneously using NNLO predictions. Although these observables are highly statistically correlated, this was made possible by a simultaneous analysis of inclusive jet and dijet data, where the statistical uncertainties and their correlations were measured as well [242, 324]. The analysis further includes inclusive jet data from H1 from HERA-I and when restricting the data to $\mu > 28$ GeV the result yields a value of [320]

$$\alpha_S(m_Z^2) = 0.1166(19)_{\text{exp}}\,(24)_{\text{th}}. \tag{7.6}$$

Since the inclusive jet and dijet data are highly correlated, the result improves only moderately over the result from the respective inclusive jet data alone. The smallest experimental uncertainty is achieved with relaxed cut on μ and yields an experimental uncertainty of $\delta\alpha_S = \pm 0.0009$, which motivates future improved predictions to underbid the experimental precision.

7.1.1. The running of α_S from HERA jet cross sections. Measurements of jet cross sections at HERA can be employed to test the running of the strong coupling, because these measurements cover a wide kinematic range. Once the renormalization scale μ_r is identified with final-state observables, every single cross section measurement of the double-differential data sets covers a well-defined range in μ_r. Hence, determinations of $\alpha_S(m_Z^2)$ from selected data points with similar values of μ_r provide a determination of α_S, where the validity of the renormalization group equation (RGE) is employed only within a limited μ_r range. The value of $\alpha_S(m_Z^2)$ can be translated to $\alpha_S(\mu_r^2)$, using a representative value of μ_r of the selected data sets, and multiple measurements at different μ_r provide a test of the running of α_S.

The running of the strong coupling constant is tested using NNLO predictions together with inclusive jet and dijet data from H1 [320], or solely inclusive jet data but from H1 and ZEUS were exploited [245], respectively. The $\overline{\text{MS}}$ renormalization scheme with 5 active

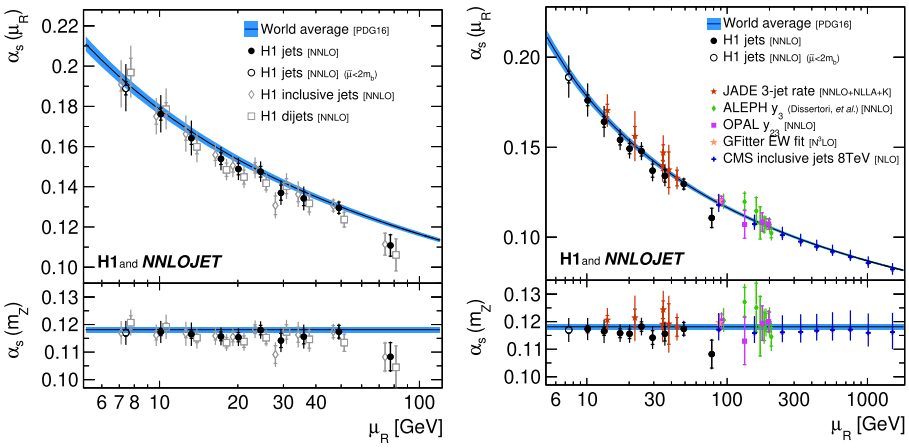

Figure 29. Left: tests of the running of α_S using NNLO pQCD predictions together with H1 inclusive jet data, dijet data, or both together. The lower panel displays $\alpha_S(m_Z^2)$ as obtained in the fit to selected data points, and the upper panel the respective value of $\alpha_S(\mu_r^2)$ for a representative value of μ_r. The blue shaded band shows the expectation when assuming the world average value from PDG 2016. Right: a comparison of $\alpha_S(m_Z^2)$ and corresponding $\alpha_S(\mu_r^2)$ from different measurements [236, 434, 435, 470, 471]. Both figures taken from [320].

flavours is used. Results from [320] are displayed in figure 29 and compared to the world average value and other determinations. Good consistency between results from inclusive jet and from dijet cross sections is observed, and all results are in good agreement with the world average value and the expectation from the RGE.

The HERA jet data are capable of testing the running of α_S in the range from about 7 to 90 GeV with a considerable precision of about 2.5 to 4%.

7.1.2. Further processes. In the recent years, the determination of $\alpha_S(m_Z^2)$ from e−p collision data focused mainly on inclusive jet and dijet data from HERA. This is because the recently achieved NNLO calculations [328, 329] provided a significant improvement over previously available NLO predictions [320], and since H1 provided a comprehensive set of jet measurements from the HERA-II running period [242, 324]. However, many further observables and final states can be exploited for $\alpha_S(m_Z^2)$, either once HERA data are further analyzed or when theoretical advancements are achieved.

Some examples, where future improvements could be possible, would be three-jet cross sections, heavy-flavour cross sections, event-shape observables, jet substructure observables or observables in photoproduction. As an example, three-jet cross sections from measurements by H1 were proven to provide small experimental uncertainties in α_S of about 1% [242, 324], but only NLO [472] predictions are available and thus largely limit the precision, and no corresponding measurement from ZEUS is published either. Similarly, in photoproduction, a precision measurement of inclusive jet cross sections by ZEUS exhibits high sensitivity to α_S [473], but no corresponding measurement from H1 is available, and no theoretical advancements were achieved for this process since then. The measurements of various event-shape observables in NC DIS by H1 [474] and ZEUS [475] from HERA-I data proved a significant sensitivity to α_S. However, although recent theoretical improvements were achieved [476] and new calculation techniques and observables [477–479], or

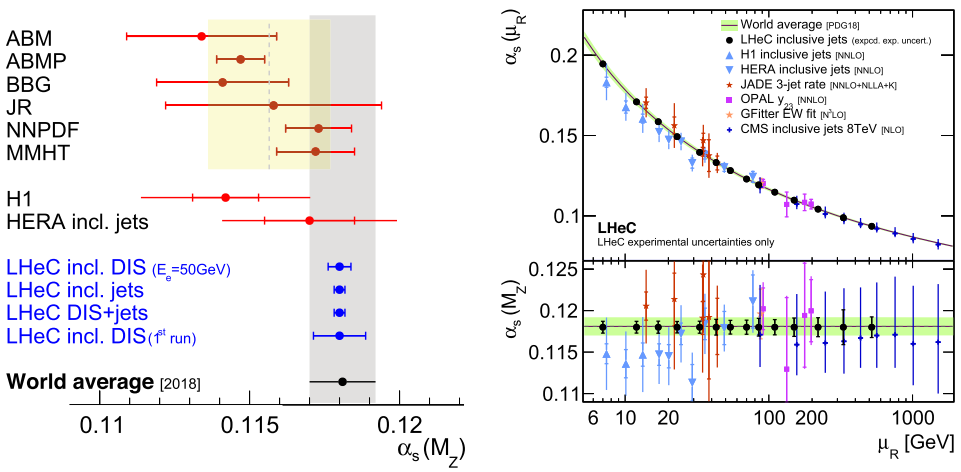

Figure 30. Left: comparison of prospected determination of $\alpha_S(m_Z^2)$ from inclusive DIS data at the LHeC and (global) PDF fits. Right: an illustration of the prospected experimental uncertainties in a study of the running of α_S from inclusive jet cross sections at the proposed LHeC experiment. Both figs. taken from [246].

substructure [455] could be studied, no suitable measurement of any such observable was published by the HERA experiments from HERA-II data (though, note the ongoing work in [480]). A recent measurement of lepton-jet correlation observables in NC DIS [481], where the jets are defined in the laboratory rest-frame, may provide high sensitivity to $\alpha_S(m_Z^2)$, and also theoretical predictions with considerable precision are available.

7.1.3. Future prospects. Future electron-proton collider experiments provide many opportunities for precision determinations of α_S. At lower center-of-mass energies, the electron-ion collider in the USA (EIC) [307, 482] and in China (EicC) [483] will provide new high-luminosity data. Early studies investigate a measurement of the 1-jettiness global event shape observable and prospect a determination of $\alpha_S(m_Z^2)$ at a level of a few percent [482].

The proposed Large-Hadron-electron-Collider experiment at CERN (LHeC) [162, 246] will provide $e^{\pm}$-p collision data at a center-of-mass energy of 1.3 TeV and hence the measurements of hadronic final state observables cover a considerably larger range than it was possible at HERA. These data will provide new precision measurements of inclusive NC and CC DIS cross section data. Because of an excellent detector acceptance and high-luminosity, also the high-x region will be measured with high precision. This will provide the opportunity to determine α_S from inclusive DIS data alone, something that was not possible with HERA data, and an experimental uncertainty of [246]

$$\delta\alpha_S(m_Z^2) = \pm 0.00022\ (\text{exp}+\text{PDF}), \tag{7.7}$$

can be expected in combined determination of PDFs and $\alpha_S(m_Z^2)$. The prospected uncertainties are compared with recent determinations in global PDF fits in figure 30.

From a simulation of inclusive jet cross section data with a complete set of systematic uncertainties, a determination of $\alpha_S(m_Z^2)$ with uncertainties of

$$\delta\alpha_S(m_Z^2) = \pm 0.00013\ (\text{exp})\ \pm\ 0.00010\ (\text{PDF}), \tag{7.8}$$

where the first uncertainties accounts for experimental uncertainties only and the second for PDF uncertainties, is expected in the LHeC/HL-LHC era. While experimental uncertainties can be well estimated, it is not quite possible to estimate the size of theoretical uncertainties reliably.

Similarly as at HERA, the running of α_S can be tested because of the dynamic scale of the jet data. Prospects for scale-dependent determinations of $\alpha_S(m_Z^2)$ (and corresponding values $\alpha_S(\mu_r^2)$) are displayed in figure 30. It is observed that, from LHeC inclusive jet cross sections, the running can be tested in the range from a few GeV up to about 600 GeV with permille precision. These measurements will become an indispensable experimental confirmation of its validity, which will allow to combine the low-scale α_S determinations from τ-decays or lattice QCD with those at the electroweak scale.

7.2. $\alpha_S(m_Z^2)$ from inclusive W and Z cross sections in p−p collisions[94]

A new determination of $\alpha_S(m_Z^2)$ has been recently proposed [484, 485] based on comparing the fiducial cross sections of electroweak (EW) boson production in p−p collisions at the LHC, $pp \to W, Z + X$ (with the EW bosons decaying into clean final states with electrons or muons) to the corresponding theoretical cross sections computed at next-to-next-to-leading-order (NNLO) accuracy. The method employed follows a similar approach to that used to derive $\alpha_S(m_Z^2)$ from inclusive top-quark pair cross sections [486]. Such an extraction exploits the fact that, first, there are many W and Z boson cross sections available and that those are the most precisely measured ones at the LHC (with typical $\pm 0.5\%$ statistical uncertainties and $\pm 2\%$ systematic uncertainties, dominated by the integrated luminosity), and, second, that their theoretical values can also be precisely computed (with scale and PDF uncertainties amounting to 0.5%–1% and 2%–4%, respectively). Theoretically, the cross sections can be derived from the convolution of parton densities $f_i(x_i, \mu_F)$ (evaluated at fractional momentum x_i and factorization scale μ_F) and elementary parton-parton cross sections (evaluated at renormalization scale μ_R) written as an expansion in the QCD coupling,

$$\sigma_{pp\to W,Z+X} = \int\int dx_1 dx_2\, f_1(x_1, \mu_F) f_2(x_2, \mu_F)[\hat{\sigma}_{LO} + \alpha_S(\mu_R)\hat{\sigma}_{NLO} + \alpha_S^2(\mu_R)\hat{\sigma}_{NNLO} + \cdots]. \tag{7.9}$$

Although the bulk of the cross section, given by $\hat{\sigma}_{LO}$, is a pure EW quantity, the contributions of NLO and NNLO higher-order pQCD corrections increase the overall $\sigma_{W,Z}$ value [487–491], and provide the dependence on $\alpha_S(m_Z^2)$ that allows extracting this parameter from a combined data-theory comparison. The size of the higher-order corrections, encoded in the so-called K-factor given by the ratio of NNLO to LO cross sections, amounts to $K = \sigma_{NNLO}/\sigma_{LO} \approx$ 1.22, 1.33, and 1.29 in the typical ATLAS, CMS, and LHCb fiducial acceptance for $W^{\pm}$ and Z final states, respectively. Such a result indicates that indeed W and Z boson production in p−p collisions is sensitive to $\alpha_S(m_Z^2)$, through ∼25% higher-order matrix-elements direct contributions to their total cross sections.

Up to the year 2019, there were $12 + 9 + 7 = 28$ $W^{\pm}$ and Z fiducial cross sections measured in p−p collisions by CMS, LHCb, and ATLAS, respectively, that have been exploited in [484, 485] to determine $\alpha_S(m_Z^2)$ by comparing them to the corresponding NNLO theoretical predictions computed with MCFM v.8 [490, 491] for a variety of PDF sets (CT14 [223], HERAPDF2.0 [215], MMHT14 [252], and NNPDF3.0 [492]) and $\alpha_S(m_Z^2) = 0.115$–0.121 values. The absolute $W^{\pm}$ and Z cross section data exploited here were not used by any of these PDF sets in their global fits to extract the parton densities themselves, so there is no

[94] Authors: D d'Enterria (CERN).

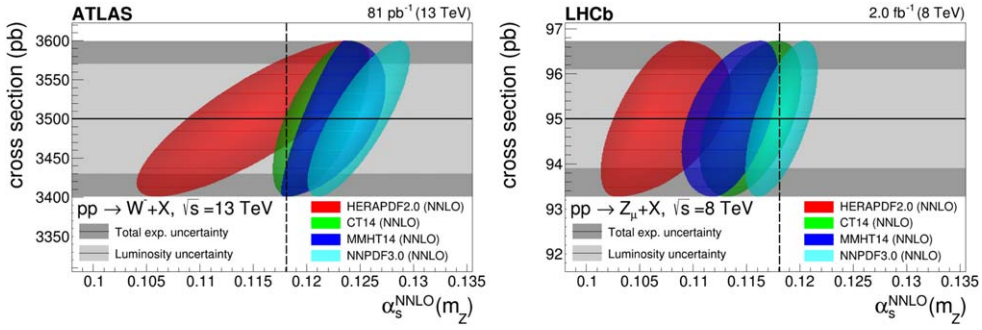

Figure 31. Examples of data-theory comparisons for EW fiducial cross sections in p−p collisions measured by ATLAS (W^+ bosons at $\sqrt{s} = 13$ TeV, left) [494] and LHCb (Z boson at $\sqrt{s} = 8$ TeV, right) [231]. The experimental cross sections are plotted as horizontal black lines with outer darker (inner grey) bands indicating their total (integrated luminosity) uncertainties. The theoretical predictions are computed for each PDF set as a function of $\alpha_S(m_Z^2)$, and combined with the experimental results into Jpdfs shown as filled ellipses. The vertical dashed line indicates the expected predictions for $\alpha_S(m_Z^2) = 0.118$.

'double counting' of the same data samples in the $\alpha_S(m_Z^2)$ determination. The final numerical accuracy of the calculations is 0.2%–0.6%, comparable to ∼1% differences found with alternative NNLO calculators such as FEWZ [489] or DYNNLO [488]. In the theoretical cross sections, we included corrections (mostly negative, of a few percent size) due to EW and photon-induced production processes evaluated at NLO accuracy with MCSANC v.1.01 [493].

Figure 31 shows examples of experimental ATLAS (left) and LHCb (right) cross sections (horizontal lines and bands) compared to the corresponding theoretical predictions per PDF as a function of $\alpha_S(m_Z^2)$ (coloured ellipses). From the computed cross sections, a linear dependence of $\sigma^{\rm th}_{\rm W,Z}$ on $\alpha_S(m_Z^2)$ is derived, and the filled ellipses are constructed to represent the contours of the joint probability density functions (Jpdfs) of the theoretical and experimental results, with a width representing a two-dimensional one standard-deviation obtained from the product of both probability densities for each PDF. The uncertainty in the theoretical cross sections is given by the quadratic sum of its associated PDF, scale, and numerical uncertainties.

The predictions are consistent with data within uncertainties but not systematically for the same $\alpha_S(m_Z^2)$ value (in particular, HERAPDF2.0 results do not always overlap with any of the others within the 1 std.-dev. region). For a fixed $\alpha_S(m_Z^2)$ value, HERAPDF2.0 (NNPDF3.0) predict larger (smaller) cross sections. Namely, HERAPDF2.0 (NNPDF3.0) favour systematically smaller (larger) $\alpha_S(m_Z^2)$ values, whereas MMHT14 and CT14 predictions are in between and less scattered over the 28 measurements considered. The predictions derived with HERAPDF2.0 (MMHT14) always feature the smallest (largest) slope, i.e. HERAPDF2.0 (MMHT14) cross sections are the least (most) sensitive to underlying $\alpha_S(m_Z^2)$ variations. With the 28 fiducial cross sections computed, we find that for the baseline QCD coupling constant value of $\alpha_S(m_Z^2) = 0.118$ of all PDF sets, the data-theory accord is overall better for the predictions calculated with CT14 and MMHT14 (goodness-of-fit per degree of freedom, $\chi^2/n_{\rm dof} \approx 1$) than those obtained with the HERAPDF2.0 and NNPDF3.0 sets ($\chi^2/n_{\rm dof} \approx 2.1$).

The cross sections calculated with different $\alpha_S(m_Z^2)$ values are fitted (using χ^2-minimization) to a first-order polynomial and the corresponding slope k is extracted for each PDF and measurement. The value of $\alpha_S(m_Z^2)$ preferred by each individual measurement is determined by the crossing point of the fitted linear theoretical curve with the experimental horizontal line. All the individual 28 $\alpha_S(m_Z^2)$ derived per PDF set, and the correlation matrices associated with all their uncertainties, are given as inputs of the CONVINO v1.2 [495] program employed to determine the final best estimate of all combined values. Table 10 lists the $\alpha_S(m_Z^2)$ values, along with the uncertainty breakdowns from every source, determined for each PDF set through the combination of the 28 individual determinations. The total symmetrized uncertainties amount to ∼1.4% for CT14, ∼2.1% for HERAPDF2.0, ∼1.3% for MMHT14 and ∼1.6% for NNPDF3.0. The last column of table 10 lists the $(\chi^2/n_{\rm dof})$ of the final single combined result compared to the 28 individual $\alpha_S(m_Z^2)$ extractions.

The final $\alpha_S(m_Z^2)$ values determined for each individual PDF are plotted in figure 32 (left) compared with the 2018 world average of $\alpha_S(m_Z^2) = 0.1181 \pm 0.0011$ (orange band) [226]. The (asymmetric) parabolas are constructed to have a minimum at the combined value and are fitted to go through $\Delta\chi^2 = 1$ (horizontal black lines) at the one std. deviation uncertainties quoted in table 10. The robustness and stability of the final $\alpha_S(m_Z^2)$ determination per PDF is cross-checked by varying key experimental and theoretical ingredients and uncertainties. For this purpose, the CONVINO combination is redone as follows: (i) for a fraction of the data subsets (ATLAS, CMS, or LHCb alone; or for 7, 8, 13 TeV c.m. energies only), (ii) varying the correlation factors of the PDF/scale uncertainties between 0 and 1, (iii) shifting the central values of the computed cross sections by $\pm 1\sigma$ of the theoretical uncertainty prior to combination, and (iv) adding±1% uncorrelated theoretical uncertainty (to cover differences among NNLO calculators). The results of such tests indicate that the MMHT14 result is the most stable against any variations in the analysis, whereas a few larger-than-1-standard-deviation changes appear in some cases for the results of the other PDF sets. The preferred QCD coupling value extracted from this study is that of MMHT14, $\alpha_S(m_Z^2) = 0.1188 \pm 0.0016$ plotted in figure 32 (right), because (i) it features the largest sensitivity (slope) of $\sigma_{W,Z}$ to α_S, (ii) it shows the lowest $\chi^2/n_{\rm dof}$ of the final single combined result compared to the 28 individual $\alpha_S(m_Z^2)$ extractions, (iii) it has the smallest (symmetrized) propagated uncertainties, and (iv) it is the most stable against any data or theory analysis variations.

This study confirms that the total inclusive $W^{\pm}$ and Z boson cross sections at hadron colliders are new promising observables that can provide useful constraints on the value of the QCD coupling constant, and that can eventually help improve the precision of the $\alpha_S(m_Z^2)$ world average. The recent availability of N^{3}LO codes [496, 497] for the calculation of inclusive $W^{\pm}$ and Z boson production cross sections, with one extra higher degree of theoretical accuracy compared to the one used here, will allow for further reductions of the propagated scale uncertainties, provided that PDF uncertainties are available at the same level of pQCD accuracy. Such theoretical developments, combined with upcoming EW boson measurements at the LHC with $\mathcal{O}(1\%)$ experimental uncertainties, mostly thanks to further reduced integrated luminosity uncertainties, will enable future $\alpha_S(m_Z^2)$ extractions with propagated uncertainties below the 1% level.

Table 10. Strong coupling constant $\alpha_S(m_Z^2)$ values extracted per PDF set by combining all the individual results obtained for each $W^{\pm}$ and Z boson production cross section measurements, listed along with their propagated total and individual uncertainties. The last column tabulates the χ^2/n_{dof} of the final single combined result compared to the 28 individual $\alpha_S(m_Z^2)$ determinations.

PDF	$\alpha_S(m_Z^2)$	δ (stat)	δ (lumi)	δ (syst)	δ(PDF)	δ(scale)	δ (num)	χ^2/n_{dof}
CT14	$0.1172^{+0.0015}_{-0.0017}$	0.0003	0.0005	0.0006	$^{+0.0011}_{-0.0013}$	0.0006	0.0003	23.5/27
HERAPDF2.0	$0.1097^{+0.0022}_{-0.0023}$	0.0004	0.0009	0.0009	$^{+0.0015}_{-0.0016}$	0.0007	0.0005	27.0/27
MMHT14	$0.1188^{+0.0019}_{-0.0013}$	0.0002	0.0008	0.0003	$^{+0.0015}_{-0.0007}$	0.0007	0.0002	19.3/27
NNPDF3.0	0.1160 ± 0.0018	0.0006	0.0004	0.0005	0.0013	0.0006	0.0007	56.9/27

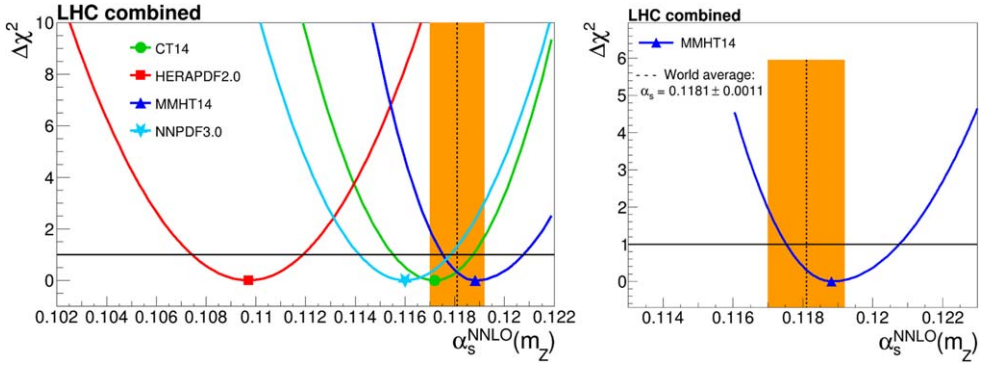

Figure 32. Final $\alpha_S(m_Z^2)$ values determined from the analysis of the EW boson inclusive cross sections at the LHC using the CT14, HERAPDF2.0, MMHT14, and NNPDF3.0 PDF sets (left), and $\alpha_S(m_Z^2)$ extraction from the MMHT14 PDF alone (right), compared to the 2018 world average (vertical orange band).

7.3. $\alpha_S(m_Z^2)$ from the transverse-momentum distribution of Z bosons[95]

A new determination of $\alpha_S(m_Z^2)$, using QCD resummed theory predictions and based on a semi-inclusive (i.e. radiation inhibited) observable at hadron-hadron colliders, has been recently proposed in [498]. The strong-coupling constant $\alpha_S(m_Z^2)$ is determined from the transverse-momentum distribution of Z bosons measured at $\sqrt{s} = 1.96$ TeV with the CDF experiment, using predictions based on q_t-resummation at N^3LO+N^3LL accuracy, as implemented in the `DYTurbo` [497, 499] program. The measurement is performed through a simultaneous fit of $\alpha_S(m_Z^2)$ and the nonperturbative Sudakov form factor. This measurement has all the desirable features for a precise determination of $\alpha_S(m_Z^2)$: large observable's sensitivity to $\alpha_S(m_Z^2)$ compared to the experimental precision; high accuracy of the theoretical prediction; small size of nonperturbative QCD effects.

Measuring $\alpha_S(m_Z^2)$, or equivalently $\Lambda_{\rm QCD}^{\overline{\rm MS}}$, from semi-inclusive Drell–Yan cross sections was first proposed in [500], by using Monte Carlo parton showers to determine $\Lambda_{\rm QCD}^{\rm MC}$ and later convert it to $\Lambda_{\rm QCD}^{\overline{\rm MS}}$. The conversion is based on resummation arguments showing that a set of universal QCD corrections can be absorbed in coherent parton showers by applying a simple rescaling, the so-called Catani-Marchesini-Webber (CMW) rescaling.

The Z-boson transverse-momentum distribution at small transverse momentum is one of such semi-inclusive observables. The recoil of Z bosons produced in hadron collisions is mainly due to QCD initial-state radiation, and the Sudakov form factor is responsible for the existence of a Sudakov peak in the distribution, at transverse-momentum values of approximately 4 GeV. The position of the peak is sensitive to the value of the strong-coupling constant.

For the measurement of $\alpha_S(m_Z^2)$ from the Z-boson transverse-momentum distribution it is necessary to rely on fast computing codes which allow the calculation of variations in the input parameters with small numerical uncertainties. To this end, the `DYTurbo` program was used.

The CDF measurement of Z-boson transverse-momentum distribution [501] at the Tevatron collider is ideal for testing the extraction of $\alpha_S(m_Z^2)$ with `DYTurbo` predictions. This

[95] Authors: S Camarda (CERN), M Schott (JGU Mainz).

measurement was performed with the angular coefficients technique, which allows extrapolating the cross section to full-lepton phase space with small theoretical uncertainties. The full-lepton phase space cross section allows fast predictions and avoid any theoretical uncertainties on the modelling of the Z-boson polarization. Another advantage of this measurement with respect to similar measurements performed at the LHC is the fact that Tevatron is a proton-antiproton collider, and the Z-boson production has reduced contribution from heavy-flavour-initiated processes compared to proton-proton collisions at the LHC.

The CDF measurement is performed in the electron channel, with central ($|\eta^e| < 1.1$) and forward ($1.2 < |\eta^e| < 2.8$) electrons, allowing a coverage up to Z-boson rapidity of $y = 2.8$, and a small extrapolation to the full rapidity range $|y_{\text{max}}| \approx 3.1$ of Z-boson production at $\sqrt{s} = 1.96$ TeV. The data sample is characterized by low values of the average number of interactions per bunch crossing, and by good electron resolution, at the level of 1 GeV for central electrons, and 1.5 GeV for forward electrons. The good resolution allows fine transverse-momentum binning (0.5 GeV) while keeping the bin-to-bin correlations smaller than 30%.

The nonperturbative QCD corrections to the Z-boson transverse-momentum distribution are modelled by including a nonperturbative term in the Sudakov form factor: $S(b) \rightarrow S(b) \cdot S_{\text{NP}}(b)$. The general form of $S_{\text{NP}}(b)$ is mass and centre-of-mass energy dependent [502]. However, at fixed invariant mass $q = m_Z$, and for one value of centre-of-mass energy, the form of $S_{\text{NP}}(b)$ can be simplified to depend on a single parameter g: $S_{\text{NP}}(b) = \exp(-g \cdot b^2)$. The nonperturbative parameter g is generally determined from the data, and its value depends on the chosen prescription to avoid the Landau pole in the impact-parameter b-space, which corresponds to a divergence of the Sudakov form factor. The divergence is avoided by using the so-called $b_\star$ prescription, which freezes b at a given value b_{lim}: $b \rightarrow b_\star = \frac{b}{1 + b^2 / b_{\text{lim}}^2}$. In this analysis b_{lim} is set to the value of $3\ \text{GeV}^{-1}$.

The sensitivity of the Z-boson transverse-momentum distribution to $\alpha_S(m_Z^2)$ mainly comes from the position of the Sudakov peak, and is related to the average recoil scale $\langle p_{\text{T}} \rangle \approx 10$ GeV. The sensitivity of the Z-boson transverse-momentum distribution to g also comes from the position of the Sudakov peak. However, the scale of the nonperturbative smearing governed by g corresponds to the value of primordial k_T. Typical values of $g \approx 0.6$ GeV^2 corresponds to a primordial k_T of approximately 1.5 GeV. It is possible to disentangle the perturbative contribution to the Sudakov form factor, governed by $\alpha_S(m_Z^2)$, from the nonperturbative one, determined by g, thanks to their different scale, as shown in figure 33.

The statistical analysis leading to the determination of $\alpha_S(m_Z^2)$ is performed by interfacing DYTURBO to xFitter [503]. The agreement between data and predictions is assessed by means of a χ^2 function, which includes experimental and PDFs theoretical uncertainties [504]. The nonperturbative form factor is added as unconstrained nuisance parameter in the χ^2 definition, i.e. it is left free in the fit. The fit to the data is performed in the region of transverse momentum $p_{\text{T}} < 30$ GeV by minimising the χ^2 as a function of $\alpha_S(m_Z^2)$, with α_S variations as provided in LHAPDF.

The corrections to the Z-boson transverse-momentum distribution due to QED initial-state radiation are estimated with PYTHIA8 and the AZ tune [505] of the parton shower parameters, and applied as multiplicative corrections. They are the level of 1%, and are responsible for a shift in the measured value of $\alpha_S(m_Z^2)$ of $\delta\alpha_S(m_Z^2) = -0.0004$.

The determination of $\alpha_S(m_Z^2)$ with the NNLO NNPDF4.0 PDF set [260] yields $\alpha_S(m_Z^2) = 0.1187$, with a statistical uncertainty of ± 0.0007, a systematic experimental uncertainty of ± 0.0001, and a PDF uncertainty of ± 0.0004. The value of g determined in the fit is $g = 0.66 \pm 0.05$ GeV^2, and the value of the χ^2 function at minimum is 41 per 53

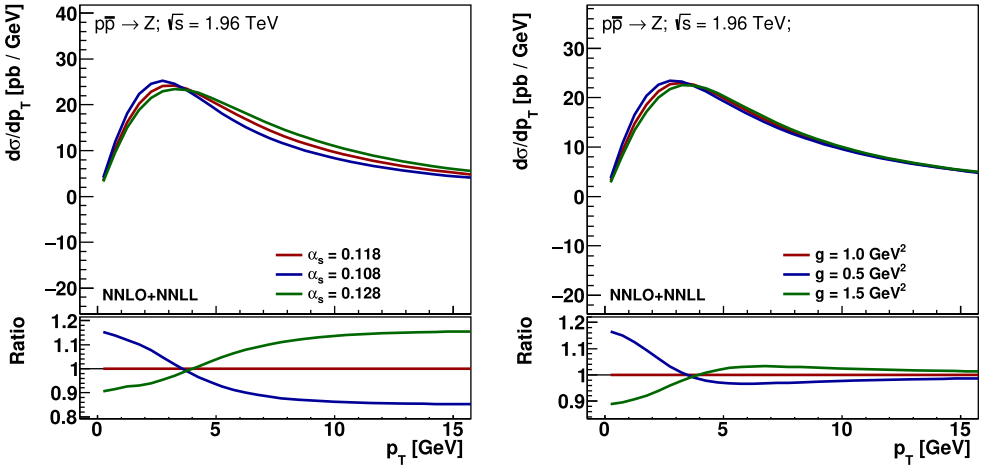

Figure 33. Sensitivity of the Z-boson transverse-momentum distribution to $\alpha_S(m_Z^2)$ (left) and to the nonperturbative QCD parameter g (right).

degrees of freedom. Various alternative NNLO PDF sets are considered: CT18 [222], CT18Z, MSHT20 [247], HERAPDF2.0 [215], and ABMP16 [208]. The determined values of $\alpha_S(m_Z^2)$ range from a minimum of 0.1178 with the ABMP16 PDF set to a maximum of 0.1192 with the CT18Z PDF set. The midpoint value in this range of $\alpha_S(m_Z^2) = 0.1185$ is considered as nominal result, and the PDF envelope of ± 0.0007 as an additional source of uncertainty. Missing higher order uncertainties are estimated through independent variations of μ_R, μ_F and Q in the range $m_{\ell\ell}/2 \leqslant \{\mu_R,\ \mu_F,\ Q\} \leqslant 2m_{\ell\ell}$ with the constraints $0.5 \leqslant \{\mu_F/\mu_R,\ Q/\mu_R,\ Q/\mu_F\} \leqslant 2$, leading to 14 variations. The determined values of $\alpha_S(m_Z^2)$ range from a minimum of 0.1177 to a maximum of 0.1193, yielding a scale-variation envelope of ± 0.0008. Alternative fits with a value of $b_{\text{lim}} = 2\ \text{GeV}^{-1}$ in the b_* regularization procedure and with the minimal prescription yields an uncertainty of $^{+0.0006}_{-0.0004}$. A fit in which the NNPDF4.0 PDF set is evolved with a variable-flavour number scheme yields $\delta\alpha_S(m_Z^2) = -0.0002$. The stability of the results upon variations of the fit range is tested by performing fits in the regions of Z-boson transverse momentum $p_{\text{T}} < 20$ GeV and $p_{\text{T}} < 40$ GeV. The spread in the determined values of $\alpha_S(m_Z^2)$ is at the level of ± 0.0001 and is not considered as a source of uncertainty. Since the region $20 < p_{\text{T}} < 40$ GeV is sensitive to the matching of the resummed cross section to the fixed order prediction, this test provides a strong confirmation that the missing $\text{O}(\alpha_S^3)$ contributions to the asymptotic term and the V+jet finite-order cross section are negligible for this analysis. The measured value of the strong-coupling constant is $\alpha_S(m_Z^2) = 0.1185^{+0.0015}_{-0.0014}$, with a statistical uncertainty of ± 0.0007, an experimental systematic uncertainty of ± 0.0001, a PDF uncertainty of ± 0.0008, missing higher order uncertainties of ± 0.0008, and additional theory uncertainties of $^{+0.0007}_{-0.0004}$. The post-fit predictions are compared to the measured Z-boson transverse-momentum distribution in figure 34 (left).

We make some observations on this determination of $\alpha_S(m_Z^2)$. Contrary to other hadron collider observables, the Z-boson transverse-momentum distribution in the Sudakov region is not included in PDF fits, therefore this determination does not have any issue of correlations with existing PDF sets. The PDF uncertainties are estimated with a conservative approach, including the envelope of six different PDF sets. Missing higher order uncertainties are estimated with the standard approach of computing an envelope of scale variations. The model for nonperturbative QCD effects based on a Gaussian form factor is simple but

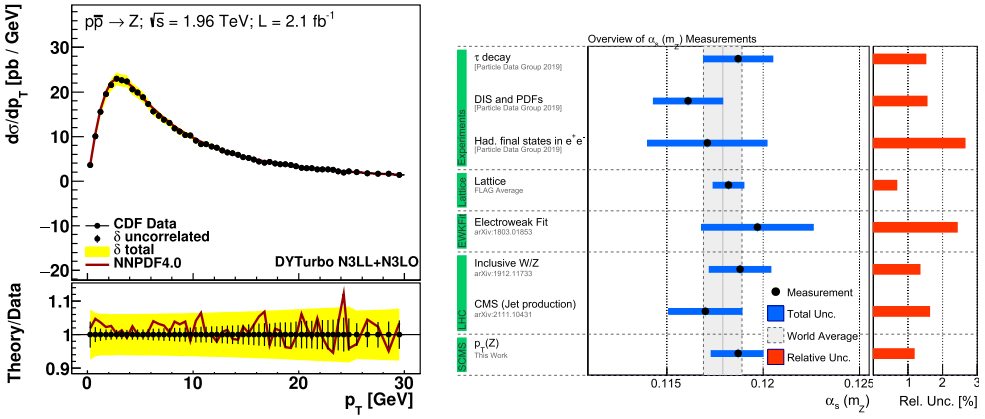

Figure 34. Left: comparison of the N^{3}LO+N^{3}LL `DYTurbo` prediction to the measured Z-boson transverse-momentum distribution. Right: comparison of the $\alpha_S(m_Z^2)$ derived here to the results of other categories of the world-average value.

effective, as it describes the data very well. Generous uncertainties on this model are estimated with variations of the Landau pole prescription. The measured value of $\alpha_S(m_Z^2)$ has a relative uncertainty of 1.2%, and is compatible with other determinations and with the world-average value, as illustrated in figure 34 (right).

Finally, we outline our personal wish-list for experimental and theoretical developments. LHC measurement of Z-boson transverse-momentum distributions are significantly more precise than measurements at the Tevatron. By analysing LHC data it is likely to reach a few 10^{-4} experimental uncertainty on $\alpha_S(m_Z^2)$ with the LHC Run-2 and Run-3 data samples. The main experimental limitation will be the lepton momentum/energy scale, currently known at $\sim 10^{-3}$. Improving the lepton scale to 10^{-4} will help to reach high precision on $\alpha_S(m_Z^2)$. Measurements of Drell–Yan transverse-momentum distributions at high mass will bring further sensitivity to $\alpha_S(m_Z^2)$, but resolution may be a limiting factor. Precise measurements of Drell–Yan transverse-momentum at low and intermediate masses will help reducing the nonperturbative uncertainties.

From the point of view of theory predictions, the analysis will clearly benefit from even higher order predictions. The N^{4}LL accuracy is likely to be possible in the near future, and approximate N^{4}LL' could also be on reach in the coming years. The required ingredients for N^{4}LL are the 5-loop cusp anomalous dimension, the 4-loop rapidity anomalous dimension. For N^{4}LL' also N^{3}LO PDFs, N^{4}LO TMD, and the 4-loop quark form factor are needed. In order to make full usage of the extremely precise LHC measurements, it is needed to have an improved heavy-flavour treatment, with variable-flavour number scheme and/or massive corrections. The inclusion of joint q_T/small-x resummation [506] may also be relevant or even required. The precision of the measurement will greatly benefit from first-principle understanding of nonperturbative corrections. As a last remark, the availability of public software for Z+jet predictions at NNLO would help the inclusion of currently missing $O(\alpha_S^3)$ terms in the matching to fixed order. In conclusion, prospects to reach subpercent precision in the next 5–10 years mostly rely on theory developments.

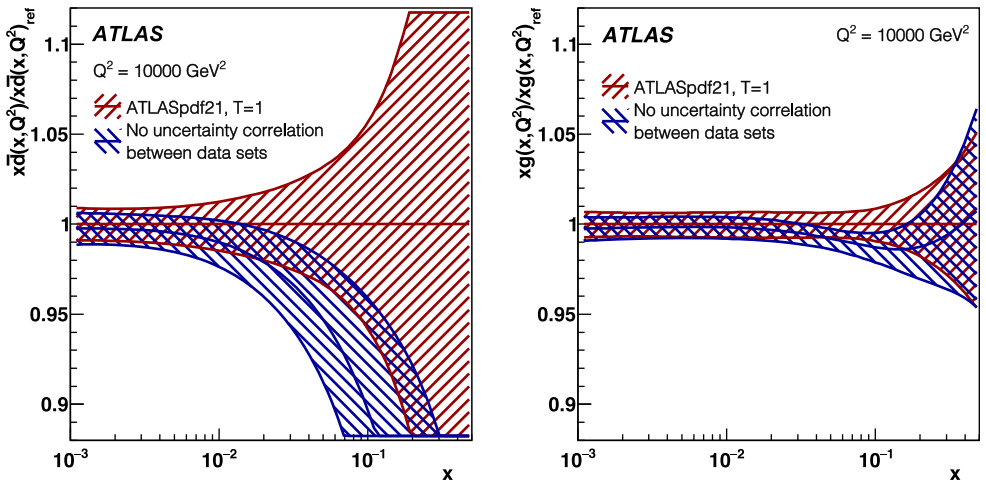

Figure 35. Difference in the gluon and the $x\bar{d}$ PDFs shown in ratio to the ATLASpdf21 (default) PDFs at scale $Q^2 = 10^4\,\mathrm{GeV}^2$. The default (red) analysis applies the full correlation of specified systematic sources among the data sets which use jet data, and the alternative (blue) analysis does not apply any correlation of systematics sources (apart from the integrated luminosities) among the data sets.

7.4 Crucial aspects of PDF fits relevant for $\alpha_S(m_Z^2)$ determination[96]

Parton densities uncertainties play an important role in $\alpha_S(m_Z^2)$ determinations from hadron collider measurements. A novel analysis at NNLO accuracy for the determination of a new set of proton PDFs using diverse measurements in p−p collisions at $\sqrt{s} = 7$, 8 and 13 TeV performed by the ATLAS experiment at the LHC, and combined with DIS data from e−p collisions at the HERA collider, has been presented in [507] with the resulting set of PDFs called ATLASpdf21. In this analysis, particular attention is paid to the correlation of systematic uncertainties within and among the various ATLAS data sets and to the inclusion of theoretical scale uncertainties, two crucial aspects of PDF fits if an ultimate precision below $\mathcal{O}(1\%)$ is sought on PDFs determination.

Specifically, the correlations of various systematic sources have been considered between different analyses that use jet data: $t\bar{t}$ data in the lepton+jets channel [234, 508], W/Z + jets data [509, 510], and inclusive jet data [511]. The difference in the resulting $x\bar{d}$ and gluon xg PDFs, when such correlations among the input data sets are considered and when they are not, is shown in figure 35. Such differences are still visible at LHC energy scales, indeed this figure is made for the scale $Q^2 = 10^4\,\mathrm{GeV}^2$ to illustrate so.

It is visible how correlations of sources of systematic uncertainty both within and among data sets need to be carefully considered in PDF fits and although the difference between the resulting PDFs is not large in the best-known kinematic region (namely $0.01 < x < 0.1$, corresponding to mass scales ∼100 GeV →1 TeV at the LHC) it can nevertheless be large enough to have an impact. In the less well-known regions, at smaller and larger mass scales, the impact can be considerably greater.

Another important aspect to be considered is the inclusion of theoretical scale uncertainties, which are evaluated as follows. The K-factors are evaluated for separate changes of the renormalization (μ_R) and factorization (μ_F) scales by factors of 2 and 0.5. The magnitude

[96] Author: F Giuli (CERN).

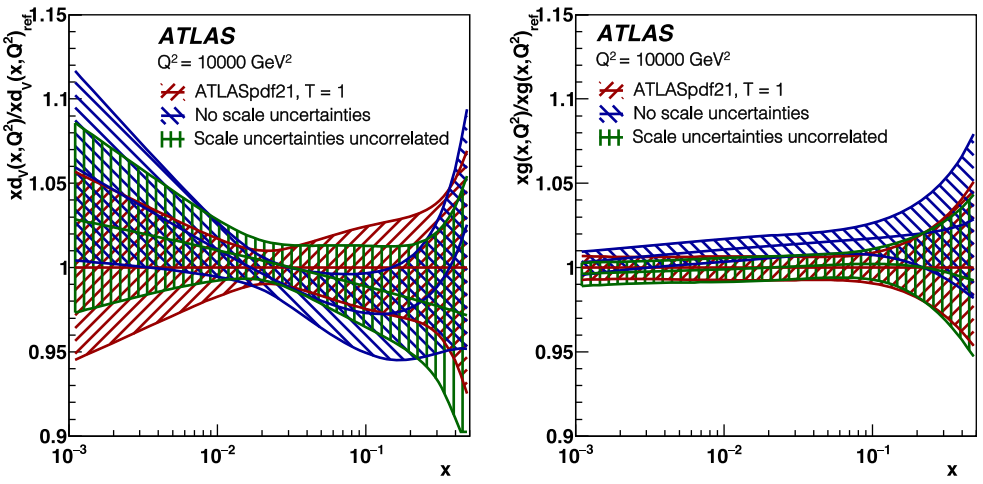

Figure 36. ATLASpdf21, showing the ratios of a fit not including theoretical scale uncertainties in the inclusive W, Z data to the central fit which does include these uncertainties, at the scale $Q^2 = 10^4\,\mathrm{GeV}^2$, for xd_v (eft) and xg (right).

of the K-factor difference is symmetrized as $(K[\mu_R(2)] - K[\mu_R(0.5)])/2$ and $(K[\mu_F(2)] - K[\mu_F(0.5)])/2$ and its sign is preserved as positive if the upward variation of μ_R or μ_F makes the K-factor increase, and negative if it makes the K-factor decrease. In the ATLASpdf21 analysis, for the ATLAS W and Z/γ^* inclusive data sets at both 7 and 8 TeV, both the total experimental uncertainty and the scale uncertainties approach $\sim$0.5%, so the scale uncertainties are considered as additional theoretical uncertainties (the effect of scale uncertainties for the other data sets entering in the fit was studied and was found to be negligible). Due to the similarity of the W and Z processes, both the μ_R and μ_F scales are considered correlated within the W, Z data sets at 7 TeV and between the W and Z data sets at 8 TeV. They are also considered to be correlated between the W and Z data sets at 7 and 8 TeV for the central fit.

Different choices for the treatment of the scale uncertainties in inclusive W, Z data are considered, and two alternative cases are considered:

1. The scale uncertainties are not correlated between the 7 and 8 TeV data,
2. Scale uncertainties are not applied at all.

Figure 36 shows the results of fits for these two cases, compared with the central fit, shown as a ratio at a scale $Q^2 = 10^4\,\mathrm{GeV}^2$, relevant for LHC physics. The uncertainties are very similar in size. The differences between the shapes of the PDFs are not large, but they can be important if the desired accuracy of the PDFs is $\mathcal{O}(1\%)$. The difference between the cases where the scale uncertainties are applied as being correlated or uncorrelated between the 7 and 8 TeV inclusive W, Z data sets is shown by the green line in these figures and it can be seen that it is generally a smaller effect.

The two aforedescribed effects should be taken into account properly when performing future precision data analyses, such as the measurement of m_W, $\sin^2\theta_{\mathrm{W}}$ or $\alpha_S(m_Z^2)$, because fits to these quantities can be very sensitive to (even) small changes.

7.5 Exact fixed-order pQCD predictions for cross section ratios[97]

In the standard approach, pQCD predictions for ratios of cross sections are computed as the ratio of the fixed-order predictions for the numerator and the denominator. Beyond the lowest order in the perturbative expansion, this result does, however, not correspond to a fixed-order prediction for the ratio. This contribution describes how exact fixed-order results for ratios of arbitrary cross sections can be obtained. Differences between the standard approach and the exact fixed-order results should be regarded as uncertainties of the predictions, related to possible higher-order contributions to the perturbative expansion. While this idea was motivated by our group's α_S determinations from ratios of jet cross sections in hadron collisions (for which pQCD predictions are currently available up to NLO), the method can be applied at any order pQCD, for any processes, and arbitrary cross sections. The full details of the method are documented in [512]. Here, we describe the general method for the computation of the exact fixed-order results and provide specific results for the NLO and NNLO cases. For various multijet cross section ratios in hadron collisions that were previously used in α_S determinations, we compare the NLO pQCD predictions for the two methods, and study how they describe the experimental data.

A measurable quantity $R = \frac{\sigma_n}{\sigma_d}$ is defined as the ratio of two cross sections σ_n and σ_d. It is assumed that the quantity R is defined in bins of an energy or transverse momentum related variable p which is defined for both σ_n and σ_d. At a fixed value (or in a given bin) of p, the quantity R is given by $R(p) = \frac{\sigma_n(p)}{\sigma_d(p)}$, and it is assumed that in a pQCD calculation the renormalization scale μ_r can be related to p by the same simple function (like $\mu_r = p$ or $\mu_r = p/2$) for both, σ_n and σ_d. In other words, in a given bin of p, the ratio R is probing α_S and the pQCD matrix elements for σ_n and σ_d at the same μ_r. For the sake of brevity, the dependence on p is omitted in the following.

In phenomenological analyses of experimental data, the LO, NLO, and NNLO pQCD prediction for R are usually computed from the ratios of the corresponding pQCD predictions for the numerator and denominator, σ_n and σ_d, as

$$R_{\mathrm{LO}} = \frac{\sigma_{n,\mathrm{LO}}}{\sigma_{d,\mathrm{LO}}} \quad \text{and} \quad R_{\mathrm{NLO}} = \frac{\sigma_{n,\mathrm{NLO}}}{\sigma_{d,\mathrm{NLO}}} \quad \text{and} \quad R_{\mathrm{NNLO}} = \frac{\sigma_{n,\mathrm{NNLO}}}{\sigma_{d,\mathrm{NNLO}}}. \tag{7.10}$$

While the LO pQCD prediction for R is uniquely defined, the higher-order pQCD predictions can be obtained in different ways. In the following, we refer to the above results as the 'standard' approach. Note that, beyond LO, these ratios are not exact fixed-order pQCD results for the quantity R.

We write the perturbative expansion for σ_n as $\sigma_n = \sigma_{n,\mathrm{LO}} \cdot (1 + k_{n,1} + k_{n,2} + ...)$ where $k_{n,1}$ is related to the NLO correction $\left(k_{n,1} = \frac{\sigma_{n,\mathrm{NLO}} - \sigma_{n,\mathrm{LO}}}{\sigma_{n,\mathrm{LO}}}\right)$ and $k_{n,2}$ to the NNLO correction $\left(k_{n,2} = \frac{\sigma_{n,\mathrm{NNLO}} - \sigma_{n,\mathrm{NLO}}}{\sigma_{n,\mathrm{LO}}}\right)$. The variables $k_{n,i}$ for $i \geqslant 3$ (corresponding to corrections beyond NNLO) are defined correspondingly, and also the corresponding variables $k_{d,i}$ $i \geqslant 1$ for the denominator σ_d. The ratio R is then given by

$$R = R_{\mathrm{LO}} \cdot (1 + k_{n,1} + k_{n,2} + \cdots) \cdot (1 + k_{d,1} + k_{d,2} + \cdots)^{-1}. \tag{7.11}$$

To obtain an exact fixed-order result for R, the second parenthesis is expanded in a Taylor series $(1+x)^{-1} = 1 - x + x^2 - x^3 + \cdots$ with $x = k_{d,1} + k_{d,2} + \cdots$. The terms of this series are multiplied with the terms in the left parenthesis, and the resulting products of $k_{n,i}$ and $k_{d,j}$ are sorted in powers of α_S. The infinite series is then truncated at the corresponding order at

[97] Authors: L Sawyer, C Waits, M Wobisch (Louisana Tech Univ.).

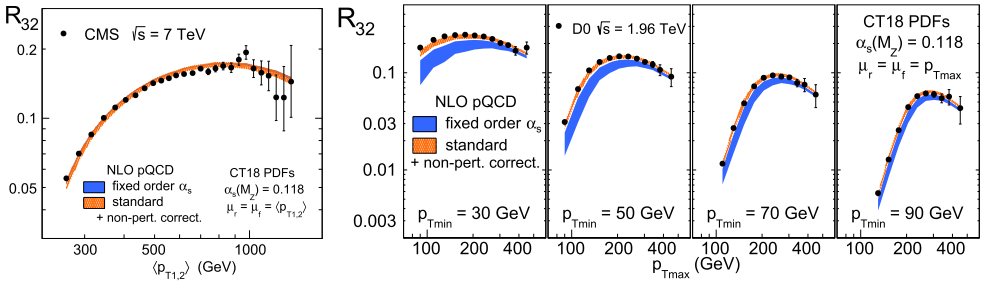

Figure 37. The multijet cross section ratio $R_{3/2}$, measured in p−p collisions at $\sqrt{s} = 7$ TeV as a function of $\langle p_{\mathrm{T}1,2}\rangle$ in the CMS experiment [255], and in p-$\bar{\mathrm{p}}$ collisions at $\sqrt{s} = 1.96$ TeV as a function of $p_{\mathrm{T}}^{\mathrm{max}}$ in the D0 experiment [516]. Two sets of pQCD predictions, corrected for nonperturbative contributions, are compared to the data: the fixed-order results for $R_{3/2}$, and the results from the 'standard' approach, computed from the ratio of the fixed-order results for the two cross sections. The shaded areas represent the ranges of the scale dependencies of the calculations.

which σ_n and σ_d were computed. This is the general procedure by which exact fixed-order results for R are obtained at arbitrary orders in pQCD. At NLO, (with $x = k_{d,1}$ in the Taylor series) this yields

$$R_{\mathrm{NLO}} = R_{\mathrm{LO}} \cdot (1 + k_{n,1} - k_{d,1}), \tag{7.12}$$

and at NNLO (with $x = k_{d,1} + k_{d,2}$ in the Taylor series)

$$R_{\mathrm{NNLO}} = R_{\mathrm{LO}} \cdot [1 + (k_{n,1} - k_{d,1}) + (k_{n,2} - k_{d,2} - k_{d,1}(k_{n,1} - k_{d,1})]. \tag{7.13}$$

In the following discussion, these results are referred to as the 'fixed-order' results for R.

The obtained formulas for the 'standard' and 'fixed-order' expressions are now used to compute NLO pQCD predictions for selected quantities which are then compared to each other and to the results from experimental measurements. For this purpose, we focus on five measurements of different multijet cross section ratios at the CERN LHC (in p−p collisions at $\sqrt{s} = 7$ and 8 TeV) and the Fermilab Tevatron Collider (in p-$\bar{\mathrm{p}}$ collisions at $\sqrt{s} = 1.96$ TeV). These include measurements of the quantities $R_{3/2}$, $R_{\Delta\phi}$, and $R_{\Delta R}$, which are different ratios of three-jet and two-jet production processes. The theoretical predictions for the ratios at NLO are obtained from the LO and NLO pQCD results for the two-jet and three-jet cross section calculations, which are computed using NLOJET [513, 514] with fastNLO [331, 515]. The proton PDFs are taken from the results of the CT18 global analysis [222]. The renormalization, μ_{r}, and factorization scales, μ_{f}, are set to the same values as used in the experimental publications of the measurement results, either to one of the relevant jet p_{T} variables, or to half of the total jet p_{T} sum, $H_{\mathrm{T}}/2$. The uncertainty of the pQCD results due to the $\mu_{\mathrm{r,f}}$ dependence is computed from independent variations of μ_{r} and μ_{f} by factors of 0.5–2 around the nominal choices. The corresponding range of variations is referred to as 'scale dependence'. Correction factors, to account for nonperturbative contributions are taken from the estimates that were obtained in the experimental analyses. PDF uncertainties are not relevant for the following discussions and have not been evaluated. The computations are referred to as 'fixed-order' results and 'standard' method, respectively.

The CMS Collaboration has measured the ratio of the inclusive three-jet and two-jet cross sections, $R_{3/2}$, for jets with $p_{\mathrm{T}} > 150$ GeV and rapidities of $|y| < 2.5$ [255]. The results are published as a function of the average transverse momentum of the two leading jets in the event, $\langle p_{\mathrm{T}1,2}\rangle$, over the range $0.42 < \langle p_{\mathrm{T}1,2}\rangle < 1.39$ TeV, as displayed in figure 37 (left).

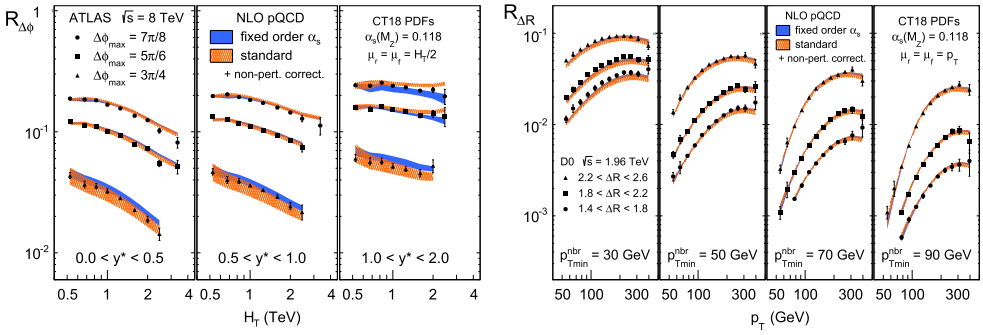

Figure 38. The multijet cross section ratio $R_{\Delta\phi}$, measured in p−p collisions at $\sqrt{s} = 8$ TeV in the ATLAS experiment [518] (left) as a function of H_{T}, in three regions of y^* and for three values of $\Delta\phi_{\mathrm{max}}$, and the multijet cross section ratio $R_{\Delta R}$, measured in p-$\bar{\mathrm{p}}$ collisions at $\sqrt{s} = 1.96$ TeV in the D0 experiment [517] (right) as a function of p_{T}, in four values of $p_{T\,\mathrm{min}}^{\mathrm{nbr}}$ and in three regions of ΔR. Two sets of pQCD predictions, corrected for nonperturbative contributions, are compared to the data: the fixed-order results for $R_{\Delta\phi}$ and $R_{\Delta R}$, and the results from the 'standard' approach, computed from the ratio of the fixed-order results for the two cross sections. The shaded areas represent the ranges of the scale dependencies of the calculations.

Another measurement of the ratio $R_{3/2}$ was made by the D0 Collaboration for jets with rapidities $|y| < 2.4$ and for various lower jet p_{T} requirements, $p_{\mathrm{T}}^{\mathrm{min}}$. The results are published as a function of the leading jet p_{T}, $p_{\mathrm{T}}^{\mathrm{max}}$, over the range $80 < p_{\mathrm{T}}^{\mathrm{max}} < 500$ GeV and for four $p_{\mathrm{T}}^{\mathrm{min}}$ choices from 30 to 90 GeV, as displayed in figure 37 (right). The results of the fixed-order and 'standard' calculations for the CMS and D0 measurements are compared to the data, with their error bands representing the range of their respective scale dependences. For the CMS results, both methods results are in agreement, and both describe the data equally well. For the D0 data, the fixed-order calculation predicts lower values everywhere and the scale uncertainty bands of the two calculations do either not, or hardly, overlap. Only towards larger $p_{\mathrm{T}}^{\mathrm{min}}$ and larger $p_{\mathrm{T}}^{\mathrm{max}}$, the uncertainty bands get closer.

The D0 Collaboration also published measurements of a new quantity, $R_{\Delta R}$, which also probes the ratio of three-jet and two-jet production [517]. The starting point is an inclusive jet sample (which probes the two-jet production process). The presence of a neighboring jet with $\Delta R < \pi$ is a sign of an event topology with three or more jets. The fraction of all inclusive jets with a neighboring jet, $R_{\Delta R}$, is therefore also a three- over two-jet cross section ratio. The quantity $R_{\Delta R}$ was measured for different p_T requirements, $p_{T\,\mathrm{min}}^{\mathrm{nbr}}$, and different angular separations, ΔR, for the neighboring jets, as a function of inclusive jet p_T from 50 to 450 GeV. The results of the fixed-order and the 'standard' calculations for $R_{\Delta R}$ are compared to the data in figure 38 (right). In almost all of the phase space the conclusions mirror those for the theoretical description of the CMS $R_{3/2}$ data in figure 37 (left): the fixed-order pQCD predictions agree with those from the 'standard' method, and both give a good description of all data with $p_{T\,\mathrm{min}}^{\mathrm{nbr}} \geqslant 50$ GeV. Only in the softer regime, for $p_{T\,\mathrm{min}}^{\mathrm{nbr}} = 30$ GeV at smaller p_T, they slightly underestimate the experimental measurement results.

The measurements of the multijet cross section ratio $R_{\Delta\phi}$ by the D0 and ATLAS Collaborations [518, 519] probe the azimuthal decorrelations of the two leading p_T jets in an event, and both analyses follow the recommendations from the original proposal [520]. The ATLAS result is shown in figure 38 (left). The D0 result is shown in [512]. Both measurements are performed in the same three rapidity regions, y^*, and for the same azimuthal decorrelation

requirements, $\Delta\phi_{\rm max}$. The ATLAS (D0) data are presented as a function of the scalar p_T sum of all jets in an event, H_T, over the range 0.46–4 TeV (180–900 GeV). The degree of agreement between the NLO pQCD predictions from the fixed-order and the 'standard' calculations and how they describe the data is pretty much the same for the ATLAS and D0 data sets. In different y^* and $\Delta\phi_{\rm max}$ regions, however, the two calculations exhibit a rather different behavior. For $0 < y^* < 1$ and $\Delta\phi_{\rm max} = 7\pi/8$ and $5\pi/6$, both calculations agree very well, exhibit a relatively small scale dependence, and both describe the data. At $\Delta\phi_{\rm max} = 3\pi/4$, the two predictions start to deviate from each other, and in some cases their larger scale uncertainty bands have only a small overlap. The data are described by both predictions. At $1 < y^* < 2$, for $\Delta\phi_{\rm max} = 7\pi/8$ and $5\pi/6$, the two predictions have a different H_T dependence and disagree at high H_T. In these regions, the fixed-order calculation gives a better description of the overall H_T shape for both data sets.

The results from these comparisons can be summarized as follows: in all cases where the results from the two methods agree with each other (as seen for the CMS $R_{3/2}$, the D0 $R_{\Delta R}$, and some regions of the ATLAS and D0 $R_{\Delta\phi}$ measurements), they also both describe the data. In all cases where the two methods disagree (meaning that their scale uncertainty bands do not overlap, as seen for the D0 $R_{3/2}$ data and the high H_T tails in some of the ATLAS and D0 $R_{\Delta\phi}$ data at $y^* > 1$), one of them (but not always the same) describes the data. In some intermediate cases, where the scale uncertainty bands from the two methods have little overlap (as for the ATLAS and D0 $R_{\Delta\phi}$ data with $\Delta\phi_{\rm max} = 3\pi/4$), both predictions are somehow consistent with the data.

It has to be noted that the 'fixed-order' and 'standard' method both stand on the same footing. In any given order pQCD, the results from both methods are equally valid representations of the perturbative expansion, and they only differ in higher-order terms. Therefore their discrepancy should be regarded as a genuine uncertainty of a fixed-order calculation, in addition to the scale dependence (since the latter does not always cover the spread of the two methods). The central value can be chosen from either method; there is no fundamental argument, to pick one over the other, and the choice may depend on the specific goal. In α_S determinations, where one assumes that the pQCD predictions are able to describe the data, one should possibly pick the method that gives a better description of the data. The proposed treatment of the spread of the two methods as additional uncertainty will provide more realistic estimates of theoretical uncertainties in future α_S determinations and other phenomenological studies. A small spread of the two methods can also be a criterion for identifying robust measurable quantities for which the theoretical approximations are more reliable.

7.6. Energy range for the RGE test and PDF sensitivity in α_S evaluations from jet cross section ratios[98]

A series of determinations of α_S are performed at the LHC e.g. using jet-based observables, which include the three-jet mass [521], R_{32} [255, 522, 523], transverse energy-energy correlations (TEECs) [524] and $R_{\Delta\phi}$ [518]. We discuss the relevant energy range on which running of the coupling, determined by the renormalization group equation (RGE), is probed through jet cross-section ratio and event shape observables at hadron colliders, as well as the PDF sensitivity in the corresponding α_S evaluations. This contribution is based mainly on remarks made in [525, 526].

[98] Authors: B Malaescu (LPNHE, Paris).

For fixed incoming parton kinematics, constructing the ratios between the cross sections for three-jet and two-jet final states can reduce the PDF dependence. At the same time, the resulting R_{32} ratio is still sensitive to α_S [255, 522]. The angular decorrelation observable $R_{\Delta\phi}$ in two-jet final states is defined as the ratio between the cross section of events with an azimuthal angular separation below some upper limit and respectively the inclusive dijet cross section. It also allows to probe three-parton final state kinematics and has been used for an α_S evaluation [518].

TEECs are event shape variables computed as energy-weighted angular distributions of all individual object pairs in the event. Similarly to e.g. the case of the inclusive jet cross section, a TEEC distribution receives multiple contributions from each event. Since analytical predictions for their distributions can be computed from first principles [527], probing hence fundamental symmetries of QCD, the TEECs are particularly attractive observables. The TEECs and the associated asymmetries (ATEEC) were measured by ATLAS and used for a determination of α_S [524]. It is interesting to note that in this study the theoretical prediction is also provided by a three-jet to two-jet cross-section ratio evaluated using NLOJET++ [513, 514], complemented by nonperturbative corrections based on PYTHIA8 [528] and HERWIG++ [529].

The choice of the scale used in the theoretical calculations for observables like R_{32}, $R_{\Delta\phi}$, and (A)TEECs is often based on event-level quantities. Typical examples are the average transverse momentum of the two leading jets [255, 523, 524], the transverse momentum of the leading jet [522], or half of the scalar sum of the transverse momenta of all the selected jets in the event [518]. The evaluated α_S values are typically displayed as a function of this same scale, reaching values up to a few TeV (see e.g. [251]). However, we note that the sensitivity to α_S for such observables is actually directly related to the probability for emission of extra radiation (yielding a third or higher order jet). This implies that these α_S determinations probe the prediction of the renormalization group equation in QCD at energy scales related to the transverse momentum of the third jet (p_{T3}), rather than to the event-level quantities above. It is to be noted that the typical values for p_{T3} are indeed significantly lower than the scale based on such event-level quantities. Indeed, in the case of the (A)TEEC studies at 8 TeV [524], if the average scales used in the theoretical calculations range between 412 and 810 GeV (depending on the bin), the corresponding average p_{T3} values are between 169 and 215 GeV.

It is desirable to achieve consistency between scale used for theory calculation and the scale at which the RGE test is claimed, while taking into account the remarks above. The MiNLO procedure [530] may indeed provide a way forward towards this goal.

The α_S determinations from ratios of three-parton-like over two-parton-like final states (i.e. from observables like R_{32}, $R_{\Delta\phi}$, (A)TEEC) are impacted by residual PDF uncertainties that have been quantified in the corresponding experimental studies [255, 518, 521–524]. Contrary to what one may have initially expected, the PDF uncertainties (originating from the PDF eigenvectors/replicas, as well as from the differences among various PDF sets) are found to be nonnegligible, being typically larger than the combined experimental uncertainties, but smaller than the NLO scale uncertainty (table 11). Furthermore, in cases where direct comparisons are possible, it can be noted that the α_S determinations from ratio observables can have even larger PDF uncertainties compared to the corresponding absolute cross sections.

Actually, these features reflect the fact that the three-parton and two-parton processes that are used to define the respective cross section ratios have different composition of partonic initial states (see also contribution by BM in [531]). Indeed, the probability of extra radiation (which is what makes these observables nontrivial) is correlated, through the

Table 11. List of $\alpha_S(m_Z^2)$ values obtained from various LHC observables, together with their corresponding uncertainties from various sources (experimental, PDF eigenvectors/replicas, nonperturbative NP, scale variations) or their quadratic sum. The last column lists the range of $\alpha_S(m_Z^2)$ values probed for various PDF sets. See the corresponding references for any details, in particular for the ensemble of PDF sets considered in each study.

Observable [Ref.]	$\alpha_S(m_Z^2)$	Range PDF variations
R_{32} [522]	$0.111 \pm 0.006\,(\text{exp})^{+0.016}_{-0.003}\,(\text{PDF, NP, scale})$	0.109 – 0.116
R_{32} [255]	$0.1148 \pm 0.0014\,(\text{exp}) \pm 0.0018\,(\text{PDF}) \pm 0.0050\,(\text{theory})$	0.1135 – 0.1148
3-jet mass [521]	$0.1171 \pm 0.0013\,(\text{exp}) \pm 0.0024\,(\text{PDF}) \pm 0.0008\,(\text{NP})^{+0.0069}_{-0.0040}\,(\text{scale})$	0.1143 – 0.1183
2-jets [523]	$0.1159 \pm 0.0025\,(\text{exp, PDF, NP})$	0.1159 – 0.1183
3-jets [523]	$0.1161 \pm 0.0021\,(\text{exp, PDF, NP})$	0.1159 – 0.1179
2- and 3-jets [523]	$0.1161 \pm 0.0021\,(\text{exp, PDF, NP})$	0.1161 – 0.1188
R_{32} [523]	$0.1150 \pm 0.0010\,(\text{exp}) \pm 0.0013\,(\text{PDF}) \pm 0.0015\,(\text{NP})^{+0.0050}_{-0.0000}\,(\text{scale})$	0.1139 – 0.1184
TEEC [524]	$0.1162 \pm 0.0011\,(\text{exp}) \pm 0.0018\,(\text{PDF}) \pm 0.0003\,(\text{NP})^{+0.0076}_{-0.0061}\,(\text{scale})$	0.1151 – 0.1177
ATEEC [524]	$0.1196 \pm 0.0013\,(\text{exp}) \pm 0.0017\,(\text{PDF}) \pm 0.0004\,(\text{NP})^{+0.0061}_{-0.0013}\,(\text{scale})$	0.1185 – 0.1206
$R_{\Delta\phi}$ [518]	$0.1127^{+0.0019}_{-0.0018}\,(\text{exp}) \pm 0.0006\,(\text{PDF})^{+0.0003}_{-0.0001}\,(\text{NP})^{+0.0052}_{-0.0019}\,(\text{scale})$	0.1127 – 0.1156

relevant matrix elements, to the type of partons in the initial state. Furthermore, both the α_S and PDF sensitivities of the observables are reduced when taking ratios. Both aspects are relevant for the corresponding evaluations of α_S, hence the presence of two competing effects resulting in residual PDF uncertainties. This residual PDF sensitivity is especially relevant in phase-space regions where PDFs are not strongly constrained. It can hence be related to the slopes observed in some comparisons of the energy dependence for the extracted α_S values, with the corresponding RGE predictions (see e.g. [518, 524]).

Up to now, the precision of the α_S determinations from three-jet-type observables has been limited by the NLO QCD theory uncertainty. This limitation will be overcome due to the NNLO corrections to three-jet production computed recently [532], which will allow to perform precision QCD studies with these observables. On the timescale of the FCC projects [139], even more progress on the theoretical predictions for these observables is desirable, allowing to further enhance the precision of these α_S evaluations.

7.7. New results on α_S and PDFs: QCD and SMEFT interpretation with inclusive jets at $\sqrt{s} = 13$ TeV[99]

Jet production in proton-proton collisions is instrumental for the extraction of the strong coupling constant α_S and the parton distribution functions (PDFs) of the proton. Furthermore, it is sensitive to the presence of physics beyond the standard model (BSM). In the following, the most recent QCD analysis [533] of the inclusive jet cross sections in p−p collisions at the LHC at a center-of-mass energy of 13 TeV is discussed. The data are collected by the CMS Collaboration. The jets are reconstructed using the anti-k_T algorithm [534] with distance parameters $R = 0.4$ and $R = 0.7$, and the cross sections are measured double-differentially as a function of the individual jet p_{T} and the absolute rapidity $|y|$. The measurements using $R = 0.7$ are used in the PDF analysis and correspond to an integrated luminosity of 33.5 fb^{-1}.

In the PDF analysis, the jet cross sections measured for $R = 0.7$ are used, together with the HERA combined [215] inclusive charged- and neutral-current deep inelastic scattering (DIS) cross sections. The fit is performed at NLO and NNLO. In the NLO version of the analysis, together with DIS and CMS jet measurements, the normalized triple-differential cross section of top quark-antiquark ($t\bar{t}$) production measured by the CMS collaboration [535], are utilized. In the NNLO (NLO) versions of the analysis, the PDFs, the value of $\alpha_S(m_Z)$ (as well as the value of the top quark pole mass, m_t^{pole}) are determined simultaneously.

Furthermore, an alternative SMEFT analysis is performed at NLO, where the cross section for the inclusive jet production is extended to include the effective contributions of 4-quark contact interactions (CI), exploring three different CI models. In this version of the analysis, the relevant Wilson coefficient is fitted simultaneously with the PDFs and SM parameters, avoiding the possibility of absorbing new physics in the PDF fit. No primary assumptions on the values of the QCD parameters are applied, such that constraints on the SM and BSM parameters are obtained simultaneously, mitigating their possible bias.

The fixed-order QCD predictions for inclusive jet production in p−p collisions are available at NLO and NNLO, obtained with NLOJet++ [513, 514] and NNLOJET (rev5918) [330, 536, 537], respectively, with the NLO calculations implemented in FASTNLO [331]. The NLO cross-section is improved to NLO+NLL by using corrections computed using the NLOJET calculation, provided by the authors of [538], and the MEKS [539] code. Electroweak and nonperturbative corrections are applied, and their details are given in [533]. The factorization scale μ_f and renormalization scale μ_r are set to the individual jet p_{T} for the inclusive jet cross

[99] Authors: K Lipka, T Mäkelä (DESY) on behalf of the CMS Collaboration.

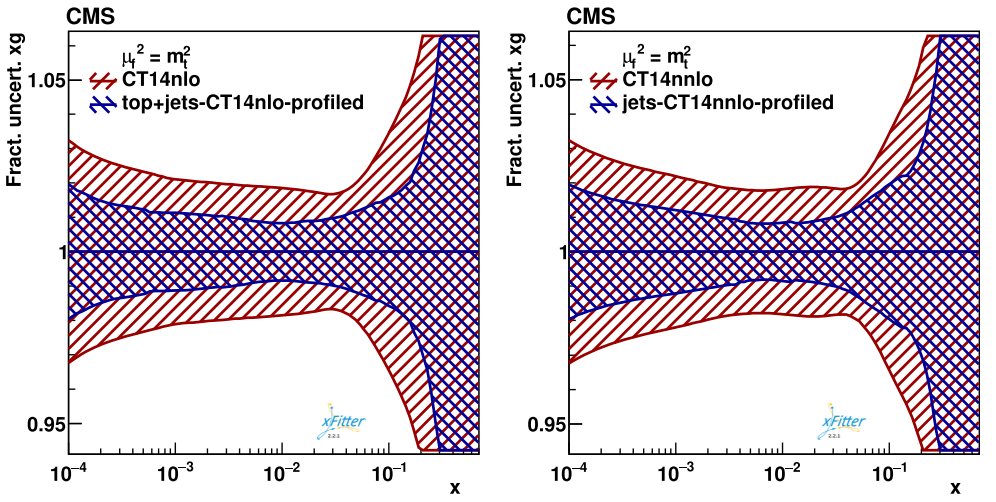

Figure 39. Fractional uncertainties in the gluon distribution, shown as functions of x for the scale μ_f set to the top quark mass. The profiling is performed at NLO with CT14nlo PDF (left) and at NNLO with CT14nnlo, by using the CMS inclusive jet cross section at $\sqrt{s} = 13$ TeV. The original uncertainty (red) and the profiled result (blue) uncertainty are shown. The figure is taken from [533].

section, and to the four-momentum transfer Q for the DIS data. In the theory predictions at NLO for the used $t\bar{t}$ production measurements, μ_r and μ_f are set to half the sum of the transverse masses of the partons, following [535]. The QCD analysis is performed using the XFITTER QCD analysis framework [503, 540] with an interface to CIJET [541, 542] for SMEFT predictions, which are available at NLO.

To illustrate the impact of the 13 TeV data on a global PDF, the profiling procedure [504, 543, 544] is used. The CT14 [223] sets at NLO or NNLO, where appropriate, are chosen. Both the $t\bar{t}$ and jet cross sections are observed to improve the precision of the gluon PDF significantly, as illustrated in figure 39. Profiling of the non-PDF parameters, such as the value of $\alpha_S(m_Z^2)$, m_t^{pole}, and CI Wilson coefficients is also performed and the results are summarized in [533]. The disadvantage of the profiling approach is that the simultaneous extraction of the PDFs and non-PDF parameters is currently not available. The full QCD analyses, implying the simultaneous fit of the PDF and non-PDF parameters, are performed using SM predictions at NNLO and NLO, or, alternatively, as a SMEFT fit, assuming three SM + CI models. In the SMEFT analyses, the scale of the BSM interaction Λ is assumed and the Wilson coefficient c_1 is a free parameter of the fit, together with the PDF parameters and the values of $\alpha_S(m_Z^2)$ and m_t^{pole}. For each of the NLO and NNLO fits, and also for the SMEFT fit, the investigation of the PDF parameterizations is performed independently. The SM fits at NLO and NNLO result in slightly different parameterizations, due to inclusion of the $t\bar{t}$ measurements in the NLO analysis. The SM and SMEFT fits at NLO result in the same solution for the preferred parameterizations.

The uncertainties are estimated following the HERAPDF approach [215], which accounts for the fit, parameterizations and model uncertainties. The Hessian fit uncertainty emerges from the uncertainties in the experimental measurements and is estimated by Hessian method using the tolerance criterion of $\Delta\chi^2 = 1$. The uncertainty is also estimated using the Monte Carlo replica method, and the results agree with those obtained by using the Hessian method. The quality of the fit is estimated by χ^2 divided by the number of degrees of freedom of

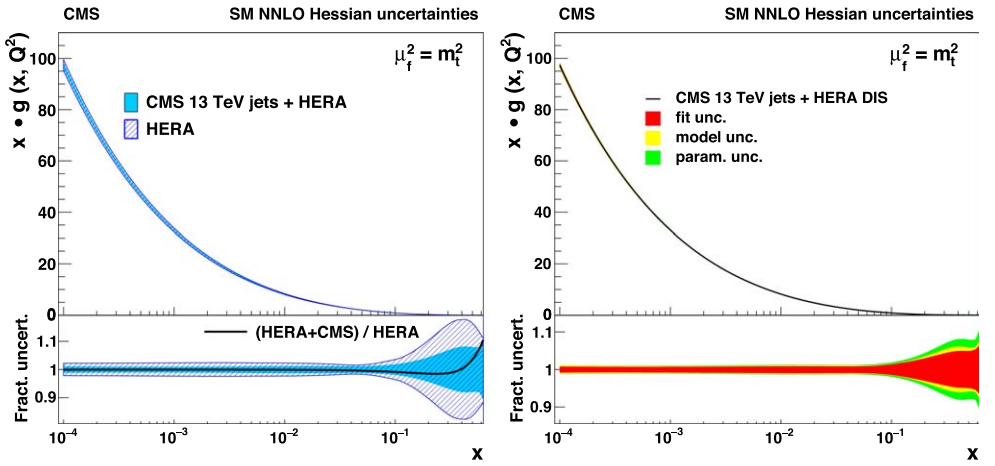

Figure 40. Total (left) and individual (right) fractional uncertainties in the gluon distributions resulting form the NNLO fit, shown as functions of x at the scale μ_f of the top quark mass. The filled (hatched) band represents the results of the fit using HERA DIS and the CMS inclusive jet cross section together (using the HERA DIS data only). The line corresponds to the ratio of the central PDF values of the two variants of the fit. The figure is taken from [533].

1321/1118, with somewhat large value driven by the fit to the inclusive DIS data, investigated in detail in [215]. The model uncertainties are obtained by varying the assumed non-PDF parameter values such as quark masses, the value of the starting evolution scale, strangeness fraction and the minimum value of Q^2 of the used DIS data. The theory uncertainties due to missing higher order contributions are obtained by an independent variation of the QCD scales up and down by a factor of two (avoiding cases $\mu_f/\mu_f = 4,\ 1/4$). For each of the independent scale choices, the QCD analysis is performed and the difference of the resulting parameters to those obtained for the central scale choice is taken as an uncertainty, which is treated as a model uncertainty. The parameterizations uncertainty arises from adding and removing additional parameters in the PDF parameterizations, one at a time, and constructing a maximum-difference envelope. The total uncertainty in the PDFs is obtained by adding the fit and the model uncertainties in quadrature, while the parameterizations uncertainty is added linearly. To illustrate the improvement in the PDF uncertainty by adding the CMS jet measurements at 13 TeV, the NNLO fit is also performed using only DIS data. A significant improvement in the uncertainty, in particular for the gluon distribution is observed (figure 40). In the same figure, also individual contributions of model, parameterizations and fit uncertainties are shown. In the SM fit at NNLO, the strong coupling constant $\alpha_S(m_Z^2)$ is obtained simultaneously with the PDFs and results in

$$\alpha_S(m_Z^2) = 0.1170 \pm 0.0014\,(\text{fit}) \pm 0.0007\,(\text{model}) \pm 0.0008\,(\text{scale}) \pm 0.0001\,(\text{param}), \tag{7.14}$$

which agrees with the previous extractions of the strong coupling constant at NNLO at hadron colliders [545, 546], of which it has best precision.

In the SMEFT analysis, the SM Lagrangian is extended with effective operators of dimension 6, introducing vertices with 4 quark legs. The considered operators are colour-singlets and lead to purely left-handed, vector-like and axial vector-like CI models, depending on how the quarks' handedness may change in the interaction. The operators' Wilson coefficients are fitted simultaneously with the PDFs, $\alpha_S(m_Z^2)$, and m_t^{pole} at NLO. Independent

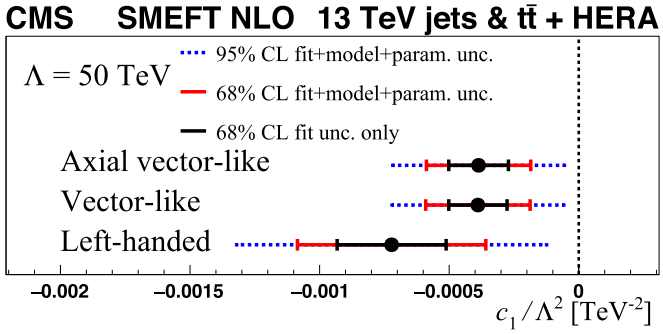

Figure 41. The Wilson coefficients c_1 obtained in the SMEFT analysis at NLO, divided by Λ^2, for $\Lambda = 50$ TeV. The solid (dashed) lines represent the total uncertainty at 68 (95)% confidence level (CL). The inner (outer) error bars show the fit (total) uncertainty at 68% CL.

of the value of Λ, the strong coupling constant and the top quark mass in these SMEFT fits result to $\alpha_S(m_Z^2) = 0.1187 \pm 0.0016_{(\text{fit})} \pm 0.0005_{(\text{model})} \pm 0.0023_{(\text{scale})} \pm 0.0018_{(\text{param.})}$, and $m_t^{\text{pole}} = 170.4 \pm 0.6_{(\text{fit})} \pm 0.1_{(\text{model})} \pm 0.1_{(\text{scale})} \pm 0.2_{(\text{param.})}$ GeV. The Wilson coefficients are obtained for different assumed values of Λ. For illustration, the values of c_1 are shown for three investigated CI models in figure 41 for $\Lambda = 50$ TeV.

To compare to a conventional search for CI, the Wilson coefficients obtained in the SMEFT analysis are translated into unbiased 95% confidence level exclusion limits on Λ with $c_1 = -1$, resulting in the limits of 24 TeV for left-handed, 32 TeV for vector-like, and 31 TeV for axial vector-like CI. The present analysis provides for the first time such limits using hadron collider data while following an unbiased search strategy. To compare the PDFs and QCD parameters obtained in the SMEFT fit to respective SM results, the NLO analysis is performed considering only the standard model. The resulting QCD parameters obtained in both variants of the fit, SM and SMEFT, agree well, however the SM results have smaller parametrization uncertainty. The fit quality of both fits expressed in χ^2 divided by number of degrees of freedom results in $1411/1141$ for the SM and $1401/1140$ for SMEFT fits, respectively. The PDFs resulting from the SMEFT fit are shown in figure 42 in comparison to the results of the SM fit. Both results agree within the fit uncertainties.

For the future developments, the authors of this measurement and interpretation would appreciate the public availability of the fast-grid techniques for the NNLO prediction of the inclusive jet cross section. Furthermore, the used $t\bar{t}$ data are interpreted at NLO, since the measurements are split into categories according to the presence of an additional jet. In spite of the strong sensitivity of these measurements to the top quark mass, strong coupling constant and to the gluon distribution, these could not be used in the NNLO analysis. A stronger effort in development of the theory calculation for the $t\bar{t}$ production associated with a jet is highly desirable.

The performed SMEFT analysis is only a step towards the global SM + BSM interpretation of the LHC measurements and implies only colour-singlet CI contributions. The availability of colour-octet contributions and also of the corresponding EFT corrections for the $t\bar{t}$ cross section predictions at NLO, as well as to the other processes, probing the operators of similar structure, would be necessary. Finally, bringing the EFT corrections to the QCD processes to at least NNLO accuracy would be the ultimate goal for the interpretation of the HL-LHC measurements.

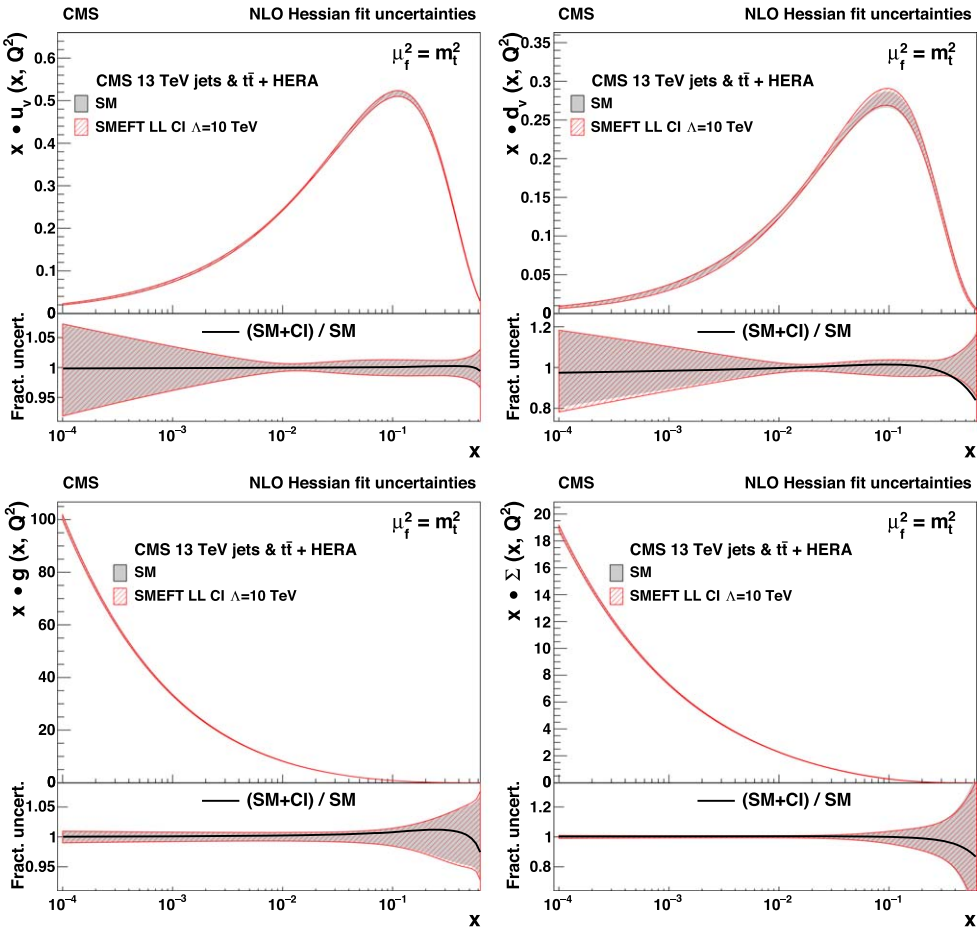

Figure 42. The u-valence (upper left), d-valence (upper right), gluon (lower left), and sea quark (lower right) distributions, shown as functions of x resulting from the fits with and without the CI terms. The SMEFT fit is performed with the left-handed CI model with $\Lambda = 10$ TeV. The figure is taken from [533].

7.8. The strong coupling constant and quark masses[100]

The determination of the strong coupling constant is strongly tied to the determination of other fundamental parameters of the SM and, in particular, with the quark masses in the QCD Lagrangian. Precise determinations of quark masses typically relies on a comparison of QCD predictions beyond leading-order accuracy with the measurement of experimental observables. These measurements are often sensitive to both the strong coupling constant and the mass value, and both parameters should ideally be treated in a simultaneous fit.

Like the strong coupling constant, quark masses are renormalized, scheme-dependent quantities. In the $\overline{\text{MS}}$ scheme the value of the quark mass depends at a given order in perturbation theory on the dimensionful renormalization scale μ. The evolution with this scale, or 'running' of the mass, forms a testable prediction of the theory. QCD yields a precise prescription for the scale evolution: given a value for a quark mass at a reference scale, its

[100] Authors: M Vos (IFIC, València).

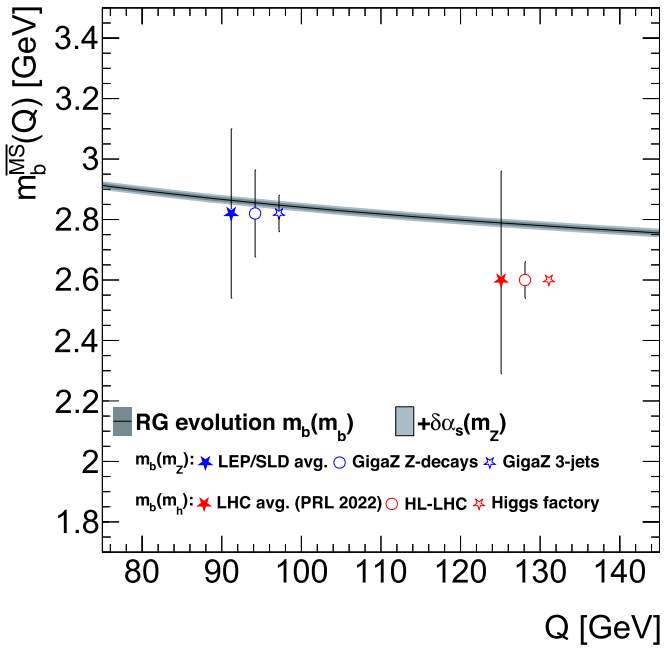

Figure 43. The scale evolution of the bottom quark $\overline{\text{MS}}$ mass. The markers are projections for $m_b(m_Z)$ from three-jet rates at the Z-pole and for $m_b(m_H)$ from Higgs boson branching fractions. The prediction of the evolution of the mass is calculated at five-loop precision with REvolver [551]. The grey error band includes the effect of missing higher orders and the projected parametric uncertainties from $m_b(m_b)$ and $\alpha_S(m_Z^2)$. [Figure from [562]].

value at any other scale can be determined using the renormalization group equation (RGE). RGE calculations for the the running quark masses have by now reached the 5-loop $\mathcal{O}(\alpha_S^5)$ level [547–549], and software packages such as RunDec [550] and REvolver [551] provide access to state-of-the-art renormalization evolution and scheme conversions.

A large number of measurements over a broad range of energies characterize the evolution of the strong coupling $\alpha_S(\mu)$ [251]. Experimental tests of the running of quark masses have been performed for the charm [552], bottom [553–560] and top [561] quarks.

Two recent studies revisit the running of the bottom quark mass using Higgs decay measurements at the LHC [563] and Z-decay rates to bottom quarks at LEP [564]. The measurement of $m_b(m_H)$ reaches a competitive precision of 14% using LHC Run-2 measurements. The precision could improve to 2% after the complete LHC programme, including the high-luminosity phase. The method has the potential for a subpercent-level determination at a future electron–positron 'Higgs factory'. The three-jet rates in a high-luminosity 'GigaZ/TeraZ' Z-pole run at future 'Higgs/EW/top factory' electron–positron collider can improve the measurement of $m_b(m_Z)$ by a factor of two [565]. The determination of $m_b(m_Z)$ from the $Z \to b\bar{b}$ decay rate is currently not competitive, but could reach an interesting precision (5%) with a new Z-pole run.

Together, these measurements take the test of the scale evolution of quark masses to a new level of precision [562]. Figure 43 from [562] compares the projections for $m_b(m_Z)$ and $m_b(m_H)$ to the current averages and the predicted evolution of the $m_b(m_b)$ world average. The precision of $m_b(m_H)$ is expected to increase rapidly in Run-3 of the LHC and the HL-LHC

programme. A new electron–positron collider operated at the Z-pole and the optimal Higgs-strahlung cross section (∼240–250 GeV) can improve $m_b(m_Z)$ and $m_b(m_H)$ further and take tests of the 'running' of the bottom quark mass into the precision regime.

The scale evolution of the strong coupling and the quark masses is sensitive to the presence of unknown, massive states that carry colour charge [10, 566]. A combined analysis of the scale evolution of the bottom quark mass and the strong coupling constant is required to consistently treat the impact of the new state on both quantities. A joint fit could possibly include also the charm and top quark masses, that can also be improved with an electron–positron collider [567].

With data collected in the next decades at the HL-LHC and a Higgs factory operated at $\sqrt{s} = m_Z$ and $\sqrt{s} \sim 250$ GeV, the precision of high-scale determinations of the bottom quark mass is expected to increase very significantly, with $m_b(m_H)$ reaching subpercent precision. A joint analysis of the scale evolution of the strong coupling and the quark masses then provides a powerful and model-independent handle on new coloured states in the mass range between m_b and m_H.

8. $\alpha_S(m_Z^2)$ from quarkonium

8.1. $\alpha_S(m_Z^2)$ from relativistic quarkonium sum rules[101]

One of the classical observables in QCD is the inclusive cross section for $e^+e^- \to$ hadrons, which is more conveniently cast in terms of the so-called R ratio defined as

$$R_{q\bar{q}}(s) = \frac{3s}{4\pi\alpha^2}\sigma_{e^+e^-\to q\bar{q}+X}(s) \simeq \frac{\sigma_{e^+e^-\to q\bar{q}+X}(s)}{\sigma_{e^+e^-\to \mu^+\mu^-}(s)}, \tag{8.1}$$

where α is the fine fine-structure constant, $\sqrt{s}$ the center-of-mass energy, and the right-hand side is exact if $\sigma_{e^+e^-\to \mu^+\mu^-}(s)$ is calculated at tree level for massless muons. Here we are interested in the case of heavy quarks, $q = c, b$.

Integrated moments of $R_{\bar{q}q}(s)$ are particularly suitable for phenomenological studies since, as opposed to local measurements, they have significantly smaller errors and suffer less from residual duality violations, allowing for a direct comparison with computations carried out with partonic degrees of freedom. Furthermore, they can be computed accurately in perturbation theory and receive small nonperturbative corrections, written as an expansion of local operators with increasing dimension. In particular, the inverse moments of $R_{\bar{q}q}(s)$, that we denote $M_q^{(n)}$, lead to the following sum rules [99, 568]

$$M_q^{(n)} = \int_{s_0}^{\infty} \frac{\mathrm{d}s}{s^{n+1}} R_{q\bar{q}}(s) = \frac{12\pi^2 Q_c^2}{n!} \frac{\mathrm{d}^n}{\mathrm{d}s^n}\Pi_q(s)\Big|_{s=0} . \tag{8.2}$$

On the left-hand side, obtained from experimental data, s_0 must be below the first $\bar{q}q$ narrow resonance with the same quantum numbers as the photon. On the right-hand side, theoretical moments can be related to derivatives of the heavy-quark vector correlator

$$(g^{\mu\nu}s - p^\mu p^\nu)\Pi_q(s) = -i\int \mathrm{d}x\, e^{i\,p\cdot x}\langle 0|T\, j_q^\mu(x) j_q^\nu(0)|0\rangle, \tag{8.3}$$

evaluated at $s = 0$ [$j_c^\mu(x) = \bar{q}(x)\gamma^\mu q(x)$]. The moments are dominated by a short-distance scale given by $\sim m_q/n > \Lambda_{\rm QCD}$ (where m_q is the quark mass), so restricting n to small values they can be computed in fixed-order QCD and their expansion is known up to $\mathcal{O}(\alpha_S^3)$ for $n \leqslant 4$

[101] Authors: D Boito (U Vienna and U Sao Paulo), V Mateu (Univ. Salamanca and UAM-CSIC Madrid).

[51, 53, 569–577]. Due to the strong sensitivity of $M_q^{(n)}$ to the heavy quark mass, which appears as a prefactor $1/[2\,\overline{m}_q(\mu_m)]^{2n}$ in their perturbative expansion, these sum rules have been used for many years to extract m_c and m_b, the masses of the charm and bottom quarks, with very good precision [48, 578–583] ($\overline{m}_q(\mu_m)$ denotes the $\overline{\rm MS}$ quark mass at scale μ_m).

Here we summarize the main results of [49, 584], where dimensionless ratios of roots of moments $M_q^{(n)}$ were considered. Since the ratios of charm-quark moments lead to a more precise determination of the strong coupling (mainly because experimental uncertainties are smaller) we restrict the presentation to the charm-quark moment ratios defined as

$$R_c^{V,n} \equiv \frac{(M_c^{(n)})^{\frac{1}{n}}}{(M_c^{(n+1)})^{\frac{1}{n+1}}}. \tag{8.4}$$

Ratios of this type were first introduced for the analysis of lattice data for the pseudoscalar correlator [55, 56] (see also the contribution of Petreczky and Weber to this volume, section 2.3). In the ratios $R_c^{V,n}$, the quark-mass dependence from the pre-factor of $M_c^{(n)}$ exactly cancels. These dimensionless ratios are suitable for precise α_S extractions for the following reasons (some of them already stated):

1. They have a very small residual dependence on the quark mass,
2. are known up to $\mathcal{O}(\alpha_S^3)$ for $1 \leqslant n \leqslant 3$,
3. contributions from nonperturbative physics are fairly small,
4. they can be determined experimentally from narrow resonance parameters and continuous $R_{\bar{q}q}(s)$ data.

The QCD fixed-order perturbative expansion of the ratios $R_c^{V,n}$ reads

$$R_c^{V,n} = \sum_{i=0}\left[\frac{\alpha_S(\mu_\alpha)}{\pi}\right]^i \times \sum_{k=0}^{[i-1]}\sum_{j=0}^{[i-2]} r_{i,j,k}^{(n)} \ln^j\left[\frac{\mu_m}{\overline{m}_c(\mu_m)}\right]\ln^k\left[\frac{\mu_\alpha}{\overline{m}_c(\mu_m)}\right], \tag{8.5}$$

where $[i-1] \equiv \mathrm{Max}(i-1, 0)$ and we use $N_{\rm f} = 4$ (the $N_{\rm f}$ dependence in α_S and the perturbative coefficients will be omitted). The running coupling $\alpha_S(\mu_\alpha)$ and quark mass $\overline{m}_c(\mu_m)$ are expressed in the $\overline{\rm MS}$ scheme and evaluated at the renormalization scales μ_α and μ_m, respectively. We do not assume these scales to be the same, as they account for different physics. This leads to a more conservative theory error estimate as argued in [48, 583]. We do avoid, however, large logarithms when varying the scales μ_α and μ_m, as discussed below. Note that the leading dependence of the ratios $R_c^{V,n}$ on the quark mass is only logarithmic and α_S^2 suppressed. Concretely, for $R_c^{V,2}$ at N^{3}LO one finds

$$\begin{aligned} R_c^{V,2} = 1.0449[1 &+ 0.57448\,a_s + (0.32576 + 2.3937L_\alpha)a_s^2 \\ &- (2.1093 + 4.7873L_m - 6.4009L_\alpha - 9.9736L_\alpha^2)a_s^3\,], \end{aligned} \tag{8.6}$$

with $a_s = \alpha_S(\mu_\alpha)/\pi$, $L_\alpha = \ln[\,\mu_\alpha/\overline{m}_c(\mu_m)]$ and $L_m = \ln[\,\mu_m/\overline{m}_c(\mu_m)]$. The total α_S corrections are about 12.5% for $R_c^{V,1}$, 7.2% for $R_c^{V,2}$, and 5.2% for $R_c^{V,3}$, which makes these observables rather sensitive to the strong coupling. The dominant nonperturbative correction to these observables stems from the gluon-condensate contribution and is known to NLO. We include it in our analysis, but the numerical impact is small.

We summarize now the determination of the moments $R_c^{V,n}$ from experimental data, which consists of three parts: the contribution from the narrow resonances (J/ψ and ψ'), a contribution from threshold data taken from [585–599], and the contribution for $\sqrt{s} > 10.538$ GeV, where there are no measurements anymore, modelled with perturbative QCD (the 'contiuum contribution'). Since charm threshold data is inclusive in all flavours,

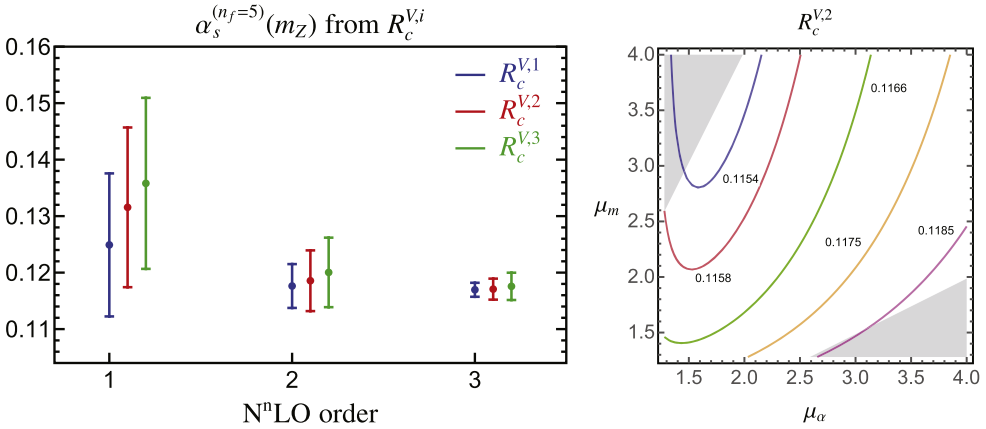

Figure 44. Left: results for α_S obtained from the analysis of $R_c^{V,n}$ with $n = 1$, 2, and 3, order-by-order in perturbation theory. Only truncation errors are shown. Right: results for α_S obtained from $R_c^{V,2}$ in the $\mu_m \times \mu_\alpha$ plane. The shaded region in gray is excluded from the analysis with $\xi = 2$ (see text).

one must also perform the subtraction of the u, d, s background and of the secondary charm production which is not accounted for in theoretical computations. (Small singlet contributions can be neglected [579]). It is important to keep the value of α_S used in the continuum contribution and the subtraction of the u, d, s background as a free parameter, otherwise the extraction of the coupling would be biased. For values not too far from the α_S world average, the dependence of $R_c^{V,n}$ on the strong coupling is linear to an excellent approximation. Parametrizing the results through $\Delta_\alpha \equiv \alpha_S^{(N_f=5)}(m_Z) - 0.1181$ we find

$$\begin{aligned} R_c^{V,1} &= (1.770 - 0.705\,\Delta_\alpha) \pm 0.017, \\ R_c^{V,2} &= (1.1173 - 0.1330\,\Delta_\alpha) \pm 0.0022, \\ R_c^{V,3} &= (1.03535 - 0.04376\,\Delta_\alpha) \pm 0.00084. \end{aligned} \tag{8.7}$$

The above errors are dominated by threshold data and are quite small. This is in part due to positive correlations between the moments $m_c^{(n)}$ which produces a partial cancellation of the errors in the ratios.

We extract α_S equating the expansions of the type of equation (8.6) with the respective experimental counterparts in equation (8.7) and solving for α_S numerically. It is mandatory to carefully and conservatively estimate the theoretical uncertainties arising from the truncation of perturbation theory. In the case of the determination of quark masses, the work of [48, 583] shows that it is important to vary the two renormalization scales μ_α and μ_m independently. We therefore vary them in the interval $\overline{m}_c \leqslant \mu_\alpha, \mu_m \leqslant 4$ GeV applying the constraint $1/\xi \leqslant (\mu_\alpha/\mu_m) \leqslant \xi$ and using $\xi = 2$ for our final results. A much less conservative choice, often adopted in related works in the literature, which leads to significantly smaller uncertainties, is to set $\mu_\alpha = \mu_m$, or equivalently $\xi = 1$. We obtain the uncertainties caused by renormalization scale variation from the spread of values of α_S in the $\mu_m \times \mu_\alpha$ plane, using a grid with 3025 points.

First, we verify the convergence of the extraction of α_S order-by-order in perturbation theory, considering solely the perturbative uncertainty—estimated through the scale variation described above. In figure 44 (left), we show that the results display a nice convergence, which indicates that the theory error bars from the truncation of perturbation theory are not

underestimated in our analysis. Further light on the perturbative uncertainty can be shed from two-dimensional α_S contour plots in the $\mu_m \times \mu_\alpha$ plane, as shown in figure 44 (right) for $R_c^{V,2}$. One sees that setting $\mu_\alpha = \mu_m$ (corresponding to $\xi = 1$) the error would be underestimated. Numerically, this choice leads to α_S errors obtained from the analysis of $R_c^{V,n}$ that are smaller by factors of 3 ($n = 1$), 2 ($n = 2$), and 1.5 ($n = 1$) than those obtained with $\xi = 2$.

We can then extract the final value of α_S from our analysis of the charmonium ratios $R_c^{V,n}$. Apart from the truncation uncertainty (labelled 'pt'), discussed in detail above, we include in the final value the experimental error ('exp'), the incertitude from the residual charm mass dependence (which happens to be negligible), and the nonperturbative error ('np', estimated from twice the gluon-condensate contribution). Ratios of moments with lower values of n lead to smaller errors in α_S from the truncation of perturbation theory but, on the other hand, have larger experimental uncertainties. It turns out that the optimal determination is obtained from the analysis of $R_c^{V,2}$, which gives, after evolving to the Z boson mass scale,

$$\alpha_S^{(N_f=5)}(m_Z) = 0.1168(15)_{\rm pt}(9)_{\rm exp}(7)_{\rm np} = 0.1168(19) \qquad \text{[charm vector current]}. \tag{8.8}$$

This result is fully compatible with the world average [251]. We remark that by setting $\mu_\alpha = \mu_m$ the total uncertainty would be reduced to 0.0013, which shows that our error estimate is indeed conservative.

We have applied our method to bottom ratios $R_b^{V,n}$ as well, but due to large experimental uncertainties the extracted value for the strong coupling is not competitive. Furthermore, we have reanalyzed lattice data on the moments of the pseudoscalar correlator. As opposed to the vector current, the pseudoscalar 0th moment $m_c^{P,0}$, which is scaleless and not sensitive to the charm quark mass, is an observable and therefore a direct comparison to perturbative computations is possible. From higher moments, one can construct ratios $R_c^{P,n}$ in the same way as displayed in equation (8.4). For either the 0th moment or the ratios, the exact same program for estimating perturbative errors can be applied, and we find uncertainties that are, in general, larger than what has been quoted in the original lattice articles. In particular, we find that the result in equation (8.8) is slightly more accurate than the extractions that we obtain with our method using lattice results quoted in [16, 54–56, 58].

A slightly more competitive determination can be obtained from a fit to $R_c^{V,2}$ and $m_c^{P,0}$ (which makes use of the fact that both theoretical and experimental uncertainties for those two observables are uncorrelated), which renders

$$\alpha_S^{(N_f=5)}(m_Z) = 0.1170 \pm (0.0014)_{\rm total} \qquad \text{[lattice + continuum]}. \tag{8.9}$$

This result can be regarded as a hybrid lattice-continuum determination.

Our ongoing efforts to improve these α_S determinations include a more refined treatment of threshold data using an iterative reclustering procedure based on linear splines, in which the new BES-III data [600] on the R-ratio below the charm production threshold has been included. Recent results for the large-order behavior of the perturbative series in the large-β_0 limit of QCD can also guide the design of new moments with reduced perturbative uncertainties, see [601]. One way of making the bottom sum rules more competitive is taking n large, such that experimental errors virtually vanish. This requires using nonrelativistic QCD (NRQCD) in the theoretical expressions, but the necessary expressions are available since some time already. Finally, as mentioned in section 9.2 on bottomonium, the method explained in the preceding paragraphs should apply equally well to the ratios of bottomonium bound-state masses, which again exhibit experimental errors negligibly small.

Acknowledgments— DB thanks the Universidad de Salamanca and VM thanks the Sao Carlos Physics Institute at Universidade de São Paulo, for hospitality. This work was supported by the FAPESP-USAL SPRINT Grant No. 2018/14967-4. DB's work is supported by the São Paulo Research Foundation (FAPESP) Grants No. 2021/06756-6, the Coordenação de Aperfeiçoamento de Pessoal de Nível Superior—Brasil (CAPES)—Finance Code 001, and by CNPq grant No. 309847/2018-4. VM is supported by the MECD grant PID2019-105439GB-C22, the EU STRONG-2020 project under the program H2020-INFRAIA-2018-1, grant agreement No. 824 093 and the COST Action CA16201 PARTICLEFACE.

8.2. $\alpha_S(m_Z^2)$ determination from bottomonium spectrum[102]

Early attempts to determine α_S from quarkonia are based on radiative $\Upsilon(1S)$ decays. The work of [602] uses the ratio of the radiative branching ratio over the nonradiative one $\Gamma(\Upsilon(1S) \to X\gamma)/\Gamma(\Upsilon(1S) \to X)$, with X the inclusive set of possible final-state hadrons. The relevant computations can be carried out with partonic degrees of freedom in the final state, and taking into account the charge conjugation of $\Upsilon(1S)$ it reduces to $\Gamma(\Upsilon(1S) \to \gamma gg)/\Gamma(\Upsilon(1S) \to gg)$, where interesting cancellations take place. Hadronic matrix elements also play a role, and need to be computed in the lattice or in the continuum. The theoretical prediction was compared to CLEO data [603] and the value $\alpha_S^{(N_f=5)}(m_Z) = 0.119^{+0.006}_{-0.005}$ was found.

In [604], charmonium and bottomonium spectra were studied within NRQCD, employing the short-distance low-scale scheme for the heavy quark mass known as MSR [605, 606] to remove the renormalon inherited from the static potential. Since the bottom and charm quarks are no longer dynamical degrees of freedom they have to be integrated out in the MSR mass as well: this prevents the appearance of large logarithms and the power counting of the theory is not upset. It was shown that, for a conservative estimate of perturbative uncertainties, the renormalization scales of α_S and the MSR mass should be varied independently in a given range determined by the principal quantum number. Furthermore, for a global analysis the scales corresponding to the different excited states should be correlated. Even though the main aim of the article was to determine m_c and m_b from global fits (data for quarkonium masses was taken from the PDG, see [251] for updated results), the possibility of obtaining α_S from a 2-parameter fit to bottomonium masses was also explored. Since experimental errors on $b\bar{b}$ bound states are tiny, their impact in α_S is immaterial. However, the very strong correlation between m_b and α_S translates into a sizable perturbative uncertainty: $\alpha_S^{(N_f=5)}(m_Z) = 0.1178 \pm 0.0051$, very similar to that quoted in [602].

A related study [607] obtains the strong coupling from a renormalon-free combination of charm and bottom bound-state masses, including $b\bar{c}$, namely $m_{B_c} - m_{\eta_b}/2 - m_{\eta_c}/2$, which is also less sensitive to ultrasoft effects. Using the experimental values for the charm and bottom masses as obtained from fits to the masses of η_c and η_b, respectively, the value $\alpha_S^{(N_f=5)}(m_Z) = 0.1195 \pm 0.0053$ was obtained, with experimental values for the quarkonium masses taken from the PDG. The uncertainty is very similar to that of [604], which opens up the possibility of improving the determination through global fits (determining m_c, m_b and α_S simultaneously) to $b\bar{b}$, $c\bar{c}$ and $b\bar{c}$ bound states. Another promising way of obtaining a precise value for the strong coupling is to adapt the strategy of [49], see also section 9.1, to bottomonium. Taking the ratio of bound-states' masses with different quantum numbers would cancel most of the heavy-quark mass dependence, along with the leading renormalon: the ratios are dimensionless and almost exclusively sensitive to α_S. Results on this direction will be reported soon.

[102] Authors: V Mateu (Univ. Salamanca and UAM-CSIC Madrid).

Acknowledgments—VM is supported by the MECD grant PID2019-105439GB-C22, the EU STRONG-2020 project under the program H2020-INFRAIA-2018-1, grant agreement No. 824 093 and the COST Action CA16201 PARTICLEFACE.

9. $\alpha_S(m_Z^2)$ world average[103]

9.1. Preliminary considerations

We summarize here the current procedure used in the Particle Data Group (PDG) [251] to obtain the world average value of $\alpha_S(m_Z^2)$ and its uncertainty, and we discuss future prospects for its improvement.

Any physics observables where the strong interaction is involved (directly, or through loop corrections) depend on the value of the strong coupling constant. This implies that a number of different observables can be used to determine the QCD coupling constant, provided that a suitable pQCD theoretical prediction is available for that observable. The following considerations are taken into account to assess if a particular observable is suitable for use in the determination of the strong coupling constant:

- The observable's sensitivity to α_S as compared to the experimental precision. For example, for the e^+e^- cross section to hadrons (e.g. the R ratio), QCD effects are only a small correction, since the perturbative series starts at order α_S^0, but the experimental precision is high. Three-jet production, or event shapes, in e^+e^- annihilation are directly sensitive to α_S since they start at order α_S. Four- and five-jet cross-sections start at α_S^2 and α_S^3 respectively, and hence are very sensitive to α_S. However, the precision of the measurements deteriorates as the number of jets involved increases.
- The accuracy of the perturbative prediction, or equivalently of the relation between α_S and the value of the observable. The minimal requirement is generally considered to be an NLO prediction. The PDG imposes now that at least NNLO-accurate predictions be available. In certain cases where phase space restrictions require it, fixed-order predictions are supplemented with resummation. An improved perturbative accuracy is necessary to guarantee that the theoretical uncertainty is assessed in a robust way.
- The size of nonperturbative effects. Sufficiently inclusive quantities, like the e^+e^- cross section to hadrons, have small nonperturbative contributions, power corrections of order $\sim\Lambda^4/Q^4$. Other quantities, such as event-shape distributions, typically have contributions $\sim\Lambda/Q$. All other aspects being equivalent, observables with smaller nonperturbative corrections are preferable.
- The scale at which the measurement is performed. An uncertainty δ on a measurement of $\alpha_S(Q^2)$, at a scale Q, translates to an uncertainty $\delta' = (\alpha_S^2(m_Z^2)/\alpha_S^2(Q^2)) \cdot \delta$ on $\alpha_S(m_Z^2)$. For example, this enhances the already important impact of precise low-Q measurements, such as from τ decays, in combinations performed at the m_Z scale.

The PDG determination of α_S first separates measurements into a number of different categories, then calculates an average for each category. Such per-category subaverages are then used as inputs to the world average. The PDG procedure requires four specifications of:

(1) the conditions that a determination of α_S should fulfill in order be included in the average;

[103] Authors: J Huston (MSU, East Lansing), K Rabbertz (KIT, Karlsruhe), G Zanderighi (MPP, Munich).

Table 12. PDG average of the categories of observables [March'22 update of the PDG'21 results]. These are the final input to the world average of $\alpha_S(m_Z^2)$.

category	$\alpha_S(m_Z^2)$	relative $\alpha_S(m_Z^2)$ uncertainty
τ decays and low Q^2	0.1178 ± 0.0019	1.6%
$Q\overline{Q}$ bound states	0.1181 ± 0.0037	3.1%
PDF fits	0.1162 ± 0.0020	1.7%
e^+e^- jets and shapes	0.1171 ± 0.0031	2.6%
electroweak	0.1208 ± 0.0028	2.3%
hadron colliders	0.1165 ± 0.0028	2.4%
lattice	0.1182 ± 0.0008	0.7%
world average (without lattice)	0.1176 ± 0.0010	0.9%
world average (with lattice)	0.1179 ± 0.0009	0.8%

(2) the separations of the different extractions of $\alpha_S(m_Z^2)$ into the (approximately) independent categories;
(3) the procedure within each category to compute the average and its uncertainty;
(4) the manner in which the different subaverages and their uncertainties are combined to determine the final value of $\alpha_S(m_Z^2)$ and its uncertainty.

9.2. Details of the PDG averaging procedure

In the following, we summarize the procedure adopted in the last edition of the PDG [251].

9.2.1. Criteria for determinations to be included in the world average. In the PDG, the selection of results from which to determine the world average value of $\alpha_S(m_Z^2)$ is restricted to those that are

(1) accompanied by reliable estimates of all experimental and theoretical uncertainties;
(2) based on the most complete perturbative QCD predictions of at least NNLO accuracy;
(3) published in a peer-reviewed journal at the time of writing of the PDG report.

Note that the second condition to some extent follows from the first. In fact, determinations of the strong coupling from observables in e^+e^- involving e.g. five or more jets are very sensitive to α_S, and could provide additional constraints. However, these observables are currently described only at leading order (LO) or next-to-leading order (NLO), and the determination of the theoretical uncertainty is thus considered not sufficiently robust. It is also important to note that some determinations are included in the PDG, but the uncertainty quoted in the relevant publications is increased by the PDG authors to fulfil the first condition. Similarly, in some cases the central value used in the PDG differs from the one quoted in some publications, but can be extracted from the analysis performed in that work.

9.2.2. Categories of observables. All observables used in the determination of $\alpha_S(m_Z^2)$ in the PDG exercise are classified in the following categories (table 12 and figure 45):

1. 'Hadronic τ decays and low Q^2 continuum' (τ decays and low Q^2):
   Calculations for τ decays are available at N^3LO; there are different approaches to treat the perturbative and nonperturbative contributions, which result in significant differences; the value of α_S is determined at the τ mass;

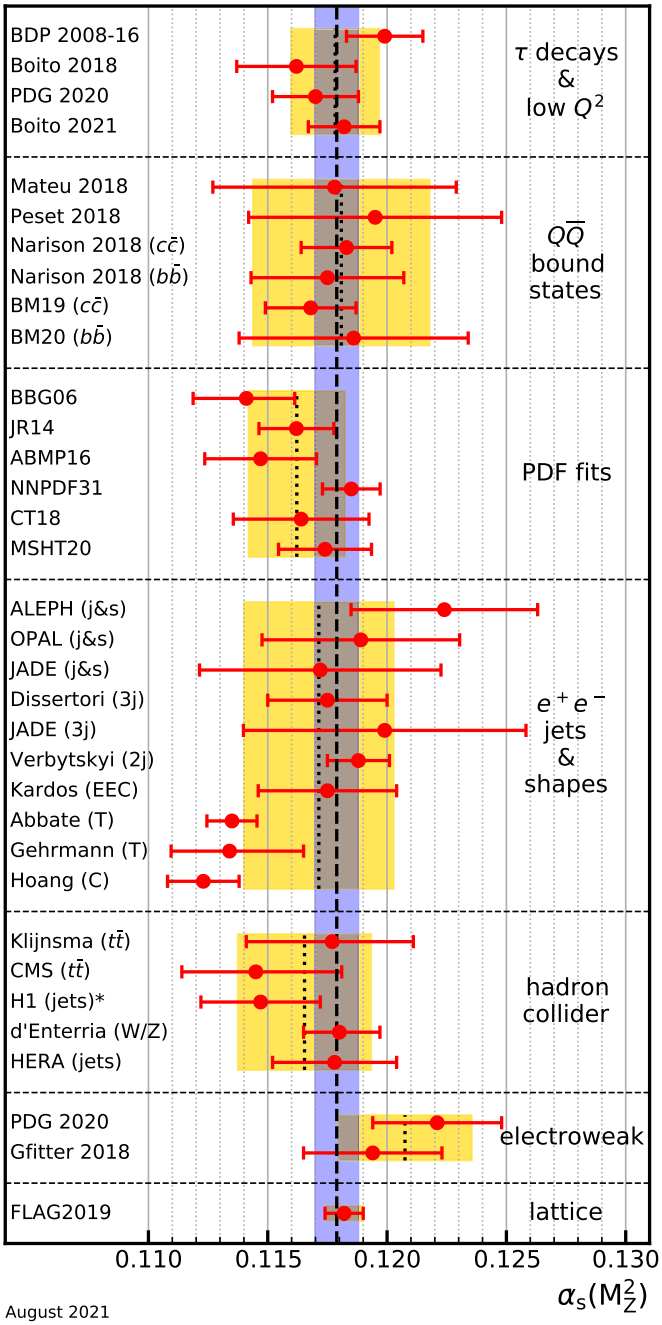

Figure 45. Summary of determinations of $\alpha_S(m_Z^2)$ from seven subfields. The yellow (light shaded) bands and dotted lines indicate the pre-average values of each subfield. The dashed line and blue (dark shaded) band represent the final $\alpha_S(m_Z^2)$ world average [March'22 update of the PDG'21 results [251]].

2. 'Heavy quarkonia decays and masses' ($Q\overline{Q}$ bound states):
   Calculations are available at NNLO and N^3LO;
3. 'PDF fits' (PDF fits)
   Taken both from global PDF fits and analyses of singlet and non-singlet structure functions; for theory uncertainty, half of the difference between results obtained with NNLO and NLO is added in quadrature;
4. 'Hadronic final states of e^+e^- annihilations' (e^+e^- jets and event shapes):
   Taken from measurements at PETRA and LEP; nonperturbative corrections are important and can be estimated either via Monte Carlo simulation or analytic modeling;
5. 'Observables from hadron-induced collisions' (hadron colliders):
   NNLO calculations for $t\bar{t}$, electroweak bosons, and jet production at both the LHC and HERA, and $Z+$jet production at the LHC have allowed measurements for these processes to be used in α_S determinations. There is still an ongoing discussion of whether a simultaneous PDF fit has to be carried out to avoid any significant bias;
6. 'Electroweak precision fit' (electroweak):
   α_S determinations are averaged from electroweak fits to data from the Tevatron, LHC, LEP and the SLC; such fits rely on the strict validity of the Standard Model; and
7. 'Lattice':
   The average determined by the FLAG group in 2019 [12] from an input of eight determinations was used; the 2021 result [11] came out too late to be included, but the 2021 α_S average is very consistent with that of 2019.

Detailed information about which observables are included in the different categories can be found in [251].

9.2.3. Average and uncertainty in each category. In order to calculate the world average value of $\alpha_S(m_Z^2)$, a preliminary step of pre-averaging results within the each category listed in section 9.2.2 is carried out. For each subfield, except for the 'Lattice' category, the *unweighted average* of all selected results is taken as the pre-average value of $\alpha_S(m_Z^2)$, and the unweighted average of the quoted uncertainties is assigned to be the respective overall error of this pre-average. An unweighted average is used to avoid the situation in which individual measurements, which may be in tension with other measurements and may have underestimated uncertainties, can considerably affect the determination of the strong coupling in a given category. As an example, the determination of $\alpha_S(m_Z^2)$ from e^+e^- jets and shapes currently averages ten determinations and arrives at $\alpha_S(m_Z^2) = 0.1171 \pm 0.0031$. Since two determinations [395, 396], both based on a similar theoretical framework, arrive at a small value of $\alpha_S(m_Z^2)$ and have a very small uncertainty, if one were to perform a weighted average one would obtain an $\alpha_S(m_Z^2)$ from e^+e^- jets and shapes of $\alpha_S(m_Z^2) = 0.1155 \pm 0.0006$, which is not compatible with the current world average. This would, in fact, considerably change the world average because of the very small uncertainties. The current procedure is instead robust against $\alpha_S(m_Z^2)$ determinations that are outliers with small uncertainties as compared to the other determinations in the same category. For the 'Lattice QCD' (lattice) subfield, we do not perform a pre-averaging step. Instead, we adopt the FLAG2019 average value and uncertainty for this subfield [12]. FLAG2019 also requires strict conditions on its own for a determination to be included in their average, which are in line with those used in the PDG. The results of the averages of the categories are given in table 12. Following the $\alpha_S(2022)$ workshop, the subfields of 'τ decays and low Q^2' and '$Q\overline{Q}$ bound states' have been updated to account for the latest studies of [121] and [49, 584], respectively. The world average value does not change.

From the table, it is clear that determinations from different categories are compatible with each other and accordingly can be combined to give rise to a final average.

9.2.4. Final average. Since the six subfields (excluding lattice) are largely independent of each other, the PDG determines a nonlattice world average value using a standard 'χ^2 *averaging*' method. This result in the final average of the six categories of

$$\alpha_S(m_Z^2) = 0.1175 \pm 0.0010, \qquad \text{(without lattice)}, \tag{9.1}$$

which is fully compatible with the lattice determination (figure 45). In a last step the PDG performs an unweighted average of the values and uncertainties of $\alpha_S(m_Z^2)$ from the nonlattice result and the lattice result presented in the FLAG2019 report [12], which results in the final average of

$$\alpha_S(m_Z^2) = 0.1179 \pm 0.0009, \qquad \text{(final average)}. \tag{9.2}$$

Performing a weighted average of all seven categories would instead give rise to $\alpha_S(m_Z^2) = 0.1180 \pm 0.0006$. The PDG uncertainty is instead more conservative and about 50% larger.

9.3. Outlook

While the strong coupling remains the least well-known gauge coupling, with an uncertainty of about 1%, it is remarkable that the determinations from all categories agree remarkably well with each other, all within one standard deviation. Future improvements will be driven by categories which have smallest uncertainties, currently lattice and τ decays and low Q^2. The uncertainty quoted in the latter category includes the difference in the extractions that are obtained using contour improved perturbation theory (CIPT) and fixed order perturbation theory (FOPT). Recent arguments suggest that FOPT are to be preferred, see also dedicated discussions on this point in this white paper. If confirmed, this would slightly shift the value of $\alpha_S(m_Z^2)$ in this category to lower values, and would allow one to quote a reduced theoretical uncertainty since this additional source of uncertainty would be completely removed. Further improvements could come from a better understanding of nonperturbative effects. Some progress is also likely to come in the category e^+e^- jets and shapes where the calculation of power corrections in the 3-jet region [412, 413] could have a sizeable impact, and improve fits of the coupling from event shapes. In fact, the region used in the fits are dominated by events with an additional hard emission, therefore the applicability of nonperturbative power corrections computed in the two-jet limit has been questioned and a treatment of these corrections in the three-jet region is certainly more appropriate. The impact of this on $\alpha_S(m_Z^2)$ in this category has still to be assessed. For the hadron collider category, it is an open discussion how to deal with correlations between PDF parameters and $\alpha_S(m_Z^2)$ in the cases where a full PDF + α_S fit is not performed simultaneously. In view of many more NNLO results to come we can expect some advances here. Particularly, NNLO for 3-jet production will enable to perform fits of $\alpha_S(m_Z^2)$ from ratios with at least partial cancellation of some uncertainties. Some doubts were raised whether this reduction in uncertainty also holds for the PDF dependence of such ratio predictions. Moreover, for predictions of ratios of cross sections, the central scale definition in numerator and denominator will require more elucidation. Finally, it is important to mention that the last years have seen remarkable advances in the determination of $\alpha_S(m_Z^2)$ from lattice gauge theory, also thanks to the FLAG effort which imposes strict quality criteria for lattice determinations to be

included in the FLAG average. This is now the single most precise result of all categories included in the PDG. The challenge is on to still beat it.

10. Summary

In this summary section we provide first an outline of the main points that were the subject of discussions during the $\alpha_S(2022)$ workshop, and secondly we recapitulate the current $\alpha_S(m_Z^2)$ uncertainties of each extraction method as well as the expected experimental and theoretical developments that will help reduce those in the coming years (and, in some cases, in the longer term of the next generation of collider facilities).

10.1. Summary of the discussions

We provide here a brief summary of the most relevant contributions of the live discussions of the $\alpha_S(2022)$ workshop meeting preparatory for this document.

Lattice: the FLAG collaboration uses a set of criteria accepted in the lattice community to classify the analyses. Only analyses ranking high in all criteria are used to derive the final FLAG determination of the strong coupling. This procedure is very similar to that adopted by the PDG. It was suggested that the FLAG and PDG procedures should be harmonized as much as possible. It was also pointed out that there were updates to individual analyses since the current FLAG 2021 report [11] was published.

τ decays: the discussions covered broadly two areas. The first area concerned the treatment of duality violations (DV) (incomplete asymptotic OPE) terms. One defines moments of the tau spectral function to control and suppress DV terms. However, stronger DV term suppression is correlated with more contributions of gluon condensates leading to a truncated OPE. This was referred to as a kind of 'seesaw mechanism' by S Peris.

The presentation by A Hoang (section 3.4) providing an explanation in terms of renormalon effects of the FOPT versus CIPT differences in the pQCD predictions, generated considerable interest. The analysis is not yet complete, and further important information would be the value of the gluon condensate normalization. New data would not help directly. The renormalon effects could possibly be studied on the lattice, but this would need a dedicated effort. One would need input from hadronic τ decay theory to derive observables to be measured on the lattice.

The second topic of discussion involved uncertainties connected with nonperturbative contributions to predictions for the τ hadronic width that are not directly related to the FOPT versus CIPT discussion. More and better spectral function data from τ decays at B-factories or at new e^+e^- colliders, and from e^+e^- annihilation to hadrons at low energies could help to understand and constrain the DV and/or OPE truncation effects.

Global PDF analyses: one focus of the discussion in this session was the treatment of theoretical (missing higher-order) uncertainties in the comparison of the predictions with data. The global fit analyses use $\mathcal{O}(1000)$ data points and thus classical χ^2-probabilities are hard to interpret, and estimation of parameter uncertainties is difficult. Some authors recommend including the prediction uncertainties in the fits. A critique to this procedure is that this influences and possibly biases the fitted parameter values, including α_S.

The ATLAS analysis of PDFs (talk by F Giuli, section 7.4) emphasized the importance of a detailed analysis of systematic uncertainties and their correlations in the p−p collision data

used in the fit. This was welcomed by global PDF fit groups who would like more detailed information on experimental uncertainties and their correlations.

K Rabbertz collected a list of open problems[104] in the area of $\alpha_S(m_Z^2)$ determinations from global PDF analyses. This was welcomed in the discussion and could serve as a reference to study and resolve pending and new issues.

e^+e^- annihilation to hadronic final states: the discussions in this area concentrated on the level of understanding of nonperturbative (NP) corrections. The latest results providing a better understanding of power corrections for the *C*-parameter observable (presentation by Monni and Nason, section 6.3) were seen as an important step. It was pointed out that a deeper understanding of NP corrections is also needed for other event-shape and for jet-based observables. Other items for improvements were raised such as: NNLO calculations for $e^+e^- \to b\bar{b}g$, NNLL precision parton-shower algorithms and their matching to fixed order predictions and the corresponding retuning of the MC event generators NP parameters (hadronization, colour/flavour/spin correlations, etc). As a potentially useful approach to reduce the NP corrections, groomed observables were discussed. It was stated that by pursuing such an agenda, a better consistency and precision of $\alpha_S(m_Z^2)$ results from e^+e^- annihilation hadronic final states should be possible.

The improved prediction for the *R*-ratio at low energies (A Nesterenko, section 6.1) was discussed as promising, but needs more precise measurements than currently available.

Lepton–hadron colliders: analyses at the only so-far operating lepton–hadron collider HERA showed high sensitivity to α_S through a large variety of processes with precision measurements available. These include inclusive cross sections, single- or multi-jet production cross sections, event-shape observables, jet-substructure observables, and heavy-flavour cross sections. Unfortunately, most of these measurements were not performed by the experiments using their larger HERA-II data samples, and the only useful published data from HERA-II that achieves 1%–2% experimental uncertainties are jet cross sections in neutral-current DIS by H1, and inclusive jet cross section in photoproduction by ZEUS. Since considerable progress on the theory side was made since the HERA times, the H1 and ZEUS collaborations should feel encouraged to continue analyzing their data.

Future e−p experiments provide excellent opportunities for many precision measurements of $\alpha_S(m_Z^2)$. The use of polarized PDFs was highlighted as a novel interesting opportunity at the future EIC. Beyond that, the PDFs from LHeC/FCC-ep will also allow improving many α_S analyses done at the HL-LHC.

Hadron colliders: the analysis presented by D. d'Enterria (section 8.2) was discussed for two reasons. First, it was claimed that the use of the MCFM v.8.0 generator to compute inclusive fiducial NNLO cross sections for W and Z bosons could be sensitive to power corrections connected with its subtraction scheme [608]. However, in the publication a cross check with a different generator (FEWZ) gave consistent (within few %) results. The second topic was the correlation of $\alpha_S(m_Z^2)$ results from this analysis with results from global PDF analyses, since a few of the more recent PDF global fits also use differential cross section distributions of W- and Z-bosons measured at LHC.

The discussion on this second point moved on to considering merging the results from hadron collider data and global PDF fits into the same $\alpha_S(m_Z^2)$ category, at least before the inclusive hadron collider cross sections ($t\bar{t}$ and EW bosons at the LHC, and jets at HERA) are not directly into the global PDF + α_S fits. The hadron collider extractions use the $\alpha_S(m_Z^2)$ dependence of the public PDF sets to derive the QCD coupling itself, but it was pointed out that this may not converge to the same result as a global PDF + α_S fit [271]. A complete

[104] Link: https://docs.google.com/spreadsheets/d/13KpbCaTpgIP7zrOJL3eveCvLoynBoiT50shzIz1HCzo.

merging of the 'DIS and PDF' and 'hadron collider' categories was seen as problematic, since in a global fit with many data sets the impact of a given data set is difficult to quantify. The 'Lagrange multiplier' approach of the CT18 group is an advanced example of such studies. One improvement could be to combine a new data set with a PDF fit in order to constrain the PDFs, but report as main result only the obtained α_S. An example of data sets for individual analysis, possibly together with a PDF fit, are ratios of jet production cross sections. A further problem of global analysis including specific data sets for α_S studies is the missing information on correlations of experimental uncertainties between data sets. In addition, the global PDF fits have an intrinsic theory theoretical uncertainty from missing higher-order terms, and any independent $\alpha_S(m_Z^2)$ determination from inclusive cross sections (not used in the fit) provides also a useful cross-check. In any case, since updated PDF (or PDF + α_S) sets are only released every ∼5 years, it was clear that keeping the independent measurements of the 'hadron collider' α_S category of the PDG world-average is appropriate as long as those are not directly incorporated into the global PDF + α_S fits.

Other discussions concerned with finding the appropriate choice of renormalization scale in the pQCD predictions, especially in multiscale observables such as event shapes in p−p collisions (e.g. TEEC, ATEEC, transverse thrust) or (multi)jet production. In addition, the problem of properly determining the correlations between measurements of the different LHC experiments was discussed. Jet production measurements are systematics limited and sensitive to many not easy to control experimental effects. M Wobisch's presentation (section 7.5) of a different formulation of cross section ratios was seen as another way to estimate theory uncertainties.

The determination of α_S from the Z-boson transverse momentum distribution (Camarda, section 7.3) was seen as a good example of an $\alpha_S(m_Z^2)$ extraction of the hadron collider category, since its precision is high (1.3%) and its dependence on PDFs is smaller than other extractions of this subfield. The measurements as well as the theory can further improve in the future.

10.2. Prospects and wish-lists for high-precision extractions

In table 13, we summarize the current precision of the seven extraction methods that contribute today to the PDG world average (table 12), as well as the expected improvements in the next ∼10 years (or in the longer future, in parenthesis) for each one of them. For each category, we list the dominant sources of theoretical and experimental uncertainties that propagate into $\alpha_S(m_Z^2)$ today, and the anticipated progress in the next years (or in the longer term of planned future collider facilities) that will lead to a corresponding reduction of the uncertainties. The last row list the relative uncertainty of the current world-average (0.8%) and of the one expected within the next decade (≈0.4%) obtained from taking a weighted average of the individual per-category uncertainties (in parenthesis, we provide the permil precision expected in the longer term from lattice-QCD and/or electroweak fits at a future high-luminosity e^+e^- facility). Of course, the latter result assumes that no new physics impacts any of the extraction methods and, as a matter of fact, significant inconsistency among independent determinations would indicate either a problem in our theoretical/experimental understanding of any given observable, or provide a potential indirect evidence of BSM physics.

Lattice: the current ±0.7% precision of the lattice-QCD extraction of $\alpha_S(m_Z^2)$ can be reduced by about a factor of two within the next ∼10 years. In order to improve the lattice-QCD based determinations of α_S, it would be important to reach higher renormalization scales for more observables, which can be achieved by implementing elements of the step-

Table 13. Summary of current and expected future (within the decade ahead or, in parenthesis, longer time scales) uncertainties in the $\alpha_S(m_Z^2)$ extractions used today to derive the world average. Acronyms and symbols: CIPT = 'contour-improved perturbation theory', FOPT = 'fixed-order perturbation theory', NP = 'nonperturbative QCD', SF = 'structure functions', PS = 'Monte Carlo parton shower'.

	Relative $\alpha_S(m_Z^2)$ uncertainty	
Method	Current theory and exp. uncertainties sources	Near (long-term) future theory and experimental progress
(1) Lattice	0.7% Finite lattice spacing and stats. $N^{2,3}LO$ pQCD truncation	≈0.3% (0.1%) Reduced latt. spacing. Add more observables Add $N^{3,4}LO$, (active charm, QED effects) Higher renorm. scale via step-scaling to more observ.
(2) τ decays	1.6% N^3LO CIPT versus FOPT diffs. Limited τ spectral data	<1% Add N^4LO terms. Solve CIPT–FOPT diffs. Improved τ spectral functions at Belle II
(3) $Q\overline{Q}$ bound states	3.3% $N^{2,3}LO$ pQCD truncation $m_{c,b}$ uncertainties	≈1.5% Add $N^{3,4}LO$ and more $(c\overline{c})$, $(b\overline{b})$ bound states Combined $m_{c,b} + \alpha_S$ fits
(4) DIS and PDF fits	1.7% $N^{2,(3)}LO$ PDF (SF) fits Span of PDF-based results	≈1% (0.2%) N^3LO fits. Add new SF fits: $F_2^{p,d}$, g_i (EIC) Better corr. matrices. More PDF data (LHeC/FCC-eh)
(5) e^+e^- jets and evt shapes	2.6% NNLO+$N^{(1,2,3)}LL$ truncation Different NP analytical and PS corrs. Limited datasets w/ old detectors	≈1.5% (<1%) Add $N^{2,3}LO+N^3LL$, power corrections Improved NP corrs. via: NNLL PS, grooming New improved data at B factories (FCC-ee)
(6) Electroweak fits	2.3% N^3LO truncation Small LEP+SLD datasets	(≈0.1%) N^4LO, reduced param. uncerts. ($m_{W,Z}$, α, CKM) Add W boson. Tera-Z, Oku-W datasets (FCC-ee)
(7) Hadron colliders	2.4% NNLO(+NNLL) truncation, PDF uncerts. Limited data sets ($t\bar{t}$c, W, Z, e−p jets)	≈1.5% N^3LO+NNLL (for colour-singlets), improved PDFs Add more datasets: Z p_T, p−p jets, σ_i/σ_j ratios, …
World average	0.8%	≈0.4% (0.1%)

scaling technique even in infinite space-time volumes. This requires resources for dedicated lattice simulations. In addition, it would be very helpful to push the corresponding pQCD calculations to higher orders. Depending on the process under study, this will require to calculate N^{3}LO, N^{4}LO, and/or N^{3}LL contributions. In some cases it may also be beneficial to compute lattice artifacts perturbatively, in order to improve the control of the continuum limit. For extractions based on moments of quarkonium correlators, one should perform more accurate lattice calculations with hadron masses $m_h \geqslant 2m_c$, where the truncation errors are subleading in the current results. In view of the fully recursive step-scaling strategies, also nonstandard perturbative techniques for selected finite volume renormalization schemes should be developed. Aiming for 0.1% uncertainties will likely require the explicit inclusion of charm quark effects (2+1+1 calculations) and of QED and isospin-breaking effects in the determination of both the physical scale and the running of α_S.

τ decays: the present $\alpha_S(m_Z^2)$ value of the τ lepton category has a $\pm 1.6\%$ uncertainty as derived from the pre-averaging of four different determinations. Solving the CIPT versus FOPT discrepancies, e.g. through the method proposed in [122], is a basic prerequisite to reduce in about a half the current theoretical uncertainty assigned to this extraction method. Although hard to compute, a calculation of the $\mathcal{O}(\alpha_S^5)$ pQCD term (N^{4}LO) would be also beneficial, given the sometimes slow convergence of terms with typical weights. On the nonperturbative side, increased data precision would allow more stringent tests of the duality-violation contributions. In the near future, more precise 2-pion and 4-pion exclusive-mode τ data from Belle II would also help to disentangle perturbative and nonperturbative contributions.

$Q\overline{Q}$ bound states: the $\alpha_S(m_Z^2)$ value derived from quarkonium decays and masses has today a $\pm 3.1\%$ uncertainty from the pre-averaging of six different determinations at NNLO or N^{3}LO accuracy. Improved determinations can be obtained by performing combined fits of α_S and charm and/or bottom quark masses, adding one extra degree of pQCD accuracy to the NNLO predictions, and/or adding more $c\overline{c}$, $b\overline{b}$ bound-states data.

Structure functions and global PDF analyses: the current $\alpha_S(m_Z^2)$ value of the parton densities category has a $\pm 1.7\%$ uncertainty as derived from the pre-averaging of six different determinations (two analyses of structure functions, and four from global PDF fits). With complete N^{3}LO predictions for DIS, the residual theoretical uncertainty due to the scale variation and the truncation of the perturbative series will be limited to $\approx 1\%$ in the range of parton kinematics relevant for the current world DIS data and the EIC. In general, progress is expected from analyses at future e$-$p colliders such as the EIC, LHeC, or FCC-eh. Adding new observables, such as e.g. deuteron and spin-dependent structure functions, which can be both measured at the EIC, will provide new useful constraints. Ultimately, an experimental precision of $\delta\alpha_S(m_Z^2) \sim 0.2\%$ is projected at the LHeC/FCC-eh.

For PDF + α_S extractions, future N^{3}LO fits (or, in the shorter term, an improved quantification of the impact of missing higher-order corrections) are required to reach $\approx 1\%$ precision on $\alpha_S(m_Z^2)$. Achieving such a higher degree of pQCD accuracy will likely reduce the present broad span of $\alpha_S(m_Z^2)$ central values among global PDF fits. In addition, the availability of LHC experimental data with more complete information on correlations would improve the global fit analyses.

e$^+$e$^-$ *annihilation to hadronic final states:* the present precision of the $\alpha_S(m_Z^2)$ determination from the e$^+$e$^-$ category of the PDG world-average is of $\pm 2.6\%$, as obtained by pre-averaging 10 different extractions based on event shapes or jet rates. Such a comparatively large uncertainty is driven by the large span among central values derived from measurements where NP corrections have been obtained with Monte Carlo parton showers or analytically. The former (latter) corrections tend to give larger (smaller) QCD couplings than the world average. The

main reduction of this uncertainty will therefore come through an improved convergence between the theoretical (analytical and MC) descriptions of NP effects. First, detailed analytical studies of nonperturbative power corrections exists now for the *C*-parameter that need to be applied to other similar observables, such as thrust, to clarify the current discrepancies. Second, improved parton-shower algorithms (e.g. of the PanXX family) reaching NNLL accuracy are needed, followed by matching to fixed-order (NNLO) predictions plus a full retuning of the hadronization and other final-state parameters (colour reconnection, spin correlations, …) of the event generators. In parallel, improved soft-drop grooming techniques should be applied to the e^+e^- data to evaluate their impact in the reduction of NP effects.

Electroweak fits: the $\alpha_S(m_Z^2)$ uncertainty of the EW category is of $\pm 2.3\%$ and is dominantly driven by the statistical uncertainty in the measurements of the Z-boson pseudoobservables at LEP (the W-boson determination is even much less precise, and features a $\pm 30\%$ uncertainty). Such an $\alpha_S(m_Z^2)$ determination is extremely clean, and can reach the 0.1% precision provided one collects the 10^{12} and 10^8 Z- and W-bosons data samples expected at a future high-luminosity e^+e^- collider such as the FCC-ee. To reach such a level of precision will require also to compute missing higher-order pQCD (N^4LO), EW $\mathcal{O}(\alpha^{2,3})$, and mixed pQCD+EW $\mathcal{O}(\alpha\alpha_S^2,\ \alpha\alpha_S^3,\ \alpha^2\alpha_S)$ corrections that, today, are negligible compared to the experimental uncertainties.

Hadron colliders: the QCD coupling derived from the hadron-collider category, obtained from the pre-averaging of 5 different extractions at NNLO accuracy, has a $\pm 2.4\%$ precision today. Theoretical (experimental) uncertainties are driven mostly by the scale and PDF (luminosity) uncertainties. A natural way to reduce the $\alpha_S(m_Z^2)$ uncertainties would be to incorporate N^3LO corrections, but this seems realistically feasible in the next years only for colour-singlet cross sections, and requires PDFs at the same level of accuracy. A faster way to reduce the current uncertainties by about a half may come from the expected addition of many more upcoming observables (Z p_T peak at N^3LO, p−p jets and σ_i/σ_j ratios at NNLO, …) and/or extended high-precision datasets (integrated luminosity uncertainties at the LHC have been lately reduced to the $\approx 1\%$ level).

Final wish-list: the determination of the strong coupling has the potential to witness considerable improvements in the decade ahead, with an anticipated reduction in the $\alpha_S(m_Z^2)$ world average uncertainty by a factor of about two (from 0.8% down to $\approx 0.4\%$) over this time scale through well-identified experimental and theoretical developments. Such a progress will have an important impact in the theoretical calculations and associated interpretation of upcoming LHC data and in searches for new physics through high-precision SM studies. Such advances will be facilitated by:

1. Sufficient dedicated computing resources to generate state-of-the-art samples for lattice QCD analyses. Enough person-power to develop perturbation theory for selected observables in a finite space-time volume, and compute identified higher-order pQCD corrections to match improved lattice QCD samples as necessary basis for α_S extractions.
2. Beyond lattice-related calculations, person-power is needed for all other important theory efforts. These include the completion of the hadronic τ decay renormalon analysis, the three-jet power corrections for e^+e^- event shapes and jet algorithms, NNLL accuracy parton shower algorithms and their matching to fixed order, NNLO MC simulations for complex final states in e^+e^-, e−p or p−p scattering, and differential NNLO predictions for HERA and LHC multi-jet observables, among others.
3. Incorporation of multiple new precision observables and/or datasets measured at the LHC into NNLO hadron-collider- or PDF- based extractions, with an improved treatment

of the experimental correlation uncertainties among measurements, will lead to a visible improvement of the accuracy and precision of the world $\alpha_S(m_Z^2)$ average.

4. Measurements of DIS with new high-energy facilities (EIC first and, in the longer term LHeC/FCC-eh) will allow determining PDFs + α_S over a large phase space covering LHC kinematics. This would resolve PDF-α_S ambiguities in hadron-collider analyses, and provide new precision $\alpha_S(m_Z^2)$ determinations. A direct extraction of α_S and studies of its energy evolution will also benefit from high-precision PDFs over a large kinematic range.
5. Arguably, the only way known to actually reach permil $\alpha_S(m_Z^2)$ uncertainty from purely experimental measurements, without lattice-QCD data simulations, is through the study of hadronic Z (and W) decays. A high-energy lepton collider (Higgs factory, ILC, FCC-ee) with a Giga- or Tera-Z program and low-energy ($\sqrt{s} < m_Z$) runs will massively improve e^+e^- determinations of $\alpha_S(m_Z^2)$ via Z- and W-boson hadronic decays, τ decays, jets rates and event shapes, significantly also improving our understanding of parton showers and nonperturbative effects, and providing accurate tests of the α_S evolution.

Acknowledgments

Support from the EU STRONG-2020 project under the program H2020-INFRAIA-2018-1, grant agreement No. 824093 is acknowledged.

Data availability statement

All data that support the findings of this study are included within the article (and any supplementary files).

ORCID iDs

D d'Enterria https://orcid.org/0000-0002-5754-4303
C Ayala https://orcid.org/0000-0001-8730-9796
J Blümlein https://orcid.org/0000-0002-0565-4906
D Boito https://orcid.org/0000-0002-4426-7984
G Cvetič https://orcid.org/0000-0003-4564-5796
M Dalla Brida https://orcid.org/0000-0001-7583-4067
A H Hoang https://orcid.org/0000-0002-8424-9334
B Malaescu https://orcid.org/0000-0002-8813-3830
A V Nesterenko https://orcid.org/0000-0003-4747-699X
R Pérez-Ramos https://orcid.org/0000-0002-4243-0063
A Ramos https://orcid.org/0000-0003-1654-1816
S Schumann https://orcid.org/0000-0003-0330-3990
M Vos https://orcid.org/0000-0001-8474-5357

References

[1] Workman R L *et al* (Particle Data Group Collaboration) 2022 Review of particle physics *Progress Theor. Exp. Phys.* **2022** 083C01

[2] Aguilar-Benitez M *et al* (Particle Data Group Collaboration) 1986 Review of particle properties. Particle data group *Phys. Lett.* B **170** 1

[3] Anastasiou C, Duhr C, Dulat F, Furlan E, Gehrmann T, Herzog F, Lazopoulos A and Mistlberger B 2016 High precision determination of the gluon fusion Higgs boson cross-section at the LHC *J. High Energy Phys.* JHEP05(2016)058

[4] Cooper-Sarkar A M, Czakon M, Lim M A, Mitov A and Papanastasiou A S 2010 *Simultaneous extraction of α_s and m_t from LHC $t\bar{t}$ differential distributions* arXiv:2010.04171 [hep-ph]

[5] Blondel A, Gluza J, Jadach S, Janot P and Riemann T (ed) 2019 *Theory for the FCC-ee: report on the 11th FCC-ee Workshop Theory and Experiments, vol. 3/2020 of CERN Yellow Reports: monographs. CERN, Geneva, May* arXiv:1905.05078 [hep-ph]

[6] Heinemeyer S, Jadach S and Reuter J 2021 Theory requirements for SM Higgs and EW precision physics at the FCC-ee *Eur. Phys. J. Plus* **136** 911

[7] Blondel A *et al* 2018 *Standard model theory for the FCC-ee Tera-Z stage, in Mini Workshop on Precision EW and QCD Calculations for the FCC Studies: methods and Techniques, vol. 3/ 2019 of CERN Yellow Reports: monographs* arXiv:1809.01830 [hep-ph]

[8] Hoang A H 2020 What is the top quark mass? *Ann. Rev. Nucl. Part. Sci.* **70** 225

[9] Chetyrkin K G and Zoller M F 2016 Leading QCD-induced four-loop contributions to the β-function of the Higgs self-coupling in the SM and vacuum stability *J. High Energy Phys.* JHEP06(2016)175

[10] Llorente J and Nachman B P 2018 Limits on new coloured fermions using precision jet data from the Large Hadron Collider *Nucl. Phys.* B **936** 106

[11] Aoki Y *et al* (Flavour Lattice Averaging Group (FLAG) Collaboration) 2022 *Eur. Phys. J.* C **82** 869

[12] Aoki S *et al* (Flavour Lattice Averaging Group Collaboration) 2020 FLAG Review 2019: flavour lattice averaging group (FLAG) *Eur. Phys. J.* C **80** 113

[13] Del Debbio L and Ramos A 2021 Lattice determinations of the strong coupling *Phys. Rep.* **920** 1–71

[14] Maltman K, Leinweber D, Moran P and Sternbeck A 2008 The realistic lattice determination of $\alpha_s(M_Z)$ revisited *Phys. Rev.* D **78** 114504

[15] Aoki S *et al* (PACS-CS Collaboration) 2009 Precise determination of the strong coupling constant in $N_f = 2+1$ lattice QCD with the Schrodinger functional scheme *J. High Energy Phys.* JHEP10(2009)053

[16] McNeile C, Davies C T H, Follana E, Hornbostel K and Lepage G P 2010 High-precision c and b masses, and QCD coupling from current-current correlators in lattice and continuum QCD *Phys. Rev.* D **82** 034512

[17] Chakraborty B, Davies C T H, Galloway B, Knecht P, Koponen J, Donald G C, Dowdall R J, Lepage G P and McNeile C 2015 High-precision quark masses and QCD coupling from $n_f = 4$ lattice QCD *Phys. Rev.* D **91** 054508

[18] Bruno M, Dalla Brida M, Fritzsch P, Korzec T, Ramos A, Schaefer S, Simma H, Sint S, Sommer R and (ALPHA Collaboration) 2017 QCD Coupling from a Nonperturbative Determination of the Three-Flavor Λ Parameter *Phys. Rev. Lett.* **119** 102001

[19] Bazavov A, Brambilla N, Garcia i Tormo X, Petreczky P, Soto J, Vairo A, Weber J H and (TUMQCD Collaboration) 2019 Determination of the QCD coupling from the static energy and the free energy *Phys. Rev.* D **100** 114511

[20] Ayala C, Lobregat X and Pineda A 2020 Determination of $\alpha(M_z)$ from an hyperasymptotic approximation to the energy of a static quark-antiquark pair *J. High Energy Phys.* JHEP09 (2020)016

[21] Cali S, Cichy K, Korcyl P and Simeth J 2020 Running coupling constant from position-space current-current correlation functions in three-flavor lattice QCD *Phys. Rev. Lett.* **125** 242002

[22] Athenodorou A, Finkenrath J, Knechtli F, Korzec T, Leder B, Marinković Krstić M and Sommer R 2019 How perturbative are heavy sea quarks? *Nucl. Phys.* B **943** 114612

[23] Bernreuther W and Wetzel W 1982 Decoupling of heavy quarks in the minimal subtraction scheme *Nucl. Phys.* B **197** 228 [Erratum: Nucl. Phys. B 513 (1998) 758]

[24] Grozin A G, Hoeschele M, Hoff J and Steinhauser M 2011 Simultaneous decoupling of bottom and charm quarks *J. High Energy Phys.* JHEP09(2011)066

[25] Chetyrkin K G, Kühn J H and Sturm C 2006 QCD decoupling at four loops *Nucl. Phys.* B **744** 121

[26] Schröder Y and Steinhauser M 2006 Four-loop decoupling relations for the strong coupling *J. High Energy Phys.* JHEP01(2006)051
[27] Kniehl B A, Kotikov A V, Onishchenko A I and Veretin O L 2006 Strong-coupling constant with flavor thresholds at five loops in the anti-MS scheme *Phys. Rev. Lett.* **97** 042001
[28] Gerlach M, Herren F and Steinhauser M 2018 Wilson coefficients for Higgs boson production and decoupling relations to $\mathcal{O}(\alpha_s^4)$ *J. High Energy Phys.* JHEP11(2018)141
[29] Lüscher M, Narayanan R, Weisz P and Wolff U 1992 The Schrödinger functional: a Renormalizable probe for nonAbelian gauge theories *Nucl. Phys.* B **384** 168
[30] Weinberg S 1973 New approach to the renormalization group *Phys. Rev.* D **8** 3497
[31] Lüscher M, Weisz P and Wolff U 1991 A Numerical method to compute the running coupling in asymptotically free theories *Nucl. Phys.* B **359** 221
[32] Husung N, Nada A and Sommer R 2020 Yang Mills short distance potential and perturbation theory *PoS* **LATTICE2019** 263
[33] Dalla Brida M, Höllwieser R, Knechtli F, Korzec T, Ramos A, Sommer R and (ALPHA Collaboration) 2020 Non-perturbative renormalization by decoupling *Phys. Lett.* B **807** 135571
[34] Dalla Brida M 2021 Past, present, and future of precision determinations of the QCD parameters from lattice QCD *Eur. Phys. J.* A **57** 66
[35] Dalla Brida M and Ramos A 2019 The gradient flow coupling at high-energy and the scale of SU(3) Yang–Mills theory *Eur. Phys. J.* C **79** 720
[36] Nada A and Ramos A 2021 An analysis of systematic effects in finite size scaling studies using the gradient flow *Eur. Phys. J.* C **81** 1
[37] Dalla Brida M, Höllwieser R, Knechtli F, Korzec T, Nada A, Ramos A, Sint S, Sommer R and (ALPHA Collaboration) 2022 Determination of $\alpha_s(m_Z)$ by the non-perturbative decoupling method *Eur. Phys. J.* C **82** 1092
[38] Dalla Brida M, Fritzsch P, Korzec T, Ramos A, Sint S, Sommer R and (ALPHA Collaboration) 2018 A non-perturbative exploration of the high energy regime in $N_{\rm f} = 3$ QCD *Eur. Phys. J.* C **78** 372
[39] Dalla Brida M, Fritzsch P, Korzec T, Ramos A, Sint S, Sommer R and (ALPHA Collaboration) 2016 Determination of the QCD Λ parameter and the accuracy of perturbation theory at high energies *Phys. Rev. Lett.* **117** 182001
[40] Sommer R and Wolff U 2015 Non-perturbative computation of the strong coupling constant on the lattice *Nucl. Part. Phys. Proc.* **261** 155
[41] Jansen K *et al* 1996 Nonperturbative renormalization of lattice QCD at all scales *Phys. Lett.* B **372** 275
[42] Dalla Brida M, Fritzsch P, Korzec T, Ramos A, Sint S, Sommer R and (ALPHA Collaboration) 2017 Slow running of the Gradient Flow coupling from 200 MeV to 4 GeV in $N_f = 3$ QCD *Phys. Rev.* D **95** 014507
[43] Weinberg S 1980 Effective gauge theories *Phys. Lett.* B **91** 51
[44] Bruno M, Finkenrath J, Knechtli F, Leder B, Sommer R and (ALPHA Collaboration) 2015 Effects of heavy sea quarks at low energies *Phys. Rev. Lett.* **114** 102001
[45] Knechtli F, Korzec T, Leder B, Moir G and (ALPHA Collaboration) 2017 Power corrections from decoupling of the charm quark *Phys. Lett.* B **774** 649
[46] Höllwieser R, Knechtli F, Korzec T and (ALPHA Collaboration) 2020 Scale setting for $N_f = 3 + 1$ QCD *Eur. Phys. J.* C **80** 349
[47] Dalla Brida M, Höllwieser R, Knechtli F, Korzec T, Nada A, Ramos A, Sint S, Sommer R and (ALPHA Collaboration) 2022 Results for α_s from the decoupling strategy *PoS* **LATTICE2021** 492
[48] Dehnadi B, Hoang A H and Mateu V 2015 Bottom and Charm Mass Determinations with a Convergence Test *J. High Energy Phys.* JHEP08(2015)155
[49] Boito D and Mateu V 2020 Precise determination of α_S from relativistic quarkonium sum rules *J. High Energy Phys.* JHEP03(2020)094
[50] Komijani J, Petreczky P and Weber J H 2020 Strong coupling constant and quark masses from lattice QCD *Prog. Part. Nucl. Phys.* **113** 103788
[51] Sturm C 2008 Moments of Heavy Quark Current Correlators at Four-Loop Order in Perturbative QCD *J. High Energy Phys.* JHEP09(2008)075
[52] Kiyo Y, Maier A, Maierhofer P and Marquard P 2009 Reconstruction of heavy quark current correlators at $O(\alpha_S^3)$ *Nucl. Phys.* B **823** 269

[53] Maier A, Maierhofer P, Marquard P and Smirnov A V 2010 Low energy moments of heavy quark current correlators at four loops *Nucl. Phys.* B **824** 1
[54] Allison I *et al* (HPQCD Collaboration) 2008 High-Precision Charm-Quark Mass from Current-Current Correlators in Lattice and Continuum QCD *Phys. Rev.* D **78** 054513
[55] Maezawa Y and Petreczky P 2016 Quark masses and strong coupling constant in 2+1 flavor QCD *Phys. Rev.* D **94** 034507
[56] Petreczky P and Weber J H 2019 Strong coupling constant and heavy quark masses in (2+1)-flavor QCD *Phys. Rev.* D **100** 034519
[57] Petreczky P and Weber J H 2022 Strong coupling constant from moments of quarkonium correlators revisited *Eur. Phys. J.* C **82** 64
[58] Nakayama K, Fahy B and Hashimoto S 2016 Short-distance charmonium correlator on the lattice with Möbius domain-wall fermion and a determination of charm quark mass *Phys. Rev.* D **94** 054507
[59] Lepage G P and Mackenzie P B 1993 On the viability of lattice perturbation theory *Phys. Rev.* D **48** 2250
[60] Weber J H 2020 Strong coupling constant and heavy quark masses in (2.1)-flavor QCD *PoS* **LATTICE2019** 101
[61] Wilson K G 1974 Confinement of quarks *Phys. Rev.* D **10** 2445
[62] Brambilla N, Pineda A, Soto J and Vairo A 2000 Potential NRQCD: an Effective theory for heavy quarkonium *Nucl. Phys.* B **566** 275
[63] Brambilla N, Pineda A, Soto J and Vairo A 1999 The Infrared behavior of the static potential in perturbative QCD *Phys. Rev.* D **60** 091502
[64] Anzai C, Kiyo Y and Sumino Y 2010 Static QCD potential at three-loop order *Phys. Rev. Lett.* **104** 112003
[65] Smirnov A V, Smirnov V A and Steinhauser M 2010 Three-loop static potential *Phys. Rev. Lett.* **104** 112002
[66] Pineda A and Soto J 2000 The Renormalization group improvement of the QCD static potentials *Phys. Lett.* B **495** 323
[67] Brambilla N, Garcia i Tormo X, Soto J and Vairo A 2007 The Logarithmic contribution to the QCD static energy at N^4LO *Phys. Lett.* B **647** 185
[68] Brambilla N, Vairo A, Garcia i Tormo X and Soto J 2009 The QCD static energy at NNNLL *Phys. Rev.* D **80** 034016
[69] Appelquist T, Dine M and Muzinich I J 1977 The Static Potential in Quantum Chromodynamics *Phys. Lett.* B **69** 231
[70] Pineda A and Soto J 1998 Effective field theory for ultrasoft momenta in NRQCD and NRQED *Nucl. Phys. B Proc. Suppl.* **64** 428
[71] Bazavov A, Brambilla N, Garcia i Tormo X, Petreczky P, Soto J and Vairo A 2012 Determination of α_S from the QCD static energy *Phys. Rev.* D **86** 114031
[72] Necco S and Sommer R 2002 The N(f) = 0 heavy quark potential from short to intermediate distances *Nucl. Phys.* B **622** 328
[73] Pineda A 2003 The Static potential: lattice versus perturbation theory in a renormalon based approach *J. Phys.* G **29** 371
[74] Brambilla N, Garcia i Tormo X, Soto J and Vairo A 2010 Precision determination of $r_0\Lambda_{\overline{\rm MS}}$ from the QCD static energy *Phys. Rev. Lett.* **105** 212001 [Erratum: Phys. Rev. Lett. 108 (2012) 269 903]
[75] Bazavov A, Brambilla N, Tormo X G, Petreczky I, P, Soto J and Vairo A 2014 Determination of α_S from the QCD static energy: an update *Phys. Rev.* D **90** 074038 [Erratum: Phys. Rev. D 101 (2020) 119 902]
[76] Weber J H, Bazavov A and Petreczky P 2019 Equation of state in (2.1) flavor QCD at high temperatures *PoS* **Confinement2018** 166
[77] Bazavov A, Petreczky P and Weber J H 2018 Equation of state in 2+1 flavor QCD at high temperatures *Phys. Rev.* D **97** 014510
[78] Steinbeißer S, Brambilla N, Delgado R L, Kronfeld A S, Leino V, Petreczky P, Vairo A, Weber J H and (TUMQCD Collaboration) 2022 The static energy in 2+1+1-flavor QCD *PoS* **LATTICE2021** 521
[79] Brambilla N, Delgado R L, Kronfeld A S, Leino V, Petreczky P, Steinbeißer S, Vairo A and Weber J H 2023 Static energy in (2 + 1 + 1)-flavor lattice QCD: scale setting and charm effects *Phys. Rev.* D **107** 074503

[80] Takaura H, Kaneko T, Kiyo Y and Sumino Y 2019 Determination of α_S from static QCD potential: OPE with renormalon subtraction and lattice QCD *J. High Energy Phys.* JHEP04 (2019)155
[81] Takaura H, Kaneko T, Kiyo Y and Sumino Y 2019 Determination of α_S from static QCD potential with renormalon subtraction *Phys. Lett.* B **789** 598
[82] Bazavov A *et al* (HotQCD Collaboration) 2014 Equation of state in (2+1)-flavor QCD *Phys. Rev.* D **90** 094503
[83] Kaneko T, Aoki S, Cossu G, Fukaya H, Hashimoto S, Noaki J and (JLQCD Collaboration) 2014 Large-scale simulations with chiral symmetry *PoS* **LATTICE2013** 125
[84] Vairo A 2016 A low-energy determination of α_S at three loops *EPJ Web Conf.* **126** 02031
[85] Brambilla N, Leino V, Philipsen O, Reisinger C, Vairo A and Wagner M 2022 Lattice gauge theory computation of the static force *Phys. Rev.* D **105** 054514
[86] Leino V, Brambilla N, Mayer-Steudte J and Vairo A 2022 The static force from generalized Wilson loops using gradient flow *EPJ Web Conf.* **258** 04009
[87] Berwein M, Brambilla N, Petreczky P and Vairo A 2017 Polyakov loop correlator in perturbation theory *Phys. Rev.* D **96** 014025 [Addendum: Phys.Rev.D 101, 099 903 (2020)]
[88] Bazavov A, Brambilla N, Petreczky P, Vairo A, Weber J H and (TUMQCD Collaboration) 2018 Color screening in (2+1)-flavor QCD *Phys. Rev.* D **98** 054511
[89] Wilson K G 1969 Nonlagrangian models of current algebra *Phys. Rev.* **179** 1499
[90] Symanzik K 1983 Continuum limit and improved action in lattice theories: I. Principles and ϕ^4 theory *Nucl. Phys.* B **226** 187
[91] Symanzik K 1983 Continuum limit and improved action in lattice theories: II. O(n) nonlinear sigma model in perturbation theory *Nucl. Phys.* B **226** 205
[92] Zyla P A *et al* (Particle Data Group Collaboration) 2020 Review of Particle Physics *Progress Theor. Exp. Phys.* **2020** 083C01
[93] Bali G S, Bauer C and Pineda A 2014 Perturbative expansion of the plaquette to $\mathcal{O}(\alpha^{35})$ in four-dimensional SU(3) gauge theory *Phys. Rev.* D **89** 054505
[94] Bali G S, Bauer C and Pineda A 2014 Model-independent determination of the gluon condensate in four-dimensional SU(3) gauge theory *Phys. Rev. Lett.* **113** 092001
[95] Mason Q, Trottier H D, Davies C T H, Foley K, Gray A, Lepage G P, Nobes M, Shigemitsu J and (HPQCD Collaboration) 2005 Accurate determinations of α_s from realistic lattice QCD *Phys. Rev. Lett.* **95** 052002
[96] Davies C T H, Hornbostel K, Kendall I D, Lepage G P, McNeile C, Shigemitsu J, Trottier H and (HPQCD Collaboration) 2008 Update: accurate determinations of α_s from realistic lattice QCD *Phys. Rev.* D **78** 114507
[97] Pich A 2021 Precision physics with inclusive QCD processes *Prog. Part. Nucl. Phys.* **117** 103846
[98] Braaten E, Narison S and Pich A 1992 QCD analysis of the tau hadronic width *Nucl. Phys.* B **373** 581
[99] Shifman M A, Vainshtein A I and Zakharov V I 1979 QCD and Resonance Physics. Theoretical Foundations *Nucl. Phys.* B **147** 385
[100] Baikov P A, Chetyrkin K G and Kuhn J H 2008 Order α_s^4 QCD corrections to Z and τ decays *Phys. Rev. Lett.* **101** 012002
[101] Le Diberder F and Pich A 1992 Testing QCD with tau decays *Phys. Lett.* B **289** 165
[102] González-Alonso M, Pich A and Rodríguez-Sánchez A 2016 Updated determination of chiral couplings and vacuum condensates from hadronic τ decay data *Phys. Rev.* D **94** 014017
[103] Davier M, Höcker A, Malaescu B, Yuan C-Z and Zhang Z 2014 Update of the ALEPH non-strange spectral functions from hadronic τ decays *Eur. Phys. J.* C **74** 2803
[104] Pich A and Rodríguez-Sánchez A 2016 Determination of the QCD coupling from ALEPH τ decay data *Phys. Rev.* D **94** 034027
[105] Schael S *et al* (ALEPH Collaboration) 2005 Branching ratios and spectral functions of tau decays: final ALEPH measurements and physics implications *Phys. Rep.* **421** 191
[106] Coan T *et al* (CLEO Collaboration) 1995 Measurement of α_S from tau decays *Phys. Lett.* B **356** 580
[107] Ackerstaff K *et al* (OPAL Collaboration) 1999 Measurement of the strong coupling constant α_S and the vector and axial vector spectral functions in hadronic tau decays *Eur. Phys. J.* C **7** 571
[108] Pich A 2014 Precision Tau Physics *Prog. Part. Nucl. Phys.* **75** 41

[109] Le Diberder F and Pich A 1992 The perturbative QCD prediction to $R(\tau)$ revisited *Phys. Lett.* B **286** 147
[110] Pivovarov A A 1992 Renormalization group analysis of the tau lepton decay within QCD *Z. Phys.* C **53** 461 [Sov. J. Nucl. Phys. 54 (1991) 676; Yad. Fiz. 54 (1991) 1114]
[111] Pich A and Rodríguez-Sánchez A 2016 Updated determination of $\alpha_S(m_\tau^2)$ from tau decays *Mod. Phys. Lett.* A **31** 1630032
[112] Pich A 2019 Tau-decay determination of the strong coupling *SciPost Phys. Proc.* **1** 036
[113] Pich A and Rodríguez-Sánchez A 2022 Violations of quark-hadron duality in low-energy determinations of α_s *J. High Energy Phys.* JHEP07(2022)145
[114] Ayala C, Cvetic G and Teca D 2022 Using improved operator product expansion in Borel–Laplace sum rules with ALEPH τ decay data, and determination of pQCD coupling *Eur. Phys. J.* C **82** 362
[115] Barate R *et al* (ALEPH Collaboration) 1998 Measurement of the spectral functions of axial—vector hadronic tau decays and determination of $\alpha_S(m_\tau^2)$ *Eur. Phys. J.* C **4** 409
[116] Beneke M 1999 Renormalons *Phys. Rep.* **317** 1
[117] Beneke M and Jamin M 2008 α_s and the τ hadronic width: fixed-order, contour-improved and higher-order perturbation theory *J. High Energy Phys.* JHEP09(2008)044
[118] Beneke M, Boito D and Jamin M 2013 Perturbative expansion of tau hadronic spectral function moments and α_S extractions *J. High Energy Phys.* JHEP01(2013)125
[119] Hoang A H and Regner C 2022 Borel representation of τ hadronic spectral function moments in contour-improved perturbation theory *Phys. Rev.* D **105** 096023
[120] Hoang A H and Regner C 2021 On the Difference between FOPT and CIPT for Hadronic Tau Decays *Eur. Phys. J. ST* **230**
[121] Boito D, Golterman M, Maltman K, Peris S, Rodrigues M V and Schaaf W 2021 Strong coupling from an improved τ vector isovector spectral function *Phys. Rev.* D **103** 034028
[122] Benitez-Rathgeb M A, Boito D, Hoang A H and Jamin M 2022 Reconciling the contour-improved and fixed-order approaches for τ hadronic spectral moments: I. Renormalon-free gluon condensate scheme *J. High Energy Phys.* JHEP07(2022)016
[123] Poggio E C, Quinn H R and Weinberg S 1976 Smearing the Quark Model *Phys. Rev.* D **13** 1958
[124] Blok B, Shifman M A and Zhang D-X 1998 An Illustrative example of how quark hadron duality might work *Phys. Rev.* D **57** 2691 [Erratum: Phys. Rev. D 59 (1999) 019 901]
[125] Bigi I I Y, Shifman M A, Uraltsev N and Vainshtein A I 1999 Heavy flavor decays, OPE and duality in two-dimensional 't Hooft model *Phys. Rev.* D **59** 054011
[126] Boito D, Caprini I, Golterman M, Maltman K and Peris S 2018 Hyperasymptotics and quark-hadron duality violations in QCD *Phys. Rev.* D **97** 054007
[127] Catà O, Golterman M and Peris S 2005 Duality violations and spectral sum rules *J. High Energy Phys.* JHEP08(2005)076
[128] Boito D, Catà O, Golterman M, Jamin M, Maltman K, Osborne J and Peris S 2011 A new determination of α_S from hadronic τ decays *Phys. Rev.* D **84** 113006
[129] Boito D, Golterman M, Jamin M, Mahdavi A, Maltman K, Osborne J and Peris S 2012 An Updated determination of α_S from τ decays *Phys. Rev.* D **85** 093015
[130] Boito D, Golterman M, Maltman K and Peris S 2017 Strong coupling from hadronic τ decays: a critical appraisal *Phys. Rev.* D **95** 034024
[131] Boito D, Golterman M, Maltman K and Peris S 2019 Evidence against naive truncations of the OPE from $e^+e^- \to$ hadrons below charm *Phys. Rev.* D **100** 074009
[132] Boito D, Golterman M, Maltman K, Osborne J and Peris S 2015 Strong coupling from the revised ALEPH data for hadronic τ decays *Phys. Rev.* D **91** 034003
[133] Keshavarzi A, Nomura D and Teubner T 2018 Muon $g-2$ and $\alpha(M_Z^2)$: a new data-based analysis *Phys. Rev.* D **97** 114025
[134] Keshavarzi A, Nomura D and Teubner T 2020 $g-2$ of charged leptons, $\alpha(M_Z^2)$, and the hyperfine splitting of muonium *Phys. Rev.* D **101** 014029
[135] Boito D, Golterman M, Keshavarzi A, Maltman K, Nomura D, Peris S and Teubner T 2018 Strong coupling from $e^+e^- \to$ hadrons below charm *Phys. Rev.* D **98** 074030
[136] Ayala C, Cvetic G and Teca D 2021 Determination of perturbative QCD coupling from ALEPH τ decay data using pinched Borel–Laplace and Finite Energy Sum Rules *Eur. Phys. J.* C **81** 930
[137] Lees J P *et al* (BaBar Collaboration) 2018 Measurement of the spectral function for the $\tau^- \to K^- K_S \nu_\tau$ decay *Phys. Rev.* D **98** 032010

[138] Davier M, Descotes-Genon S, Hocker A, Malaescu B and Zhang Z 2008 The determination of α_S from tau decays revisited, *Eur. Phys. J.* C **56** 305
[139] Abada A *et al* (FCC Collaboration) 2019 FCC-ee: the Lepton Collider: future Circular Collider Conceptual Design Report Volume 2 *Eur. Phys. J. ST* **228** 261
[140] Dam M 2021 The τ challenges at FCC-ee *Eur. Phys. J. Plus* **136** 963
[141] Fujikawa M *et al* (Belle Collaboration) 2008 High-Statistics Study of the $\tau^- \to \pi^-\pi^0\nu_\tau$ Decay *Phys. Rev.* D **78** 072006
[142] Amhis Y S *et al* (HFLAV Collaboration) 2021 Averages of b-hadron, c-hadron, and τ-lepton properties as of 2018 *Eur. Phys. J. C.* **81** 226
[143] Kataev A L and Starshenko V V 1995 Estimates of the higher order QCD corrections to $R(s)$, R_τ and deep inelastic scattering sum rules *Mod. Phys. Lett.* A **10** 235
[144] Boito D, Masjuan P and Oliani F 2018 Higher-order QCD corrections to hadronic τ decays from Padé approximants *J. High Energy Phys.* JHEP08(2018)075
[145] Cvetič G 2019 Renormalon-motivated evaluation of QCD observables *Phys. Rev.* D **99** 014028
[146] Boito D, Hornung D and Jamin M 2015 Anomalous dimensions of four-quark operators and renormalon structure of mesonic two-point correlators *J. High Energy Phys.* JHEP12(2015)090
[147] Ayala C, Cvetic G, Kogerler R and Kondrashuk I 2018 Nearly perturbative lattice-motivated QCD coupling with zero IR limit *J. Phys.* G **45** 035001
[148] Caprini I 2020 Conformal mapping of the Borel plane: going beyond perturbative QCD *Phys. Rev.* D **102** 054017
[149] Benitez-Rathgeb M A, Boito D, Hoang A H and Jamin M 2022 Reconciling the contour-improved and fixed-order approaches for τ hadronic spectral moments: II. Renormalon norm and application in α_s determinations *J. High Energy Phys.* JHEP09(2022)223
[150] Boito D, Jamin M and Miravitllas R 2016 Scheme Variations of the QCD Coupling and Hadronic τ Decays *Phys. Rev. Lett.* **117** 152001
[151] Beneke M 2021 Pole mass renormalon and its ramifications *Eur. Phys. J. ST* **230** 2565
[152] Herzog F, Ruijl B, Ueda T, Vermaseren J A M and Vogt A 2017 On Higgs decays to hadrons and the R-ratio at N^{4}LO *J. High Energy Phys.* JHEP08(2017)113
[153] Hoang A H, Jain A, Scimemi I and Stewart I W 2010 R-evolution: improving perturbative QCD *Phys. Rev.* D **82** 011501
[154] Bethke S *et al* (ed) 2011 *Workshop on Precision Measurements of* α_S arXiv:1110.0016 [hep-ph]
[155] Alekhin S, Blümlein J and Moch S O 2016 α_S from global fits of parton distribution functions *Mod. Phys. Lett.* A **31** 1630023
[156] Moch S *et al High precision fundamental constants at the TeV scale* arXiv:1405.4781 [hep-ph]
[157] Alekhin S *et al The PDF4LHC Working Group Interim Report* arXiv:1101.0536 [hep-ph]
[158] Accardi A *et al* 2016 A Critical Appraisal and Evaluation of Modern PDFs *Eur. Phys. J.* C **76** 471
[159] Blümlein J, Böttcher H and Guffanti A 2007 Non-singlet QCD analysis of deep inelastic world data at $O(\alpha_S^3)$ *Nucl. Phys.* B **774** 182
[160] Blümlein J and Saragnese M 2021 The N^{3}LO scheme-invariant QCD evolution of the non-singlet structure functions $F_2^{NS}(x, Q^2)$ and $g_1^{NS}(x, Q^2)$ *Phys. Lett.* B **820** 136589
[161] Boer D *et al* 1713 *Gluons and the quark sea at high energies: distributions, polarization, tomography* arXiv:1108.1713 [nucl-th]
[162] Abelleira Fernandez J L *et al* (LHeC Study Group Collaboration) 2012 A large hadron electron collider at CERN: report on the physics and design concepts for machine and detector *J. Phys.* G **39** 075001
[163] Moch S, Vermaseren J A M and Vogt A 2004 The Three loop splitting functions in QCD: the nonsinglet case *Nucl. Phys.* B **688** 101
[164] Blümlein J, Marquard P, Schneider C and Schönwald K 2021 The three-loop unpolarized and polarized non-singlet anomalous dimensions from off shell operator matrix elements *Nucl. Phys.* B **971** 115542
[165] Baikov P A and Chetyrkin K G 2006 New four loop results in QCD *Nucl. Phys. B Proc. Suppl.* **160** 76
[166] Moch S, Ruijl B, Ueda T, Vermaseren J A M and Vogt A 2017 Four-loop non-singlet splitting functions in the planar limit and beyond *J. High Energy Phys.* JHEP10(2017)041
[167] Vermaseren J A M, Vogt A and Moch S 2005 The third-order QCD corrections to deep-inelastic scattering by photon exchange *Nucl. Phys.* B **724** 3

[168] Ablinger J, Behring A, Blümlein J, De Freitas A, Hasselhuhn A, von Manteuffel A, Round M, Schneider C and Wißbrock F 2014 The 3-loop non-singlet heavy flavor contributions and anomalous dimensions for the structure function $F_2(x, Q^2)$ and Transversity *Nucl. Phys.* B **886** 733
[169] Buza M, Matiounine Y, Smith J, Migneron R and van Neerven W L 1996 Heavy quark coefficient functions at asymptotic values $Q^2 \gg m^2$ *Nucl. Phys.* B **472** 611
[170] Blümlein J, Falcioni G and Freitas A De 2016 The complete $O(\alpha_S^2)$ Non-Singlet Heavy Flavor Corrections to the Structure Functions $g_{1,2}^{ep}(x, Q^2)$, $F_{1,2,L}^{ep}(x, Q^2)$, $F_{1,2,3}^{\nu(\bar{\nu})}(x, Q^2)$ and the Associated Sum Rules *Nucl. Phys.* B **910** 568
[171] Guyot C, Milsztajn A, Ouraou A, Staude A and Teichert K 1988 *A new fixed target experiment for a precise test of QCD*
[172] Alexopoulos T *et al* 2003 Electron deuteron scattering with HERA, a letter of intent for an experimental programme with the H1 detector **12**
[173] Alekhin S, Blümlein J and Moch S 2012 Parton distribution functions and benchmark cross sections at NNLO *Phys. Rev. D* **86** 054009 arXiv:1202.2281 [hep-ph]
[174] Whitlow L W, Riordan E M, Dasu S, Rock S and Bodek A 1992 Precise measurements of the proton and deuteron structure functions from a global analysis of the SLAC deep inelastic electron scattering cross-sections *Phys. Lett.* B **282** 475
[175] Whitlow L W 1990 Deep inelastic structure functions from electron scattering on hydrogen, deuterium, and iron at 0.6 GeV $^2 \leqslant Q^2 \leqslant 30$ GeV^2 *PhD thesis*
[176] Arneodo M *et al* (New Muon Collaboration) 1997 Measurement of the proton and deuteron structure functions, F_2^p and F_2^d, and of the ratio σ_L/σ_T *Nucl. Phys.* B **483** 3
[177] Benvenuti A C *et al* (BCDMS Collaboration) 1989 A high statistics measurement of the proton structure functions $F_2(x, Q^2)$ and R from deep inelastic muon scattering at high Q^2 *Phys. Lett.* B **223** 485
[178] Benvenuti A C *et al* (BCDMS Collaboration) 1990 A high statistics measurement of the deuteron structure functions $F_2(x, Q^2)$ and R from deep inelastic muon scattering at high Q^2 *Phys. Lett.* B **237** 592
[179] Benvenuti A C *et al* (BCDMS Collaboration) 1987 A high statistics measurement of the nucleon structure function $F_2(x, Q^2)$ from deep inelastic muon-carbon scattering at high Q^2 *Phys. Lett.* B **195** 91
[180] Altarelli G, Ellis R K and Martinelli G 1978 Leptoproduction and drell-yan processes beyond the leading approximation in chromodynamics *Nucl. Phys.* B **143** 521 [Erratum: Nucl. Phys. B 146 (1978) 544]
[181] Shaikhatdenov B G, Kotikov A V, Krivokhizhin V G and Parente G 2010 QCD coupling constant at NNLO from DIS data *Phys. Rev.* D **81** 034008 [Erratum: Phys. Rev. D 81 (2010) 079 904]
[182] Kotikov A V, Krivokhizhin V G and Shaikhatdenov B G 2015 Improved nonsinglet QCD analysis of fixed-target DIS data *J. Phys.* G **42** 095004
[183] Kotikov A V, Krivokhizhin V G and Shaikhatdenov B G 2018 Gottfried sum rule in QCD NS analysis of DIS fixed target data *Phys. Atom. Nucl.* **81** 244
[184] Krivokhizhin V G and Kotikov A V 2005 A systematic study of QCD coupling constant from deep-inelastic measurements, *Phys. Atom. Nucl.* **68** 1873
[185] Krivokhizhin V G and Kotikov A V 2009 Functions of the nucleon structure and determination of the strong coupling constant *Phys. Part. Nucl.* **40** 1059
[186] Buras A J 1980 Asymptotic freedom in deep inelastic processes in the leading order and beyond *Rev. Mod. Phys.* **52** 199
[187] Kazakov D I and Kotikov A V 1988 Total α_S Correction to Deep Inelastic Scattering Cross-section Ratio, R $= \sigma_L/\sigma_T$ in QCD. Calculation of Longitudinal Structure Function *Nucl. Phys.* B **307** 721 [Erratum: Nucl. Phys. B 345 (1990) 299]
[188] Kotikov A V and Velizhanin V N *Analytic continuation of the Mellin moments of deep inelastic structure functions* arXiv:hep-ph/0501274
[189] Kotikov A V 1994 Gluon distribution for small *x Phys. Atom. Nucl.* **57** 133
[190] Parisi G and Sourlas N 1979 A simple parametrization of the q^2 dependence of the quark distributions in QCD *Nucl. Phys.* B **151** 421
[191] Krivokhizhin V G, Kurlovich S P, Sanadze V V, Savin I A, Sidorov A V and Skachkov N B 1987 QCD analysis of singlet structure functions using Jacobi polynomials: the description of the method *Z. Phys.* C **36** 51

[192] Krivokhizhin V G, Kurlovich S P, Lednicky R, Nemecek S, Sanadze V V, Savin I A, Sidorov A V and Skachkov N B 1990 Next-to-leading order QCD analysis of structure functions with the help of Jacobi polynomials *Z. Phys.* C **48** 347
[193] James F and Roos M 1975 Minuit: a System for Function Minimization and Analysis of the Parameter Errors and Correlations *Comput. Phys. Commun.* **10** 343
[194] Kotikov A V, Krivokhizhin V G and Shaikhatdenov B G 2012 Analytic and 'frozen' QCD coupling constants up to NNLO from DIS data *Phys. Atom. Nucl.* **75** 507
[195] Shirkov D V and Solovtsov I L 1997 Analytic model for the QCD running coupling with universal $\alpha_S(0)$ value *Phys. Rev. Lett.* **79** 1209
[196] Cvetic G, Illarionov A Y, Kniehl B A and Kotikov A V 2009 Small-x behavior of the structure function F(2) and its slope $\partial \ln F(2)/\partial \ln(1/x)$ for 'frozen' and analytic strong-coupling constants *Phys. Lett.* B **679** 350
[197] Kotikov A V and Parente G 1999 Small x behavior of parton distributions with soft initial conditions *Nucl. Phys.* B **549** 242
[198] Illarionov A Y, Kotikov A V and Parente Bermudez G 2008 Small x behavior of parton distributions. A Study of higher twist effects *Phys. Part. Nucl.* **39** 307
[199] Kotikov A V, Parente G and Sanchez Guillen J 1993 Renormalization scheme invariant analysis of the DIS structure functions F2 and F(L) *Z. Phys. C.* **58** 465
[200] Parente G, Kotikov A V and Krivokhizhin V G 1994 Next to next-to-leading order QCD analysis of DIS structure functions *Phys. Lett.* B **333** 190
[201] Grunberg G 1980 Renormalization Group Improved Perturbative QCD *Phys. Lett.* B **95** 70 [Erratum: Phys. Lett. B 110 (1982) 501]
[202] Grunberg G 1984 Renormalization Scheme Independent QCD and QED: the Method of Effective Charges *Phys. Rev.* D **29** 2315
[203] Vogt A, Moch S and Vermaseren J A M 2004 The Three-loop splitting functions in QCD: the Singlet case *Nucl. Phys.* B **691** 129
[204] van Neerven W L and Zijlstra E B 1991 Order α_s^2 contributions to the deep inelastic Wilson coefficient *Phys. Lett.* B **272** 127
[205] Zijlstra E B and van Neerven W L 1992 Order α_s^2 QCD corrections to the deep inelastic proton structure functions F_2 and F_L *Nucl. Phys.* B **383** 525
[206] Zijlstra E B and van Neerven W L 1992 Order α_s^2 correction to the structure function $F_3(x, Q^2)$ in deep inelastic neutrino-hadron scattering *Phys. Lett.* B **297** 377
[207] Moch S and Vermaseren J A M 2000 Deep inelastic structure functions at two loops *Nucl. Phys.* B **573** 853
[208] Alekhin S, Blümlein J, Moch S and Placakyte R 2017 Parton distribution functions, α_S, and heavy-quark masses for LHC Run II *Phys. Rev.* D **96** 014011
[209] Laenen E, Riemersma S, Smith J and van Neerven W L 1993 Complete $O(\alpha_s)$ corrections to heavy flavor structure functions in electroproduction *Nucl. Phys.* B **392** 162
[210] Alekhin S, Blümlein J and Moch S 2020 Heavy-flavor PDF evolution and variable-flavor number scheme uncertainties in deep-inelastic scattering *Phys. Rev.* D **102** 054014
[211] Bodek A *et al* 1979 Experimental Studies of the Neutron and Proton Electromagnetic Structure Functions *Phys. Rev.* D **20** 1471
[212] Mestayer M D, Atwood W B, Bloom E D, Cottrell R L, DeStaebler H C, Prescott C Y, Rochester L S, Stein S, Taylor R E and Trines D 1983 The ratio σ_l/σ_t from deep inelastic electron scattering, *Phys. Rev.* D **27** 285
[213] Whitlow L W, Rock S, Bodek A, Riordan E M and Dasu S 1990 A Precise extraction of $R = \sigma_L/\sigma_T$ from a global analysis of the SLAC deep inelastic e−p and e-d scattering cross-sections *Phys. Lett.* B **250** 193
[214] Aaron F D *et al* (H1, ZEUS Collaboration) 2010 Combined Measurement and QCD Analysis of the Inclusive $e^{\pm}$p Scattering Cross Sections at HERA *J. High Energy Phys.* JHEP01(2010)109
[215] Abramowicz H *et al* (H1, ZEUS Collaboration) 2015 Combination of measurements of inclusive deep inelastic $e^{\pm}$p scattering cross sections and QCD analysis of HERA data *Eur. Phys. J. C* **75** 580 arXiv:1506.06042 [hep-ex]
[216] Patrignani C *et al* (Particle Data Group Collaboration) 2016 Review of Particle Physics *Chin. Phys.* C **40** 100001
[217] Moch S, Ruijl B, Ueda T, Vermaseren J A M and Vogt A 2022 Low moments of the four-loop splitting functions in QCD *Phys. Lett.* B **825** 136853

[218] Moch S and Rogal M 2007 Charged current deep-inelastic scattering at three loops *Nucl. Phys.* B **782** 51
[219] Moch S, Rogal M and Vogt A 2008 Differences between charged-current coefficient functions *Nucl. Phys.* B **790** 317
[220] Moch S, Vermaseren J A M and Vogt A 2009 Third-order QCD corrections to the charged-current structure function F_3 *Nucl. Phys.* B **813** 220
[221] Moch S, Ruijl B, Ueda T, Vermaseren J A M and Vogt A 2018 On quartic colour factors in splitting functions and the gluon cusp anomalous dimension *Phys. Lett.* B **782** 627
[222] Hou T-J *et al* 2021 New CTEQ global analysis of quantum chromodynamics with high-precision data from the LHC *Phys. Rev.* D **103** 014013
[223] Dulat S, Hou T-J, Gao J, Guzzi M, Huston J, Nadolsky P, Pumplin J, Schmidt C, Stump D and Yuan C P 2016 New parton distribution functions from a global analysis of quantum chromodynamics *Phys. Rev.* D **93** 033006
[224] Hou T-J, Dulat S, Gao J, Guzzi M, Huston J, Nadolsky P, Pumplin J, Schmidt C, Stump D and Yuan C P 2017 CTEQ-TEA parton distribution functions and HERA Run I and II combined data *Phys. Rev.* D **95** 034003
[225] Aaboud M *et al* (ATLAS Collaboration) 2017 Precision measurement and interpretation of inclusive W^+, W^- and Z/γ^* production cross sections with the ATLAS detector *Eur. Phys. J.* C **77** 367
[226] Tanabashi M *et al* (Particle Data Group Collaboration) 2018 Review of Particle Physics *Phys. Rev.* D **98** 030001
[227] Lai H-L, Huston J, Li Z, Nadolsky P, Pumplin J, Stump D and Yuan C P 2010 Uncertainty induced by QCD coupling in the CTEQ global analysis of parton distributions *Phys. Rev.* D **82** 054021
[228] Stump D, Pumplin J, Brock R, Casey D, Huston J, Kalk J, Lai H L and Tung W K 2001 Uncertainties of predictions from parton distribution functions. 1. The Lagrange multiplier method *Phys. Rev.* D **65** 014012
[229] Kovařík K, Nadolsky P M and Soper D E 2020 Hadronic structure in high-energy collisions *Rev. Mod. Phys.* **92** 045003
[230] Aad G *et al* (ATLAS Collaboration) 2016 Measurement of the transverse momentum and ϕ^*_η distributions of Drell–Yan lepton pairs in proton–proton collisions at $\sqrt{s} = 8$ TeV with the ATLAS detector *Eur. Phys. J.* C **76** 291
[231] Aaij R *et al* (LHCb Collaboration) 2016 Measurement of forward W and Z boson production in pp collisions at $\sqrt{s} = 8$ TeV *J. High Energy Phys.* JHEP01(2016)155
[232] Aad G *et al* (ATLAS Collaboration) 2015 Measurement of the inclusive jet cross-section in proton-proton collisions at $\sqrt{s} = 7$ TeV using 4.5 fb^{-1} of data with the ATLAS detector *J. High Energy Phys.* JHEP02(2015)153 [Erratum: J. High Energy Phys. JHEP09(2015)141]
[233] Abazov V M and (VM Collaboration) 2008 Measurement of the inclusive jet cross-section in $p\bar{p}$ collisions at $\sqrt{s} = 1.96$ TeV *Phys. Rev. Lett.* **101** 062001
[234] Aad G *et al* (ATLAS Collaboration) 2016 Measurements of top-quark pair differential cross-sections in the lepton+jets channel in pp collisions at $\sqrt{s} = 8$ TeV using the ATLAS detector *Eur. Phys. J.* C **76** 538
[235] Chatrchyan S *et al* (CMS Collaboration) 2014 Measurement of the ratio of inclusive jet cross sections using the anti-k_t algorithm with radius parameters $r = 0.5$ and 0.7 in pp collisions at $\sqrt{s} = 7$ TeV *Phys. Rev.* D **90** 072006
[236] Khachatryan V *et al* (CMS Collaboration) 2017 *Measurement and QCD analysis of double-differential inclusive jet cross sections in pp collisions at* $\sqrt{s} = 8$ *TeV and cross section ratios to 2.76 and 7 TeV, J. High Energy Phys.* JHEP03(2017)156
[237] Barlow R 2002 Systematic errors: facts and fictions *Conference on Advanced Statistical Techniques in Particle Physics* 134
[238] Guzzi M *et al* 2022 NNLO constraints on proton PDFs from the SeaQuest and STAR experiments and other developments in the CTEQ-TEA global analysis *v* **8** 005
[239] Gribov V N and Lipatov L N 1972 Deep inelastic e−p scattering in perturbation theory *Sov. J. Nucl. Phys.* **15** 438
[240] Altarelli G and Parisi G 1977 Asymptotic Freedom in Parton Language *Nucl. Phys.* B **126** 298
[241] Dokshitzer Y L 1977 Calculation of the Structure Functions for Deep Inelastic Scattering and e^+e^- Annihilation by Perturbation Theory in Quantum Chromodynamics. (In Russian) *Sov. Phys. JETP* **46** 641–53

[242] Andreev V *et al* (H1 Collaboration) 2017 Measurement of jet production cross sections in deep-inelastic ep scattering at HERA *Eur. Phys. J.* C **77** 215 [Erratum: Eur. Phys. J. C 81 (2021) 739]
[243] Abt I *et al* (H1, ZEUS Collaboration) 2022 Impact of jet-production data on the next-to-next-to-leading-order determination of HERAPDF2.0 parton distributions *Eur. Phys. J.* C **82** 243
[244] Abramowicz H *et al* (H1, ZEUS Collaboration) 2018 Combination and QCD analysis of charm and beauty production cross-section measurements in deep inelastic ep scattering at HERA *Eur. Phys. J.* C **78** 473
[245] Britzger D *et al* 2019 Calculations for deep inelastic scattering using fast interpolation grid techniques at NNLO in QCD and the extraction of α_S from HERA data *Eur. Phys. J.* C **79** 845 [Erratum: Eur. Phys. J. C 81 (2021) 957]
[246] Agostini P *et al* (LHeC, FCC-he Study Group Collaboration) 2021 The Large Hadron-Electron Collider at the HL-LHC *J. Phys.* G **48** 110501
[247] Bailey S, Cridge T, Harland-Lang L A, Martin A D and Thorne R S 2021 Parton distributions from LHC, HERA, Tevatron and fixed target data: MSHT20 PDFs *Eur. Phys. J.* C **81** 341
[248] Cridge T, Harland-Lang L A, Martin A D and Thorne R S 2022 QED parton distribution functions in the MSHT20 fit *Eur. Phys. J.* C **82** 90
[249] Cridge T, Harland-Lang L A, Martin A D and Thorne R S 2021 An investigation of the α_S and heavy quark mass dependence in the MSHT20 global PDF analysis *Eur. Phys. J.* C **81** 744
[250] Harland-Lang L A, Martin A D, Motylinski P and Thorne R S 2015 Uncertainties on α_S in the MMHT2014 global PDF analysis and implications for SM predictions *Eur. Phys. J.* C **75** 435
[251] Zyla P *et al* (Particle Data Group Collaboration) 2020 Review of Particle Physics *Progress Theor. Exp. Phys.* **2020** 083C01
[252] Harland-Lang L A, Martin A D, Motylinski P and Thorne R S 2015 Parton distributions in the LHC era: MMHT 2014 PDFs *Eur. Phys. J.* C **75** 204
[253] Martin A D, Stirling W J, Thorne R S and Watt G 2009 Parton distributions for the LHC *Eur. Phys. J. C.* **63** 189
[254] Buckley A, Ferrando J, Lloyd S, Nordström K, Page B, Rüfenacht M, Schönherr M and Watt G 2015 LHAPDF6: parton density access in the LHC precision era *Eur. Phys. J.* C **75** 132
[255] Chatrchyan S *et al* (CMS Collaboration) 2013 Measurement of the ratio of the inclusive 3-jet cross section to the inclusive 2-jet cross section in pp collisions at $\sqrt{s} = 7$ TeV and first determination of the strong coupling constant in the TeV Range *Eur. Phys. J.* C **73** 2604
[256] Ball R D, Del Debbio L, Forte S, Guffanti A, Latorre J I, Piccione A, Rojo J, Ubiali M and (NNPDF Collaboration) 2009 Precision determination of electroweak parameters and the strange content of the proton from neutrino deep-inelastic scattering *Nucl. Phys.* B **823** 195
[257] Iranipour S and Ubiali M 2022 A new generation of simultaneous fits to LHC data using deep learning *J. High Energy Phys.* JHEP05(2022)032
[258] Greljo A, Iranipour S, Kassabov Z, Madigan M, Moore J, Rojo J, Ubiali M and Voisey C 2021 Parton distributions in the SMEFT from high-energy Drell-Yan tails *J. High Energy Phys.* JHEP07(2021)122
[259] Carrazza S, Degrande C, Iranipour S, Rojo J and Ubiali M 2019 Can new physics hide inside the proton? *Phys. Rev. Lett.* **123** 132001
[260] Ball R D *et al* (NNPDF Collaboration) 2022 The path to proton structure at 1% accuracy *Eur. Phys. J.* C **82** 428
[261] Ball R D *et al* (NNPDF Collaboration) 2021 An open-source machine learning framework for global analyses of parton distributions *Eur. Phys. J.* C **81** 958
[262] Lionetti S, Ball R D, Bertone V, Cerutti F, Del Debbio L, Forte S, Guffanti A, Latorre J I, Rojo J and Ubiali M 2011 Precision determination of α_S using an unbiased global NLO parton set *Phys. Lett.* B **701** 346
[263] Ball R D, Bertone V, Del Debbio L, Forte S, Guffanti A, Latorre J I, Lionetti S, Rojo J and Ubiali M 2012 Precision NNLO determination of $\alpha_S(m_Z^2)$ using an unbiased global parton set *Phys. Lett.* B **707** 66
[264] Ball R D, Bertone V, Cerutti F, Del Debbio L, Forte S, Guffanti A, Latorre J I, Rojo J and Ubiali M 2011 Impact of heavy quark masses on parton distributions and LHC phenomenology *Nucl. Phys.* B **849** 296
[265] Ball R D, Bertone V, Cerutti F, Del Debbio L, Forte S, Guffanti A, Latorre J I, Rojo J, Ubiali M and (NNPDF Collaboration) 2012 Unbiased global determination of parton distributions and their uncertainties at NNLO and at LO *Nucl. Phys.* B **855** 153

[266] Bagnaschi E, Cacciari M, Guffanti A and Jenniches L 2015 An extensive survey of the estimation of uncertainties from missing higher orders in perturbative calculations *J. High Energy Phys.* JHEP02(2015)133
[267] Ball R D, Carrazza S, Del Debbio L, Forte S, Kassabov Z, Rojo J, Slade E and Ubiali M 2018 Precision determination of the strong coupling constant within a global PDF analysis *Eur. Phys. J.* C **78** 408
[268] Ball R D *et al* (NNPDF Collaboration) 2017 Parton distributions from high-precision collider data *Eur. Phys. J.* C **77** 663
[269] Ball R D, Del Debbio L, Forte S, Guffanti A, Latorre J I, Rojo J, Ubiali M and (NNPDF Collaboration) 2010 Fitting parton distribution data with multiplicative normalization uncertainties *J. High Energy Phys.* JHEP05(2010)075
[270] Ball R D *et al* 2013 Parton Distribution Benchmarking with LHC Data *J. High Energy Phys.* JHEP04(2013)125
[271] Forte S and Kassabov Z 2020 Why α_S cannot be determined from hadronic processes without simultaneously determining the parton distributions *Eur. Phys. J.* C **80** 182
[272] Abdul Khalek R *et al* 2020 Phenomenology of NNLO jet production at the LHC and its impact on parton distributions *Eur. Phys. J.* C **80** 797
[273] Campbell J M, Rojo J, Slade E and Williams C 2018 Direct photon production and PDF fits reloaded *Eur. Phys. J.* C **78** 470
[274] Abdul Khalek R *et al* (NNPDF Collaboration) 2019 Parton distributions with theory uncertainties: general formalism and first phenomenological studies *Eur. Phys. J.* C **79** 931
[275] Abdul Khalek R *et al* (NNPDF Collaboration) 2019 A first determination of parton distributions with theoretical uncertainties *Eur. Phys. J.* C **79**
[276] Deur A, Brodsky S J and De Téramond G F 2018 *The spin structure of the nucleon* 05250 1807.05250 [hep-ph]
[277] Blümlein J and Böttcher H 2010 QCD analysis of polarized deep inelastic scattering data *Nucl. Phys.* B **841** 205
[278] Kataev A L 1994 The Ellis-Jaffe sum rule: the estimates of the next to next-to-leading order QCD corrections *Phys. Rev.* D **50** R5469
[279] Kataev A L 2005 Deep inelastic sum rules at the boundaries between perturbative and nonperturbative QCD *Mod. Phys. Lett.* A **20** 2007
[280] Baikov P A, Chetyrkin K G and Kuhn J H 2010 Adler function, Bjorken sum rule, and the Crewther relation to order α_s^4 in a general gauge theory *Phys. Rev. Lett.* **104** 132004
[281] Bjorken J D 1966 Applications of the Chiral U(6)×(6) Algebra of Current Densities *Phys. Rev.* **148** 1467
[282] Bjorken J D 1970 Inelastic Scattering of Polarized Leptons from Polarized Nucleons *Phys. Rev.* D **1** 1376
[283] Altarelli G, Ball R D, Forte S and Ridolfi G 1997 Determination of the Bjorken sum and strong coupling from polarized structure functions *Nucl. Phys.* B **496** 337
[284] Guler N *et al* (CLAS Collaboration) 2015 Precise determination of the deuteron spin structure at low to moderate Q^2 with CLAS and extraction of the neutron contribution *Phys. Rev.* C **92** 055201
[285] Fersch R *et al* (CLAS Collaboration) 2017 Determination of the proton spin structure functions for $0.05 < Q^2 < 5$ GeV^2 using CLAS *Phys. Rev.* C **96** 065208
[286] Abe K *et al* (E143 Collaboration) 1998 Measurements of the proton and deuteron spin structure functions $g_1(x)$ and $g_2(x)$ *Phys. Rev.* D **58** 112003
[287] Anthony P L *et al* (E142 Collaboration) 1996 Deep inelastic scattering of polarized electrons by polarized He-3 and the study of the neutron spin structure *Phys. Rev.* D **54** 6620
[288] Abe K *et al* (E154 Collaboration) 1997 Precision determination of the neutron spin structure function $g_1(n)$ *Phys. Rev. Lett.* **79** 26
[289] Anthony P L *et al* (E155 Collaboration) 1999 Measurement of the deuteron spin structure function $g_1(d)(x)$ for 1-(GeV/c)^2 $< Q^2 <$ 40-(GeV/c)^2 *Phys. Lett.* B **463** 339
[290] Anthony P L *et al* (E155 Collaboration) 2000 Measurements of the Q^2 dependence of the proton and neutron spin structure functions $g(1)^p$ and $g(1)^n$ *Phys. Lett.* B **493** E15519
[291] Adeva B *et al* (Spin Muon Collaboration) 1993 Measurement of the spin dependent structure function $g_1(x)$ of the deuteron *Phys. Lett.* B **302** 533
[292] Adeva B *et al* (SMC Spin Muon Collaboration) 1997 The spin dependent structure function $g_1(x)$ of the proton from polarized deep inelastic muon scattering *Phys. Lett.* B **412** 414

[293] Adams D *et al* (Spin Muon (SMC) Collaboration) 1994 Measurement of the spin dependent structure function $g_1(x)$ of the proton *Phys. Lett.* B **329** 399 [Erratum: Phys. Lett. B 339 (1994) 332]
[294] Adams D *et al* (Spin Muon Collaboration) 1995 A new measurement of the spin dependent structure function $g_1(x)$ of the deuteron *Phys. Lett.* B **357** 248
[295] Adams D *et al* (Spin Muon (SMC) Collaboration) 1997 The Spin dependent structure function $g_1(x)$ of the deuteron from polarized deep inelastic muon scattering *Phys. Lett.* B **396** 338
[296] Adams D *et al* (SMC Spin Muon Collaboration) 1997 Spin structure of the proton from polarized inclusive deep inelastic muon—proton scattering *Phys. Rev.* D **56** 5330
[297] Ageev E S *et al* (COMPASS Collaboration) 2005 Measurement of the spin structure of the deuteron in the DIS region *Phys. Lett.* B **612** 154
[298] Alexakhin V Y *et al* (COMPASS Collaboration) 2007 The Deuteron Spin-dependent Structure Function $g_1(d)$ and its First Moment *Phys. Lett.* B **647** 8
[299] Alekseev M G *et al* (COMPASS Collaboration) 2010 The Spin-dependent Structure Function of the Proton g_1^p and a Test of the Bjorken Sum Rule *Phys. Lett.* B **690** 466
[300] v K *et al* (HERMES Collaboration) 1997 Measurement of the neutron spin structure function $g_1(n)$ with a polarized He-3 internal target *Phys. Lett.* B **404** 383
[301] Airapetian A *et al* (HERMES Collaboration) 1998 Measurement of the proton spin structure function $g_1(p)$ with a pure hydrogen target *Phys. Lett.* B **442** 484
[302] Airapetian A *et al* (HERMES Collaboration) 2007 Precise determination of the spin structure function $g_1(x)$ of the proton, deuteron and neutron *Phys. Rev.* D **75** 012007
[303] Deur A *et al* 2004 Experimental determination of the evolution of the Bjorken integral at low Q^2 *Phys. Rev. Lett.* **93** 212001
[304] Deur A *et al* 2008 Experimental study of isovector spin sum rules *Phys. Rev.* D **78** 032001
[305] Schmelling M 1995 Averaging correlated data *Phys. Scripta* **51** 676
[306] Deur A, Prok Y, Burkert V, Crabb D, Girod F X, Griffioen K A, Guler N, Kuhn S E and Kvaltine N 2014 High precision determination of the Q^2 evolution of the Bjorken Sum *Phys. Rev.* D **90** 012009
[307] Accardi A *et al* 2016 Electron ion collider: the next QCD frontier: understanding the glue that binds us all *Eur. Phys. J.* A **52** 268
[308] Brodsky S J, de Teramond G F, Dosch H G and Erlich J 2015 Light-Front Holographic QCD and Emerging Confinement *Phys. Rep.* **584** 1
[309] de Alfaro V, Fubini S and Furlan G 1976 Conformal invariance in quantum mechanics *Nuovo Cim.* A **34** 569
[310] Trawiński A P, Głazek S D, Brodsky S J, de Téramond G F and Dosch H G 2014 Effective confining potentials for QCD *Phys. Rev.* D **90** 074017
[311] Deur A, Brodsky S J and de Teramond G F 2015 Connecting the hadron mass scale to the fundamental mass scale of quantum chromodynamics *Phys. Lett.* B **750** 528
[312] Sufian R S, de Téramond G F, Brodsky S J, Deur A and Dosch H G 2017 Analysis of nucleon electromagnetic form factors from light-front holographic QCD: the spacelike region *Phys. Rev.* D **95** 014011
[313] de Teramond G F, Liu T, Sufian R S, Dosch H G, Brodsky S J, Deur A and (HLFHS Collaboration) 2018 Universality of generalized parton distributions in light-front holographic QCD *Phys. Rev. Lett.* **120** 182001
[314] de Téramond G F, Dosch H G, Liu T, Sufian R S, Brodsky S J, Deur A and (HLFHS Collaboration) 2021 Gluon matter distribution in the proton and pion from extended holographic light-front QCD *Phys. Rev.* D **104** 114005
[315] Liu T, Sufian R S, de Téramond G F, Dosch H G, Brodsky S J and Deur A 2020 Unified description of polarized and unpolarized quark distributions in the proton *Phys. Rev. Lett.* **124** 082003
[316] Brodsky S J, de Teramond G F and Deur A 2010 Nonperturbative QCD Coupling and its β-function from Light-Front Holography *Phys. Rev.* D **81** 096010
[317] Deur A, Brodsky S J and de Teramond G F 2016 The QCD running coupling *Nucl. Phys.* **90** 1
[318] Deur A, Brodsky S J and de Teramond G F 2016 On the interface between perturbative and nonperturbative QCD *Phys. Lett.* B **757** 275
[319] Deur A, Brodsky S J and de Teramond G F 2017 Determination of $\Lambda_{\overline{\rm MS}}$ at five loops from holographic QCD *J. Phys.* G **44** 105005

[320] Andreev V *et al* (H1 Collaboration) 2017 Determination of the strong coupling constant $\alpha_S(m_Z^2)$ in next-to-next-to-leading order QCD using H1 jet cross section measurements *Eur. Phys. J.* C **77** 791 [Erratum: Eur. Phys. J. C 81 (2021) 738].
[321] Aaron F D *et al* (H1, ZEUS Collaboration) 2010 Combined measurement and QCD analysis of the inclusive $e^{\pm}$–p scattering cross sections at HERA *J. High Energy Phys.* JHEP01(2010)109
[322] Aaron F D *et al* (H1 Collaboration) 2012 Inclusive deep inelastic scattering at high Q^2 with longitudinally polarised lepton beams at HERA *J. High Energy Phys.* JHEP09(2012)061
[323] Aktas A *et al* (H1 Collaboration) 2007 Measurement of inclusive jet production in deep-inelastic scattering at high Q^2 and determination of the strong coupling *Phys. Lett.* B **653** 134
[324] Andreev V *et al* (H1 Collaboration) 2015 Measurement of multijet production in *ep* collisions at high Q^2 and determination of the strong coupling α_S *Eur. Phys. J.* C **75** 65
[325] Aaron F D *et al* (H1 Collaboration) 2011 Measurement of the inclusive $e^{\pm}$−p scattering cross section at high inelasticity y and of the structure function F_L *Eur. Phys. J.* C **71** 1579
[326] Ball R D, Bertone V, Bonvini M, Marzani S, Rojo J and Rottoli L 2018 Parton distributions with small-x resummation: evidence for BFKL dynamics in HERA data *Eur. Phys. J.* C **78** 321
[327] Botje M 2011 QCDNUM: fast QCD evolution and convolution *Comput. Phys. Commun.* **182** 490
[328] Currie J, Gehrmann T and Niehues J 2016 Precise QCD predictions for the production of dijet final states in deep inelastic scattering *Phys. Rev. Lett.* **117** 042001
[329] Currie J, Gehrmann T, Huss A and Niehues J 2017 NNLO QCD corrections to jet production in deep inelastic scattering *J. High Energy Phys.* JHEP07(2017)018 [Erratum: J. High Energy Phys. JHEP12(2020)042]
[330] Gehrmann T *et al* 2018 Jet cross sections and transverse momentum distributions with NNLOJET *PoS* **RADCOR2017** 074
[331] Britzger D, Rabbertz K, Stober F, Wobisch M and (fastNLO Collaboration) 2012 New features in version 2 of the fastNLO project *20th International Workshop on Deep-Inelastic Scattering and Related Subjects* 217
[332] Charchula K, Schuler G A and Spiesberger H 1994 Combined QED and QCD radiative effects in deep inelastic lepton—proton scattering: the Monte Carlo generator DJANGO6 *Comput. Phys. Commun.* **81** 381
[333] Jung H 1995 Hard diffractive scattering in high-energy e−p collisions and the Monte Carlo generator RAPGAP *Comput. Phys. Commun.* **86** 147
[334] Haller J, Hoecker A, Kogler R, Mönig K, Peiffer T and Stelzer J 2018 Update of the global electroweak fit and constraints on two-Higgs-doublet models *Eur. Phys. J.* C **78** 675
[335] Erler J and Schott M 2019 Electroweak Precision Tests of the Standard Model after the Discovery of the Higgs Boson *Prog. Part. Nucl. Phys.* **106** 68
[336] d'Enterria D and Jacobsen V 2020 *Improved strong coupling determinations from hadronic decays of electroweak bosons at N^3LO accuracy* arXiv:2005.04545 [hep-ph]
[337] Dubovyk I, Freitas A, Gluza J, Riemann T and Usovitsch J 2018 Complete electroweak two-loop corrections to Z boson production and decay *Phys. Lett.* B **783** 86
[338] Dubovyk I, Freitas A, Gluza J, Riemann T and Usovitsch J 2019 Electroweak pseudo-observables and Z-boson form factors at two-loop accuracy *J. High Energy Phys.* JHEP08(2019)113
[339] Chen L and Freitas A 2020 Leading fermionic three-loop corrections to electroweak precision observables *J. High Energy Phys.* JHEP07(2020)210
[340] Voutsinas G, Perez E, Dam M and Janot P 2020 Beam-beam effects on the luminosity measurement at LEP and the number of light neutrino species *Phys. Lett.* B **800** 135068
[341] d'Enterria D and Srebre M 2016 α_S and V_{cs} determination, and CKM unitarity test, from W decays at NNLO *Phys. Lett.* B **763** 465
[342] Denner A 1993 Techniques for calculation of electroweak radiative corrections at the one loop level and results for W physics at LEP-200 *Fortsch. Phys.* **41** 307
[343] Kara D 2013 Corrections of Order $\alpha\alpha_s$ to W Boson Decays *Nucl. Phys.* B **877** 683
[344] Schael S *et al* (ALEPH, DELPHI, L3, OPAL, LEP Electroweak Collaboration) 2013 Electroweak Measurements in Electron-Positron Collisions at W-Boson-Pair Energies at LEP, Phys *Rep.* **532** 119
[345] Janot P and Jadach S 2020 Improved Bhabha cross section at LEP and the number of light neutrino species *Phys. Lett.* B **803** 135319

[346] Blondel A and Gianfelice E 2021 The challenges of beam polarization and keV-scale centre-of-mass energy calibration at the FCC-ee *Eur. Phys. J. Plus* **136** 1103
[347] Janot P 2016 Direct measurement of $\alpha_{QED}(m_Z^2)$ at the FCC-ee *J. High Energy Phys.* JHEP02(2016)053 [Erratum: J. High Energy Phys. JHEP11(2017)164].
[348] Nesterenko A V 2016 *Strong interactions in spacelike and timelike domains: dispersive approach* (Elsevier) (https://doi.org/10.1016/C2014-0-04749-1)
[349] Feynman R P 1972 *Photon-hadron interactions* (Reading, Massachusetts)
[350] Adler S L 1974 Some simple vacuum-polarization phenomenology: $e^+e^- \to$ hadrons; the muonic-atom x-ray discrepancy and $g_\mu - 2$ *Phys. Rev.* D **10** 3714
[351] Radyushkin A V 1996 Optimized Λ-parametrization for the QCD running coupling constant in spacelike and timelike regions *JINR Rapid Commun.* **78** 96 [Report JINR E2-82-159 (1982)]
[352] Krasnikov N V and Pivovarov A A 1982 The influence of the analytical continuation effects on the value of the QCD scale parameter Λ extracted from the data on charmonium and ϒ hadron decays *Phys. Lett.* B **116** 168
[353] Moorhouse R G, Pennington M R and Ross G G 1977 What can asymptotic freedom say about $e^+e^- \to$ hadrons? *Nucl. Phys.* B **124** 285
[354] Pennington M R and Ross G G 1981 Perturbative QCD for timelike processes: what is the best expansion parameter? *Phys. Lett.* B **102** 167
[355] Pennington M R, Roberts R G and Ross G G 1984 How to continue the predictions of perturbative QCD from the spacelike region where they are derived to the timelike regime where experiments are performed *Nucl. Phys.* B **242** 69
[356] Pivovarov A A 1992 Renormalization group summation of perturbative series in timelike momentum region *Nuovo Cim.* A **105** 813
[357] Nesterenko A V 2013 Dispersive approach to QCD and inclusive τ lepton hadronic decay *Phys. Rev.* D **88** 056009
[358] Nesterenko A V 2015 Hadronic vacuum polarization function within dispersive approach to QCD *J. Phys.* G **42** 085004
[359] Baikov P A, Chetyrkin K G and Kuhn J H 2009 $R(s)$ and hadronic τ-decays in order α_s^4: technical aspects *Nucl. Phys. B Proc. Suppl.* **189** 49
[360] Baikov P A, Chetyrkin K G, Kuhn J H and Rittinger J 2012 Vector correlator in massless QCD at order $\mathcal{O}(\alpha_s^4)$ and the QED β-function at five loop *J. High Energy Phys.* JHEP07(2012)017
[361] Nesterenko A V 2019 Explicit form of the R-ratio of electron–positron annihilation into hadrons *J. Phys.* G **46** 115006
[362] Nesterenko A V 2020 Recurrent form of the renormalization group relations for the higher-order hadronic vacuum polarization function perturbative expansion coefficients *J. Phys.* G **47** 105001
[363] Baikov P A, Chetyrkin K G, Kuhn J H and Rittinger J 2012 Adler function, sum rules and Crewther relation of order $\mathcal{O}(\alpha_s^4)$: the singlet case *Phys. Lett.* B **714** 62
[364] Baikov P A, Chetyrkin K G and Kühn J H 2017 Five-loop running of the QCD coupling constant *Phys. Rev. Lett.* **118** 082002
[365] Herzog F, Ruijl B, Ueda T, Vermaseren J A M and Vogt A 2017 The five-loop beta function of Yang-Mills theory with fermions *J. High Energy Phys.* JHEP02(2017)090
[366] Luthe T, Maier A, Marquard P and Schroder Y 2017 The five-loop beta function for a general gauge group and anomalous dimensions beyond Feynman gauge *J. High Energy Phys.* JHEP10(2017)166
[367] Chetyrkin K G, Falcioni G, Herzog F and Vermaseren J A M 2017 Five-loop renormalisation of QCD in covariant gauges *J. High Energy Phys.* JHEP10(2017)179 [Addendum: J. High Energy Phys. JHEP12(2017)006]
[368] Schrempp B and Schrempp F 1980 QCD at low Q^2: a correspondence relation for moments of structure functions *Z. Phys.* C **6** 7
[369] Jones H F and Solovtsov I L 1995 QCD running coupling constant in the timelike region *Phys. Lett.* B **349** 519
[370] Milton K A and Solovtsov I L 1997 Analytic perturbation theory in QCD and Schwinger's connection between the beta function and the spectral density *Phys. Rev.* D **55** 5295
[371] Milton K A and Solovtsov I L 1999 Can the QCD effective charge be symmetrical in the Euclidean and the Minkowskian regions? *Phys. Rev.* D **59** 107701
[372] Solovtsov I L and Shirkov D V 1999 Analytic approach in Quantum Chromodynamics *Theor. Math. Phys.* **120** 1220

[373] Nesterenko A V and Simolo C 2010 QCDMAPT: program package for analytic approach to QCD *Comput. Phys. Commun.* **181** 1769
[374] Nesterenko A V and Simolo C 2011 QCDMAPT_F: fortran version of QCDMAPT package *Comput. Phys. Commun.* **182** 2303
[375] Nesterenko A V 2017 Electron-positron annihilation into hadrons at the higher-loop levels *Eur. Phys. J.* C **77** 844
[376] Bjorken J D 1989 Two topics in Quantum Chromodynamics *1989 Cargese Summer Institute in Particle Physics.* 11
[377] Prosperi G M, Raciti M and Simolo C 2007 On the running coupling constant in QCD *Prog. Part. Nucl. Phys.* **58** 387
[378] Perez-Ramos R and d'Enterria D 2014 Energy evolution of the moments of the hadron distribution in QCD jets including NNLL resummation and NLO running-coupling corrections *J. High Energy Phys.* JHEP08(2014)068
[379] d'Enterria D and Perez-Ramos R 2014 Extraction of α_S from the energy evolution of jet fragmentation functions at low z *49th Rencontres de Moriond on QCD and High Energy Interactions* 315
[380] d'Enterria D and Pérez-Ramos R 2016 Uncertainties on the determination of the strong coupling α_S from the energy evolution of jet fragmentation functions at low z *Nucl. Part. Phys. Proc.* **273** 1943
[381] Pérez-Ramos R and d'Enterria D 2015 Determination of α_S at NLO*+NNLL from a global fit of the low-z parton-to-hadron fragmentation functions in e^+e^- and DIS collisions *EPJ Web Conf.* **90** 04001
[382] d'Enterria D and Pérez-Ramos R 2015 α_S determination at NNLO *+NNLL accuracy from the energy evolution of jet fragmentation functions at low z *50th Rencontres de Moriond on QCD and High Energy Interactions* 117
[383] Dokshitzer Y L, Fadin V S and Khoze V A 1983 On the sensitivity of the inclusive distributions in parton jets to the coherence effects in QCD gluon cascades *Z. Phys.* C **18** 37
[384] Dokshitzer Y L, Khoze V A and Troian S I 1992 Inclusive particle spectra from QCD cascades *Int. J. Mod. Phys.* A **7** 1875
[385] Fong C P and Webber B R 1991 One and two particle distributions at small x in QCD jets *Nucl. Phys.* B **355** 54
[386] Perez-Ramos R and d'Enterria D *in preparation*
[387] Pérez-Ramos R and d'Enterria D 2019 α_S from soft QCD jet fragmentation functions *PoS* **ALPHAS2019** 94
[388] d'Enterria D 2018 α_S status and perspectives (2018) *PoS* **DIS2018** 109
[389] d'Enterria D *et al* (ed) 2017 *Proceedings, Parton Radiation and Fragmentation from LHC to FCC-ee: CERN, Geneva, Switzerland, November 22-23, 2016* arXiv:1702.01329 [hep-ph]
[390] Mueller A H 1983 Multiplicity and hadron distributions in QCD jets: nonleading terms *Nucl. Phys.* B **213** 85
[391] Mitov A, Moch S and Vogt A 2006 Next-to-Next-to-Leading Order Evolution of Non-Singlet Fragmentation Functions *Phys. Lett.* B **638** 61
[392] Albino S, Bolzoni P, A Kniehl B and Kotikov A 2011 Fully double-logarithm-resummed cross sections *Nucl. Phys.* B **851** 86
[393] Neill D 2021 The fragmentation spectrum from space-time reciprocity *J. High Energy Phys.* JHEP03(2021)081
[394] Kotikov A V and Teryaev O V 2021 SUSY, Casimir scaling, and probabilistic properties of gluon and quark-jet evolution *Phys. Rev.* D **103** 034002
[395] Abbate R *et al* 2011 Thrust at N^{3}LL with power corrections and a precision global fit for $\alpha_S(m_Z^2)$ *Phys.Rev.* D **83** 074021
[396] Hoang A *et al* 2015 Precise determination of α_S from the C-parameter distribution *Phys. Rev.* D **91** 094018
[397] Verbytskyi A, Banfi A, Kardos A, Monni P F, Kluth S, Somogyi G, Szőr Z, Trócsányi Z, Tulipánt Z and Zanderighi G 2019 High precision determination of α_S from a global fit of jet rates *J. High Energy Phys.* JHEP08(2019)129
[398] Gehrmann T, Luisoni G and Monni P F 2013 Power corrections in the dispersive model for a determination of the strong coupling constant from the thrust distribution *Eur. Phys. J.* C **73** 2265

[399] Manohar A V and Wise M B 1995 Power suppressed corrections to hadronic event shapes *Phys. Lett.* B **344** 407
[400] Webber B R 1994 Estimation of power corrections to hadronic event shapes *Phys. Lett.* B **339** 148
[401] Korchemsky G P and Sterman G F 1995 Nonperturbative corrections in resummed cross-sections *Nucl. Phys.* B **437** 415
[402] Korchemsky G P and Sterman G F 1999 Power corrections to event shapes and factorization *Nucl. Phys.* B **555** 335
[403] Dokshitzer Y L and Webber B R 1995 Calculation of power corrections to hadronic event shapes *Phys. Lett.* B **352** 451
[404] Dokshitzer Y L, Marchesini G and Webber B R 1996 Dispersive approach to power behaved contributions in QCD hard processes *Nucl. Phys.* B **469** 93
[405] Nason P and Seymour M H 1995 Infrared renormalons and power suppressed effects in e^+e^- jet events *Nucl. Phys.* B **454** 291
[406] Dasgupta M and Webber B R 1997 Power corrections and renormalons in e^+e^- fragmentation functions *Nucl. Phys.* B **484** 247
[407] Dokshitzer Y L, Lucenti A, Marchesini G and Salam G P 1998 Universality of $1/Q$ corrections to jet-shape observables rescued *Nucl. Phys.* B **511** 396 [Erratum: Nucl. Phys. B 593 (2001) 729]
[408] Dasgupta M, Magnea L and Smye G 1999 Universality of $1/Q$ corrections revisited *J. High Energy Phys.* JHEP11(1999)025
[409] Beneke M, Braun V M and Magnea L 1997 Phenomenology of power corrections in fragmentation processes in e^+e^- annihilation *Nucl. Phys.* B **497** 297
[410] Gardi E and Magnea L 2003 The C parameter distribution in e^+e^- annihilation *J. High Energy Phys.* JHEP08(2003)030
[411] Davison R A and Webber B R 2009 Non-perturbative contribution to the thrust distribution in e^+e^- annihilation *Eur. Phys. J.* C **59** 13
[412] Luisoni G, Monni P F and Salam G P 2021 C-parameter hadronisation in the symmetric 3-jet limit and impact on α_S fits *Eur. Phys. J.* C **81** 158
[413] Caola F, Ravasio S F, Limatola G, Melnikov K and Nason P 2022 On linear power corrections in certain collider observables *J. High Energy Phys.* JHEP01(2022)093
[414] Farhi E 1977 A QCD test for jets *Phys. Rev. Lett.* **39** 1587
[415] Ellis R, Ross D and Terrano A 1981 The perturbative calculation of jet structure in e^+e^- annihilation *Nucl. Phys.* B **178** 421
[416] Parisi G 1978 Super inclusive cross-sections *Phys. Lett.* B **74** 65
[417] Donoghue J F, Low F E and Pi S-Y 1979 Tensor analysis of hadronic jets in quantum chromodynamics *Phys. Rev.* D **20** 2759
[418] Catani S and Webber B R 1998 Resummed *C* parameter distribution in e^+e^- annihilation *Phys. Lett.* B **427** 377
[419] Dokshitzer Y L, Lucenti A, Marchesini G and Salam G P 1998 On the universality of the Milan factor for $1/Q$ power corrections to jet shapes *J. High Energy Phys.* JHEP05(1998)003
[420] Catani S and Webber B R 1997 Infrared safe but infinite: soft gluon divergences inside the physical region *J. High Energy Phys.* JHEP10(1997)005
[421] Gorishnii S G, Kataev A L and Larin S A 1991 The $O(\alpha_S^3)$-corrections to $\sigma_{tot}(e^+e^- \to \text{hadrons})$ and $\Gamma(\tau^- \to \nu_\tau + \text{hadrons})$ in QCD *Phys. Lett.* B **259** 144
[422] Banfi A, McAslan H, Monni P F and Zanderighi G 2015 A general method for the resummation of event-shape distributions in e^+e^- annihilation *J. High Energy Phys.* JHEP05(2015)102
[423] Del Duca V *et al* 2016 Three-jet production in electron–positron collisions at next-to-next-to-leading order accuracy *Phys. Rev. Lett.* **117** 152004
[424] Heister A *et al* (ALEPH Collaboration) 2004 Studies of QCD at e^+e^- centre-of-mass energies between 91 GeV and 209 GeV *Eur. Phys. J.* C **35** 457–86
[425] Movilla Fernandez P A, Biebel O, Bethke S and (JADE Collaboration) 1998 Measurement of C parameter and determinations of α_S from C parameter and jet broadening at PETRA energies, in High-energy physics *Proceedings, 29th International Conference, ICHEP'98, Vancouver, Canada, July 23-29, 1998* **1** 2
[426] Hoang A H, Kolodrubetz D W, Mateu V and Stewart I W 2015 C-parameter distribution at N^3LL' including power corrections *Phys. Rev.* D **91** 094017
[427] Huston J, Rabbertz K and Zanderighi G 2019 *2019 Update to the Quantum Chromodynamics Review* (http://pdg.lbl.gov/2019/reviews/rpp2019-rev-qcd.pdf)

[428] Catani S and Seymour M 1997 A General algorithm for calculating jet cross-sections in NLO QCD *Nucl. Phys.* B **485** 291 [Erratum: Nucl. Phys. B 510 (1998) 503].
[429] Dasgupta M, Dreyer F A, Hamilton K, Monni P F, Salam G P and Soyez G 2020 Parton showers beyond leading logarithmic accuracy *Phys. Rev. Lett.* **125** 052002
[430] Caola F, Ferrario Ravasio S, Limatola G, Melnikov K, Nason P and Ozcelik M A 2022 Linear power corrections to e^+ e $^-$ shape variables in the three-jet region *J. High Energy Phys.* JHEP12(2022)062
[431] Bethke S, Kluth S, Pahl C, Schieck J and (JADE Collaboration) 2009 Determination of the strong coupling α_S from hadronic event shapes with $o(\alpha_S^3)$ and resummed QCD predictions using JADE data *Eur. Phys. J.* C **64** 351
[432] Dissertori G, Gehrmann-De Ridder A, Gehrmann T, Glover E W N, Heinrich G, Luisoni G and Stenzel H 2009 Determination of the strong coupling constant using matched NNLO+NLLA predictions for hadronic event shapes in e^+e^- annihilations *J. High Energy Phys.* JHEP08(2009)036
[433] Dissertori G *et al* 2010 Precise determination of the strong coupling constant at NNLO in QCD from the three-jet rate in electron–positron annihilation at LEP *Phys. Rev. Lett.* **104** 072002
[434] Abbiendi G *et al* 2011 Determination of α_S using OPAL hadronic event shapes at $\sqrt{s} = 91$–209 GeV and resummed NNLO calculations *Eur. Phys. J.* C **71** 1733
[435] Schieck J, Bethke S, Kluth S, Pahl C, Trocsanyi Z and (JADE Collaboration) 2013 Measurement of the strong coupling α_S from the three-jet rate in e^+e^- annihilation using JADE data *Eur. Phys. J.* C **73** 2332
[436] Abbate R, Fickinger M, Hoang A H, Mateu V and Stewart I W 2012 Precision thrust cumulant moments at N^3LL *Phys. Rev.* D **86** 094002
[437] Larkoski A J, Marzani S, Soyez G and Thaler J 2014 Soft Drop *J. High Energy Phys.* JHEP05(2014)146
[438] Baron J, Marzani S and Theeuwes V 2018 Soft-drop thrust *J. High Energy Phys.* JHEP08(2018)105 [Erratum: J. High Energy Phys. JHEP05(2019)056]
[439] Baron J, Reichelt D, Schumann S, Schwanemann N and Theeuwes V 2021 Soft-drop grooming for hadronic event shapes *J. High Energy Phys.* JHEP07(2021)142
[440] Marzani S, Reichelt D, Schumann S, Soyez G and Theeuwes V 2019 Fitting the strong coupling constant with soft-drop thrust *J. High Energy Phys.* JHEP11(2019)179
[441] Buckley A *et al* 2011 General-purpose event generators for LHC physics *Phys. Rep.* **504** 145
[442] Bothmann E *et al* (Sherpa Collaboration) 2019 Event Generation with Sherpa 2.2 *SciPost Phys.* **7** 034
[443] Schumann S and Krauss F 2008 A Parton shower algorithm based on Catani-Seymour dipole factorisation *J. High Energy Phys.* JHEP03(2008)038
[444] Winter J-C, Krauss F and Soff G 2004 A Modified cluster hadronization model *Eur. Phys. J.* C **36** 381
[445] Fischer N, Gieseke S, Kluth S, Plätzer S, Skands P and (OPAL Collaboration) 2015 Measurement of observables sensitive to coherence effects in hadronic Z decays with the OPAL detector at LEP *Eur. Phys. J.* C **75** 571
[446] Kluth S, Verbytskyi A and (OPAL Collaboration) 2017 Measurements of jet rates with the anti-k_t and SISCone algorithms at LEP with the OPAL detector *EPJ Web Conf.* **141** 02003
[447] Chen Y, Lee Y-J, Maggi M, Chang P, Chien Y-T, McGinn C and Perepelitsa D *Analysis note: jet reconstruction, energy spectra, and substructure analyses with archived ALEPH data* arXiv:2108.04877 [hep-ex]
[448] Chen Y *et al* 2022 Jet energy spectrum and substructure in e^+e^- collisions at 91.2 GeV with ALEPH Archived Data *J. High Energy Phys.* JHEP06(2022)008
[449] Caletti S, Fedkevych O, Marzani S, Reichelt D, Schumann S, Soyez G and Theeuwes V 2021 Jet angularities in Z+jet production at the LHC *J. High Energy Phys.* JHEP07(2021)076
[450] Tumasyan A *et al* (CMS Collaboration) 2022 Study of quark and gluon jet substructure in Z+jet and dijet events from pp collisions *J. High Energy Phys.* JHEP01(2022)188
[451] Acharya S *et al* (ALICE Collaboration) 2022 Measurements of the groomed and ungroomed jet angularities in pp collisions at $\sqrt{s} = 5.02$ TeV *J. High Energy Phys.* JHEP05(2022)061
[452] Caletti S, Fedkevych O, Marzani S and Reichelt D 2021 Tagging the initial-state gluon *Eur. Phys. J.* C **81** 844
[453] Zhu J, Kang D and Maji T 2021 Angularity in DIS at next-to-next-to-leading log accuracy *J. High Energy Phys.* JHEP11(2021)026

[454] Reichelt D, Caletti S, Fedkevych O, Marzani S, Schumann S and Soyez G 2022 Phenomenology of jet angularities at the LHC *J. High Energy Phys.* JHEP03(2022)131
[455] Makris Y 2021 Revisiting the role of grooming in DIS *Phys. Rev.* D **103** 054005
[456] Les Houches 2017: physics at TeV Colliders Standard Model Working Group Report. March, 2018. arXiv:1803.07977 [hep-ph]
[457] Kardos A, Somogyi G and Trócsányi Z 2018 Soft-drop event shapes in electron–positron annihilation at next-to-next-to-leading order accuracy *Phys. Lett.* B **786** 313
[458] Frye C, Larkoski A J, Schwartz M D and Yan K 2016 Factorization for groomed jet substructure beyond the next-to-leading logarithm *J. High Energy Phys.* JHEP07(2016)064
[459] Kardos A, Larkoski A J and Trócsányi Z 2020 Groomed jet mass at high precision *Phys. Lett.* B **809** 135704
[460] Benkendorfer K and Larkoski A J 2021 Grooming at the cusp: all-orders predictions for the transition region of jet groomers *J. High Energy Phys.* JHEP11(2021)188
[461] Hoang A H, Mantry S, Pathak A and Stewart I W 2019 Nonperturbative corrections to soft drop jet mass *J. High Energy Phys.* JHEP12(2019)002
[462] Pathak A, Stewart I W, Vaidya V and Zoppi L 2021 EFT for Soft Drop Double Differential Cross Section *J. High Energy Phys.* JHEP04(2021)032
[463] Carli T, Clements D, Cooper-Sarkar A, Gwenlan C, Salam G P, Siegert F, Starovoitov P and Sutton M 2010 A posteriori inclusion of parton density functions in NLO QCD final-state calculations at hadron colliders: the APPLGRID Project *Eur. Phys. J.* C **66** 503
[464] Bertone V 2018 APFEL++: a new PDF evolution library in C++ *PoS* **DIS2017** 201
[465] Adloff C *et al* (H1 Collaboration) 2001 Measurement and QCD analysis of jet cross-sections in deep inelastic positron—proton collisions at $\sqrt{s} = 300$ GeV *Eur. Phys. J.* C **19** 289
[466] Aaron F D and (H1 Collaboration) 2010 Jet production in ep collisions at low Q^2 and determination of α_S *Eur. Phys. J.* C **67** 1
[467] Chekanov S *et al* (ZEUS Collaboration) 2002 Inclusive jet cross-sections in the Breit frame in neutral current deep inelastic scattering at HERA and determination of α_S *Phys. Lett.* B **547** 164
[468] Chekanov S *et al* (ZEUS Collaboration) 2007 Inclusive-jet and dijet cross-sections in deep inelastic scattering at HERA *Nucl. Phys.* B **765** 1
[469] Abramowicz H *et al* (ZEUS Collaboration) 2010 Inclusive dijet cross sections in neutral current deep inelastic scattering at HERA *Eur. Phys. J.* C **70** 965
[470] Baak M, Cúth J, Haller J, Hoecker A, Kogler R, Mönig K, Schott M, Stelzer J and (Gfitter Group Collaboration) 2014 The global electroweak fit at NNLO and prospects for the LHC and ILC *Eur. Phys. J.* C **74** 3046
[471] Dissertori G *et al* 2008 First determination of the strong coupling constant using NNLO predictions for hadronic event shapes in e^+e^- annihilations *J. High Energy Phys.* JHEP02 (2008)040
[472] Nagy Z and Trocsanyi Z 2001 Multijet cross-sections in deep inelastic scattering at next-to-leading order *Phys. Rev. Lett.* **87** 082001
[473] Abramowicz H *et al* (ZEUS Collaboration) 2012 Inclusive-jet photoproduction at HERA and determination of α_S *Nucl. Phys.* B **864** 1
[474] Aktas A *et al* (H1 Collaboration) 2006 Measurement of event shape variables in deep-inelastic scattering at HERA *Eur. Phys. J.* C **46** 343
[475] Chekanov S *et al* (ZEUS Collaboration) 2007 Event shapes in deep inelastic scattering at HERA *Nucl. Phys.* B **767** 1
[476] Gehrmann T, Huss A, Mo J and Niehues J 2019 Second-order QCD corrections to event shape distributions in deep inelastic scattering *Eur. Phys. J.* C **79** 1022
[477] Kang Z-B, Liu X and Mantry S 2014 1-jettiness DIS event shape: NNLL+NLO results *Phys. Rev.* D **90** 014041
[478] Kang D, Lee C and Stewart I W 2013 Using 1-jettiness to measure 2 jets in DIS 3 ways *Phys. Rev.* D **88** 054004
[479] Kang D, Lee C and Stewart I W 2015 DIS Event Shape at N^3LL *PoS* **DIS2015** 142
[480] Hessler J, Britzger D, Lee S and (H1 Collaboration) 2022 Measurement of 1-jettiness in deep-inelastic scattering at HERA *PoS* **EPS-HEP2021** 367
[481] Andreev V *et al* (H1 Collaboration) 2022 Measurement of Lepton-Jet Correlation in Deep-Inelastic Scattering with the H1 Detector Using Machine Learning for Unfolding *Phys. Rev. Lett.* **128** 132002

[482] Abdul Khalek R *et al* 2022 Science Requirements and Detector Concepts for the Electron-Ion Collider: EIC Yellow Report *Nucl. Phys.* A **1026** 122447
[483] Anderle D P *et al* 2021 Electron-ion collider in China *Front. Phys. (Beijing)* **16** 64701
[484] d'Enterria D and Poldaru A 2020 Extraction of the strong coupling $\alpha_S(m_Z^2)$ from a combined NNLO analysis of inclusive electroweak boson cross sections at hadron colliders *J. High Energy Phys.* JHEP06(2020)016
[485] Sirunyan A M *et al* (CMS Collaboration) 2020 Determination of the strong coupling constant $\alpha_S(m_Z^2)$ from measurements of inclusive $W^{\pm}$ and Z boson production cross sections in proton-proton collisions at $\sqrt{s} = 7$ and 8 TeV *J. High Energy Phys.* JHEP06(2020)018
[486] Klijnsma T, Bethke S, Dissertori G and Salam G P 2017 Determination of the strong coupling constant $\alpha_s(m_Z)$ from measurements of the total cross section for top-antitop quark production *Eur. Phys. J.* C **77** 778
[487] Anastasiou C, Dixon L J, Melnikov K and Petriello F 2004 High precision QCD at hadron colliders: electroweak gauge boson rapidity distributions at NNLO *Phys. Rev.* D **69** 094008
[488] Catani S, Cieri L, Ferrera G, de Florian D and Grazzini M 2009 Vector boson production at hadron colliders: a fully exclusive QCD calculation at NNLO *Phys. Rev. Lett.* **103** 082001
[489] Gavin R, Li Y, Petriello F and Quackenbush S 2011 FEWZ 2.0: a code for hadronic Z production at next-to-next-to-leading order *Comput. Phys. Commun.* **182** 2388
[490] Campbell J M and Ellis R K 2010 MCFM for the Tevatron and the LHC *Nucl. Phys. B Proc. Suppl.* **10** 205–6
[491] Boughezal R, Campbell J M, Ellis R K, Focke C, Giele W, Liu X, Petriello F and Williams C 2017 Color singlet production at NNLO in MCFM *Eur. Phys. J.* C **77** 7
[492] R D Ball *et al* (NNPDF Collaboration) 2015 Parton distributions for the LHC Run II *J. High Energy Phys.* JHEP04(2015)040
[493] Bondarenko S G and Sapronov A A 2013 NLO EW and QCD proton-proton cross section calculations with mcsanc-v1.01 *Comput. Phys. Commun.* **184** 2343
[494] Aad G *et al* (ATLAS Collaboration) 2016 Measurement of $W^{\pm}$ and Z-boson production cross sections in pp collisions at $\sqrt{s} = 13$ TeV with the ATLAS detector *Phys. Lett.* B **759** 601
[495] Kieseler J 2017 A method and tool for combining differential or inclusive measurements obtained with simultaneously constrained uncertainties *Eur. Phys. J.* C **77** 792
[496] Duhr C, Dulat F and Mistlberger B 2020 Charged current Drell-Yan production at N^3LO *J. High Energy Phys.* JHEP11(2020)143
[497] Camarda S, Cieri L and Ferrera G 2021 Drell–Yan lepton-pair production: qT resummation at N^3LL accuracy and fiducial cross sections at N^3LO *Phys. Rev.* D **104** L111503
[498] Camarda S, Ferrera G and Schott M 2024 Determination of the strong-coupling constant from the Z-boson transverse-momentum distribution *Eur. Phys. J.* C **84** 39
[499] Camarda S *et al* 2020 DYTurbo: fast predictions for Drell-Yan processes *Eur. Phys. J.* C **80** 251 [Erratum: Eur. Phys. J. C 80 (2020) 440]
[500] Catani S, Webber B R and Marchesini G 1991 QCD coherent branching and semiinclusive processes at large x *Nucl. Phys.* B **349** 635
[501] Aaltonen T *et al* (CDF Collaboration) 2012 Transverse momentum cross section of e^+e^- pairs in the Z-boson region from $p\bar{p}$ collisions at $\sqrt{s} = 1.96$ TeV *Phys. Rev.* D **86** 052010
[502] Landry F, Brock R, Nadolsky P M and Yuan C P 2003 Tevatron Run-1 Z boson data and Collins-Soper-Sterman resummation formalism *Phys. Rev.* D **67** 073016
[503] Alekhin S *et al* 2015 HERAFitter, open source QCD fit project *Eur. Phys. J.* C **75** 304
[504] (HERAFitter developers' team) 2015 QCD analysis of W- and Z-boson production at Tevatron *Eur. Phys. J.* C **75** 458
[505] Aad G *et al* (ATLAS Collaboration) 2014 Measurement of the Z/γ^* boson transverse momentum distribution in *pp* collisions at $\sqrt{s} = 7$ TeV with the ATLAS detector *J. High Energy Phys.* JHEP09(2014)145
[506] Marzani S and Combining Q 2016 Combining Q_T and small-x resummations *Phys. Rev.* D **93** 054047
[507] Aad G *et al* (ATLAS Collaboration) 2022 Determination of the parton distribution functions of the proton using diverse ATLAS data from pp collisions at $\sqrt{s} = 7$, 8 and 13 TeV *Eur. Phys. J.* C **82** 438
[508] Aad G *et al* (ATLAS Collaboration) 2019 Measurements of top-quark pair differential and double-differential cross-sections in the ℓ+jets channel with pp collisions at $\sqrt{s} = 13$ TeV using the ATLAS detector *Eur. Phys. J.* C **79** 1028 [Erratum: Eur. Phys. J. C 80 (2020) 1092].

[509] Aad G *et al* (ATLAS Collaboration) 2018 Measurement of differential cross sections and W^+/W^- cross-section ratios for W boson production in association with jets at $\sqrt{s} = 8$ TeV with the ATLAS detector *J. High Energy Phys.* JHEP05(2018)077 [Erratum: J. High Energy Phys. JHEP10(2020)048]
[510] Aad G *et al* (ATLAS Collaboration) 2019 Measurement of the inclusive cross-section for the production of jets in association with a Z boson in proton-proton collisions at 8 TeV using the ATLAS detector *Eur. Phys. J.* C **79** 847
[511] Aad G *et al* (ATLAS Collaboration) 2017 Measurement of the inclusive jet cross-sections in proton-proton collisions at $\sqrt{s} = 8$ TeV with the ATLAS detector *J. High Energy Phys.* JHEP09(2017)020
[512] Sawyer L, Waits C and Wobisch M *Perturbative QCD predictions in fixed order for cross section ratios* arXiv:2112.01449 [hep-ph]
[513] Nagy Z 2002 Three jet cross-sections in hadron-hadron collisions at next-to-leading order *Phys. Rev. Lett.* **88** 122003
[514] Nagy Z 2003 Next-to-leading order calculation of three jet observables in hadron-hadron collision *Phys. Rev.* D **68** 094002
[515] Kluge T, Rabbertz K and Wobisch M 2006 FastNLO: fast pQCD calculations for PDF fits *14th International Workshop on Deep Inelastic Scattering* **9** 483
[516] Abazov V M *et al* (D0 Collaboration) 2013 Measurement of the ratio of three-jet to two-jet cross sections in $p\bar{p}$ collisions at $\sqrt{s} = 1.96$ TeV *Phys. Lett.* B **720** 6
[517] Abazov V M and (D0 Collaboration) 2012 Measurement of angular correlations of jets at $\sqrt{s} = 1.96$ TeV and determination of the strong coupling at high momentum transfers *Phys. Lett.* B **718** 56
[518] (ATLAS Collaboration, ATLAS) 2018 Measurement of dijet azimuthal decorrelations in pp collisions at $\sqrt{s} = 8$ TeV with the ATLAS detector and determination of the strong coupling *Phys. Rev.* D **98** 092004
[519] Abazov V M *et al* (D0 Collaboration) 2013 Measurement of the combined rapidity and p_T dependence of dijet azimuthal decorrelations in $p\bar{p}$ collisions at $\sqrt{s} = 1.96$ TeV *Phys. Lett.* B **721** 212
[520] Wobisch M, Chakravarthula K, Dhullipudi R, Sawyer L and Tamsett M 2013 A new quantity for studies of dijet azimuthal decorrelations *J. High Energy Phys.* JHEP01(2013)172
[521] Khachatryan V *et al* (CMS Collaboration) 2015 Measurement of the inclusive 3-jet production differential cross section in proton-proton collisions at 7 TeV and determination of the strong coupling constant in the TeV range *Eur. Phys. J.* C **75** 186
[522] (ATLAS Collaboration) Measurement of multi-jet cross-section ratios and determination of the strong coupling constant in proton-proton collisions at $\sqrt{s} = 7$ TeV with the ATLAS detector *ATLAS-CONF-2013-041*
[523] (CMS Collaboration) Determination of the strong coupling constant from the measurement of inclusive multijet event cross sections in pp collisions at $\sqrt{s} = 8$ TeV *CMS-PAS-SMP-16-008*
[524] Aaboud M *et al* (ATLAS Collaboration) 2017 Determination of the strong coupling constant α_S from transverse energy–energy correlations in multijet events at $\sqrt{s} = 8$ TeV using the ATLAS detector *Eur. Phys. J.* C **77** 872
[525] Gehrmann T and Malaescu B 2022 Precision QCD Physics at the LHC *Ann. Rev. Nucl. Part. Sci.* **72** 233
[526] Malaescu B 2017 *Scale choices, uncertainties and correlations for jet observables* https://indico.cern.ch/event/555452/contributions/2495852/attachments/1436555/2222319/ScalesJetObservables_Malaescu.pdf, 2017. talk at the workshop: taming Unphysical Scales for Physical Predictions.
[527] Dixon L J, Moult I and Zhu H X 2019 Collinear limit of the energy-energy correlator *Phys. Rev.* D **100** 014009
[528] Sjöstrand T, Mrenna S and Skands P Z 2008 A Brief Introduction to PYTHIA 8.1 *Comput. Phys. Commun.* **178** 852
[529] Gieseke S, Rohr C and Siodmok A 2012 Colour reconnections in Herwig++ *Eur. Phys. J.* C **72** 2225
[530] Hamilton K, Nason P and Zanderighi G 2012 MINLO: multi-scale improved NLO *J. High Energy Phys.* JHEP10(2012)155
[531] d'Enterria D and Skands P Z (ed) 2015 *Proceedings, High-Precision* α_S *Measurements from LHC to FCC-ee. CERN, Geneva, Oct.* arXiv:1512.05194 [hep-ph]

[532] Czakon M, Mitov A and Poncelet R 2021 Next-to-next-to-leading order study of three-jet production at the LHC *Phys. Rev. Lett.* **127** 152001
[533] Tumasyan A *et al* 2022 Measurement and QCD analysis of double-differential inclusive jet cross sections in proton-proton collisions at $\sqrt{s} = 13$ TeV *J. High Energy Phys.* JHEP02(2022)142
[534] Cacciari M, Salam G P and Soyez G 2008 The anti-k_t jet clustering algorithm *J. High Energy Phys.* JHEP04(2008)063
[535] Sirunyan A M *et al* (CMS Collaboration) 2020 Measurement of $t\bar{t}$ normalised multi-differential cross sections in pp collisions at $\sqrt{s} = 13$ TeV, and simultaneous determination of the strong coupling strength, top quark pole mass, and parton distribution functions *Eur. Phys. J.* C **80** 658
[536] Currie J, Glover E W N and Pires J 2017 Next-to-next-to leading order QCD predictions for single jet inclusive production at the LHC *Phys. Rev. Lett.* **118** 072002
[537] Currie J, Gehrmann-De Ridder A, Gehrmann T, Glover E W N, Huss A and Pires J 2018 Infrared sensitivity of single jet inclusive production at hadron colliders *J. High Energy Phys.* JHEP10(2018)155
[538] Liu X, Moch S-O and Ringer F 2018 Phenomenology of single-inclusive jet production with jet radius and threshold resummation *Phys. Rev.* D **97** 056026
[539] Gao J, Liang Z, Soper D E, Lai H-L, Nadolsky P M and Yuan C P 2013 MEKS: a program for computation of inclusive jet cross sections at hadron colliders *Comput. Phys. Commun.* **184** 1626
[540] Bertone V, Botje M, Britzger D *et al* 2018 `xFitter` 2.0.0: an open source QCD fit framework *PoS* **DIS2017** 203
[541] Gao J, Li C S and Yuan C P 2012 NLO QCD corrections to dijet production via quark contact interactions *J. High Energy Phys.* JHEP07(2012)037
[542] Gao J 2013 CIJET: a program for computation of jet cross sections induced by quark contact interactions at hadron colliders *Comput. Phys. Commun.* **184** 2362
[543] Paukkunen H and Zurita P 2014 PDF reweighting in the Hessian matrix approach *J. High Energy Phys.* JHEP12(2014)100
[544] Schmidt C, Pumplin J, Yuan C P and Yuan P 2018 Updating and optimizing error parton distribution function sets in the Hessian approach *Phys. Rev.* D **98** 094005
[545] Andreev V *et al* (H1 Collaboration) 2017 Determination of the strong coupling constant $\alpha_S(m_Z^2)$ in next-to-next-to-leading order QCD using H1 jet cross section measurements *Eur. Phys. J.* C **77** 791
[546] Sirunyan A M *et al* (CMS Collaboration) 2019 Measurement of the $t\bar{t}$ production cross section, the top quark mass, and the strong coupling constant using dilepton events in p−p collisions at $\sqrt{s} = 13 TeV$ *Eur. Phys. J.* C **79** 368
[547] Vermaseren J A M, Larin S A and van Ritbergen T 1997 The four loop quark mass anomalous dimension and the invariant quark mass *Phys. Lett.* B **405** 327
[548] Chetyrkin K G 1997 Quark mass anomalous dimension to $O(\alpha_S^4)$ *Phys. Lett.* B **404** 161
[549] Baikov P A, Chetyrkin K G and Kühn J H 2014 Quark Mass and Field Anomalous Dimensions to $\mathcal{O}(\alpha_S^5)$ *J. High Energy Phys.* JHEP10(2014)076
[550] Herren F and Steinhauser M 2018 Version 3 of RunDec and CRunDec *Comput. Phys. Commun.* **224** 333
[551] Hoang A H, Lepenik C and Mateu V 2022 REvolver: automated running and matching of couplings and masses in QCD *Comput. Phys. Commun.* **270** 108145
[552] Gizhko A *et al* 2017 Running of the charm-quark mass from HERA deep-inelastic scattering data *Phys. Lett.* B **775** 233–8
[553] Abreu P *et al* (DELPHI Collaboration) 1998 m_b at M_Z *Phys. Lett.* B **418** 430–42
[554] Rodrigo G, Santamaria A and Bilenky M S 1997 Do the quark masses run? Extracting $m_b(m_Z)$ from LEP data *Phys. Rev. Lett.* **79** 193–6
[555] Abe K *et al* (SLD Collaboration) 1999 An Improved test of the flavor independence of strong interactions *Phys. Rev.* D **59** 012002
[556] Brandenburg A, Burrows P N, Muller D, Oishi N and Uwer P 1999 Measurement of the running b quark mass using $e^+e^- \to b\bar{b}g$ events *Phys. Lett.* B **468** 168
[557] Barate R *et al* (ALEPH Collaboration) 2000 A Measurement of the b quark mass from hadronic Z decays *Eur. Phys. J.* C **18** 1
[558] Abbiendi G *et al* (OPAL Collaboration) 2001 Determination of the b quark mass at the Z mass scale *Eur. Phys. J.* C **21** 411

[559] Abdallah J *et al* (DELPHI Collaboration) 2006 Determination of the b quark mass at the M(Z) scale with the DELPHI detector at LEP *Eur. Phys. J.* C **46** 569
[560] Abdallah J *et al* (DELPHI Collaboration) 2008 Study of b-quark mass effects in multijet topologies with the DELPHI detector at LEP *Eur. Phys. J.* C **55** 525
[561] (CMS collaboration) 2020 Running of the top quark mass from proton-proton collisions at $\sqrt{s} =$ 13 *Phys. Lett.* B **803** 135263
[562] Aparisi J *et al Snowmass White Paper: prospects for measurements of the bottom quark mass* arXiv:2203.16994 [hep-ex]
[563] Aparisi J *et al* 2022 mb at mH: the Running Bottom Quark Mass and the Higgs Boson *Phys. Rev. Lett.* **128** 122001
[564] Kluth S 2022 $m_{\mathrm{b}}(m_{Z^0})$ revisited with Zedometry *Eur. Phys. J.* C **82** 240
[565] Fuster J, Irles A, Tairafune S, Rodrigo G, Vos M, Yamamoto H and Yonamine R *Prospects for the measurement of the bottom quark mass at the ILC, ILD note, ILD-PHYS-PUB-2021-001*
[566] Jezabek M and Kuhn J H 1993 Light gluinos in Z0 decays? *Phys. Lett.* B **301** 121
[567] Boronat M, Fullana E, Fuster J, Gomis P, Hoang A, Mateu V, Vos M and Widl A 2020 Top quark mass measurement in radiative events at electron–positron colliders *Phys. Lett.* B **804** 135353
[568] Shifman M A, Vainshtein A I and Zakharov V I 1979 QCD and Resonance Physics: applications *Nucl. Phys.* B **147** 448–518
[569] Chetyrkin K G, Kühn J H and Steinhauser M 1996 Heavy quark vacuum polarization to three loops *Phys. Lett.* B **371** 93–8
[570] Chetyrkin K G, Kühn J H and Steinhauser M 1996 Three loop polarization function and $O(\alpha_S^2)$ corrections to the production of heavy quarks *Nucl. Phys.* B **482** 213–40
[571] Boughezal R, Czakon M and Schutzmeier T 2006 Four-loop tadpoles: applications in QCD *Nucl. Phys. Proc. Suppl.* **160** 160
[572] Czakon M and Schutzmeier T 2008 Double fermionic contributions to the heavy-quark vacuum polarization *J. High Energy Phys.* JHEP07(2008)001
[573] Maier A, Maierhofer P and Marquard P 2008 Higher Moments of Heavy Quark Correlators in the Low Energy Limit at $O(\alpha_S^2)$ *Nucl. Phys.* B **797** 218
[574] Chetyrkin K G, Kühn J H and Sturm C 2006 Four-loop moments of the heavy quark vacuum polarization function in perturbative QCD *Eur. Phys. J.* C **48** 107
[575] Boughezal R, Czakon M and Schutzmeier T 2006 Charm and bottom quark masses from perturbative QCD *Phys. Rev.* D **74** 074006
[576] Maier A, Maierhofer P and Marquard P 2008 The second physical moment of the heavy quark vector correlator at $O(\alpha_S^3)$ *Phys. Lett.* B **669** 88–91
[577] Maier A and Marquard P 2018 Validity of Padé approximations in vacuum polarization at three- and four-loop order *Phys. Rev.* D **97** 056016
[578] Kühn J H and Steinhauser M 2001 Determination of α_S and heavy quark masses from recent measurements of $R(s)$ *Nucl. Phys.* B **619** 588 [Erratum: Nucl. Phys. B 640 (2002) 415]
[579] Kühn J H, Steinhauser M and Sturm C 2007 Heavy quark masses from sum rules in four-loop approximation *Nucl. Phys.* B **778** 192
[580] Chetyrkin K G *et al* 2009 Charm and Bottom Quark Masses: an Update *Phys. Rev.* D **80** 074010
[581] Chetyrkin K, Kühn J H, Maier A, Maierhofer P, Marquard P, Steinhauser M and Sturm C 2012 Precise Charm- and Bottom-Quark Masses: theoretical and Experimental Uncertainties *Theor. Math. Phys.* **170** 217
[582] Chetyrkin K G, Kühn J H, Maier A, Maierhofer P, Marquard P, Steinhauser M and Sturm C 2017 Addendum to Charm and bottom quark masses: an update *Phys. Rev.* D **96** 116007
[583] Dehnadi B, Hoang A H, Mateu V and Zebarjad S M 2013 Charm Mass Determination from QCD Charmonium Sum Rules at Order α_S^3 *J. High Energy Phys.* JHEP09(2013)103
[584] Boito D and Mateu V 2020 Precise α_S determination from charmonium sum rules *Phys. Lett.* B **806** 135482
[585] Bai J Z *et al* (BES Collaboration) 2000 Measurement of the Total Cross Section for Hadronic Production by e^+e^- Annihilation at Energies between 2.6–5 GeV *Phys. Rev. Lett.* **84** 594–7
[586] Bai J Z *et al* (BES Collaboration) 2002 Measurements of the Cross Section for $e^+e^- \rightarrow$ hadrons at Center-of-Mass Energies from 2 to 5 GeV *Phys. Rev. Lett.* **88** 101802
[587] Ablikim M *et al* (BES Collaboration) 2004 Measurement of Cross Sections for $D^0\bar{D}^0$ and D^+D^- Production in e^+e^- Annihilation at $\sqrt{s} = 3.773$ GeV *Phys. Lett.* B **603** 130

[588] Ablikim M *et al* (BES Collaboration) 2006 Measurements of the cross sections for $e^+e^- \to$ hadrons at 3.650 GeV, 3.6648 GeV, 3.773 GeV and the branching fraction for $\psi(3770) \to$ non D $\bar{D}$ *Phys. Lett.* B **641** 145
[589] Ablikim M *et al* 2006 Measurements of the continuum R_{uds} and R values in e^+e^- annihilation in the energy region between 3.650 GeV and 3.872 GeV *Phys. Rev. Lett.* **97** 262001
[590] Ablikim M *et al* (BES Collaboration) 2009 *R* value measurements for e^+e^- annihilation at 2.60, 3.07 and 3.65 GeV *Phys. Lett.* B **677** 239
[591] Osterheld A *et al* 1986 Measurements of total hadronic and inclusive D^* cross-sections in e^+e^- annihilations between 3.87 GeV and 4.5 GeV *SLAC-PUB-4160*
[592] Edwards C *et al* 1990 Hadron production in e^+e^- annihilation from $s^{1/2} = 5$ GeV to 7.4 GeV *SLAC-PUB-5160*
[593] Ammar R *et al* (CLEO Collaboration) 1998 Measurement of the total cross section for $e^+e^- \to$ hadrons at $s^{1/2} = 10.52$ GeV *Phys. Rev.* D **57** 1350
[594] Besson D *et al* (CLEO Collaboration) 1985 Observation of new structure in the e^+e^- annihilation cross-section above B $\bar{B}$ threshold *Phys. Rev. Lett.* **54** 381
[595] Besson D *et al* (CLEO Collaboration) 2007 Measurement of the total hadronic cross section in e^+e^- annihilations below 10.56 GeV *Phys. Rev.* D **76** 072008
[596] Cronin-Hennessy D *et al* (CLEO Collaboration) 2009 Measurement of Charm Production Cross Sections in e^+e^- Annihilation at Energies between 3.97 and 4.26 GeV *Phys. Rev.* D **80** 072001
[597] Blinov A E *et al* 1996 The Measurement of R in e^+e^- annihilation at center-of- mass energies between 7.2 GeV and 10.34 GeV *Z. Phys.* C **70** 31–8
[598] Criegee L and Knies G 1982 Review of e^+e^- experiments with PLUTO from 3 GeV to 31 GeV, Phys *Rep.* **83** 151
[599] Abrams G S *et al* 1980 Measurement of the parameters of the $\psi''(3770)$ resonance, *Phys. Rev.* D **21** 2716
[600] Ablikim M *et al* (BESIII Collaboration) 2022 Measurement of the Cross Section for $e^+e^- \to$ Hadrons at Energies from 2.2324 to 3.6710 GeV *Phys. Rev. Lett.* **128** 062004
[601] Boito D, Mateu V and Rodrigues M V 2021 Small-momentum expansion of heavy-quark correlators in the large-β_0 limit and α_S extractions *J. High Energy Phys.* JHEP08(2021)027
[602] Brambilla N, Garcia i Tormo X, Soto J and Vairo A 2007 Extraction of α_S from radiative $\Upsilon(1S)$ decays *Phys. Rev.* D **75** 074014
[603] Besson D *et al* (CLEO Collaboration) 2006 Measurement of the direct photon momentum spectrum in $\Upsilon(1S)$, $\Upsilon(2S)$, and $\Upsilon(3S)$ decays *Phys. Rev.* D **74** 012003
[604] Mateu V and Ortega P G 2018 Bottom and Charm Mass determinations from global fits to $Q\bar{Q}$ bound states at N^3LO *J. High Energy Phys.* JHEP01(2018)122
[605] Hoang A H, Jain A, Scimemi I and Stewart I W 2008 Infrared renormalization group flow for heavy quark masses *Phys. Rev. Lett.* **101** 151602
[606] Hoang A H, Jain A, Lepenik C, Mateu V, Preisser M, Scimemi I and Stewart I W 2018 The MSR mass and the $\mathcal{O}\Lambda_{QCD}$ renormalon sum rule *J. High Energy Phys.* JHEP04(2018)003
[607] Peset C, Pineda A and Segovia J 2018 The charm/bottom quark mass from heavy quarkonium at N^3LO *J. High Energy Phys.* JHEP09(2018)167
[608] Alekhin S, Kardos A, Moch S and Trócsányi Z 2021 Precision studies for Drell–Yan processes at NNLO *Eur. Phys. J.* C **81** 573